THE UNIVERSITY OF MICHIGAN

INDUSTRY PROGRAM OF THE COLLEGE OF ENGINEERING

ON THE FLOW OF TWO IMMISCIBLE INCOMPRESSIBLE FLUIDS IN POROUS MEDIA

Russell L. Nielsen

A dissertation submitted in partial fulfillment
of the requirements for the degree of
Doctor of Philosophy in the
University of Michigan
Chemical and Metallurgical Department
1962

December, 1962

IP-594

"J'ai cherché par des expériences précises à déterminer les lois de l'écoulement de l'eau à travers les filtres....Ces expériences démontrent positivement que le volume d'eau qui passe à travers une couche de sable d'une nature donnée est proportionnel à la pression et en raison inverse de l'épaisseur des couches traversées...."

"...il résulte que le volume d'eau qui traverse une couche sablonneuse est proportionnel à la pression, et non pas à la racine carrée de cette pression, comme le suppose M. Genieys, dans son Essai sur les moyens d'élever, de conduire et de distribuer les eaux."

M. Henry Darcy
Inspecteur Général des Ponts et Chaussées
Les Fontaines Publiques de la Ville de Dijon
Paris, 1856

ACKNOWLEDGEMENTS

I wish to express my gratitude to the many persons and organizations who have contributed to this research. Thanks are due particularly to:

Professor M. R. Tek, chairman of the doctoral committee for his efficient handling of administrative matters, his help in defining the area of research and in interpreting the results.

Doctor K. H. Coats, committee member, for his suggestions during the early phases of the numerical work.

Professors D. L. Katz, E. F. Brater, J. R. Street and Doctor L. A. Rapoport, committee members, for their interest and helpful suggestions.

Professor R. C. F. Bartels, Director, and the personnel of the Computing Center at the University of Michigan for their generous donation of computing time and services.

The late Professor W. A. Hedrich for the use of his photometry laboratory.

Messers J. E. Briggs, S. C. Jones, H. B. Kristinsson, M. C. Miller, and D. A. Saville for their interest and constructive criticisms throughout the course of the investigation.

The office and shop personnel of the Chemical and Metallurgical Engineering Department for their help in securing materials and constructing equipment.

The consumers Power Company and the Michigan Gas Association for financial aid in the form of fellowships.

The Jersey Production Research Company for the loan of the laboratory flow model used in the experimental portion of this research.

My wife, Colleen, and mother, Mrs. J. J. Nielsen for typing the draft of this dissertation.

Messers R. E. Carroll, D. L. Danford and the personnel of the Industry Program of the College of Engineering for their masterful production of the final form of this dissertation.

TABLE OF CONTENTS

TABLE OF CONTENTS CONT'D

LIST OF TABLES

LIST OF TABLES (CONT'D)

LIST OF TABLES (CONT'D)

LIST OF FIGURES

LIST OF FIGURES (CONT'D)

LIST OF FIGURES (CONT'D)

LIST OF APPENDICES

NOMENCLATURE

Defining equations will be cited for all characters unless meaning is obvious. Multiple meanings have been avoided as much as possible without resorting to extensive use of cumbersome distinguishing marks such as super bars, sub bars, etc. When multiple meanings occur, the correct meaning will depend upon context. Normally, multiple meanings occur only for constants.

a	constant defined by Equations (73a), (74a), (110b)
A	constant defined by Equations (23), (48), (107), (119), (112e), (I-13)
A_1	constant defined by Equations (36), (I-15)
A_2	constant defined by Equations (37), (I-15)
$\bar{A}_1$	constant defined by Equation (I-15)
$\bar{A}_2$	constant defined by Equation (I-15)
b	constant defined by Equations (73b), (74b)
B	constant defined by Equations (24), (119)
$\bar{B}_1$	constant defined by Equation (I-17)
$\bar{B}_2$	constant defined by Equation (I-17)
c	constant defined by Equations (73c), (74c)
C	constant defined by Equations (25), (100), (106a), (106b), (111), (112)
C_x	constant defined by Equation (79)
C_y	constant defined by Equation (82)
$\bar{C}_x$	constant defined by Equation (88)

	$\bar{C}_y$		constant defined by Equation (91)
	C_1		constant defined by Equation (121b)
	C_2		constant defined by Equation (121c)
	d		constant defined by Equations (73d), (74d), (110c), (110d)
	D		constant defined by Equations (26), (100), (120)
	e		constant defined by Equations (73e), (74e)
	E		constant defined by Equation (27)
or	E	=	P*-P, error; defined by Equation (I-2c)
	f	=	porosity (dimensionless)
	F		constant defined by Equations (28), (108a), (108b)
or	F		geometric attenuation factor; defined by Equation (122c)
	g		constant defined by Equation (73f), (74f)
or	g	=	9.66×10^{-4} atm cm^2/gm, gravitational acceleration
	G		constant defined by Equations (29a), (29b), (72a), (72b)
	$\bar{G}$		constant defined by Equations (85a), (85b)
	h		height above datum (cm)
	H		iteration parameter; defined by Equations (77a), (77b)
	HK		"pure" iteration parameter; defined by Equation (84e)
	i		position index, x- (or r-) direction
	I		i-component of error, E; defined by Equation (I-6)
	I_b		base light intensity; defined by Equation (122b)
	I_t		total light intensity; defined by Equation (122a)
	j		position index, y-direction
	J		j-component of error, E; defined by Equation (I-6)
or	J		Leverett J-function (dimensionless); defined by Equation (4)

	k	relative permeability (dimensionless)
	K	single phase permeability (Darcys)
or	K	k-component of error, E; defined by Equation (I-6)
	L	over-all length dimension
	M	sum of phase mobilities; defined by Equation (54c)
	n	time index
	N	difference between phase mobilities; defined by Equation (54d)
	p	pressure (atm)
	P	sum of phase potentials (atm); defined by Equation (54a)
	P*	exact solution of difference equation; defined by Equation (I-2a)
	p_c	capillary pressure (atm); defined by Equation (3)
	PV	pore volume (cc)
	Q	injection rate (cc/sec)
	QT	total injection rate (cc/sec)
	r,y,Θ	position coordinates, cylindrical coordinate system
	R	difference between phase potentials (atm); defined by Equation (54b)
	$\bar{R}$	average R; defined by Equation (93b)
	S	phase saturation (dimensionless)
	S'	dS/dpc, reciprocal slope of capillary pressure curve (atm^{-1})
	t	time (sec)
	Δt	time increment (sec)
	T	constant defined by Equation (86)

	u,v,w	x-, y-, z-, or r-, y-, Θ- components of velocity vector (cm/sec)
	U	dummy dependent variable
	$\bar{v}$	velocity vector (cm/sec)
	W	water in pore volume (cc)
	x,y,z	position coordinates, cartesian coordinate system
	$\bar{y}$	elevation of the surface y = 0, domal coordinate system; defined by Equation (45)
	y_o	elevation of the surface y = 0, domal grid system; defined by Equation (63)
	Δx	x-direction dimension, cartesian grid element
or	Δx	logarithmic r-direction dimension, domal grid element; defined by Equation (64a)
	Δy	y-direction dimension, cartesian or domal grid element
	Δz	z-direction dimension, cartesian grid element

Greek Letters

	α	constant defined by Equation (94)
or	α	difference equation eigenvalue; defined by Equations (I-12a), (I-12b)
or	α	geometric factor defined by Equation (67)
	β	constant defined by Equation (94)
or	β	difference equation variable; defined by Equation (I-13)
or	β	geometric factor defined by Equation (68)
	γ	constant defined by Equations (94), (I-8)
	γ_1	constant defined by Equation (I-9)
	γ_2	constant defined by Equation (I-21)
	γ_x	geometric factor defined by Equations (I-36a), (I-36b)
	γ_y	geometric factor defined by Equations (I-36c), (I-36d)
	Γ	constant defined by Equation (29b)

	δ	constant defined by Equations (94), (II-1)
	Δ	denotes difference
	Δ_x	difference operator defined by Equation (58)
	Δ_y	difference operator defined by Equation (59)
	$\bar{\Delta}_r$	difference operator defined by Equation (69)
	$\bar{\Delta}_y$	difference operator defined by Equation (70)
	ϵ	constant defined by Equation (I-31)
	θ	contact angle
or	θ	angle of tilt from horizontal, cartesian coordinate system
or	θ	angular position, cylindrical coordinate system
	λ_1	constant defined by Equation (I-10)
	λ_2	constant defined by Equation (I-22)
	μ	viscosity (centipoise)
	ρ	fluid density (g/cc)
	$\Delta\rho$	$\rho_w - \rho_n$, density difference (g/cc)
	σ	interfacial tension (dynes/cm)
	Σ	denotes summation
	Φ	flow potential, compressible fluid (atm cm^3/gm); defined by Equation (6)
	Φ	flow potential, incompressible fluid (atm); defined by Equation (5)
	Φ	well bore potential (atm); defined by Equation (105a)
	ψ_1	mobility function; defined by Equation (21a)
	ψ_2	mobility function; defined by Equation (21b)

Subscripts

1,2	denote particular phases, systems, or grid elements
av	denotes average property
B	denotes bottom of laboratory model
c	denotes well at center of grid element
e	denotes well at edge of grid element
i	denotes general phase, position index (x- or r-direction)
j	denotes position index (y-direction)
ℓ	dummy index
m	dummy index; or when associated with position index, denotes maximum index in grid system
n	denotes time index, or non-wetting phase
w	denotes wetting phase
wb	denotes well-bore property

Superscripts

k	iteration number
—	denotes average property
primes	used to distinguish properties of a scaled laboratory model from corresponding properties of its reservoir prototype

Miscellaneous

∇	differential operator denoting the gradient of a scalar quantity or the divergence of a vector quantity
log	logarithm to base e
max	denotes maximum value
min	denotes minimum value

ABSTRACT

The purpose of the research was to study the simultaneous flow of two fluid phases in porous media by experimental means and through simulation on a digital computer.

Drainage and imbibition displacements of a gas - water system were performed in a two-dimensional laboratory flow model. The transient phase distributions were determined through an original technique based on the attenuation of transmitted light. The reproducibility of the measurement technique and of the over-all displacement processes was found to be very good. The experimental results compared favorably to numerical solutions of the differential equations describing the flow of two immiscible, incompressible fluids in porous media.

Scaling laws derived from the same differential equations state the relationships which must be satisfied by dynamically similar two-phase flow systems of this type. The scaling laws presuppose conditions which are unattainable in the laboratory for practical reasons. The effects of the unscalable properties have been evaluated through computer-simulation of a hypothetical laboratory model of a natural gas reservoir.

Natural gas storage operations often are carried out underground in dome-shaped formations of porous rock. When a saddle is present in the contour of the formation, the gas storage capacity is limited. Numerical simulation of such a storage operation indicated that water injection at the saddle would increase the effective capacity of the reservoir.

I. INTRODUCTION

Petroleum hydrocarbons are a most important natural resource. Since the advent of the internal combustion engine production and refining of crude oil and, more recently, natural gas have increased continually. Today petroleum products serve both as a source of energy and as starting materials for the chemical industry. So far, proven and estimated reserves have kept pace with the growing demand for petroleum products. Although discovered and still undiscovered reserves are vast, they are by no means inexhaustible. This plus the fact that most reservoirs are abandoned with as little as one half the potential yield realized points out the need for conservation measures. Vital to the improvement of the yield realized in production operations is an understanding of the physical phenomena involved in recovering the crude petroleum hydrocarbons from their native environment. To this end most major oil companies participate significantly in production research activities.

Underground rock formations in which petroleum hydrocarbons have been discovered fall into several classes. Common to most of these is a layer of dense impermeable rock situated on top of a porous, water-bearing layer of rock. The water-bearing rock is called an aquifer. Faults or domes in the bedding planes of the rock layers cause the overlying impermeable cap rock to act as a trap for hydrocarbon fluids which were produced over a span of geologic time from the decomposition of once-living matter.

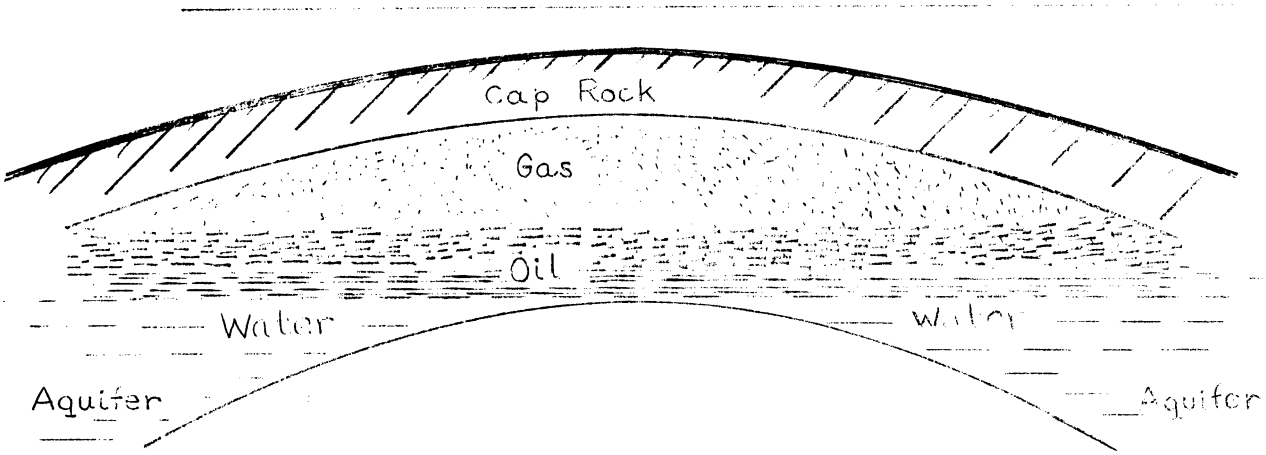

Figure 1. Typical Petroleum Reservoir.

A vertical cross-section of a typical dome-shaped reservoir is illustrated in Figure 1. The composition of the petroleum fluids varies among reservoirs, but normally an uncountable number of components are present ranging from methane to high molecular weight fractions generally termed asphalt. Lighter components including methane and ethane along with nitrogen, carbon dioxide and occasionally helium normally predominate in the gas phase, with heavier components in the oil phase. Saline water normally underlies the petroleum phases. As indicated in Figure 1, phases are not separated by a sharp interface, but rather by a zone of gradual transition. This is caused by interaction of gravitational segregation and capillary effects associated with the fluids in the network of interconnecting void spaces permeating the porous medium.

When reservoir fluids are withdrawn (or injected in some types of operation), simultaneous motion of all phases results. A major objective of production research is mathematical description of the motion of the multiphase system.

As with most physical phenomena, multiphase flow in porous media can be subjected either to macroscopic or microscopic analysis. Because the macroscopic approach is inherently simpler and requires only a bulk description of the porous medium, it has been used in practically all work to date, and it will be used exclusively here. However, the opinion of this author is that significant contributions eventually will result through the microscopic approach applied in a statistical manner.

Once valid and practical mathematical description of the multiphase flow system has been achieved, the effect of controllable operating variables such as well spacing, well penetration and production (or injection) rates can be studied systematically. The result will surely be more efficient reservoir operation.

Although the study of multiphase flow in porous media is of particular importance in petroleum production, it also has applications in packed bed separation processes used in chemical and petroleum refining operations.

II. HISTORICAL DEVELOPMENT AND LITERATURE SURVEY

In 1856, the French engineer Henry Darcy[12] empirically established that the flow rate of a single phase fluid through a porous medium is proportional to the imposed pressure gradient. This relationship has come to be known as Darcy's law and it has served as the cornerstone for conventional means of describing fluid flow systems in porous media. It is valid for systems of this type in which flow velocities are such that inertial forces are negligible in comparison to viscous forces. A comprehensive discussion of Darcy's work is given by Hubbert[22], who also shows how Darcy's law can be deduced from the Navier-Stokes equations.

Darcy's law may be written as:

$$\bar{v} = -\frac{K}{\mu} \nabla \Phi \qquad (1)$$

General background information on the production of oil and natural gas is given by Katz, et al.[25], Pirson[41], Muskat[34], and Scheidegger[47], among a number of other authors. They dwell mainly on the highly developed theory of single phase flow.

Interest in the flow of two immiscible fluids in porous media seems to have germinated in the early 1930's. Experimental studies by a number of investigators[9,52] made it evident that the presence of a second phase lowers the permeability of the medium to both phases.

Extension of Darcy's law to two phase systems was suggested by Muskat and Meres[35] who postulated the relative permeability concept.

$$\bar{v}_1 = -K \frac{k_1}{\mu_1} \nabla \Phi_1 \tag{2a}$$

$$\bar{v}_2 = -K \frac{k_2}{\mu_2} \nabla \Phi_2 \tag{2b}$$

Experimental work to substantiate the concept appears first to have been performed by Wyckoff and Botset[59]. Their data show the relative permeability to each phase of an immiscible two-phase system to be, within limits, only a function of the relative amounts of each phase present within the porous medium. Their work on unconsolidated media is regarded as classic, and their data are widely used today. A typical pair of relative permeability curves is shown in Figure 22. Other investigators[7,51] have found relative permeability functions to be approximately the same for any non-wetting, wetting system in unconsolidated media. A summary of the methods for measurement of relative permeability are given by Osaba, et al.[38].

The concept of capillary pressure was introduced by Leverett[28]. Capillary pressure is defined as the difference in pressure existing on either side of an interface between fluid phases. The pressure difference is due to the interfacial tension between phases, the curvature of the interface separating the phases, and the wettability of the walls of the capillary container by the phases. The experimental work performed by Leverett on wetting-non-wetting immiscible two phase systems showed capillary pressure to be a function of the saturation within the pore

space on a macroscopic basis. Actually, a hysteretic effect was observed in which the capillary pressure function depended upon whether the equilibrium wetting phase saturation was approached from above or below. The function associated with the former is termed drainage (for decreasing wetting phase saturation) and the latter imbibition (for increasing wetting phase saturation).

$$p_c(S) = p_n - p_w \tag{3}$$

Leverett was also able to correlate the capillary pressure functions on a dimensionless basis for a number of unconsolidated media of different porosity and permeability.

$$J(S) = \frac{p_c(S)}{\sigma \cos\theta}\sqrt{K/f} \tag{4}$$

In view of the hysteresis observed in the capillary pressure function, it is not unreasonable to expect similar hysteretic effects in the relative permeability function. Data demonstrating such effects have been reported recently by Naar, et al.[37] These effects are associated with the degree of wetting of the surfaces within the porous matrix by the separate phases. Normally wettability is taken into account by multiplying the interfacial tension by the cosine of the contact angle. The contact angle, θ a microscopic property of the system, is defined as the angle formed by the phase interface with the solid surface. It is measured through the wetting phase. Several authors[54,13] describe the concept of wettability in rather qualitative terms but the most basic treatment has been given by Melrose[33]. These investigators all point out that the inclusion of wettability effects by means of the cos θ

factor is a far too superficial approach. However at present, at least on the macroscopic scale, a better, yet practical, treatment of weattability is not available.

The generalized form of Darcy's law stated in Equations (2a) and (2b) includes gravitational forces through the use of the flow potential Φ instead of pressure.

$$\Phi_i = p_i + \rho_i g h \tag{5}$$

Pressure and potential are related according to Equation (5) for incompressible fluids. For compressible fluids it is convenient to employ a different potential function φ defined by Equation (6).[22]

$$\phi_i = gh + \int \frac{dp_i}{\rho_i} \tag{6}$$

For use of this potential function a different form of Darcy's law is necessary.

$$\bar{v}_i = -K \frac{k_i}{\mu_i} \rho_i \nabla \phi_i \tag{7}$$

It is apparent that Equation (7) reduces to the form of Equations (2a) and (2b) for incompressible fluids.

For a system of immiscible phases, mathematical analysis consists of formulating differential equations obtained by combining Darcy's law, capillary pressure relationships and an equation of state for each phase with the continuity equation for each phase. The result is a number of simultaneous, non-linear partial differential equations, the number of equations being equal to the number of phases. For miscible or partially

miscible fluids, the resulting mathematical description is obtained by performing similar analysis on a component basis.

Due to the complexity of the differential equations general analytic solution will in all probability never be achieved. Before the advent of high-speed digital computing facilities, serious attempt at numerical solution for all but the most simple systems was out of the question.

In 1942, the "fractional flow" equations were derived by Buckley and Leverett[6] for the flow of two immiscible phases in one-dimensional media. By neglecting gravitational and capillary effects, the fractional flow equations were simplified to allow saturation distribution during displacement to be obtained by a graphical means of solution. Later Welge[55] presented a simplified method based on the work of Buckley and Leverett for obtaining oil recovery in the presence of gas or water drive.

In 1951, Terwilliger, et al.[50] used the fractional flow equations retaining capillary and gravitational contributions to describe gravity drainage experiments on a one-dimensional gas-water system. Their work appears to be the first to employ numerical methods with machine calculations (punched card calculator). Using an explicit means of attack, they were able to obtain good agreement with experimental data. Also of significance was their conclusion that steady state relative permeability and static capillary pressure relationships can be used in the treatment of transient systems.

Several years later West, Garvin, and Sheldon[57], with much improved computing facilities (IBM 701) studied horizontal linear and radial systems produced under gas drive neglecting capillary effects. Their numerical treatment employed the more sophisticated implicit finite difference grid system. Implicit difference formulations are normally superior to explicit ones because of stability considerations, and they have been used in virtually all of the recent work.

A recent numerical simulation of the one-dimensional inclined flow of two immiscible incompressible fluids has been reported by Hovanessian and Fayers[21]. They showed that the inclusion of capillary and gravitational forces has a pronounced effect on phase saturation and pressure distributions. Several other studies[2,32] have been made on horizontal one-dimensional systems to demonstrate the effect of capillary forces. The general conclusion is that the numerical solutions in which capillary effects have been included approach the Buckley-Leverett simplified solution at high flow rates.

All mathematical analyses cited so far were carried out within the framework of an Eulerian coordinate system. In such a coordinate system, the position vector of a point on the porous surface is constant. An equally valid coordinate system is the Lagrangian, in which the position vector of a fluid particle (or some transient property of the system) remains constant.

Sheldon, Zondek and Cardwell[49] have transformed the Eulerian equations describing the one-dimensional vertical flow of two immiscible, incompressible phases into a Lagrangian system with saturation and time

as the independent variables. The dependent variable defines position within the porous medium. The authors have demonstrated the use of the method of characteristics in obtaining a numerical solution. This method is often used in the theory of supersonic compressible flow. Although their results are the same as those obtained by previous methods, these authors feel their approach is more logical and has more general applicability. Fayers and Sheldon[17] applied this method to a one-dimensional inclined system. However, they state that the Eulerian methods are superior for systems operated at low flow rates, and also for calculations after breakthrough regardless of flow rate.

All of the preceding numerical solutions have dealt with various one-dimensional systems. In 1958, a very important paper was published by Douglas[15], in which a numerical technique called the "Implicit Alternating Direction Method" for treatment of two-dimensional problems was presented. Earlier two-dimensional techniques all suffered from either excessive computational time requirements or stability considerations. This technique possesses stability equivalent to one-dimensional implicit methods, and can be employed in solution of both parabolic and elliptic equations.

The classic finite difference treatment of the two-dimensional flow of two immiscible, incompressible fluids was done by Douglas, Peaceman, and Rachford[16] who used the alternating direction method. They simulated two experimental water-flood displacements in a horizontal plane (no gravity). Although experimentally determined phase saturation distributions were not available, the agreement with integral data (recovery curve) was

very good. Their study serves as the basis for the numerical work done in this thesis.

Peaceman and Rachford[40] also made a significant contribution in two-dimensional miscible displacement. Using numerical methods similar to those above, good agreement was obtained with laboratory data. This study dealt mainly with finger formation due to small randomly distributed permeability inhomogeneities under conditions of adverse mobility ratio.

So far, little numerical work has been reported on studies of partially miscible systems. Welge, et al.[56] have reported a one-dimensional study of "condensing gas drive." The method gives good agreement with laboratory recovery data. The work of West, Garvin, and Sheldon[57] cited earlier dealt with solution gas drive in the absence of capillary effects. It is probable that additional work in this important area will be published soon.

Also very little work of any nature has been reported on three-phase systems, and none on three-dimensional multiphase systems. Leverett and Lewis[29] in 1941, and Naar and Wygal[36] in 1961 have reported three-phase relative permeability data. Presumably further three-phase studies are under way. It is the author's personal knowledge that at least one production research organization is actively working on numerical techniques for handling three-dimensional two-phase flow systems.

Prior to and during the early 1950's digital computing facilities and techniques had not been developed sufficiently to allow numerical solution of multiphase flow problems. Consequently solution to a number of problems was sought through experimental studies on scaled laboratory models of reservoir systems. The theoretical background for this work was

supplied by Rapoport and Leas[44] and later Rapoport[42]. Combining the three-dimensional partial differential equations describing immiscible, incompressible two-phase flow systems to obtain a single equation, they proceeded by dimensional analysis to formulate a set of scaling requirements. These requirements, or scaling laws state the relationships between field and model properties which must be satisfied in order that the same phase saturation distribution exists at corresponding times in both systems. A portion of this thesis is devoted to an evaluation of these scaling laws.

The objective of experimental work is to collect physical data on a system for the purpose of confirming or rejecting existing mathematical description of the system. In the latter case the data normally lead to further understanding of the system, which, in turn, is transformed into an improved mathematical description of the system.

Single phase flow systems can be described adequately by experimental measurement of the pressure distribution existing within the porous medium. Description of two-or three- phase systems is considerably more difficult. Because of capillary pressure effects, the separate phases exist at different pressures at any given point within the porous medium. Hence pressure measurements must be made on each phase separately. This is done through the use of special devices permeable only to the phase in question. Due to the difficulty in making the measurements, they are seldom attempted except in experiments where relative permeability relationships are the objective.

A considerable number of two-phase displacements mostly on oil-water systems have been reported in terms of production history before and after breakthrough of the injected phase. A typical example is that reported by Rapoport, et al.[43] Although data of this type give an adequate integral description of the system, they give little information about the phase distributions existing within the porous medium during the displacement.

To obtain comprehensive description of a multiphase flow system, measurement of local phase saturation during displacement is required. In two-phase systems, saturation measurements have been made by a number of techniques. Certainly the most obvious and direct method of measurement, especially in one-dimensional unconsolidated media, is physical sampling. This method was employed by Leverett, et al.,[30] and Gorring[18] by running parallel displacements in several identical cores and sampling each at a specific time. Some work has been reported in which a radioactive tracer has been introduced into one phase.[11,23] Research with which this author is acquainted, presently being carried out by Briggs[5] employs this method to study one-dimensional "gravity counterflow segregation." Several interesting publications have described the use of fluids and media with matched refractive indices.[19,14] The latter two methods find application in studies of miscible as well as immiscible systems. Measurements of electrical resistivity have been used in a number of investigations[1,31,50] Other methods employ magnetic susceptibility[58], and x-ray transmission[4,27]. These methods and the one to be developed here, which employs the transmission

of visible light, all have advantages and disadvantages. Consideration of the geometry, fluid properties, and method of operation of the system must be made in choosing a suitable technique for phase saturation measurements.

III. SCOPE OF THIS RESEARCH

This study deals with the flow of two immiscible, incompressible fluids in a two-dimensional porous medium. Its purpose is basically twofold.

1. Experimental data are to be taken to allow a critical evaluation of the accuracy that can be expected from numerical solution of the partial differential equations taken to describe the system.

2. The same numerical techniques are to be employed in the study of several systems, including applications on the reservoir scale.

The most significant work to have appeared in this area is that by Douglas, Peaceman, and Rachford[16]. The major purpose of their paper was to present a numerical method for solution of the two-dimensional differential equations describing the flow of two immiscible, incompressible phases. For the sake of completeness solutions were carried out for two laboratory displacements performed by Rapoport, et al.[43], and Richardson and Perkins[45].

The first of the two experimental displacements was done in a homogeneous glass bead pack 32 x 16 x 2 inches. It was horizontally oriented with injection and production occurring through 19 wells to give a repeating five-spot pattern. Prior to operation the bead pack was treated to render it oil-wet and filled with oil. During operation water was injected and an oil recovery curve was generated. The numercial simulation of this displacement showed good agreement with experimental data, particularly up to the occurrence of water breakthrough.

The second displacement was done in a two-layered glass bead pack 6 feet by 6 inches by 3/8 inch thick. The layers had permeabilities of 21 and 3 Darcys. Each layer was 3 inches wide and ran the entire length of the model. The model was oriented in a horizontal plane. The oil-wet pack was filled with dyed oil prior to operation, and water was injected along one end with production occurring along the other end. Again good agreement was obtained between computed and observed oil recovery curves up to water breakthrough, with poor agreement after breakthrough. A computed saturation distribution was included for purposes of qualitative comparison to a photograph taken by reflected light.

The good agreement obtained on the integral basis of oil recovery up to water breakthrough is not of particular significance. Indeed, it is a necessary requirement, but certainly not a sufficient one to guarantee the validity of the numerical solution. In fact, it is automatic due to material balance considerations. Accurate prediction of breakthrough time is governed by the value used for residual oil saturation. Likewise, qualitatively good comparison on the basis of a photograph does not supply conclusive evidence of the validity of the solution.

Of more significance is the good agreement in oil recovery following breakthrough obtained in the case of the five-spot waterflood. The author does not wish to take issue with the poor agreement obtained after breakthrough for the second displacement. No doubt this could be attributed to failure in describing the wells accurately and to packing considerations which were not as important in the case of the homogeneous five-spot.

Absolutely conclusive evidence as to the validity of the solution could be obtained only through experimental measurement of the time-space distributions of two dependent variables such as water saturation and water potential. Two variables would be required because the system is described by two simultaneous differential equations. The use of any two variables among oil potential, water potential and water saturation is legitimate.

In practice, agreement between computed and experimental distributions of one variable, such as water saturation would be considered sufficient to substantiate the validity of the numerical solution. Obviously these data would provide a much more critical test than recovery data.

In the present investigation, two-dimensional water saturation distributions are to be measured experimentally during several gas-water displacements. The data will be compared to the computed saturation distributions at several stations in time for each displacement. The basic numerical methods of Douglas, Peaceman, and Rachford will be used. The gas phase will be considered to behave as an incompressible fluid. This is reasonable for low flow rates because of the resulting low pressure (or potential) gradients in the gas phase.

To the author's knowledge, no two-dimensional experimental work has been reported in which phase saturation (or potential) distributions have been measured. Likewise, the experimental technique of water saturation measurement by means of the attenuation in intensity of transmitted light is thought to be novel. Details of the experimental methods are taken up in a later section.

The Douglas, Peaceman and Rachford work was done within the framework of a two-dimensional cartesian coordinate system. Such a system has applicability in many problems. It may be oriented in a vertical, horizontal or inclined plane. However, a number of problems can be described better in a two-dimensional cylindrical (radius and height) coordinate system. In this work, the difference equations will be formulated and treated in both types of coordinate systems.

In addition to simulation of the laboratory displacements, other applications of the numerical techniques fall into two categories.

1. An evaluation of the scaling laws derived for the flow of two immiscible incompressible phases will be made. This will be accomplished on the basis of numerical solutions for a hypothetical reservoir and several versions of a scaled laboratory model of the reservoir.

2. An analysis will be made to determine the effect of water injection on the phase distribution existing within a gas storage reservoir. Solutions will be generated for several rates of water injection through a well located at the spillpoint of the hypothetical reservoir.

The scaling laws formulated by Rapoport[42] set forth the scaling considerations required in order for the performance of a laboratory model to be homologous to that of the reservoir prototype. The laws were deduced by performing dimensional analysis on the partial differential equation describing phase saturation distribution in a porous medium subject to the simultaneous flow of two immiscible incompressible phases.

Rapoport's treatment was based on the premise of having identical relative permeability curves, linearly related capillary pressure curves

and identical boundary conditions in the field and laboratory systems. These three requirements are not easily satisfied in practice.

Normally field media will be consolidated, while laboratory media will be unconsolidated due to practical considerations. Comparison of relative permeability curves representative of consolidated and unconsolidated media shows the curves to be considerably different. Also further differences can arise where an oil-water system is used to simulate behavior of a gas-water system (see Figures 39a and 39b).

Capillary pressure curves always exhibit the familiar "J" shape. Hence it is usually possible to superpose one curve upon another to a fair approximation by linear transformation. Agreement will be closest in the mid range of phase saturation, and normally poorest near residual phase saturations. This is because of the differences usually existing between connate water and residual gas (or oil) saturations for consolidated and unconsolidated media (see Figure 38b).

Generally it will be impossible to duplicate boundary conditions associated with the reservoir on the laboratory scale. The geographical extent of a field medium is usually very large, and is often considered to be infinite. Practical considerations limit the size of the laboratory model. Consequently, a discontinuity in the porous medium non-existent in the prototype often occurs at the boundaries of the laboratory model. Symmetry conditions such as those present in a repeating five-spot pattern sometimes render this consideration unimportant. Accurate well scaling, however, can seldom be accomplished since a well in the prototype will scale down to microscopic dimensions for the laboratory model.

In view of these considerations, it is apparent that even the most carefully designed and constructed laboratory model probably will violate the scaling laws in some respects. The objective of this portion of the work will be to determine how closely laboratory behavior can be expected to conform to field performance when the requirements related to relative permeability and capillary pressure curves and the boundary conditions are met only approximately.

The analysis performed by Rapoport was done in three-dimensional cartesian coordinates. Since this work is concerned with two-dimensional systems, appropriate revision of the scaling laws will be made.

Natural gas storage operations are often carried out in dome-shaped formations such as illustrated in Figure 1 of the Introduction. The presence of a saddle in the formation will effectively limit the storage capacity of the formation. After a critical amount of gas has been injected, the saddle will serve as a spillpoint, and leakage will result upon further injection. The use of water injection at the spill-point has been considered as a possible means for increasing the capacity of a reservoir of this geometry[26]. The same principle logically might be extended to allow storage in a horizontal aquifer by injecting water through a series of wells completed on a circle centrally enclosing the gas injection well.

Gas containment by water injection will be investigated by carrying out solutions for a hypothetical reservoir described in an inclined two-dimensional cartesian coordinate system.

IV. MATHEMATICAL ANALYSIS

The mathematical bases for this work are developed in the following sequence:

A. Derivation of the partial differential equations describing the flow of two immiscible, incompressible phases in porous media.

B. Combination of the differential equations to yield a single equation for purposes of deducing the scaling laws.

C. Reduction of the differential equations to two-dimensional difference equations in cartesian and domal coordinates.

D. Enumeration of the numerical method of solution including treatment of boundary conditions.

For the sake of compactness, vector notation, as set forth by Kaplan[24], will be used whenever convenient. The basic differential equations will appear in three-dimensional cartesian coordinates with subsequent reduction to the specific two-dimensional systems to be employed here.

A. Basic Differential Equations

Derivation of the equations for incompressible, immiscible fluids, has been presented by many authors including Douglas, Peaceman, and Rachford[16]. For the sake of generality, the equations will be

developed here for immiscible but compressible fluids with later simplification to the incompressible case. Isothermal conditions will be assumed to prevail in the porous medium.

Darcy's law for compressible fluids, as expressed in Equations (6) and (7), is written for wetting and non-wetting phases:

$$\bar{v}_w = -K \frac{k_w}{\mu_w} \rho_w \nabla \phi_w \tag{8a}$$

$$\bar{v}_n = -K \frac{k_n}{\mu_n} \rho_n \nabla \phi_n \tag{8b}$$

$$\phi_w = gh + \int \frac{dp_w}{\rho_w} \tag{9a}$$

$$\phi_n = gh + \int \frac{dp_n}{\rho_n} \tag{9b}$$

Limits are not specified for the integrals since each potential may be referred to arbitrary base.

For a compressible fluid equations of state are required to relate density and viscosity to pressure. In the case of a non-isothermal system, temperature will appear in the equations of state.

$$\rho_w = \rho_w (p_w) \tag{10a}$$

$$\rho_n = \rho_n (p_n) \tag{10b}$$

$$\mu_w = \mu_w (p_w) \tag{10c}$$

$$\mu_n = \mu_n (p_n) \tag{10d}$$

From Equations (10a) and (10b) the potentials defined by Equations (9a) and (9b) are seen to be functions of pressure and height.

The continuity or material balance equations for compressible fluids in porous media are:

$$\nabla\cdot(\rho_w \bar{v}_w) = -f\,\partial(\rho_w S_w)/\partial t \tag{11a}$$

$$\nabla\cdot(\rho_n \bar{v}_n) = -f\,\partial(\rho_n S_n)/\partial t \tag{11b}$$

Phase saturations are defined such that

$$S_w + S_n = 1 \tag{12}$$

Combination of Darcy's law and the continuity equations results in:

$$\nabla\cdot\left(K\frac{k_w}{\mu_w}\rho_w^2\nabla\phi_w\right) = +f\,\partial(\rho_w S_w)/\partial t \tag{13a}$$

$$\nabla\cdot\left(K\frac{k_n}{\mu_n}\rho_n^2\nabla\phi_n\right) = +f\,\partial(\rho_n S_n)/\partial t \tag{13b}$$

The capillary pressure concept relates pressures in the separate phases.

$$p_n - p_w = p_c(S_w) \tag{14}$$

Use of the non-wetting phase saturation would be equivalent because of Equation (12).

Without assuming a specific functional form for the equations of state, no simplification arises from further substitution. Hence the system is described by the simultaneous, nonlinear, second-order partial differential equations (13a) and (13b), in combination with the defining equations (9a), (9b), (10a), (10b), (10c), (10d), (12) and (14). The

most logical choice of dependent variable is φ_w and φ_n. However, one of these could be replaced by Sw or Sn.

Considerable simplification results for incompressible fluids. In this case it is convenient to define potentials according to Equation (5).

$$\Phi_w = \rho_w g h + p_w \tag{15a}$$

$$\Phi_n = \rho_n g h + p_n \tag{15b}$$

Darcy's law takes the form:

$$\bar{v}_w = -K \frac{k_{rw}}{\mu_w} \nabla \Phi_w \tag{16a}$$

$$v_n = -K \frac{k_{rn}}{\mu_n} \nabla \Phi_n \tag{16b}$$

The continuity equations reduce for each phase to:

$$\nabla \cdot \bar{v}_w = -f \frac{\partial S_w}{\partial t} \tag{17a}$$

$$\nabla \cdot \bar{v}_n = -f \frac{\partial S_n}{\partial t} = +f \frac{\partial S_w}{\partial t} \tag{17b}$$

and overall to:

$$\nabla \cdot (\bar{v}_w + \bar{v}_n) = 0 \tag{17c}$$

From the capillary pressure relationship it follows that:

$$\frac{\partial S_w}{\partial t} = \left(\frac{dS_w}{dp_c}\right) \frac{\partial p_c}{\partial t} \tag{18a}$$

$$= S_w' \frac{\partial \{\Phi_n - \Phi_w + (\rho_w - \rho_n) g h\}}{\partial t} \tag{18b}$$

$$= S_w' \frac{\partial (\Phi_n - \Phi_w)}{\partial t} \tag{18c}$$

Substitution of Darcy's law, Equations (16a) and (16b), into the continuity equations, Equations (17a) and (17b), and using Equation (18c), there results:

$$\nabla\cdot\left(K\frac{k_w}{\mu_w}\nabla\Phi_w\right) = +f\,S_w'\frac{\partial(\Phi_n-\Phi_w)}{\partial t} \tag{19a}$$

$$\nabla\cdot\left(K\frac{k_n}{\mu_n}\nabla\Phi_n\right) = -f\,S_w'\frac{\partial(\Phi_n-\Phi_w)}{\partial t} \tag{19b}$$

Equations (19a) and (19b) are the equations describing the flow of two immiscible, incompressible phases. Again, the result is a system of simultaneous non-linear, second order partial differential equations. The non-linearity is introduced through the functional dependence on wetting phase saturation, S_w of relative permeabilities, k_n and k_w and the reciprocal slope of the capillary curve, S_w'. Wetting phase saturation is in turn dependent on the differences between wetting and non-wetting phase potentials, Φ_w and Φ_n through the inverse of Equation (14).

Complete description of the flow system requires statements of the appropriate boundary conditions. These are more conveniently treated in the sub-section dealing with the numerical solution, and discussion will be deferred until then.

B. Phase Saturation Distribution Equation and Dimensional Analysis

For purposes of dimensional analysis, it is convenient to combine Equations (14), (16a), (16b), (17a) and (17c) to obtain a single equation. This has been done by Rapoport[42] and also by Gorring[18], who presents the necessary manipulations in considerable detail. The resulting equation is based on the assumptions of immiscibility and incompressibility.

$$f\frac{\partial S_w}{\partial t} + \frac{d\psi_1}{dS_w}\bar{v}_t\cdot(\nabla S_w) - \frac{K}{\mu_n}\nabla\cdot\left(\psi_2\frac{dp_c}{dS_w}\nabla S_w\right)$$

$$-\frac{K}{\mu_n}g\Delta\rho\frac{d\psi_2}{dS_w}(\nabla h)\cdot(\nabla S_w) = 0 \qquad (20)$$

with the functional definitions:

$$\psi_1 = \frac{k_w/\mu_n}{k_w/\mu_n + k_n/\mu_w} \qquad (21a)$$

$$\psi_2 = k_n\psi_1 \qquad (21b)$$

and

$$\Delta\rho = \rho_w - \rho_n \qquad (22)$$

Equation (20) is written in a general three-dimensional cartesian coordinate system in which the x-y plane may be inclined from the horizontal. As a result, the elevation, h is constant for any horizontal plane in the system. This has little advantage over normal (horizontal-vertical) orientation in three dimensions, but it makes the treatment in inclined two-dimensional geometry more straightforward. In normally oriented three-dimensional geometry, h is identical to the vertical coordinate z.

Dimensional analysis is accomplished by defining the following scale ratios where unprimed and primed variables are associated with the reservoir and laboratory systems, respectively.

$$L/L' = x/x' = y/y' = z/z' = A \quad \text{(spatial coordinates)} \qquad (23)$$

$$Q/Q' = B \quad \text{(injection or production rates)} \qquad (24)$$

$$f/f' = C \quad \text{(porosities)} \qquad (25)$$

$$K/K' = D \quad \text{(permeabilities)} \tag{26}$$

$$\Delta\rho/\Delta\rho' = E \quad \text{(density differences)} \tag{27}$$

$$\mu_n/\mu_n' = \mu_w/\mu_w' = F \quad \text{(viscosities)} \tag{28}$$

$$(dp_c/dS_w)/(dp_c/dS_w)' = G \quad \text{(capillary pressures)} \tag{29a}$$

or equivalently

$$p_c' = G p_c + \Gamma \tag{29b}$$

Having selected the above scale ratios, velocity and time scale ratios are necessarily defined as:

$$u/u' = v/v' = w/w' = (Q/L^2)/(Q/L^2)' = B/A^2 \tag{30}$$

$$t/t' = (L^3 f/Q)/(L^3 f/Q)' = A^3 C/B \tag{31}$$

Taking Equation (20) to apply in the reservoir system, the same equation involving primed variables applies in the laboratory system. Substitution of Equations (23) to (31) replaces primed variables by unprimed variables. Comparison of the differential equations for the two systems shows the relationships that must exist among the scale ratios in order for the phase distributions in the two systems to be identical at corresponding times.

Rapoport's results, to be referred to henceforth as the "three-dimensional scaling laws" can be stated in the following form:

$$G = EA \tag{32}$$

$$FB = DGA \tag{33}$$

In addition, the functions ψ_1 and ψ_2 must be identical for both systems. In effect, this requirement demands that the relative permeability curves for the reservoir and laboratory systems must be the same. Because

of the similarities postulated to exist with respect to velocities in the systems by Equation (30) it is apparent that boundary conditions must be duplicated. The use of these relationships is demonstrated in the section Evaluation of Scaling Laws.

In inclined two-dimensional cartesian coordinates, some relaxation of the scaling requirements results.

With the x-axis inclined from the horizontal by the angle θ, the elevation function is:

$$h(x,y) = x \sin\theta + y \cos\theta \tag{34}$$

Upon insertion of Equation (34) into Equation (20), the differential equation describing the reservoir prototype becomes:

$$\phi \frac{\partial S_w}{\partial t} + \frac{d\psi_1}{dS_w}\left[u \frac{\partial S_w}{\partial x} + v \frac{\partial S_w}{\partial y}\right] - \frac{K}{\mu_n}\left[\frac{\partial}{\partial x}\left(\psi_2 \frac{dp_c}{dS_w} \frac{\partial S_w}{\partial x}\right) + \frac{\partial}{\partial y}\left(\psi_2 \frac{dp_c}{dS_w} \frac{\partial S_w}{\partial y}\right)\right]$$

$$- \frac{K g \Delta\rho}{\mu_n} \frac{d\psi_2}{dS_w}\left[\sin\theta \frac{\partial S_w}{\partial x} + \cos\theta \frac{\partial S_w}{\partial y}\right] = 0 \tag{35}$$

All scale ratios are defined to be the same as for the three-dimensional case (Equations 24 through 29) except the ratio of spatial coordinates, for which:

$$x/x' = y/y' = A_1 \qquad \text{(variant spatial coordinates)} \tag{36}$$

$$z/z' = A_2 \qquad \text{(invariant spatial coordinates)} \tag{37}$$

The velocity and time scale ratios are:

$$u/u' = (Q/yz)/(Q/yz)' = B/(A_1 A_2) \tag{38}$$

$$v/v' = (Q/xz)/(Q/xz)' = B/(A_1 A_2) \tag{39}$$

$$t/t' = (xyzf/Q)/(xyzf/Q) = A_1^2 A_2 C/B \tag{40}$$

Equation (35) describes the laboratory system when written in terms of primed variables.

$$f'\frac{\partial S_w}{\partial t'} + \frac{d\psi_1}{dS_w}\left[u'\frac{\partial S_w}{\partial x'} + v'\frac{\partial S_w}{\partial y'}\right] - \frac{K'}{\mu_n'}\left[\frac{\partial}{\partial x'}\left(\psi_2 \frac{dp_c'}{dS_w}\frac{\partial S_w}{\partial x'}\right)\right.$$
$$\left. + \frac{\partial}{\partial y'}\left(\psi_2 \frac{dp_c'}{dS_w}\frac{\partial S_w}{\partial y'}\right)\right] - \frac{K'g\Delta\rho'}{\mu_n'}\frac{d\psi_2}{dS_w}\left[\sin\theta\frac{\partial S_w}{\partial x'} + \cos\theta\frac{\partial S_w}{\partial y'}\right] = 0 \tag{41}$$

Substitution of the scale ratios, Equations (24) through (29), (36), (38) through (40) into Equation (41), the laboratory equation becomes:

$$f\frac{\partial S_w}{\partial t} + \frac{d\psi_1}{dS_w}\left[u\frac{\partial S_w}{\partial x} + v\frac{\partial S_w}{\partial y}\right] - \left(\frac{FB}{A_2 DG}\right)\frac{K}{\mu_n}\left[\frac{\partial}{\partial x}\left(\psi_2 \frac{dp_c}{dS_w}\frac{\partial S_w}{\partial x}\right)\right.$$
$$\left. + \frac{\partial}{\partial y}\left(\psi_2 \frac{dp_c}{dS_w}\frac{\partial S_w}{\partial y}\right)\right] - \left(\frac{FB}{A_1 A_2 DE}\right)\frac{Kg\Delta\rho}{\mu_n}\frac{d\psi_2}{dS_w}\left[\sin\theta\frac{\partial S_w}{\partial x}\right.$$
$$\left. + \cos\theta\frac{\partial S_w}{\partial y}\right] = 0 \tag{42}$$

Equation (42) describes the phase saturation distribution in the laboratory system in terms of variables associated with the reservoir system. For the saturation distributions in the two systems to be identical at corresponding or "homologous" times in the two systems, it is necessary for Equation (42) to be identical to Equation (35). Thus, the two-dimensional scaling laws are stated:

$$G = EA_1 \tag{43}$$

$$FB = DGA_2 \tag{44}$$

The additional requirements of identical boundary conditions and identical functions ψ_1 and ψ_2 remain as for the three-dimensional scaling laws.

The relaxation resulting from two-dimensional analysis is that the third or invariant dimension may be scaled independently of the variant dimensions. This is a significant practical advantage since it allows the scaled laboratory model to be built with any convenient thickness.

Dimensional analysis also shows that scaling in the x, y, and z directions of the three-dimensional system must be the same. That is, if a scale ratio R_1 is defined for the x-direction, R_2 for the y-direction and R_3 for the z-direction, the ratios R_1, R_2, and R_3 must be identical. Similarly, in two-dimensional geometry, the x-and y-directions must be scaled in the same ratio and the angle of inclination, θ, cannot be changed by scaling.

If Equation (20) is transformed into the two-dimensional domal system of coordinates, the corresponding scaling laws can be deduced from the same type of analysis.

In domal coordinates, the elevation function is defined as:

$$h(r,y) = y + \bar{y}(r) \tag{45}$$

with

$$\frac{\partial h}{\partial r} = \frac{d\bar{y}}{dr} \tag{46}$$

The function $\bar{y}(r)$ is the elevation above an arbitrary horizontal plane for any point on the dome-shaped surface for y = 0. The y-axis is vertical.

If the curvature of the surfaces corresponding to constant values of y is small, the correct differential equation corresponding to Equation (20) is closely approximated by the equation to follow. The restriction of low curvature is required in order that the radial distance from a point (r_p, y_p) to the y-axis measured on the surface $y = y_p$ is approximately the same as the distance from the point to the y-axis measured on the horizontal plane passing through (r_p, y_p).

Bearing this restriction in mind, the differential equation is:

$$f\frac{\partial S_w}{\partial t} + \frac{d\psi_1}{dS_w}\left[u\frac{\partial S_w}{\partial r} + v\frac{\partial S_w}{\partial y}\right] + \frac{K}{\mu_n}\left[\frac{1}{r}\frac{\partial}{\partial r}\left(r\psi_2\frac{dp_c}{dS_w}\frac{\partial S_w}{\partial r}\right)\right.$$

$$\left. + \frac{\partial}{\partial y}\left(\psi_2\frac{dp_c}{dS_w}\frac{\partial S_w}{\partial y}\right)\right] - \frac{Kg\Delta\rho}{\mu_n}\frac{d\psi_2}{dS_w}\left[\frac{1}{r}\frac{\partial}{\partial r}\left(r\frac{d\bar{y}}{dr}S_w\right) + \frac{\partial S_w}{\partial y}\right] = 0 \qquad (47)$$

Applying the same type of dimensional analysis illustrated for two-dimensional cartesian coordinates, the scaling laws result. All scale ratios again are defined by Equations (24) through (29) except the scale ratio for spatial coordinates, for which:

$$r/r' = y/y' = A \qquad (48)$$

Velocity and time scale ratios will occur as:

$$u/u' = v/v' = B/A^2 \qquad (49)$$

$$t/t' = A^3C/B \qquad (50)$$

Upon substitution of the scale ratios, the domal scaling laws turn out to be the same as the three-dimensional cartesian scaling laws, as might be expected. Restated they are:

$$G = EA \tag{51}$$

$$FB = DGA \tag{52}$$

The dimensional analysis also shows that the base elevation function $\bar{y}(r)$ must be scaled in the same ratio as the spatial coordinates r and y.

C. Finite Difference Equations

The flow of two incompressible immiscible fluids in porous media is described by Equations (19a) and (19b). As discussed earlier, these simultaneous partial differential equations are non-linear due to the functional dependence of the coefficients on the dependent variables. Their solution must be accomplished by numerical means since analytic methods are not available.

The finite difference representation of the differential equations and the method of solution closely follow the work of Douglas, Peaceman and Rachford[16]. The primary difference existing between their methods and those used here lies in the treatment of boundary conditions. In addition, their basic methods are extended to treat two-dimensional domal coordinates.

Discussions of finite difference forms, and stability and convergence of finite difference equations appear in standard texts on numerical analysis such as Hildebrand[20]

1. Cartesian Coordinates

Equations (19a) and (19b) restated are:

$$\nabla\cdot\left(K\frac{k_w}{\mu_w}\nabla\Phi_w\right) = +f S_w'\frac{\partial(\Phi_n-\Phi_w)}{\partial t} \tag{53a}$$

$$\nabla\cdot\left(K\frac{k_n}{\mu_n}\nabla\Phi_n\right) = -f S_w'\frac{\partial(\Phi_n-\Phi_w)}{\partial t} \tag{53b}$$

Addition and subtraction of the equations yields equations which simplify numerical treatment. The following variables are defined:

$$P = \tfrac{1}{2}\left(\Phi_n+\Phi_w\right) \tag{54a}$$

$$R = \tfrac{1}{2}\left(\Phi_n-\Phi_w\right) \tag{54b}$$

$$M = K\left(k_n/\mu_n + k_w/\mu_w\right) \tag{54c}$$

$$N = K\left(k_n/\mu_n - k_w/\mu_w\right) \tag{54d}$$

The differential equations become:

$$\nabla\cdot(M\nabla P) + \nabla\cdot(N\nabla R) = 0 \tag{55a}$$

$$\nabla\cdot(N\nabla P) + \nabla\cdot(M\nabla R) = -4f S_w'\frac{\partial R}{\partial t} \tag{55b}$$

The simplification is that Equations (55a) and (55b) may be solved separately in "leap-frog" fashion, using the alternating direction iteration procedure due to Douglas[15]. By leap-frog fashion it is meant that a time step consists of updating the P and R variables separately. This technique gives divergent results when applied to Equations (53a)

and (53b). These equations must be solved simultaneously at the expense of increased computational time.

A section of the two-dimensional cartesian grid system is shown in Figure 2. All grid elements are of the same size, Δx by Δy with thickness Δz in the invariant dimension.

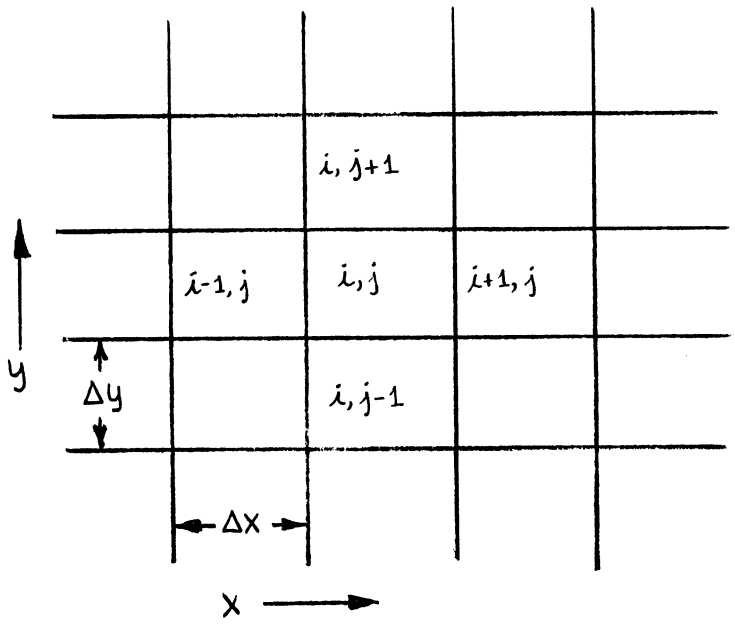

Figure 2. Interior Section of Cartesian Grid System.

Mesh points are at the centers of the blocks of the grid system with the point associated with the block i, j having coordinates:

$$x_i = x_o + i\,\Delta x \tag{56a}$$

$$y_j = y_o + j\,\Delta y \tag{56b}$$

The derivatives in Equations (55a) and (55b) are replaced by difference forms directly.

The x-component of the first term of Equation (55a) is abbreviated:

$$\frac{\partial}{\partial x}\left(M\frac{\partial P}{\partial x}\right) \cong \Delta_x\left(M\,\Delta_x P\right)_{i,j} \tag{57}$$

The difference form is:

$$\Delta_x(M\Delta_x P)_{i,j} = \frac{1}{\Delta x^2}\Big\{M_{i+1/2,j}\,P_{i+1,j} - \left(M_{i+1/2,j} + M_{i-1/2,j}\right)P_{i,j} + M_{i-1/2,j}\,P_{i-1,j}\Big\} \tag{58}$$

The subscripts i + 1/2 and i - 1/2 denote the use of "interblock" properties. Evaluation of the interblock properties is taken up later.

The difference forms for the other derivatives are analogous. For example, the y-component of the second term in Equation (55b) is:

$$\frac{\partial}{\partial y}\left(M\frac{\partial R}{\partial y}\right) \cong \Delta_y(M\Delta_y R)_{i,j} = \frac{1}{\Delta y^2}\Big\{M_{i,j+1/2}\,R_{i,j+1} - \left(M_{i,j+1/2} + M_{i,j-1/2}\right)R_{i,j} + M_{i,j-1/2}\,R_{i,j-1}\Big\} \tag{59}$$

The subscript n denotes the time variable which is conveniently defined for non-constant intervals such that:

$$t_n = t_o + \sum_{m=1}^{n}\Delta t_m \tag{60}$$

Using the difference forms indicated by Equations (58) and (59), the implicit difference equations in two-dimensional cartesian coordinates become:

$$\Delta_x(M_n\Delta_x P_{n+1})_{i,j} + \Delta_y(M_n\Delta_y P_{n+1})_{i,j} + \Delta_x(N_n\Delta_x R_n)_{i,j} + \Delta_y(N_n\Delta_y R_n)_{i,j} + \frac{(Q_n+Q_w)}{\Delta x\,\Delta y\,\Delta z}_{i,j,n+1/2} = 0 \tag{61a}$$

$$\Delta_x(N_n \Delta_x P_{n+1})_{i,j} + \Delta_y(N_n \Delta_y P_{n+1})_{i,j} + \Delta_x(M_n \Delta_x R_{n+1})_{i,j}$$

$$+ \Delta_y(M_n \Delta_y R_{n+1})_{i,j} + \frac{(Q_n - Q_w)}{\Delta x \Delta y \Delta z}_{i,j,n+1/2}$$

$$= -4 \frac{f_{i,j}}{\Delta t_{n+1}} S'_{w_{i,j,n+1/2}} (R_{i,j,n+1} - R_{i,j,n}) \qquad (61b)$$

The Q terms have been introduced to account for any external injection or production of either or both phases associated with the block i,j. Positive Q terms denote injection. Normally, operation will be such that injection or production occurs only for a small number of blocks on a boundary.

Reference to the difference equations illustrates the meaning of leap-frog fashion. The P variable is updated to the advanced time t_{n+1} using values of R at t_n through Equation (61a). Then the R variable is updated through solution of Equation (61b). P and R together fix the new phase saturation distribution. The coefficients M and N are evaluated from S_w at the time level t_n. The coefficient S'_w is evaluated at the half interval time $t_{n+\frac{1}{2}}$. This is done iteratively by averaging values at t_n and t_{n+1}. The method of evaluation will be taken up later. Although computations would increase considerably, it is possible to evaluate coefficients M and N at the more representative half interval time level.

The numerical techniques for solving Equations (61a) and (61b) are presented later.

2. Domal Coordinates

With the restrictions of low curvature discussed previously, Equations (55a) and (55b) become:

$$\frac{1}{r}\frac{\partial}{\partial r}\left(rM\frac{\partial P}{\partial r}\right)+\frac{\partial}{\partial y}\left(M\frac{\partial P}{\partial y}\right)+\frac{1}{r}\frac{\partial}{\partial r}\left(rN\frac{\partial R}{\partial r}\right)+\frac{\partial}{\partial y}\left(N\frac{\partial R}{\partial y}\right)=0 \qquad (62a)$$

$$\frac{1}{r}\frac{\partial}{\partial r}\left(rN\frac{\partial P}{\partial r}\right)+\frac{\partial}{\partial y}\left(N\frac{\partial P}{\partial y}\right)+\frac{1}{r}\frac{\partial}{\partial r}\left(rM\frac{\partial R}{\partial r}\right)+\frac{\partial}{\partial y}\left(M\frac{\partial R}{\partial y}\right)=-4fS'_{w}\frac{\partial R}{\partial t} \qquad (62b)$$

The variables P, R, M and N are again defined by Equations (54a) through (54d).

A three-dimensional sketch of a section of the domal grid system is shown in Figure 3.

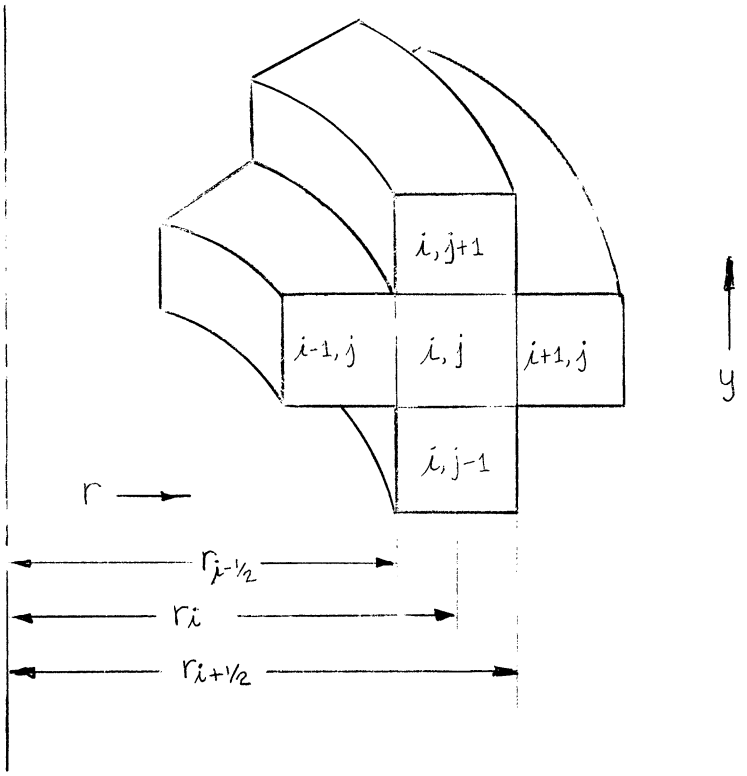

Figure 3. Interior Section of Domal Grid System.

Once again equal grid spacing is used in the y-direction such that:

$$y_j = y_o(r_i) + j\Delta y \qquad (63)$$

The elevation function $y_o(r_i)$ is equivalent to $\bar{y}(r)$ appearing in Equation (45).

In the r-direction logarithmic spacing is desirable. This follows from integration of Darcy's law as does the choice of inter-block radii which will be recognized as the log-mean between the radii of the adjacent grid elements.

$$r_i = r_1 e^{(i-1)\Delta x} \tag{64a}$$

$$r_{i+1/2} = r_i \left(\frac{e^{\Delta x} - 1}{\Delta x}\right) = r_1 e^{(i-1)\Delta x} \left(\frac{e^{\Delta x} - 1}{\Delta x}\right) \tag{64b}$$

Specification of r_1, the interior radius, r_m the exterior radius and the number of radial increments of the grid system, i_m fixes the logarithmic increment size Δx as:

$$\Delta x = \frac{1}{i_m - 1} \log r_m/r_1 \tag{64c}$$

Using this grid system, difference equations may be obtained from Equations (62a) and (62b). However, more accurate difference equations will result if they are derived directly from a material balance around the finite ring shaped element of the grid system. The reason the two difference equations are not the same is that the volume of the differential ring used in derivation of the differential equation is $2\pi r dr dy$, while the correct volume of the finite grid element is $\pi \Delta y (r^2_{i+\frac{1}{2}} - r^2_{i-\frac{1}{2}})$. These expressions are identical only in the limit as Δr approaches zero.

For purposes of derivation, it is more straightforward to work with each phase separately and obtain equations in Φ_w and Φ_n. Addition

and subtraction of the resulting equations yields equations in P and R analogous to Equations (62a) and (62b).

Stated in words, the material balance is:

$$\text{IN} - \text{OUT} + \text{INJECTION} = \text{ACCUMULATION} \tag{65}$$

For the wetting phase, material balance around the grid element i,j is:

$$\text{IN} = \frac{2\pi\Delta y}{\mu_w}(Kr\,k_w)_{i-1/2,j}\left\{\frac{\Phi_{wi-1,j}-\Phi_{wi,j}}{r_i - r_{i-1}}\right\} + \frac{\pi}{\mu_w}(K\,k_w)_{i,j-1/2}\left(r_{i+1/2}^2 - r_{i-1/2}^2\right)\left\{\frac{\Phi_{wi,j-1}-\Phi_{wi,j}}{\Delta y}\right\} \tag{66a}$$

$$\text{OUT} = \frac{2\pi\Delta y}{\mu_w}(Kr\,k_w)_{i+1/2,j}\left\{\frac{\Phi_{wi,j}-\Phi_{wi+1,j}}{r_{i+1} - r_i}\right\} + \frac{\pi}{\mu_w}(K\,k_w)_{i,j+1/2}\left(r_{i+1/2}^2 - r_{i-1/2}^2\right)\left\{\frac{\Phi_{wi,j}-\Phi_{wi,j+1}}{\Delta y}\right\} \tag{66b}$$

$$\text{INJECTION} = Q_{wi,j,n+1/2} \tag{66c}$$

$$\text{ACCUMULATION} = f_{i,j}\,\pi\Delta y\left(r_{i+1/2}^2 - r_{i-1/2}^2\right)\left\{\frac{S_{wi,j,n+1} - S_{wi,j,n}}{\Delta t_{n+1}}\right\} \tag{66d}$$

The time index has been omitted in Equations (64a) and (64b) to eliminate undue confusion. In the technique of solution to be employed, relative permeabilities bear the subscript n. Since the difference equations will be written in the P and R forms for solution by the leap-frog technique, wetting phase potentials will appear both at time levels n and n+1.

The difference equation analogous to Equation (19a) for cartesian coordinates results upon substitution of Equations (66a) through (66d) into Equation (65) followed by use of the relationship exhibited by Equation (18c).

The material balance for the non-wetting phase is accomplished in the same manner. Addition and subtraction of the two difference equations again yield the P and R form.

Use of the following definitions condenses the final result.

$$\alpha_i = 2\Delta x \Big/ \left\{ r_1^2 e^{2(i-1)\Delta x} \left[1 - e^{-2\Delta x}\right] \left[e^{\Delta x} - 1\right]^2 \right\} \tag{67}$$

$$\beta_i = \left(\frac{\Delta x}{2\pi \Delta y}\right) \alpha_i \tag{68}$$

The difference operators denote:

$$\bar{\Delta}_r (M \bar{\Delta}_r P)_{i,j} = M_{i+1/2,j} P_{i+1,j} - (M_{i+1/2,j} + M_{i-1/2,j}) P_{i,j} + M_{i-1/2,j} P_{i-1,j} \tag{69}$$

$$\bar{\Delta}_y (M \bar{\Delta}_y P)_{i,j} = M_{i,j+1/2} P_{i,j+1} - (M_{i,j+1/2} + M_{i,j-1/2}) P_{i,j} + M_{i,j-1/2} P_{i,j-1} \tag{70}$$

Using these definitions, the difference equations reduce to:

$$\alpha_i \left\{ \bar{\Delta}_r (M_n \bar{\Delta}_r P_{n+1}) + \bar{\Delta}_r (N_n \bar{\Delta}_r R_n) \right\}_{i,j} + \frac{1}{\Delta y^2} \left\{ \bar{\Delta}_y (M_n \bar{\Delta}_y P_{n+1}) + \bar{\Delta}_y (N_n \bar{\Delta}_y R_n) \right\}_{i,j} + \beta_i (Q_n + Q_w)_{i,j,n+1/2} = 0 \tag{71a}$$

$$\alpha_i \left\{ \bar{\Delta}_r (N_n \bar{\Delta}_r P_{n+1}) + \bar{\Delta}_r (M_n \bar{\Delta}_r R_{n+1}) \right\}_{i,j} + \frac{1}{\Delta y^2} \left\{ \bar{\Delta}_y (N_n \bar{\Delta}_y P_{n+1}) + \bar{\Delta}_y (M_n \bar{\Delta}_y R_{n+1}) \right\}_{i,j} + \beta_i (Q_n - Q_w)_{i,j,n+1/2} = -\phi_{i,j} S'_{w i,j,n+1/2} \left\{ \frac{R_{i,j,n+1} - R_{i,j,n}}{\Delta t_{n+1}} \right\} \tag{71b}$$

The numerical techniques for solution of Equations (71a) and (71b) are presented in the following sub-section.

D. Numerical Solution of Difference Equations

The difference equations written in two-dimensional cartesian geometry, Equations (61a) and (61b) and those in two-dimensional domal geometry, Equations (71a) and (71b) are of very similar form. Other than differences in constant multiplying factors, the only significant difference arises in the boundary condition at the inner radius of the latter system. For the sake of compactness, the systems will be treated individually only when necessary.

The alternating directional procedure was developed specifically for treatment of parabolic equations. It has turned out to provide an efficient means of solving elliptic equations as well. The R difference equations (61b) and (71b) are classed as parabolic while the P equations (61a) and (71a) are elliptic. The obvious distinction is the appearance of the time derivative in the R equations.

Although treatment of the R equations is simpler conceptually, the treatment of the P equations will be presented first since they are solved before the R equations within a time step.

Solution of the elliptic equations involves the insertion of an artificial time derivative on the right side to obtain the form of a parabolic equation. Since the two simultaneous equations (P and R) are solved separately by the leap-frog technique, the P equation may be thought of as a steady state equation. The physical interpretation of the artificial time derivative is that the steady state solution is

approached as artificial time advances. Thus it is seen that successive iteration continually advances the solution by a series of pseudo time steps until the solution has approached a steady or stabilized state within a prescribed tolerance.

The alternating direction procedure consists of splitting a time step (actual or artificial) into two equally sized half-steps. During the first half-step, the difference equations are written implicitly in the x-(or r-) direction and explicitly in the y-direction. The procedure is reversed during the second half-step with equations being implicit in the y-direction and explicit in the x- (or r-) direction.

In the P equations only the P terms bear time subscripts n+1 associated with the advanced time level. All other terms bear time subscripts n associated with the earlier time level at which all variables were known. It is convenient to lump all of these terms into a single constant.

For the cartesian case:

$$G_{i,j,n} = -\Delta_x(N_n \Delta_x R_n)_{i,j} - \Delta_y(N_n \Delta_y R_n)_{i,j} - \frac{(Q_n + Q_w)_{i,j,n+1/2}}{\Delta x \Delta y \Delta z} \qquad (72a)$$

For the domal case:

$$G_{i,j,n} = -\alpha_i \bar{\Delta}_r(N_n \bar{\Delta}_r R_n)_{i,j} - \frac{1}{\Delta y^2}\bar{\Delta}_y(N_n \bar{\Delta}_y R_n)_{i,j} - \beta_i(Q_n + Q_w)_{i,j,n+1/2} \qquad (72b)$$

The terms on the right side of Equations (72a) and (72b) are defined according to the conventions adopted in Equations (58, (59), (67), (68), (69) and (70).

The coefficients on the P terms in Equations (61a) and (71a) are also constant within a time step. The following terms are defined:

Cartesian:

$$a_{i+1,j,n} = \frac{1}{\Delta x^2} M_{i+1/2,j,n} \tag{73a}$$

$$b_{i,j,n} = -\frac{1}{\Delta x^2}\left(M_{i+1/2,j,n} + M_{i-1/2,j,n}\right) \tag{73b}$$

$$c_{i-1,j,n} = \frac{1}{\Delta x^2} M_{i-1/2,j,n} \tag{73c}$$

$$d_{i,j+1,n} = \frac{1}{\Delta y^2} M_{i,j+1/2,n} \tag{73d}$$

$$e_{i,j,n} = -\frac{1}{\Delta y^2}\left(M_{i,j+1/2,n} + M_{i,j-1/2,n}\right) \tag{73e}$$

$$g_{i,j-1,n} = \frac{1}{\Delta y^2} M_{i,j-1/2,n} \tag{73f}$$

Domal:

$$a_{i+1,j,n} = \alpha_i M_{i+1/2,j,n} \tag{74a}$$

$$b_{i,j,n} = -\alpha_i\left(M_{i+1/2,j,n} + M_{i-1/2,j,n}\right) \tag{74b}$$

$$c_{i-1,j,n} = \alpha_i M_{i-1/2,j,n} \tag{74c}$$

$$d_{i,j+1,n} = \frac{1}{\Delta y^2} M_{i,j+1/2,n} \tag{74d}$$

$$e_{i,j,n} = -\frac{1}{\Delta y^2}\left(M_{i,j+1/2,n} + M_{i,j-1/2,n}\right) \tag{74e}$$

$$g_{i,j-1,n} = \frac{1}{\Delta y^2} M_{i,j-1/2,n} \tag{74f}$$

Using the above definitions, the difference form of the P equation in both systems of coordinates becomes:

$$a_{i+1,j,n}\,P_{i+1,j,n+1} + b_{i,j,n}\,P_{i,j,n+1} + c_{i-1,j,n}\,P_{i-1,j,n+1} + d_{i,j+1,n}\,P_{i,j+1,n+1} + e_{i,j,n}\,P_{i,j,n+1} + g_{i,j-1,n}\,P_{i,j-1,n+1} - G_{i,j,n} = 0 \tag{75}$$

Since all terms bear an n time subscript except for P terms, all of which bear n+1 time subscripts, time subscription will be omitted in further manipulations of Equation (75). The superscript k will be used to denote iteration number or equivalently, the level of the artificial time variable t_k. The following difference form will be associated with the artificial time derivative.

$$\frac{\partial P}{\partial t_k} \cong \frac{P_{i,j}^{k+1} - P_{i,j}^{k}}{\Delta t_k} \tag{76}$$

In the alternating direction method time advances by half steps alternately in the x* and y directions. To denote this the following convention is adopted:

$$\frac{P_{i,j}^{k+1/2} - P_{i,j}^{k}}{\frac{1}{2}\Delta t_k} = \mathcal{H}^{(k+1)}\left(P_{i,j}^{k+1/2} - P_{i,j}^{k}\right) \tag{77a}$$

$$\frac{P_{i,j}^{k+1} - P_{i,j}^{k+1/2}}{\frac{1}{2}\Delta t_k} = \mathcal{H}^{(k+1)}\left(P_{i,j}^{k+1} - P_{i,j}^{k+1/2}\right) \tag{77b}$$

For the x-direction, Equation (75) becomes:

$$a_{i+1,j}\,P_{i+1,j}^{k+1/2} + b_{i,j}\,P_{i,j}^{k+1/2} + c_{i-1,j}\,P_{i-1,j}^{k+1/2} + d_{i,j+1}\,P_{i,j+1}^{k} + e_{i,j}\,P_{i,j}^{k} + g_{i,j-1}\,P_{i,j-1}^{k} = \mathcal{H}^{(k+1)}\left(P_{i,j}^{k+1/2} - P_{i,j}^{k}\right) + G_{i,j} \tag{78}$$

*For simplicity this direction will be referred to as the x-direction though the r-direction is actually meant in the domal system of coordinates.

For solution in the x-direction advancing P from the k to k + $\frac{1}{2}$ level, only the P terms superscripted k + $\frac{1}{2}$ are unknown.

Defining

$$C_{x_{i,j}}^{K} = G_{i,j} - \mathcal{H}^{(K+1)} P_{i,j}^{K} - d_{i,j+1} P_{i,j+1}^{K} - e_{i,j} P_{i,j}^{K} - g_{i,j-1} P_{i,j-1}^{K} \quad (79)$$

Equation (78) becomes:

$$a_{i+1,j} P_{i+1,j}^{K+1/2} + (b_{i,j} - \mathcal{H}^{(K+1)}) P_{i,j}^{K+1/2} + c_{i-1,j} P_{i-1,j}^{K+1/2} = C_{x_{i,j}}^{K} \quad (80)$$

Along a row (constant j) a series of simultaneous linear equations of this form specifies the values $P_{1,j} \ldots P_{i_m,j}$ where the x-index $\underline{i}$ runs from 1 to i_m. Solution proceeds row by row until the entire P matrix is advanced to the k + $\frac{1}{2}$ level.

In the y-direction, Equation (75) becomes:

$$a_{i+1,j} P_{i+1,j}^{K+1/2} + b_{i,j} P_{i,j}^{K+1/2} + c_{i-1,j} P_{i-1,j}^{K+1/2} + d_{i,j+1} P_{i,j+1}^{K+1} + e_{i,j} P_{i,j}^{K+1} + g_{i,j-1} P_{i,j-1}^{K+1} = \mathcal{H}^{(K+1)} (P_{i,j}^{K+1} - P_{i,j}^{K+1/2}) + G_{i,j} \quad (81)$$

Defining

$$C_{y_{i,j}}^{K+1/2} = G_{i,j} - \mathcal{H}^{(K+1)} P_{i,j}^{K+1/2} - a_{i+1,j} P_{i+1,j}^{K+1/2} - b_{i,j} P_{i,j}^{K+1/2} - c_{i-1,j} P_{i-1,j}^{K+1/2} \quad (82)$$

Equation (81) reduces to:

$$d_{i,j+1} P_{i,j+1}^{K+1} + (e_{i,j} - \mathcal{H}^{(K+1)}) P_{i,j}^{K+1} + g_{i,j-1} P_{i,j-1} = C_{y_{i,j}}^{K+1/2} \quad (83)$$

Similarly, the P matrix is advanced to the k+1 level by column-wise solution of the simultaneous equations represented by Equation (83). The y-direction index is taken to run from 1 to j_m.

The row-wise and column-wise solutions employed in the alternating direction method are illustrated by Figures 4a and 4b.

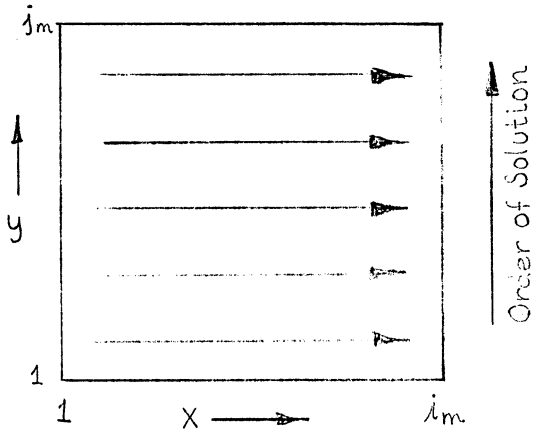

Figure 4a. x-Direction Solution.

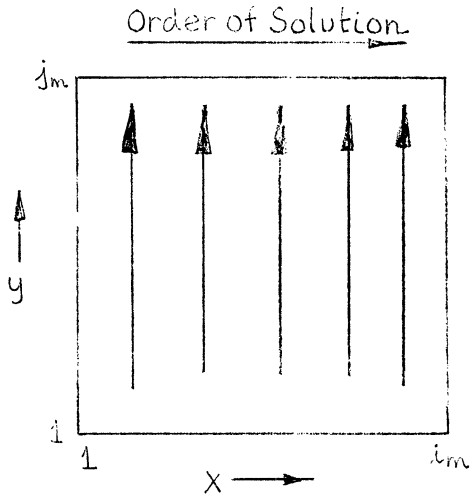

Figure 4b. y-Direction Solution.

Values of the iteration parameter are determined by performing a stability analysis. This has been done in Appendix I for both coordinate systems. Most rapid convergence of the P equation is obtained by employing a series of iteration parameters in a cyclic manner. In most calculations done here, seven iteration parameters were used per cycle. That is, H_1 was used on iterations 1, 8, 15, ... with H_2 on iterations 2, 9, 16, ... up to H_7 for iterations 7, 14, 21, ...

From stability considerations, the preferred minimum and maximum values (corresponding to H_1 and H_7) were found to be:

Cartesian:

$$HK_{min} = \min \left\{ \begin{array}{l} \frac{1}{2\Delta x^2}\left[\pi^2/(2i_m^2)\right] \\ \frac{1}{2\Delta y^2}\left[\pi^2/(2j_m^2)\right] \end{array} \right\} \tag{84a}$$

$$HK_{max} = \max \left\{ \begin{array}{l} \frac{1}{2\Delta x^2}\left[2 - \pi^2/(2i_m^2)\right] \\ \frac{1}{2\Delta y^2}\left[2 - \pi^2/(2j_m^2)\right] \end{array} \right\} \tag{84b}$$

Domal:

$$HK_{min} = \min \left\{ \begin{array}{l} \frac{\alpha_{im}}{2}\left[\pi^2/(2i_m^2)\right] \\ \frac{1}{2\Delta y^2}\left[\pi^2/(2j_m^2)\right] \end{array} \right\} \tag{84c}$$

$$HK_{max} = \max \left\{ \begin{array}{l} \frac{\alpha_1}{2}\left[2 - \pi^2/(2i_m^2)\right] \\ \frac{1}{2\Delta y^2}\left[2 - \pi^2/(2j_m^2)\right] \end{array} \right\} \tag{84d}$$

$$\mathcal{H}^{(K)} = HK^{(K)}\left(M_{i+1/2,j} + M_{i-1/2,j} + M_{i,j+1/2} + M_{i,j-1/2}\right) \tag{84e}$$

Values of the "pure" parameter HK are obtained by logarithmic interpolation between HK_{min} and HK_{max}.

The R equations are treated in much the same manner as the P equations, but in this case the purpose of iteration is to obtain the function S_w' at the half time step $n + \frac{1}{2}$. Iteration parameters are not involved since the R equations are of parabolic form.

The constant terms are lumped into $\overline{G}$ as for the P equations.

Cartesian:

$$\bar{G}_{i,j,n+1} = -\Delta_x(N_n \Delta_x P_{n+1})_{i,j} - \Delta_y(N_n \Delta_y P_{n+1})_{i,j} - (Q_n - Q_w)_{i,j,n+1/2} / (\Delta x \Delta y \Delta z) \quad (85a)$$

Domal:

$$\bar{G}_{i,j,n+1} = -\alpha_i \bar{\Delta}_r(N_n \bar{\Delta}_r P_{n+1})_{i,j} - \frac{1}{\Delta y^2} \bar{\Delta}_y(N_n \bar{\Delta}_y P_{n+1})_{i,j} - \beta_i (Q_n - Q_w)_{i,j,n+1/2} \quad (85b)$$

Definition of the coefficients a, b, c, d, e, g remains according to Equations (73a) through (74f).

Solution proceeds again by half times steps.

Defining:

$$T^{(K+1)}_{i,j,n+1} = 8 f_{i,j} S'^{(K+1)}_{w\,i,j,n+1/2} / \Delta t_{n+1} \quad (86)$$

The R Equations (61b) and (71b) assume the following form in the x-direction. Time subscripts have been omitted for all constants except T. They are understood to bear n.

$$a_{i+1,j} R^{K+1/2}_{i+1,j,n+1/2} + b_{i,j} R^{K+1/2}_{i,j,n+1/2} + c_{i-1,j} R^{K+1/2}_{i-1,j,n+1/2} + d_{i,j+1} R_{i,j+1,n} + e_{i,j} R_{i,j,n} + g_{i,j-1} R_{i,j-1,n} - \bar{G}_{i,j,n+1} = -T^{(K+1)}_{i,j,n+1} \left(R^{K+1/2}_{i,j,n+1/2} - R_{i,j,n} \right) \quad (87)$$

All quantities are known except $R^{k+\frac{1}{2}}_{n+\frac{1}{2}}$. The following definition is made:

$$\bar{C}^{k}_{x\,i,j} = \bar{G}_{i,j,n+1} - d_{i,j+1}\,R_{i,j+1,n} - (e_{i,j} - T^{(k+1)}_{i,j,n+1})\,R_{i,j,n} - g_{i,j-1}\,R_{i,j-1,n} \qquad (88)$$

Equation (87) assumes the standard form in which time subscripts on constant terms have been dropped:

$$a_{i+1,j}\,R^{k+1/2}_{i+1,j,n+1/2} + (b_{i,j} + T^{(k+1)}_{i,j,n+1})\,R^{k+1/2}_{i,j,n+1/2} + c_{i-1,j}\,R^{k+1/2}_{i-1,j,n+1/2} = \bar{C}^{k}_{x\,i,j} \qquad (89)$$

The analogous form of Equation (87) for the y-direction is:

$$a_{i+1,j}\,R^{k+1/2}_{i+1,j,n+1/2} + b_{i,j}\,R^{k+1/2}_{i,j,n+1/2} + c_{i-1,j}\,R^{k+1/2}_{i-1,j,n+1/2} + d_{i,j+1}\,R^{k+1}_{i,j+1,n+1} + e_{i,j}\,R^{k+1}_{i,j,n+1} + g_{i,j-1}\,R^{k+1}_{i,j-1,n+1} - \bar{G}_{i,j,n+1} = -T^{(k+1)}_{i,j,n+1}\,(R^{k+1}_{i,j,n+1} - R^{k+1/2}_{i,j,n+1/2}) \qquad (90)$$

Defining:

$$\bar{C}^{k}_{y\,i,j} = \bar{G}_{i,j,n+1} - a_{i+1,j}\,R^{k+1/2}_{i+1,j,n+1/2} - (b_{i,j} - T^{(k+1)}_{i,j,n+1})\,R^{k+1/2}_{i,j,n+1/2} - c_{i-1,j}\,R^{k+1/2}_{i-1,j,n+1/2} \qquad (91)$$

The standard form again results:

$$d_{i,j+1}\,R^{k+1}_{i,j+1} + (e_{i,j} + T^{(k+1)}_{i,j,n+1})\,R^{k+1}_{i,j,n+1} + g_{i,j-1}\,R^{k+1}_{i,j-1,n+1} = \bar{C}_{y\,i,j} \qquad (92)$$

Since R is closely related to capillary pressure (see Equations (18a), (18b)), wetting phase saturation is obtainable through the inverse capillary pressure function for a given value of R.

Thus, S'_w is updated according to:

$$S'^{(k+1)}_{w_{i,j,n+1/2}} = \frac{S_w(\bar{R}^k_{i,j,n+1}) - S_w(R_{i,j,n})}{\bar{R}^k_{i,j,n+1} - R_{i,j,n}} \tag{93a}$$

With $\bar{R}$ defined:

$$\bar{R}^k_{i,j,n+1} = \frac{1}{2}\left(R^k_{i,j,n+1} + R^{k-1}_{i,j,n+1}\right) \tag{93b}$$

with special cases for iterations 1 and 2:

$$S'^{1}_{w_{i,j,n+1}} = S'_w(R_{i,j,n}) \tag{93c}$$

$$S'^{2}_{w_{i,j,n+1}} = \frac{S_w(R^1_{i,j,n+1}) - S_w(R_{i,j,n})}{R^1_{i,j,n+1} - R_{i,j,n}} \tag{93d}$$

The difference equations to be solved (80), (83), (89), and (92) are all of the generic form:

$$\alpha_{m+1} U_{m+1} + \beta_m U_m + \gamma_{m-1} U_{m-1} = \delta_m \tag{94}$$

For x-direction equations, the subscript m corresponds to i with j-indices dropped, and for y-direction equations, m corresponds to j with i-indices dropped. This is convenient because of the row-wise and column-wise technique employed for solution.

Before the difference equations can be solved for the updated P and R matrices, the boundary conditions must be specified.

At all points on the boundaries not experiencing injection or production, a reflection condition is seen to apply for both phase potentials. For such points, this condition is stated mathematically as:

at $y = 0$, $y = y_{max}$ $\quad \frac{\partial \Phi_n}{\partial y} = \frac{\partial \Phi_w}{\partial y} = 0$ (95a)

at $x = 0$, $x = x_{max}$ $\quad \frac{\partial \Phi_n}{\partial x} = \frac{\partial \Phi_w}{\partial x} = 0$ (95b)

For a boundary point experiencing injection or production, specification of the rate of injection or production fixes the normal derivative. However, such a point may be treated equivalently by setting the normal derivative to zero and including the injection rate in the material balance. To see this, consider the external input to the volume element on the x = 0 boundary shown in Figure 5.

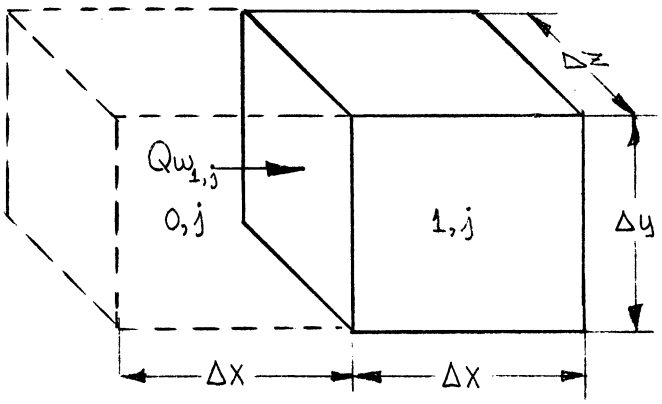

Figure 5. Boundary Element.

The volumetric injection rate of wetting phase is Q_w in cc/sec. For purposes of evaluating the derivative at the boundary in the finite difference grid system, grid element (o,j) has been included. (Production will be considered to be negative.)

Proceeding in the manner of Equation (65):

$$IN_x = \left(\frac{K k_w}{\mu_w}\right)_{\frac{1}{2},j} \frac{\Delta y \Delta z}{\Delta x} \left(\Phi_{w_{0,j}} - \Phi_{w_{1,j}}\right) \qquad (96)$$

However, in all difference forms, provision for external injection has been made for any element of the grid system. Thus it is entirely equivalent to treat injection at a boundary through specification of the Q-term.

$$IN_x = Q_{w_{1,j}} \qquad (97)$$

Similar reasoning applies for the non-wetting phase. Although Figure 5 and Equation (96) describe a boundary element in the cartesian grid system, the same analysis can be applied to a boundary element in the domal system.

This allows all boundary points to be treated the same whether injection occurs or not. In the case of no injection, the Q term is merely zero.

Since the P and R variables employed here are defined as the sum of and difference between non-wetting and wetting phase potentials, reflection of potentials implies reflection of P and R. Using the form of grid system illustrated in Figure 5, the reflection condition amounts to having identical potentials on either side of the boundary.

The generic form of all difference equations Equation (94) is expanded into the following simultaneous equations:

$$\alpha_2 U_2 + (\beta_1 + \gamma_0) U_1 = \delta_1 \qquad (98a)$$

$$\alpha_3 U_3 + \beta_2 U_2 + \gamma_1 U_1 = \delta_2 \qquad (98b)$$

$$\vdots$$

$$\alpha_{(max)} U_{(max)} + \beta_{(max-1)} U_{(max-1)} + \gamma_{(max-2)} U_{(max-2)} = \delta_{(max-1)} \qquad (98c)$$

$$(\alpha_{(max+1)} + \beta_{(max)}) U_{(max)} + \gamma_{(max-1)} U_{(max-1)} = \delta_{(max)} \qquad (98d)$$

For P and R difference equations (80) and (89) in the x-direction,

$$(max) = i_m \tag{99a}$$

and for the y-direction forms Equations (83) and (92),

$$(max) = j_m \tag{99b}$$

These equations are seen to form a tridiagonal matrix for which a simple non-iterative inversion technique is given by Richtmeyer[46] This technique is based on the existence of the following recursion relationship.

$$U_{m-1} = C_m U_m + D_m \tag{100}$$

Substitution of Equation (100) into Equation (94) yields:

$$U_m = \frac{\alpha_{m+1}}{\beta_m + \gamma_{m-1} C_m} U_{m+1} + \frac{\delta_m - \gamma_{m-1} D_m}{\beta_m + \gamma_{m-1} C_m} \tag{101}$$

Comparison of Equations (100) and (101) shows that:

$$C_{m+1} = \frac{\alpha_{m+1}}{\beta_m + \gamma_{m-1} C_m} \tag{102a}$$

and

$$D_{m+1} = \frac{\delta_m - \gamma_{m-1} D_m}{\beta_m + \gamma_{m-1} C_m} \tag{102b}$$

Equation (98a) gives C_2 and D_2 directly:

$$C_2 = -\frac{\alpha_2}{\beta_1 + \gamma_0} \tag{102c}$$

$$D_2 = \frac{\delta_1}{\beta_1 + \gamma_0} \tag{102d}$$

Since all α's, β's, and γ's are known, C_m and D_m can be calculated from Equations (102a) and (102b) for m = 3, 4 ... (max).

Equations (98d) and (100) provide the relationship:

$$U_{(max)} = \frac{\delta_{(max)} - \gamma_{(max-1)} D_{(max)}}{\alpha_{(max+1)} + \beta_{(max)} + \gamma_{(max-1)} C_{(max)}} \qquad (103)$$

Equation (101) now allows all U's to be calculated in decreasing order of m for m = (max-1), (max-2) ... 2, 1.

Evaluation of the interblock mobility properties (coefficients M and N) is straightforward. At the beginning of a time step the wetting phase saturation matrix allows relative permeability matrices to be calculated for each phase. Provided the permeability to neither phase is zero for either of two adjacent grid elements, the interblock properties are obtained by averaging the adjacent mobilities. If one of the elements has zero permeability to one of the phases, the potential gradient for that phase is investigated. If that phase would tend to flow out of the particular element, the interblock mobility of that phase must be set to zero. In other words, flow of a phase from an element having a zero mobility to that phase is not allowed, although flow into such an element is quite all right.

Normally, injection and production will occur through distributed sources or sinks. The assignment of Q terms to grid elements bounding the source or sink is treated in the following manner.

The layer-wise distribution of the total injection or production rate is obtained from assumption of a constant well-bore potential and use of relative permeabilities and insitu phase potentials existing at the beginning of the time step. The concept of constant well-bore potential neglects frictional effects in the well-bore over the span which is open to the porous medium.

The well-bore potential is defined in terms of the average density of the well-bore fluids. Determination of the correct average density deals with two phase flow in pipes and is beyond the scope of this work. For the sake of simplicity the average density is taken to be:

$$\rho_{av} = \frac{\rho_n QT_n + \rho_w QT_w}{QT_n + QT_w} \tag{104}$$

QT_n and QT_w are the total volumetric flow rates of non-wetting and wetting phases in the well-bore.

The well bore potential Φ_{wb} is:

$$\Phi_{wb} = p_{wb} + \rho_{av} g h \tag{105a}$$

Within the well-bore both phases are considered to exist at the same pressure. It will be noted that the discontinuity existing at the boundary of the well is manifest by a discontinuity in capillary pressure at the boundary. Phase potentials in the well-bore are:

$$\Phi_{n,wb} = \Phi_{wb} + (\rho_n - \rho_{av}) g h \tag{105b}$$

$$\Phi_{w,wb} = \Phi_{wb} + (\rho_w - \rho_{av}) g h \tag{105c}$$

The injection rate into block i, j along the well-bore is:

$$Q_{ni,j} = C K_{i,j} \frac{k_{ni,j}}{\mu_n} \left[\Phi_{ni,j} - \Phi_{wb} - (\rho_n - \rho_{av}) g h \right] \tag{106a}$$

$$Q_{wi,j} = C K_{i,j} \frac{k_{wi,j}}{\mu_w} \left[\Phi_{wi,j} - \Phi_{wb} - (\rho_w - \rho_{av}) g h \right] \tag{106b}$$

The constant C is a geometric factor depending on the shape of the well, the size of the grid element, and the fraction of the well-bore area open to flow.

The following well geometries may exist.

Cartesian Coordinates:

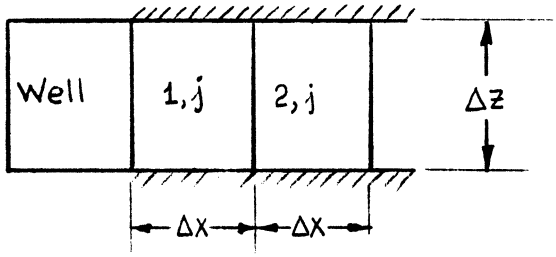

Figure 6. Rectangular Well - Top View.

This type of well may exist at the edges of a laboratory system.

$$C = 2\Delta y \Delta z A/\Delta x \tag{107}$$

Where A is the fraction of the total area of the well surface open to flow.

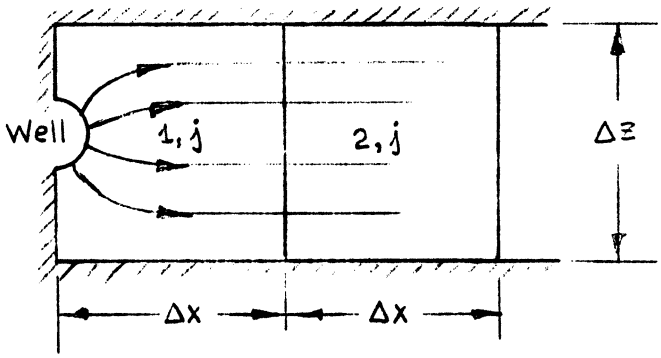

Figure 7a. Circular Well at Edge of Medium - Top View.

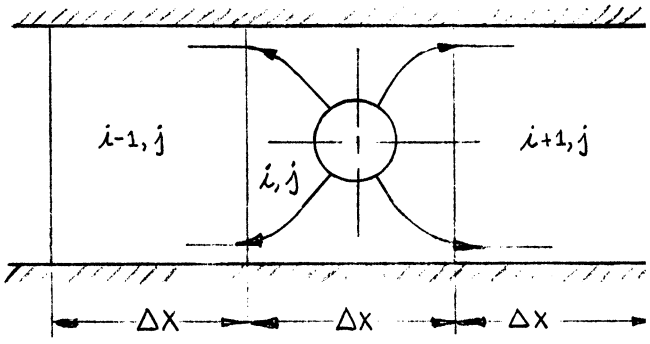

Figure 7b. Circular Well Within Medium - Top View.

Wells of these types normally will be present in the reservoir system.

For wells at the edge of an element:

$$C = 2\pi A/Fe \tag{108a}$$

For wells at the center of an element, the phase potentials in element (i,j), $\Phi_{n_{i,j}}$ and $\Phi_{w_{i,j}}$ appearing in equation (106a) and (106b) are replaced by the arithmetic average of the potentials in adjacent elements (i+1, j) and (i-1, j). The constant factor is:

$$C = 4\pi A/F_c \tag{108b}$$

The factor F is evaluated from the relationship presented by Muskat[34] which expresses the pressure distribution within a direct line-drive network. One unit of the direct line drive net-work is analogous to the flow system existing for the circular well within a volume increment.

$$F = \log\left\{\frac{\sinh[\frac{\pi}{a}(d+r_{wb})]}{\sinh[\frac{\pi}{a}r_{wb}]}\prod_{m=1}^{\infty}\left[\frac{\sinh[\frac{\pi}{a}\{r_{wb}-(m-1)d\}]\sinh[\frac{\pi}{a}\{r_{wb}+(m+1)d\}]}{\sinh[\frac{\pi}{a}\{r_{wb}+md\}]\sinh[\frac{\pi}{a}\{r_{wb}-md\}]}\right]^{(-1)^{m+1}}\right\} \tag{109}$$

Where r_{wb} = well radius (110a)

$$a = \Delta z \tag{110b}$$

For computation of F_e :

$$d = \Delta x \tag{110c}$$

For computation of F_c :

$$d = 2\Delta x \tag{110d}$$

Domal coordinates :

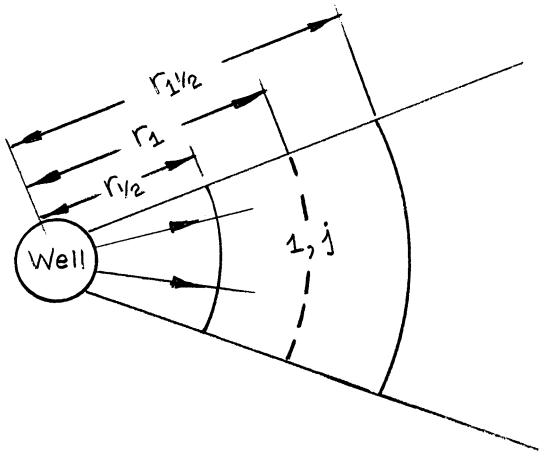

Figure 8. Axial Well - Top View.

Integration of Darcy's law yields

$$C = 2\pi \Delta y A / \log(r_1/r_{wb}) \tag{111}$$

In laboratory systems, production may occur at the outer radius. Such a producing face is analogous to the rectangular well in the cartesian system and the constant C is seen to be:

$$C = 2\pi \Delta y A / \log(r_{m+1/2}/r_m) \tag{112}$$

Because of axial symmetry, additional injection or production must occur by means of a line source or sink on a circle about the axis. This case will be handled differently.

The layer-wise distribution resulting from single phase injection must total the specified injection rate.

$$\sum_{j=1}^{jm} Q_{ni,j} = QT_{ni} \tag{113a}$$

$$\sum_{j=1}^{jm} Q_{wi,j} = QT_{wi} \tag{113b}$$

Rearrangement of Equations (106a) and (106b), with the i-index omitted but understood to correspond to the position of the well, yields:

$$\Phi_{wb} = \frac{\sum_{j=1}^{jm}\left[K_j \frac{k_{nj}}{\mu_n}\left(\Phi_{nj} - \{\rho_n - \rho_{av}\} g h\right)\right] - QT_n/C}{\sum_{j=1}^{jm}\left[K_j \frac{k_{nj}}{\mu_n}\right]} \tag{114a}$$

$$\Phi_{wb} = \frac{\sum_{j=1}^{jm}\left[K_j \frac{k_{wj}}{\mu_w}\left(\Phi_{wj} - \{\rho_w - \rho_{av}\} g h\right)\right] - QT_w/C}{\sum_{j=1}^{jm}\left[K_j \frac{k_{wj}}{\mu_w}\right]} \tag{114b}$$

If a well is completed only at selected levels of the grid system, summation is performed only over those levels affected.

In the case of the circular well shown in Figure 7b, the phase potentials appearing in Equations (114a) and (114b) are replaced by the average of the appropriate phase potentials existing in the adjacent grid elements, (i+1, j) and (i-1, j).

The well-bore potential is computed from Equation (114a) or (114b) using the appropriate value for the geometric factor C. The distribution is obtained by solution of Equation (106a) or (106b). The summation over j includes only those layers at which the well communicates with the porous medium.

Two phase injection has not been considered, but this extension is obvious.

Two-phase production is handled in a similar way. If the total production rate of a single phase is specified, the distribution of that phase is computed the same as for injection. The resulting distribution of the second phase is obtained from Equation (106a) or (106b), whichever is appropriate. If the total two-phase production rate is specified, Equations (114a) and (114b) are added and solved for the well-bore potential. The distribution of each phase is computed from Equations (106a) and (106b).

Since the circular line source or sink in the domal system has no physical counterpart, the distribution is assigned on a mobility basis. It will be noted that this is the limiting case occurring in the previous treatment when the geometric factor approaches infinity, which results when the well-bore radius approaches zero.

For this case:

$$Q_{n_{i,j}} = \frac{K_{i,j}\, k_{rn_{i,j}}}{\sum_{j=1}^{jm}\left[K_{i,j}\, k_{rn_{i,j}}\right]}\, QT_{n_i} \qquad (115a)$$

$$Q_{w_{i,j}} = \frac{K_{i,j}\, k_{rw_{i,j}}}{\sum_{j=1}^{jm}\left[K_{i,j}\, k_{rw_{i,j}}\right]}\, QT_{w_i} \qquad (115b)$$

The single phase injection distribution is computed from Equations (115a) or (115b).

Two-phase production from this type of sink is computed from the following equations:

$$Q_{n_{i,j}} = \frac{K_{i,j}\, k_{rn_{i,j}}\,(QT_{n_i} + QT_{w_i})}{\sum_{j=1}^{jm}\left[K_{i,j}\left(k_{rn_{i,j}} + \frac{\mu_n}{\mu_w}\, k_{rw_{i,j}}\right)\right]} \qquad (116a)$$

$$Q_{w_{i,j}} = \frac{K_{i,j}\, k_{rw_{i,j}}\,(QT_{n_i} + QT_{w_i})}{\sum_{j=1}^{jm}\left[K_{i,j}\left(k_{rw_{i,j}} + \frac{\mu_w}{\mu_n}\, k_{rn_{i,j}}\right)\right]} \qquad (116b)$$

Another type of boundary is useful especially in field systems where the two-phase region occupies only a very small part of the aquifer. In this case it is convenient to place an artificial boundary around the two-phase region. At this type of boundary no discontinuity in the medium exists. The total flow across the boundary is obtained by over-all material balance. The distribution is assumed to be the same as that existing

within the elements one column removed from the boundary. Figure 9 illustrates this type of boundary for either coordinate systems.

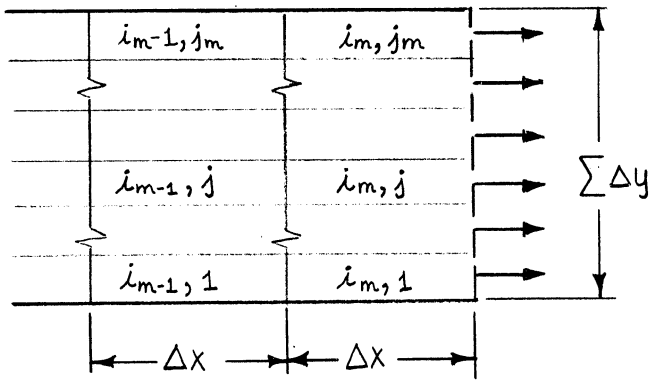

Figure 9. Vertical Cross Section Aquifer Boundary.

$$Qn_{i_m,j} = \frac{Gn_j \quad QT}{\sum_{j=1}^{j_m}\left[Gn_j + G\omega_j\right]} \tag{117a}$$

$$Q\omega_{i_m,j} = \frac{G\omega_j \quad QT}{\sum_{j=1}^{j_m}\left[Gn_j + G\omega_j\right]} \tag{117b}$$

$$Gn_j = \left(K\frac{k_n}{\mu_n}\right)_{i_{m-1/2},j}\left(\Phi n_{i_{m-1},j} - \Phi n_{i_m,j}\right) \tag{117c}$$

$$G\omega_j = \left(K\frac{k_\omega}{\mu_\omega}\right)_{i_{m-1/2},j}\left(\Phi\omega_{i_{m-1},j} - \Phi\omega_{i_m,j}\right) \tag{117d}$$

The distribution is computed according to Equations (117a) through (117d).

This treatment of injection and production is geared for systems in which rates are specified. The modifications required to handle cases where injection or production pressures are specified are obvious.

Since the phases are treated as incompressible, the pressure level does not enter. However, pressures at wells could easily be calculated if the aquifer were treated as slightly compressible according to the methods of Van Everdingen and Hurst[53]. They would enter as a boundary condition to supply the operating pressure level.

The computational sequence within a time step may be summarized as follows:

1. Relative permeability matrices are computed from the existing phase saturation distribution and these are combined to obtain the coefficients M and N.
2. Injection-production terms are computed from relative permeabilities and phase potentials (sum and difference of P and R) for all appropriate grid elements.
3. P matrix is updated by cyclic iteration on Equations (80) and (83) involving inversion of tridiagonal matrices.
4. R matrix is updated by iteration on Equations (89) and (92) also involving inversion of tridiagonal matrices.

Programs have been written in both coordinate systems embodying the numerical techniques presented in this section. Some discussion of the programs, their capabilities and limitations has been included in Appendix II.

V. EXPERIMENTAL METHOD

The experimental work was undertaken to assess the degree to which the differential equations obtained in the previous section describe a controlled two-phase displacement. The data available in the literature dealing with the two-dimensional flow of two immiscible phases are of an integral nature. To critically test the mathematical description of systems of this type, phase distributions in space and time are required. In this study the space-time distributions of water and gas phases occurring during drainage and imbibition displacements in a two-dimensional unconsolidated porous medium have been measured. The experimental methods employed in collecting the data are discussed in the following sequence:

A. Laboratory Equipment.

B. Water Saturation Measurement.

C. Operating Procedures.

D. Data Analysis.

A. Laboratory Equipment

The basic piece of equipment, the flow model was borrowed from the Jersey Production Research Company of Tulsa, Oklahoma. The construction of the model is indicated in Figures 10a, b and c.

The porous section is enclosed by a brass frame 1/2 inch thick, measuring 18 inches square on the outside and 16 inches square

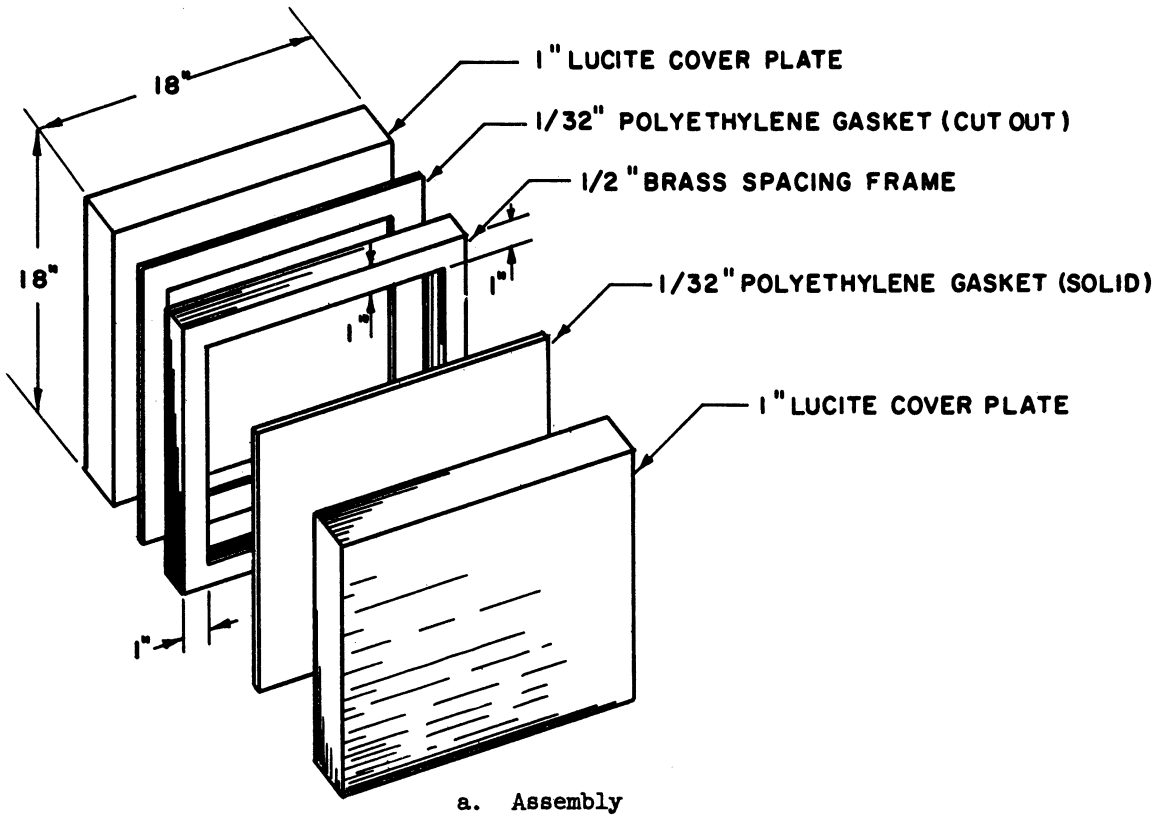

a. Assembly

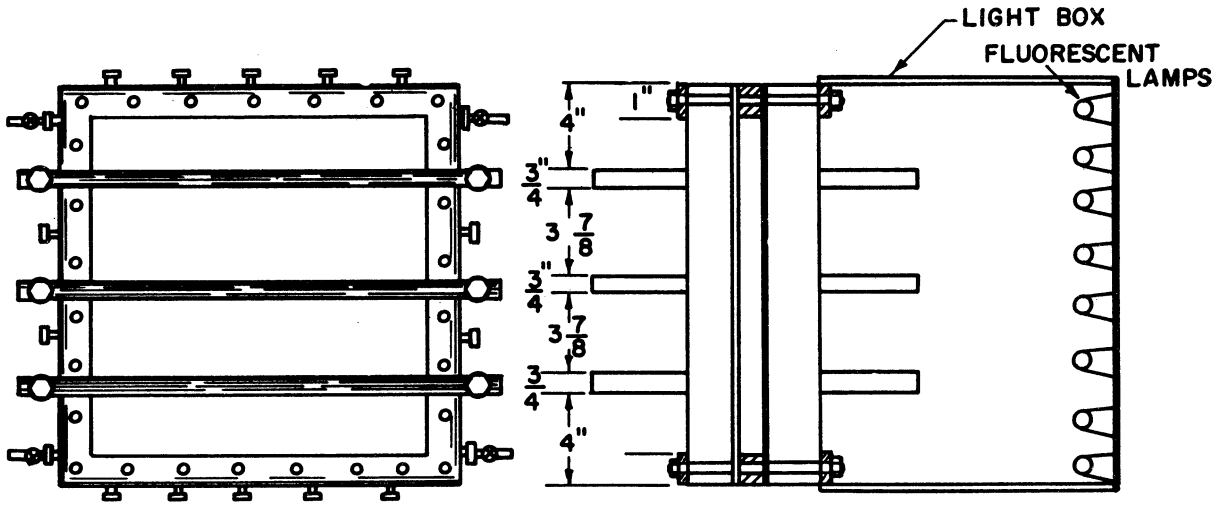

b. Front View

c. Vertical Cross Section

Figure 10. Laboratory Model.

on the inside. A lucite plate one inch thick and 18 inches square is placed on each side of the frame. Each plate is sealed to the frame with a 1/32 inch thick gasket cut from polyethylene sheet. One gasket is cut to the dimensions of the frame while the other is a solid sheet. Thus the packed section measures 16 inches square by 17/32 inch thick. The lucite plate in contact with the solid sheet of polyethylene is inscribed with a network of grooves. Water pressure is maintained at 100 psig between this plate and the polyethylene sheet to prevent shifting of the pack during operation. The complete assembly is bolted together with forty 1/4 inch bolts spaced around the edges of the face. The bolts bear on the lucite through 1 x 1/4 inch aluminum strips. Three steel bars measuring 22 x 2 x 3/4 inches are placed across the face as indicated in Figures 10b and 10c for strengthening purposes.

A total of 38 wells are tapped into the frame, with one at each corner, nine along the top and bottom edges, and eight along each side. Each well is a 1/8" Swagelock tubing fitting equipped with a screen to block passage of the packing material. "Lectromesh" is the brand name of the screen used. This type of screen is a .005 inch thick mesh of nickel-clad copper with 0.002 inch square holes. The open area is 36% of the total area of the screen.

The model was packed with spherical glass beads designated as grade No. 996 by the manufacturer, the Minnesota Mining and Manufacturing Company[8]. This is a special close cut of beads averaging 115 microns in diameter with all beads falling in the 105-125 micron range. Prior to packing, the beads were soaked in hydrochloric acid, washed and dried

to render them water wet. The beads were slurried in water and poured into the model. After the bolts had been tightened and the sleeve pressure established, the pack was flushed with distilled water until all residual HCl was removed.

The model was mounted in a vertical plane with the hold-down bars running horizontally. A tightly fitting light box illuminated by eight 15-watt fluorescent lamps was placed behind the model. The inside of the box was painted white in an effort to obtain uniform illumination over the entire packed area. For the purpose of measuring transmitted light intensities to obtain local water saturations, the 16 inch square face was partitioned off into a one inch square grid and masked with a blackened galvanized iron sheet. A 1/4 inch diameter hole was drilled through the masking at the center of each element excluding those under the reinforcing bars. Figure 11 is a photograph of the model in the operating position with the battery of photocells in place.

Mounted below the model is a set of "soap film" gas rate measuring devices. Rates were measured by timing the rise of a soap film between etched marks on the vertical glass tubes. Tube diameters of 3, 6, and 10 mm were used with etched marks 10 cm apart. Accurate measurements could be made for rise times from 10 sec. (49 cc/min, 10 mm tube) to 500 sec. (6.8 cc/hr, 3 mm tube). Outside of this range of rise time, measurements were less accurate. Helium, selected because of its low water solubility, was saturated with water prior to injection by passing it through a wet-test meter. The pressure of the injected gas phase was indicated on a differential capillary manometer not shown in the photograph.

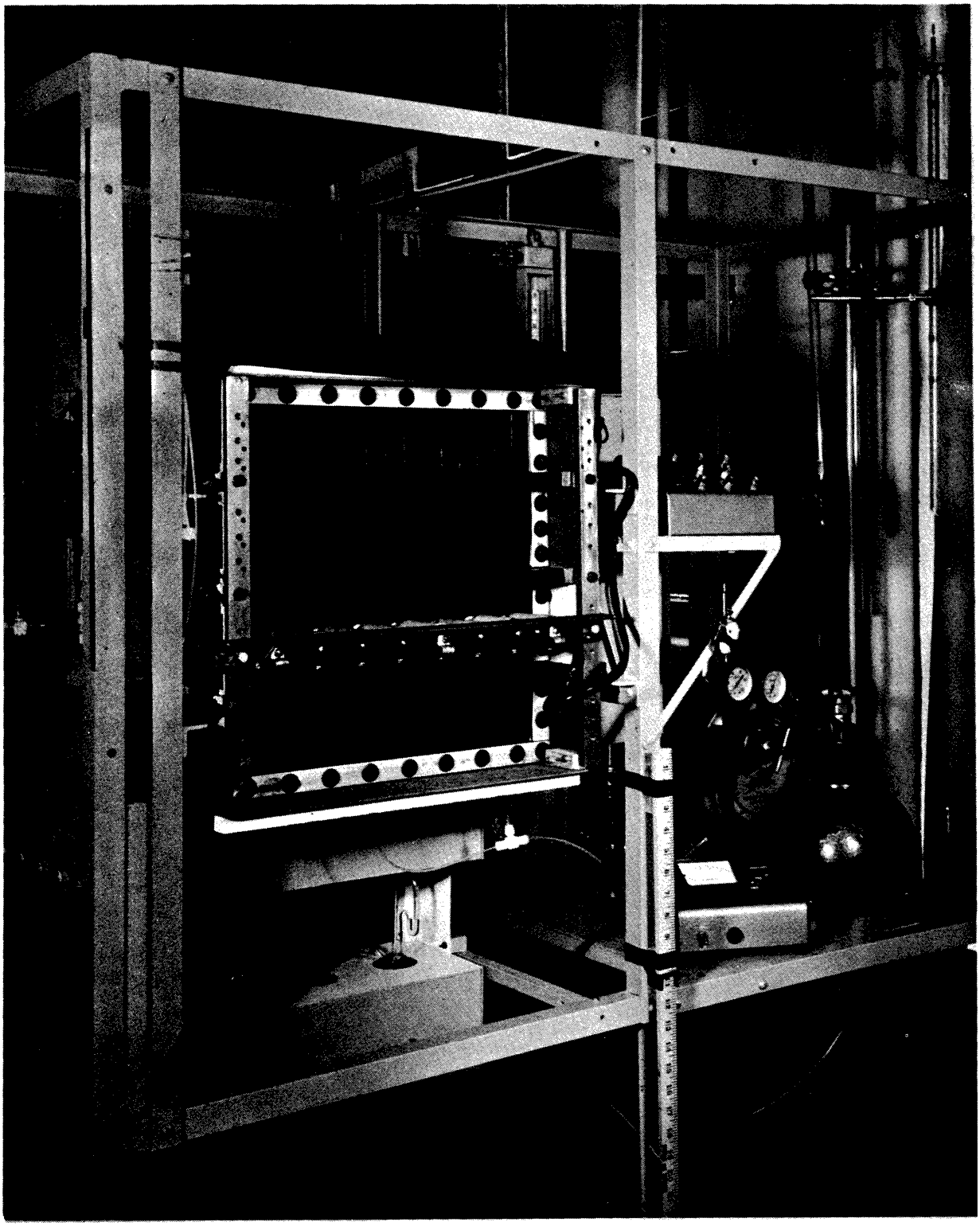

Figure 11. Experimental Apparatus

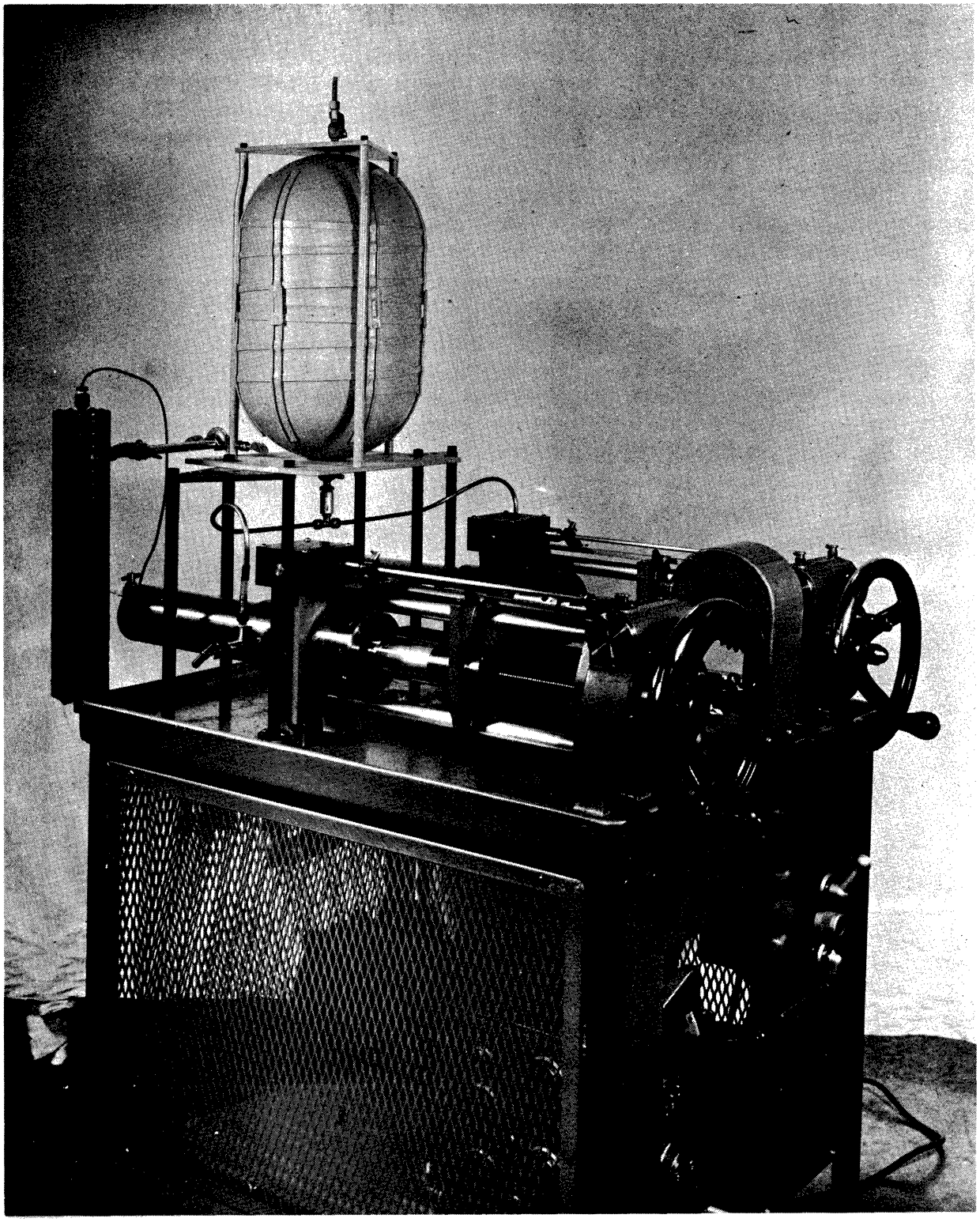

Figure 12. Ruska Pump

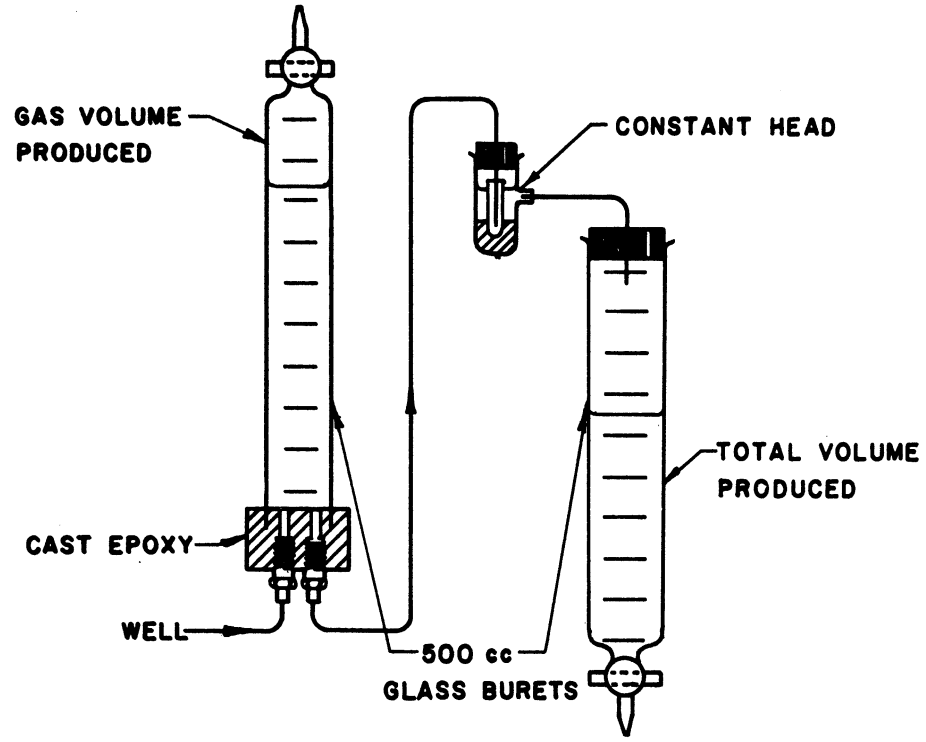

a. Drainage Displacements

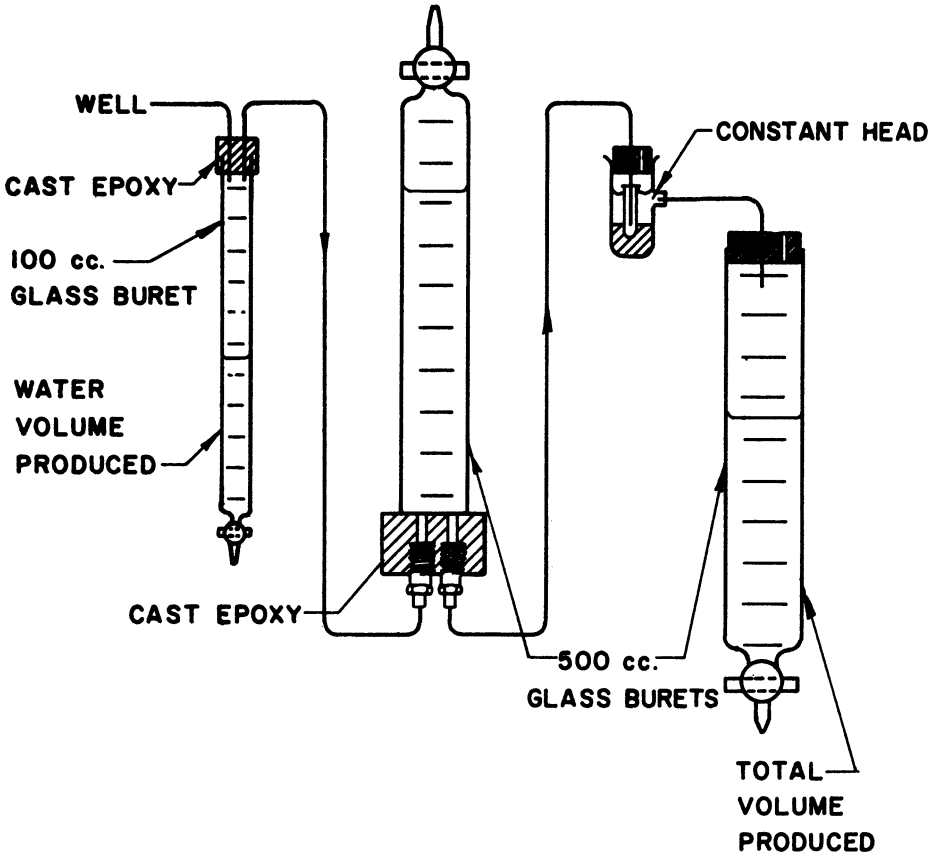

b. Imbibition Displacements

Figure 13. Effluent Collection

Constant water rates were obtained by means of the Ruska pump pictured in Figure 12. Nominal rates of 1 to 224 cc/hr (448 cc/hr for both cylinders) can be obtained by the appropriate setting on the gear box. Although the actual rates were found to be about 2% higher than the nominal rates, accurate displacement volumes for each cylinder are indicated on a scale which can be read to .01 cc. Each cylinder has a deliverable capacity of 500 cc. Distilled water was vacuum deaerated and passed through a ceramic filter prior to injection. Both phases were transported in 1/8 inch polyethylene tubing.

Produced phases were collected in burets as shown in Figures 13a and 13b. The 500 cc burets were graduated every 5 cc and the 100 cc buret every 0.2 cc. A different collection system was used for drainage and imbibition displacements to obviate the occurrence of breakthrough. In both cases, the first buret registered the produced volume of the appropriate phase, while the last registered the total of both phases. Pressure corrections had to be applied to the gas volumes.

B. Water Saturation Measurement

All of the methods of phase saturation measurement enumerated in the Literature Survey have disadvantages, especially when considered for application in two-dimensional systems operated with injection-production. Briefly, these methods were not used for the following reasons:

1. Electrical Resistivity: The use of probes is required making packing more difficult and introducing significant inhomogeneities. Also, calibration would be quite a problem in two-dimensions.
2. X-Ray Transmission: This is quite similar to the method employed but requires expensive equipment and adequate radiation shielding.
3. Radioactive Tracer: Expensive equipment and shielding again are required. Also, for injection-production operations, the quantities of radioactive fluids involved create a disposal problem.
4. Matched Refractive Indices: This method employs crushed calcium fluoride crystals which present more of a packing problem than glass beads. Fluid selection is limited because of the high refractive indices needed. Such fluids are normally reactive and much less desirable than water. Also, strict temperature controls would be necessary.
5. Magnetic Susceptibility: Elaborate equipment is required as well as special fluids. (An aqueous solution of cobaltous chloride was used by Whalen[58]).
6. Physical Sampling: This was considered by the author to be a last resort and would be very difficult in a two-dimensional system.

By the time the equipment had been built, a technique had not been chosen. However, during the first two-phase displacement it was discovered that regions of low water saturation appeared dark when viewed by transmitted light. Measurement of the light intensities over the face of the model indicated that the intensity in regions of low saturation was markedly lower than for the corresponding regions measured earlier at high water saturation.

After several crude intensity scans gave promising results, the system as it appears in Figure 11 was built. As discussed earlier, the face was partitioned off into a one-inch square grid. This grid was chosen because of the size of the photocells selected for the job and also because it would be convenient for use in the numerical work. Because of the hold down bars, four rows of elements were not viewable leaving a total of 192 points to be monitored. A mounting bracket for eight photocells was built to facilitate rapid and accurate placement of the photocells over the grid elements. With this arrangement it was possible to monitor light intensities of eight grid points (every second point in a horizontal row) before moving the mounting bracket. The remaining points were metered by sliding the bracket one inch laterally. The bracket was positioned by inserting a steel pin into prealigned holes in the bracket and the mounting rail. A quarter inch screw tapped into the rail held it firmly in place during the eight measurements.

Precautions were taken to seal off external light from the photocells. Figure 14c shows the metal sleeve used to hold each photo

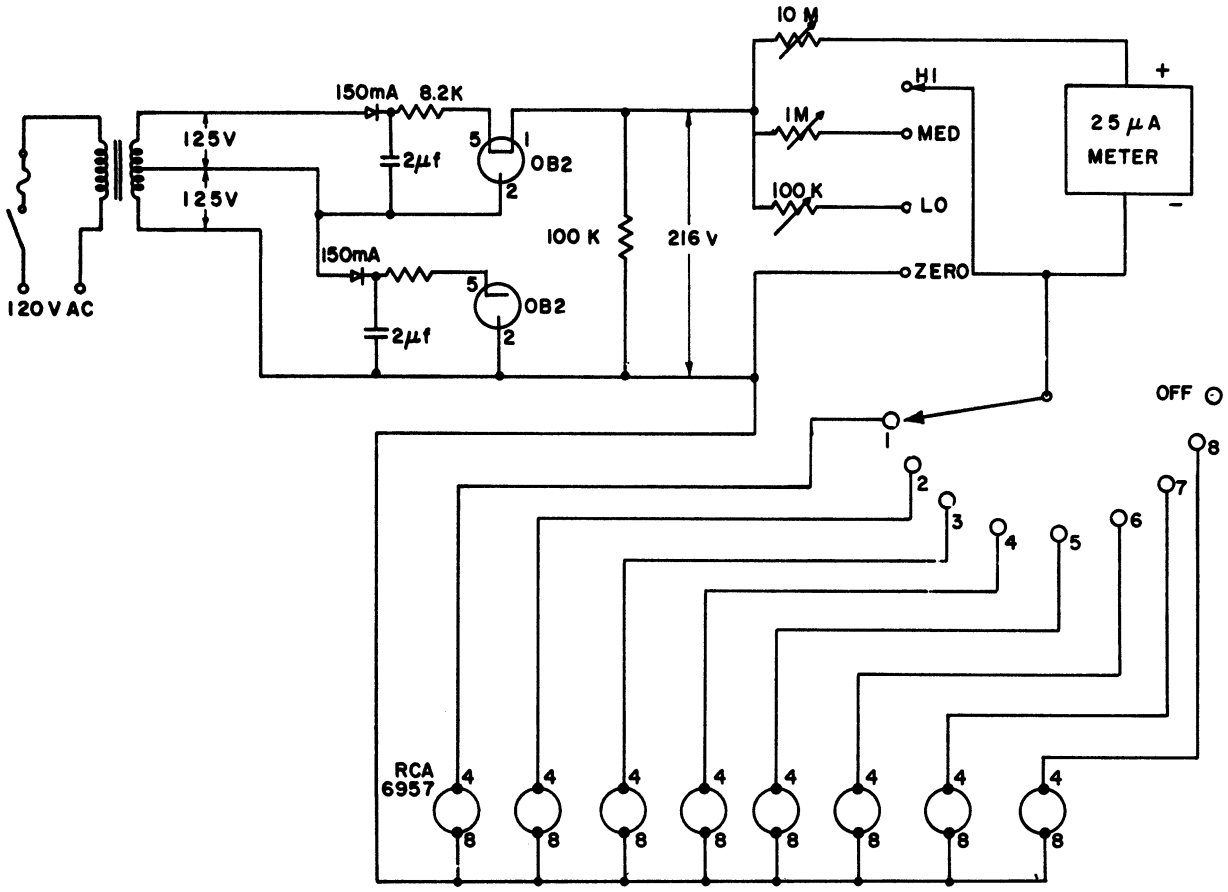

a. Metering Circuit

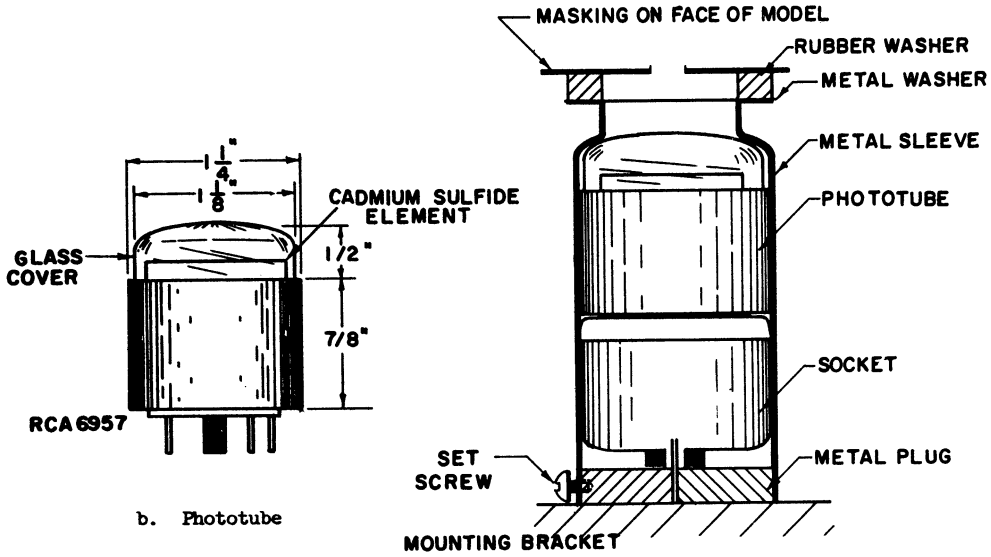

b. Phototube

c. Mounting Sleeve

Figure 14. Light Metering Equipment

tube in position on the mounting bracket. The rubber washer at the front of the sleeve is slightly compressed when bearing on the face masking of the model. The edges of the lucite plates were masked with tape and the area between the model face and the mounting rails was enclosed as shown in Figure 11. During operation a black drape was fastened over the whole assembly.

The wiring diagram of the meter circuit is shown in Figure 14a. A step-up transformer powers a parallel rectifier-voltage regulator system to produce a 216 volt DC supply. The 10 megohm potentiometer is set to give a full scale 25 microamp current through the micro ammeter with the sensitivity selector in the zero position. In the high sensitivity position the full current passes through the meter regulated by the light intensity seen by the appropriate photocell. At medium and low sensitivities additional current is shunted around the meter to supply a higher voltage to the photocell. The potentiometers governing medium and low sensitivities are set to give the desired readings for the higher intensities to be measured. It is seen that the circuit has a built-in safeguard in that the meter can draw a maximum of 25 microamps regardless of the sensitivity and light intensity.

The particular photocell employed was an RCA 6957 tube. It is a relatively inexpensive item designed for much less elegant use. Consequently, no two cells behaved alike and each cell had to be calibrated against a known intensity light source over the intensity range of interest (0.6 ft. candles at total water saturation down to the minimum detectible by each cell).

Calibration was done in a dark room equipped with an optical bench. A set of neutral filters was used to attenuate the intensity of the light emitted by a Tungsten filament lamp (4.8 ft. candles - no attentuation) into the ranges desired. Fine adjustment was made by varying the distance between the photocell and lamp. From a total of about twenty photocells, the best eight were selected on the basis of the response obtained to an intensity at the low end of the range of interest.

First, each filter combination in the sequence of increasing opaqueness was calibrated against the previous combination of the sequence at four intensity levels by positioning the photocell to give the same reading for each case. The good agreement obtained among the attentuation factors (1.5%) indicates that the photocell behavior is reasonably reproducible. Then each photocell was calibrated against approximately 65 known intensity levels spanning high, medium and low sensitivity ranges. Two of the eight curves are superimposed in Figure 15 to show the differences in photocell behavior.

The basic assumption is that light attenuation is some function of water saturation. That is, all points with the same water saturation will yield the identical ratio of the light intensity measured at that saturation to the intensity measured at total water saturation. It will be seen later, however, that an intensity characterizing zero water saturation will also be required because of differences present among the responses of each photocell at very low intensities.

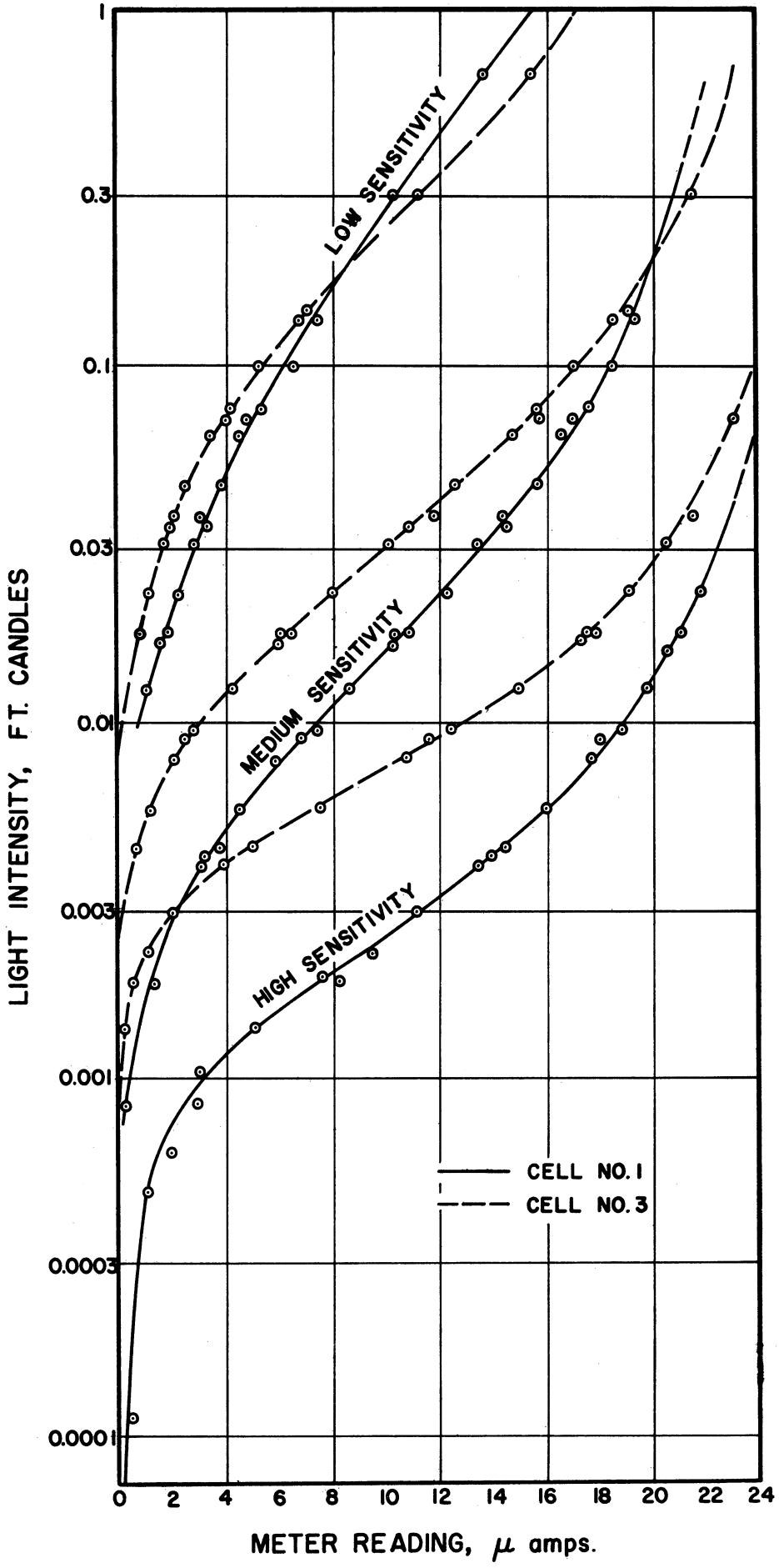

Figure 15. Typical Photocell Characteristics

For purposes of finding this functional dependence, it is necessary to obtain the water saturations corresponding to the intensity measurements. Perhaps the most direct means would be through physical sampling. This is not desirable because it would necessitate repacking of the model after each set of measurements on a given saturation distribution. Repacking would be very time consuming and it is questionable whether reproducible packing could be achieved.

Consequently, an indirect method was employed. In collaboration with Briggs[5] who was studying one-dimensional two-phase flow in the same unconsolidated medium, three sets of drainage capillary pressure data were obtained. A lucite tube as illustrated in Figure 16 was wet packed with treated 3M No. 996 beads. The pack was dried, evacuated, and filled with deaerated water to obtain its porosity. The water permeability was measured for several rates supplied by the Ruska pump. A level for the constant head was fixed and valves were opened to effect gravity drainage. Water production ceased after several days, and after about a week, samples were taken with the column remaining in place. Beads were removed inch by inch, starting at the bottom. The samples collected were weighed wet, muffled and reweighed. For all three sets of drainage data, the overall material balance was good. This consisted of a comparison of the total pore volume against the sum of the water produced and that remaining in the column. The latter contribution was obtained by graphical integration of the water saturation versus height curve defined by the sampling procedure.

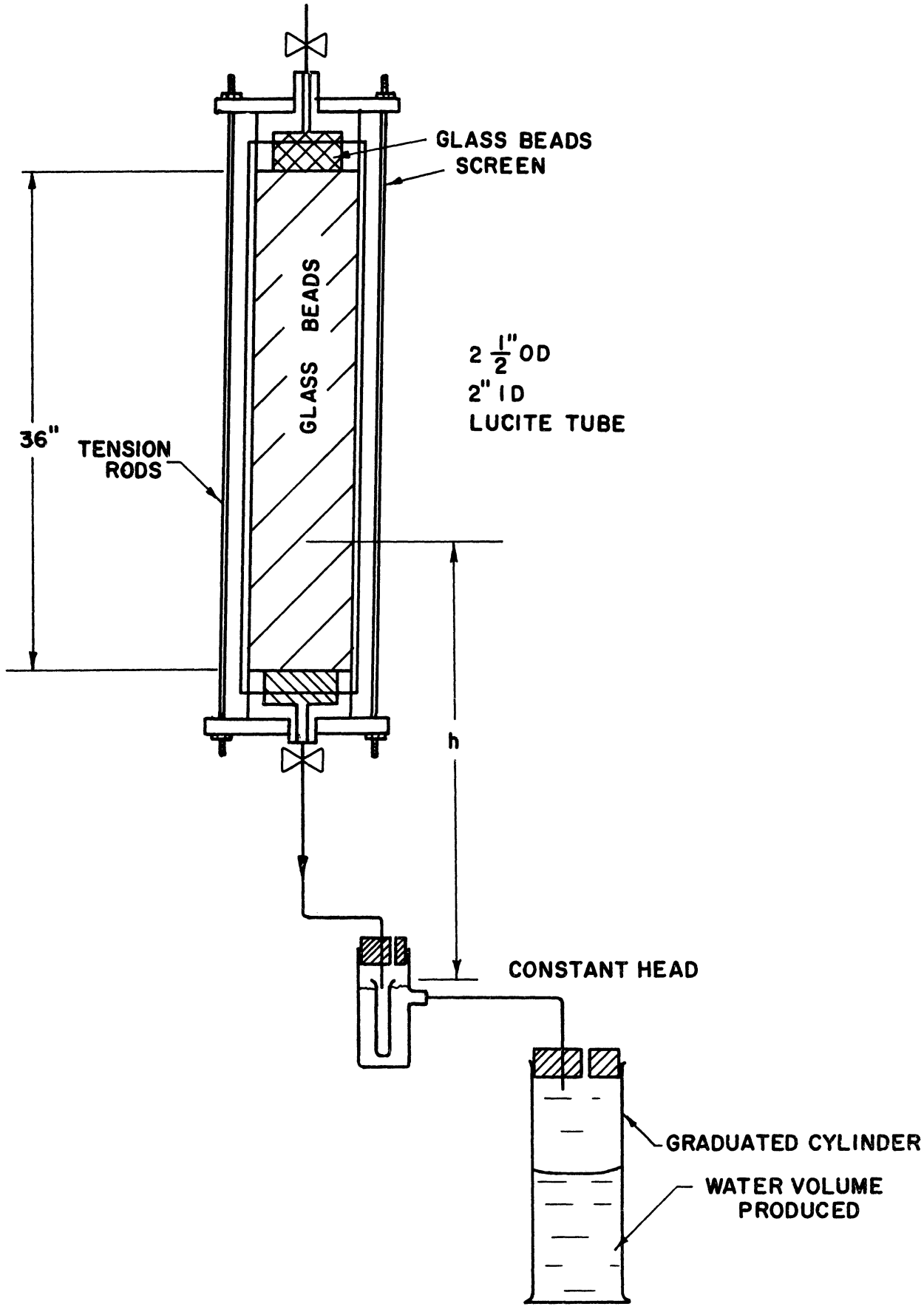

Figure 16. Capillary Pressure Apparatus

At equilibrium the difference between the pressures existing in the two phases is proportional to the height above the datum where the pressures are equal. Stated mathematically,

$$p_g(h) - p_w(h) = p_c(S_w) = (\rho_w - \rho_g) g h \qquad (118)$$

Thus, the capillary pressure curve is proportional to the height-water saturation curve.

Although efforts were made to obtain identical bead packings for each experiment, different porosity and permeability were observed each time. Using the Leverett J-function, Equation (4) to account for these differences, the sets of dimensionless capillary pressure data were similar.

The average of the three sets of data was assumed to apply under suitable linear transformation to the two-dimensional model. The use of a linear transformation is somewhat more general than the J-function approach. In the following equations, subscript 1 refers to the drainage experiments and 2 to the two-dimensional model.

$$p_c(S_w)_2 = A\, p_c(S_w)_1 + B \qquad (119)$$

The constants A and B are obtained from water production volumes obtained from the model during a series of gravity drainage displacements. If drainage is begun with the model saturated with water, and a total volume of water D is produced, from the pore volume, PV, it follows that:

$$\frac{D(p_{c2T} - p_{c2B})}{PV} = \int_{S_{wT}}^{S_{wB}} \left[p_{c_{2T}} - p_c(S_w)_2 \right] dS_w \qquad (120)$$

The additional subscripts B and T refer to the bottom and top of the model.

Substitution of Equation (119) into Equation (120) yields the following:

$$C_1 D = (C_2 - B)(S_{w_{2B}} - S_{w_{2T}}) - A\int_{S_{w_{2T}}}^{S_{w_{2B}}} p_c(S_w)_1 \, dS_w \tag{121a}$$

where

$$C_1 = (h_{2T} - h_{2B})\Delta\rho g / PV \tag{121b}$$

$$C_2 = \Delta\rho g h_{2T} \tag{121c}$$

$$\Delta\rho = \rho_w - \rho_g \tag{121d}$$

h_2 = height above constant head in model (121e)

S_{2B}, S_{2T} = water saturations at top and bottom of model (121f)

Equation (121a) is solved by trial and error to obtain the correct value of A for some choice of B. The procedure is to set B, make an initial guess at A, solve Equation (121a) for the water saturation at the top of the model (or at the bottom since the two are not independent) and recalculate A. Using the new value of A, the process if repeated until A is reproduced to the desired tolerance. Convergence was fairly rapid, normally requiring about 9 iterations. Computations were done by machine (IBM 709) using linear interpolation to obtain the integral function from tabular values. The "best" value of B was the one which gave the most constant values of A for the series of drainages.

For the nine drainages performed in calibration, Table I presents the values of A obtained for two choices of B. Also included are the constant head positions, YB, referred to the bottom of the model, the total water produced and the number of iterations required for solution. The water saturation distributions for these values of A and B are presented in Table II for each row in the grid system with Y measured from the bottom of the model. It will be noted that water saturations were reasonably insensitive to the values of A and B used. The best values of A and B were taken as 1.163 and -0.004, respectively. The capillary pressure curve resulting from application of these constants to the experimental curve is shown in Figure 23 and is used in the numerical simulation of the drainage displacement.

Prior to the drainages, the model was evacuated and filled with deaerated water. Three complete scans of the transmitted light intensity were made for all 192 viewable points across the face of the model. Where different, the meter readings for a point were averaged to obtain the characteristic unity saturation intensity for each point.

Each of the drainages cited in Tables I and II were done with all nine of the wells across the top edge open to the atmosphere. Three of the wells on the bottom edge were joined to a common line running to the constant head device. Produced water was collected in a 100 ml buret with care taken to minimize evaporation losses. Operated in this manner, the behavior was considered to be one-dimensional. That is, the water saturation should have been nearly constant along a horizontal row of grid elements.

TABLE I

LINEAR TRANSFORMATION CONSTANTS

COMPUTED VALUES OF A FOR B = -.0040 ATM				COMPUTED VALUES OF A FOR B = -.0025 ATM			
YB, INCHES	DRAINAGE, CC	ITERATIONS	A	YB, INCHES	DRAINAGE, CC	ITERATIONS	A
11.00	33.08	10	1.1621	11.00	33.08	10	1.1359
12.50	71.34	10	1.1629	12.50	71.34	9	1.1379
14.00	120.14	10	1.1638	14.00	120.14	9	1.1389
15.50	177.38	10	1.1630	15.50	177.38	9	1.1385
17.00	238.05	10	1.1630	17.00	238.05	9	1.1389
18.50	309.35	10	1.1559	18.50	309.35	9	1.1321
19.50	358.85	10	1.1499	19.50	358.85	9	1.1264
20.50	405.69	10	1.1467	20.50	405.69	9	1.1235
21.50	454.52	10	1.1341	21.50	454.52	9	1.1169

TABLE II

WATER SATURATION DISTRIBUTIONS FROM LINEAR TRANSFORMATION

	B = -.0040 ATM							
Y, IN.	A = 1.1621	1.1629	1.1638	1.1630	1.1630	1.1559	1.1499	1.1467	1.1341
.50	1.0000	1.0000	.9990	.9974	.9958	.9937	.9923	.9905	.9875
1.50	1.0000	1.0000	.9979	.9964	.9946	.9925	.9906	.9882	.9781
2.50	1.0000	.9984	.9969	.9952	.9933	.9908	.9884	.9831	.9417
3.50	.9989	.9974	.9958	.9939	.9919	.9887	.9836	.9571	.8099
4.50	.9979	.9964	.9946	.9927	.9901	.9845	.9598	.8612	.6471
5.50	.9969	.9952	.9933	.9911	.9878	.9646	.8742	.6939	.5161
6.50	.9957	.9939	.9920	.9891	.9806	.8978	.7057	.5534	.4140
7.50	.9945	.9927	.9902	.9855	.9522	.7290	.5640	.4439	.3382
8.50	.9933	.9911	.9878	.9702	.8405	.5833	.4523	.3624	.2839
9.50	.9919	.9891	.9809	.9148	.6779	.4674	.3686	.3011	.2430
10.50	.9901	.9855	.9529	.7567	.5424	.3799	.3055	.2560	.2116
11.50	.9877	.9702	.8438	.6058	.4362	.3148	.2598	.2221	.1902
12.50	.9802	.9148	.6808	.4854	.3579	.2669	.2251	.1975	.1734
13.50	.9515	.7566	.5447	.3946	.2987	.2305	.1994	.1796	.1581
14.50	.8370	.6057	.4383	.3257	.2545	.2031	.1813	.1640	.1444
15.50	.6747	.4854	.3594	.2751	.2214	.1845	.1656	.1499	.1322

	B = -.0025 ATM							
Y, IN.	A = 1.1359	1.1379	1.1389	1.1385	1.1389	1.1321	1.1264	1.1235	1.1169
.50	1.0000	1.0000	.9992	.9977	.9960	.9940	.9926	.9908	.9882
1.50	1.0000	1.0000	.9982	.9966	.9948	.9928	.9909	.9886	.9829
2.50	1.0000	.9987	.9971	.9954	.9935	.9911	.9888	.9840	.9551
3.50	.9992	.9976	.9960	.9942	.9922	.9890	.9844	.9606	.8472
4.50	.9981	.9966	.9948	.9929	.9904	.9853	.9631	.8742	.6775
5.50	.9971	.9954	.9935	.9913	.9881	.9677	.8861	.7022	.5374
6.50	.9960	.9941	.9922	.9893	.9823	.9073	.7132	.5579	.4279
7.50	.9947	.9929	.9904	.9862	.9548	.7363	.5676	.4453	.3490
8.50	.9934	.9913	.9881	.9725	.8492	.5862	.4529	.3619	.2907
9.50	.9921	.9893	.9823	.9190	.6823	.4676	.3676	.2998	.2472
10.50	.9903	.9861	.9549	.7621	.5433	.3785	.3038	.2540	.2142
11.50	.9879	.9722	.8494	.6072	.4350	.3125	.2575	.2199	.1919
12.50	.9811	.9179	.6825	.4843	.3555	.2643	.2227	.1958	.1746
13.50	.9524	.7597	.5435	.3921	.2961	.2279	.1975	.1779	.1590
14.50	.8371	.6052	.4351	.3227	.2518	.2009	.1794	.1620	.1450
15.50	.6713	.4825	.3556	.2720	.2184	.1823	.1634	.1478	.1325

Approximately one week was allowed for equilibration with the majority of the water production occurring during the first two days. Following this period for each drainage the intensity of the transmitted light was metered for all 192 viewable points. These meter readings were reduced to intensities from the calibration data, divided by intensities obtained at total water saturation for the corresponding points and plotted as relative intensities against the calculated water saturations. The correlation obtained between water saturation and relative intensity is shown in Figure 17. Each data point represents the logarithmic average relative intensity for all 16 points monitored in a horizontal row. The corresponding water saturation values are those presented in Table II for B = -0.004 atm.

The working form of Figure 17 included row numbers for all points. With each point identified in this manner it was apparent that a systematic deviation from the overall curve existed. This is not surprising because of the presence of the hold down bars and the boundaries. An effort was made to eliminate these effects by postulating that the total intensity seen at a point could be resolved into a "base intensity" for that point plus the contribution from the other elements of the system. The mathematical model was:

$$I_{t_{i,j}} = \sum_{\ell=1}^{i_m} \sum_{m=1}^{j_m} F_{\ell,m} I_{b_{\ell,m}} \tag{122a}$$

with

$$I_{b_{i,j}} = \text{base intensity, point } (i,j) \tag{122b}$$

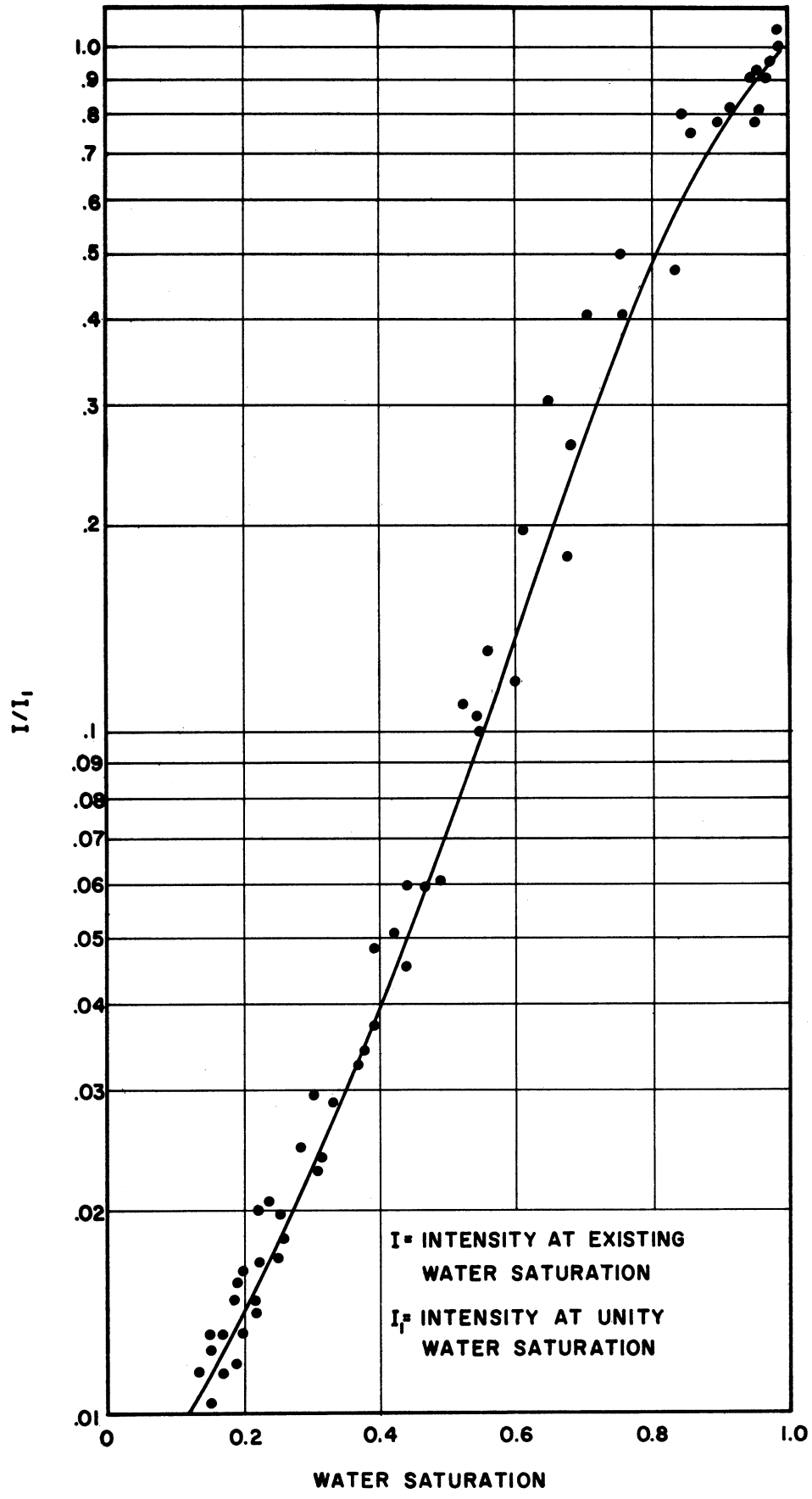

Figure 17. Overall Relative Intensity - Water Saturation Correlation.

$F_{\ell,m}$ = geometric altenuation factor, point (ℓ,m) (122c)

$$F_{i,j} = 1 \tag{122d}$$

Summation is done over the whole face.

Base intensities for elements under bars are considered to be zero. Boundaries are considered to be partially reflecting.

$$I_{b_0,j} = A\, I_{b_1,j} \tag{122e}$$

The constant A is fractional reflectance.

The geometric factors were investigated by masking the rear face of the model except for one element of the grid system. Intensities were measured for the illuminated point and the neighboring points in the horizontal row. This was repeated for four rows at which water saturations were approximately 0.20, 0.35, 0.70 and 1.00. The data obtained are plotted in Figure 18 as ratios of the intensity seen at a point to that seen at the illuminated points.

This attenuation factor theoretically allows solution of the 192 simultaneous equations represented by Equation (122a). Inversion of a matrix of this size is out of the question. Several iterative attempts at solution on a "nearest neighbors" basis failed.

As a practical solution the over-all correlation of Figure 17 was resolved into seven separate curves with each applying for one or more of the 12 rows of elements. Although this approach does not account for the vertical boundaries, the effects of the bars and

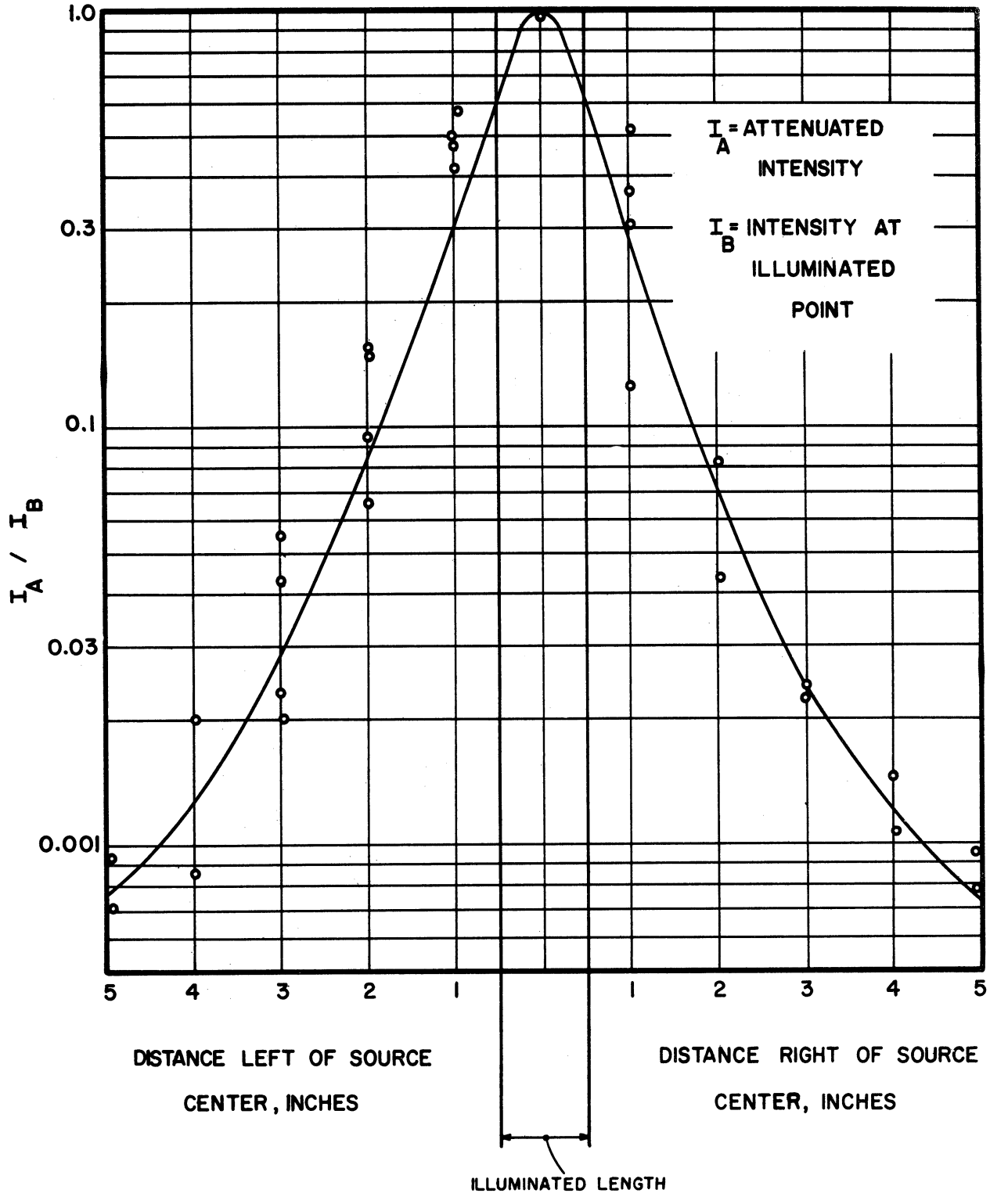

Figure 18. Geometric Attenuation Factor

horizontal boundaries are reduced. One of the resulting curves is shown in Figure 19. This curve applies to the top and third from the top rows, which behave similarly because of their positions with respect to the top boundary and upper hold-down bar. The other six curves fit the appropriate points to about the same degree as shown by this one.

After the nine successive drainages were made, the model was dried by flowing about 200 SCF of nitrogen through the packing. This was followed by two weeks of vacuum drying. A scan of transmitted light intensity was made on the dry pack for every second point to establish the zero end of the correlation for all seven curves.

Analysis of later data suggested two improvements which were subsequently employed in the conversion of meter readings to water saturations.

1. The intensity of the incident light supplied by the fluorescent lamps was found to vary during operation. This was evident from the systematic variations observed in the sets of data taken for total water saturation. Measurements showed the incident intensity to wander as much as 20 per cent on either side of the average. This must have been due to either or both line voltage fluctuation and lamp instability. Correction was applied to the set of unity water saturation intensities by frequently monitoring a point in the bottom row of elements where the water saturation did not change appreciably during displacement.

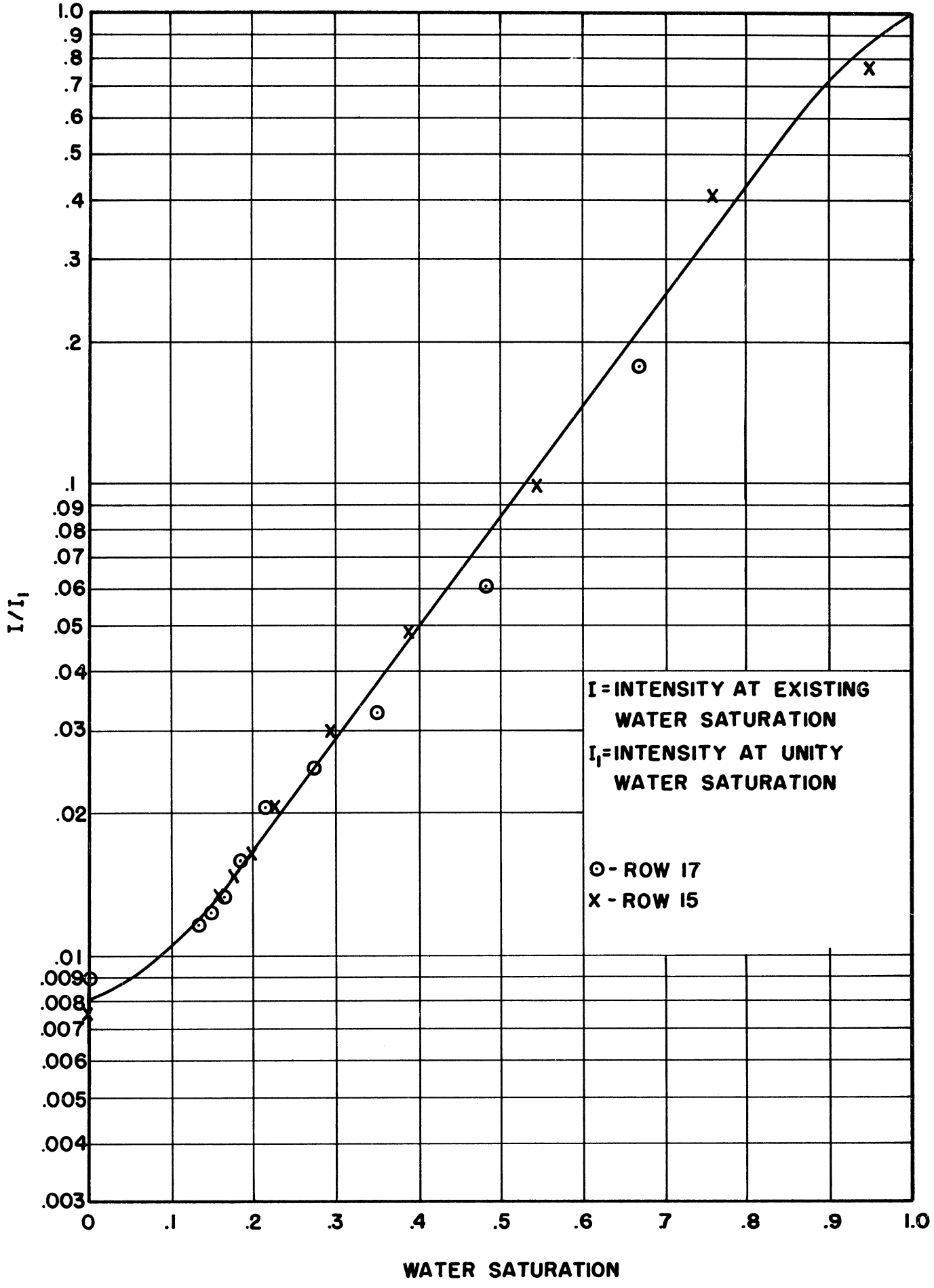

Figure 19. Row-Wise Relative Intensity - Water Saturation Correlation

2. Some improvement in the intensity matrix corresponding to zero water saturation was made. This was done on the basis of imbibition phase distributions obtained prior to the imbibition displacements. The assumption of one-dimensional phase distribution at imbibition equilibrium is more justifiable than for drainage because of physical stability considerations. Calibration, however, had to be done using drainage because of the difficulties involved in determining imbibition capillary pressure curves by the sampling technique. The average of the saturations measured across a row were taken to be the correct saturation for that row. Each point was assigned the zero saturation intensity which would result in that saturation. The average values obtained for the six data sets were used. The resulting adjustment seldom amounted to more than two saturation per cent.

It is estimated that a total of 10,000 intensity readings were taken. Due to the tremendous data processing load, machine computations were employed to convert meter readings to water saturations.

Duplicate sets of data taken prior to imbibition displacements demonstrate this technique to be reproducible to about 1.5 saturation per cent. These data appear in the Experimental Results section.

C. Operating Procedure

One drainage and three imbibition displacements were made. For all displacements, the water saturation data were obtained in the

the same manner. Viewable points were continually monitored allowing 90 seconds for photocell equilibration at each point. A complete measurement cycle including removal of the drape, positioning the mounting apparatus, replacement of the drape and metering of eight points took about 14 minutes. Readings were concentrated in zones of most rapidly changing water saturation. Displacements proceeded on a 24-hour a day basis lasting from one to three days. Light measurements normally were taken for about 16 hours of each operating day.

Prior to all displacements, the model was filled to total saturation with deaerated water. This was accomplished either by evacuation of the dry pack or by repeated pressuring to 50 psig with subsequent flushing with water. In either case, total water saturation was evidenced by a sharp rise in pressure from atmospheric on injection of a small volume of water into the model with production wells closed. Total water saturation was desired to provide a reliable material balance datum.

In the drainage displacement, water saturated helium was injected into the pack through the well at the upper left corner. A rate of 8 cc/hr was approximated over the displacement by making periodic rate checks with the soap film apparatus. The injection pressure was shown on the capillary manometer. Water production, followed later by gas production, occurred through the well at the lower right corner. The production pressure was fixed at about 2 feet of water by the constant head device. Hourly records

were kept of total phase production and gas injection pressure. Operation was continued until production was gas phase only.

The imbibition displacements were started from an equilibrium saturation distribution established by water imbibition. This was accomplished by injecting helium into the model previously saturated with water. Injection was through three wells along the top edge with production from three wells along the bottom into a buret via the constant head device. After helium breakthrough, the production line was attached to the tip of the water buret. The imbibition production apparatus shown in Figure 13b was connected to the upper left well with the pressure level set above atmospheric by about 6 inches of water. Imbibition of water was begun by elevating the water buret to the desired position. After imbibition had ceased, several days were allowed for equilibration. In each case duplicate intensity scans were made to determine the initial phase distribution. The average initial water saturation was established by over-all material balance considerations.

In the first imbibition displacement, water was injected at the lower right well at a nominal rate of 10 cc/hr controlled by the Ruska pump. The rate was obtained accurately by recording the injected volume hourly. Production occurred through the upper left well. Produced volumes were also recorded. Operation was continued for a short period following water breakthrough.

The last two displacements were run as identically as possible. Starting from essentially the same initial phase distribution,

water was injected at a nominal rate of 5 cc/hr through each of two wells located at the upper and lower right corners. Production was from the upper left corner. Except for the geometric differences, operation was the same as for the first imbibition displacement.

D. Data Analysis

During each displacement, the light intensity at each viewable grid point was metered from two to twelve times depending on the saturation change experienced by that point. Following conclusion of the displacement, the data were converted to water saturations.

The resulting water saturation values applied at a different time for each grid point. The objective was to obtain the point by point saturation distribution at a series of discrete time levels. To accomplish this, the water saturation data for all points were plotted against time on a row by row basis. Thus, if each point in a row had been metered six times, the plot for that row would contain 96 points. By passing a curve through all data points for a single element of the grid system, the water saturation was obtained at the desired time for that point. The behavior of the neighboring points in the row served as a guide in drawing the curve between data points. This was done for all 192 viewable points.

The water saturation distributions obtained in this manner were smoothed slightly by plotting the values for a horizontal row at each time level. The degree of smoothing never exceeded the estimated precision of the data.

For the four rows which were not viewable, point by point saturations were assigned by interpolation of the values obtained for the adjacent viewable rows. The water saturations measured or assigned for all 256 elements of the grid were adjusted to conform to the over-all material balance. Adjustment was done by iterative application of the following relationship:

$$S_{i,j}^{k+1} = S_{i,j}^{k}\left\{1+\frac{3}{2}\left[1-\left\{\frac{S_{i,j}^{k}-\left(\frac{S_{max}+S_{min}}{2}\right)}{\left(\frac{S_{max}-S_{min}}{2}\right)}\right\}^{2}\right]\cdot\left[\frac{S_{av}}{\sum_{i=1}^{i_m}\sum_{j=1}^{j_m}S_{i,j}^{k}}-1\right]\right\} \qquad (123a)$$

where

k = iteration number (123b)

S_{min} = minimum allowable water saturation (connate water) (123c)

S_{max} = maximum allowable water saturation (1 for drainage, residual gas for imbibition) (123d)

S_{av} = required average saturation (123e)

This method of adjustment retains the same "relative" distribution. That is, if the saturation for one point was initially lower than for a second point, the adjusted saturation would also be lower. For points at the minimum or maximum allowable saturation, no adjustment was desired. The greatest adjustment is seen to occur in the mid range of saturation with least near the minimum and maximum ends of the range. Gross adjustment was never required.

The experimental data are presented in the following section. For each data set, the smoothing and material balance adjustments are indicated.

VI. EXPERIMENTAL RESULTS

The results are presented and interpreted in the following order:

A. Porosity and Permeability.

B. Reproducibility of Saturation Measurement.

C. Two-Phase Displacements.

D. Over-all Displacement Reproducibility.

E. Discussion of Results.

Reproducibility of the light attenuation technique for measurement of water saturation is assessed by comparison of duplicate sets of initial distribution data for the last three displacements. Over-all reproducibility is assessed by comparison of the operating distributions observed during the last two displacements which were run as duplicates.

A. Porosity and Permeability

Porosity is ratio of the total pore volume to the superficial volume. The pore volume was measured by injecting deaerated water into the dried and evacuated pack. The result shown in Table III agrees to within 7 cc of the measurement supplied for the model by the Jersey Production Research Company. The pore volume measured here is the higher of the two and is considered correct because errors would be expected to cause a low measurement.

The permeability was measured with corner to corner water flow under conditions of total water saturation. Because of "well effects,"

edge wells 11/16 inch from the corner wells served as pressure taps. Pressure drop was measured with a differential manometer using an oil of 1.750 gm/cc density. The temperature of the produced water was taken in an insulated receiver to establish the water viscosity. Flow at three rates controlled by the Ruska pump was directed along both diagonals in both directions. Permeability was calculated according to the 5-spot equation given by Muskat[34].

$$Q = \frac{\pi K h \Delta p}{\mu \left[\log(d/r_w) - 0.6190\right]} \tag{124a}$$

for Q = rate, cc/hr (124b)

h = thickness, cm (17/32 inch) (124c)

d = diagonal length, cm ($16\sqrt{2}$ inches) (124d)

r_w = well radius, cm (11/16 inch) (124e)

For the model measurements and with Δp expressed in cm of oil, Equation (124a) reduces to:

$$K = 1.409\, Q\mu/\Delta p \tag{124f}$$

The average of the 12 measurements is presented in Table III. The average deviation of the measurements from this value was 2%. Since measurements were taken for flow along both diagonals, this degree of precision supports the assumption of pack homogeneity. Also, a permeability error of one per cent would be introduced through viscosity by a temperature error of 0.5°C or through pressure drop by a manometer error of 2 mm.

TABLE III

LABORATORY MODEL PROPERTIES

Pore volume	=	871 cc
Porosity	=	0.391
Permeability	=	10.2 Darcys

B. Reproducibility of Water Saturation Measurements

Duplicate measurements of the initial water saturation distributions were made for the imbibition displacements. These measurements served a dual purpose. They supplied the imbibition capillary pressure curve required for the numerical simulation of the imbibition displacements. They also provided a basis for assessment of the reproducibility of the light attenuation technique. The measured water saturations appear in Tables IVa, b and c for Displacements No. 2, 3 and 4, respectively.

These data are plotted on a row basis in Figure 26, the imbibition capillary pressure curve used in the numerical simulations.

The respective sets of data were compared point by point to yield average absolute and standard deviations. The results are presented in Table V which lists average and standard deviations on an over-all basis and by five water saturation ranges. These deviations are expressed in saturation per cent.

The comparisons indicate that the readings can be reproduced on the average to within 1.5 saturation per cent. Or, in other terms, two-thirds of the corresponding measurements of duplicate data sets lie within about two saturation per cent of each other. The best precision appears to result in the 40-80 per cent range. The author feels that this degree of reproducibility speaks well for the technique.

C. Two-Phase Displacements

Each displacement is taken up in chronological sequence. Experimental details have been discussed in the previous section.

TABLE IV

INITIAL WATER SATURATION DISTRIBUTIONS
IMBIBITION DISPLACEMENTS

a. LABORATORY DISPLACEMENT NO. 2

Set 1

EXPRESSED IN SATURATION PER CENT

.0	8.2	14.0	13.1	14.6	13.2	13.5	13.0	13.3	12.5	11.2	11.3	12.3	12.5	12.2	11.5
12.1	13.2	14.9	14.6	15.4	14.2	14.8	14.4	14.4	13.5	13.1	12.8	13.9	13.6	14.1	13.7
14.5	16.1	16.7	17.0	15.7	16.9	15.8	16.3	14.8	14.9	14.8	15.5	15.0	15.4	15.2	15.0
NOT VIEWABLE - UNDER HOLD-DOWN BAR - NOT VIEWABLE															
20.7	19.4	20.2	20.5	20.3	20.7	20.1	20.2	19.6	20.2	18.7	18.7	19.4	19.6	19.4	19.7
21.5	21.1	22.7	22.4	22.6	22.9	22.5	22.3	22.5	22.2	21.3	21.1	21.9	21.8	21.8	21.8
24.0	24.2	25.2	25.3	25.2	24.9	25.3	23.4	25.1	24.7	24.0	23.8	24.5	24.6	24.1	24.6
NOT VIEWABLE - UNDER HOLD-DOWN BAR - NOT VIEWABLE															
NOT VIEWABLE - UNDER HOLD-DOWN BAR - NOT VIEWABLE															
35.6	36.1	37.1	37.2	37.1	37.2	36.9	36.1	36.5	35.9	36.6	36.1	36.3	35.1	36.1	36.3
44.0	43.2	44.3	44.1	44.1	44.2	43.8	43.7	43.9	43.6	43.2	43.4	44.0	43.3	43.3	43.3
52.2	51.5	52.1	52.3	52.4	52.3	51.8	51.8	51.8	51.9	51.4	51.4	51.6	51.7	51.6	51.8
NOT VIEWABLE - UNDER HOLD-DOWN BAR - NOT VIEWABLE															
72.6	72.3	73.3	72.6	73.8	73.6	72.9	72.6	73.4	73.1	72.7	72.4	72.8	72.7	72.8	72.7
84.5	88.5	86.5	86.8	84.3	83.9	83.7	82.8	83.9	83.3	82.7	82.1	83.2	83.2	82.9	82.4
91.6	89.8	97.2	96.5	92.3	91.7	91.8	90.3	91.5	91.2	91.0	90.6	92.1	91.2	91.4	91.1

Set 2

EXPRESSED IN SATURATION PER CENT

18.9	14.4	9.0	10.5	7.8	10.4	10.1	10.6	10.3	11.1	12.3	12.2	11.3	11.1	11.4	12.1
14.6	13.5	11.7	12.0	11.2	12.4	11.8	12.2	12.2	13.1	13.6	13.7	12.8	13.0	12.5	12.9
15.4	13.8	13.2	12.9	14.2	12.9	14.1	13.6	15.2	15.0	15.2	14.4	14.3	14.5	14.8	15.0
NOT VIEWABLE - UNDER HOLD-DOWN BAR - NOT VIEWABLE															
17.6	19.0	18.2	17.8	18.1	17.7	18.4	18.1	18.8	18.2	19.7	19.7	19.0	18.8	19.0	18.7
21.9	22.3	20.7	21.0	20.8	20.5	20.9	21.1	20.9	21.2	22.1	22.3	21.5	21.6	21.6	21.6
25.1	24.8	23.8	23.7	23.8	24.1	23.7	25.6	23.9	24.3	25.0	25.2	24.6	24.4	24.9	24.5
NOT VIEWABLE - UNDER HOLD-DOWN BAR - NOT VIEWABLE															
NOT VIEWABLE - UNDER HOLD-DOWN BAR - NOT VIEWABLE															
37.8	37.4	36.3	36.3	36.3	36.2	36.5	37.3	36.9	37.5	36.8	37.4	37.1	38.3	37.2	37.1
43.0	43.8	42.7	42.9	42.9	42.8	43.2	43.4	43.1	43.4	43.8	43.6	43.8	43.6	43.7	43.7
51.4	52.1	51.5	51.3	51.2	51.3	51.8	51.8	51.8	51.7	52.2	52.2	52.0	51.9	52.0	51.8
NOT VIEWABLE - UNDER HOLD-DOWN BAR - NOT VIEWABLE															
73.2	73.5	72.5	73.2	72.0	72.2	72.9	73.2	72.4	72.7	73.1	73.4	73.0	73.1	73.0	73.1
83.9	80.2	81.9	81.5	84.1	84.5	84.7	85.6	84.5	85.1	85.7	86.3	85.2	85.2	85.5	86.0
92.2	94.3	87.9	88.4	91.5	92.1	92.0	93.5	92.2	92.6	92.8	93.2	91.7	92.6	92.4	92.6

b. LABORATORY DISPLACEMENT NO. 3

Set 1

EXPRESSED IN SATURATION PER CENT

18.3	17.2	20.1	19.6	18.2	18.7	21.3	20.6	17.8	17.8	17.5	17.9	19.0	19.1	18.4	17.0
6.2	19.5	24.2	23.5	22.5	23.2	23.5	24.1	22.4	22.2	20.7	21.4	22.6	22.3	22.2	23.5
24.0	23.9	26.8	27.8	26.8	26.7	28.4	27.2	27.3	27.9	24.3	24.5	26.3	26.1	26.5	25.2
NOT VIEWABLE - UNDER HOLD-DOWN BAR - NOT VIEWABLE															
33.4	32.2	35.2	35.0	35.2	34.9	35.3	35.2	34.6	34.3	33.9	33.8	34.0	34.3	34.4	35.1
42.0	39.4	42.6	42.1	42.1	42.5	42.1	42.1	42.4	42.7	41.4	41.7	40.7	41.2	41.4	43.2
49.0	48.3	49.1	48.4	49.2	48.9	49.5	49.7	49.3	49.1	49.1	48.7	48.9	48.5	49.9	49.3
NOT VIEWABLE - UNDER HOLD-DOWN BAR - NOT VIEWABLE															
NOT VIEWABLE - UNDER HOLD-DOWN BAR - NOT VIEWABLE															
76.3	77.4	76.2	75.7	75.2	76.1	76.4	77.0	76.3	74.1	75.6	76.4	76.3	76.9	77.4	78.6
87.8	83.4	85.4	82.6	85.7	85.0	85.6	84.5	86.0	84.8	84.0	84.2	84.9	83.6	83.7	85.1
87.0	85.9	82.4	80.5	86.4	84.9	86.8	86.5	88.0	86.2	86.1	86.7	88.9	87.6	89.9	88.8
NOT VIEWABLE - UNDER HOLD-DOWN BAR - NOT VIEWABLE															
86.2	85.2	86.3	86.7	92.2	92.2	91.8	91.8	90.3	92.6	95.7	92.7	90.5	94.0	93.7	88.4
81.3	85.2	82.4	82.8	88.2	91.5	96.3	100.0	99.3	97.1	96.1	96.5	94.5	95.0	91.5	90.9
82.4	94.9	85.0	85.4	89.9	92.5	93.5	97.7	93.2	94.5	95.0	98.0	94.5	95.0	94.9	94.5

Set 2

EXPRESSED IN SATURATION PER CENT

25.4	.0	17.5	18.7	18.7	19.8	16.2	15.5	19.3	20.8	18.1	18.6	18.7	20.0	20.3	23.1
24.6	24.3	21.8	20.4	22.7	22.5	20.0	20.5	23.4	22.7	21.8	22.3	21.9	21.6	23.3	23.2
27.8	25.3	24.5	24.6	25.9	24.7	24.0	23.6	26.6	27.3	25.2	25.2	25.3	25.2	25.6	24.4
NOT VIEWABLE - UNDER HOLD-DOWN BAR - NOT VIEWABLE															
35.4	34.8	35.2	34.5	35.3	35.2	33.1	33.1	35.2	34.9	34.0	33.8	34.5	34.8	34.4	34.7
42.6	40.2	41.6	41.8	42.1	42.5	40.6	40.7	42.7	43.2	41.4	41.7	40.7	41.4	41.4	42.5
48.5	49.7	48.8	48.7	49.4	48.9	47.9	48.4	49.6	48.7	48.9	48.5	48.9	48.5	49.4	49.2
NOT VIEWABLE - UNDER HOLD-DOWN BAR - NOT VIEWABLE															
NOT VIEWABLE - UNDER HOLD-DOWN BAR - NOT VIEWABLE															
77.0	78.0	76.1	76.4	76.7	77.7	76.1	77.3	77.5	75.7	77.0	77.2	77.2	76.7	77.9	79.0
84.1	83.3	80.1	80.3	83.7	84.9	84.3	85.4	85.0	84.8	84.3	85.1	83.8	83.2	84.7	86.7
84.8	87.1	78.0	82.3	85.9	86.7	85.4	86.8	87.5	87.8	85.6	87.4	88.3	88.4	90.8	91.2
NOT VIEWABLE - UNDER HOLD-DOWN BAR - NOT VIEWABLE															
85.0	84.9	86.6	83.1	93.2	92.9	93.0	93.0	91.8	94.0	94.4	92.9	91.5	94.0	93.5	89.3
81.4	84.6	84.9	85.4	90.0	91.6	95.0	100.0	100.0	96.4	94.6	95.0	93.1	94.4	92.5	93.0
86.4	93.9	88.7	87.6	90.7	91.2	92.4	96.5	93.3	93.1	95.1	96.6	93.3	95.6	95.9	95.0

TABLE IV (CONT'D)

c. LABORATORY DISPLACEMENT NO.

Set 1

EXPRESSED IN SATURATION PER CENT

17.7	18.2	20.9	21.0	20.0	20.0	21.6	21.3	19.5	19.3	18.6	18.5	19.5	19.3	19.5	19.6
21.9	22.5	23.7	23.7	22.8	22.9	24.1	24.1	22.7	21.9	21.5	21.7	22.4	22.4	22.5	22.7
25.2	25.5	27.1	27.3	25.7	26.0	27.5	27.3	25.8	24.6	25.1	25.0	25.7	26.0	25.7	25.8
NOT VIEWABLE - UNDER HOLD-DOWN BAR - NOT VIEWABLE															
34.0	34.3	35.2	35.2	35.0	35.1	35.6	35.5	34.6	34.5	33.9	34.0	34.0	34.3	34.4	34.5
41.0	40.6	41.9	41.6	41.2	41.2	42.0	42.0	40.9	40.5	40.3	40.3	41.5	41.2	40.9	40.7
48.6	48.3	49.4	49.1	49.1	49.3	49.4	49.6	48.7	48.7	48.5	48.5	48.9	48.7	48.9	49.2
NOT VIEWABLE - UNDER HOLD-DOWN BAR - NOT VIEWABLE															
NOT VIEWABLE - UNDER HOLD-DOWN BAR - NOT VIEWABLE															
78.7	77.9	79.5	78.4	79.0	78.6	79.4	78.9	78.6	78.2	78.6	78.3	78.9	78.9	78.9	78.7
89.9	85.6	91.4	89.9	87.4	86.5	87.0	85.9	86.6	85.7	85.2	85.0	86.5	85.9	85.5	85.2
89.7	90.9	91.4	91.4	90.4	91.7	92.0	91.5	90.9	91.3	91.6	91.6	91.6	91.2	91.6	92.0
NOT VIEWABLE - UNDER HOLD-DOWN BAR - NOT VIEWABLE															
92.7	92.1	92.7	91.0	93.3	92.5	93.7	93.3	93.3	92.9	94.9	94.9	92.8	93.3	94.5	93.7
93.6	92.0	94.2	93.6	93.6	93.6	94.1	93.6	93.6	93.6	94.0	93.6	93.6	93.2	93.6	93.6
88.6	94.1	91.7	94.5	92.5	92.9	94.2	96.3	93.4	93.8	94.5	94.5	93.6	93.6	94.C	93.1

Set 2

EXPRESSED IN SATURATION PER CENT

21.9	21.4	18.7	18.6	19.6	19.6	18.0	18.3	20.1	20.3	21.0	21.1	20.1	20.3	20.1	20.C
23.7	23.1	21.9	21.9	22.8	22.7	21.5	21.5	23.0	23.7	24.1	23.9	23.2	23.2	23.1	22.9
26.7	26.5	24.9	24.7	26.3	26.0	24.5	24.7	26.2	27.3	26.9	27.0	26.3	26.0	26.3	26.2
NOT VIEWABLE - UNDER HOLD-DOWN BAR - NOT VIEWABLE															
35.4	35.1	34.2	34.2	34.4	34.3	33.8	33.9	34.8	34.9	35.5	35.4	35.4	35.0	35.0	34.9
41.4	41.8	40.5	40.8	41.1	41.2	40.4	40.4	41.5	41.9	42.1	42.1	40.9	41.2	41.5	41.7
49.2	49.5	48.3	48.7	48.7	48.5	48.4	48.2	49.1	49.1	49.3	49.2	48.9	49.C	48.9	48.6
NOT VIEWABLE - UNDER HOLD-DOWN BAR - NOT VIEWABLE															
NOT VIEWABLE - UNDER HOLD-DOWN BAR - NOT VIEWABLE															
79.3	80.2	78.5	79.6	79.0	79.5	78.6	79.1	79.4	79.8	79.4	79.7	79.1	79.1	79.1	79.3
84.9	88.7	83.8	84.9	86.8	87.7	87.2	88.2	87.6	88.5	89.3	89.6	87.7	88.3	88.9	89.3
92.9	91.7	91.2	91.2	92.2	91.0	90.6	91.1	91.7	91.3	91.0	91.0	91.0	91.4	91.C	90.6
NOT VIEWABLE - UNDER HOLD-DOWN BAR - NOT VIEWABLE															
93.9	94.5	93.9	95.6	93.3	94.1	92.9	93.3	93.3	93.7	91.7	91.7	93.6	93.3	92.1	92.9
93.6	95.2	93.0	93.6	93.6	93.6	93.1	93.6	93.6	93.6	93.2	93.6	93.6	94.0	93.6	93.6
100.0	93.5	96.0	93.0	95.1	94.7	93.4	91.4	94.2	93.8	93.1	93.2	94.C	94.0	93.6	94.5

TABLE V

REPRODUCIBILITY OF TECHNIQUE

LABORATORY DISPLACEMENT NO. 2

AVERAGE AND STANDARD DEVIATION BY WATER SATURATION RANGE

EXPRESSED IN SATURATION PER CENT

FROM	TO	NO. PTS	AVG. DEV.	STD. DEV.
.0	20.0	96	1.8	2.3
20.0	40.0	58	1.3	1.5
40.0	60.0	32	.6	.8
60.0	80.0	16	.7	.8
80.0	100.0	32	2.5	3.5
OVERALL		192	1.5	2.1

LABORATORY DISPLACEMENT NO. 3

AVERAGE AND STANDARD DEVIATION BY WATER SATURATION RANGE

EXPRESSED IN SATURATION PER CENT

FROM	TO	NO. PTS	AVG. DEV.	STD. DEV.
.0	20.0	15	4.3	7.1
20.0	40.0	50	1.5	2.0
40.0	60.0	31	.4	.7
60.0	80.0	16	.8	.9
80.0	100.0	80	1.2	1.6
OVERALL		192	1.4	2.5

LABORATORY DISPLACEMENT NO. 4

AVERAGE AND STANDARD DEVIATION BY WATER SATURATION RANGE

EXPRESSED IN SATURATION PER CENT

FROM	TO	NO. PTS	AVG. DEV.	STD. DEV.
.0	20.0	12	1.5	1.9
20.0	40.0	52	1.3	1.6
40.0	60.0	32	.8	.9
60.0	80.0	16	.8	1.0
80.0	100.0	80	1.6	2.5
OVERALL		192	1.3	1.9

1. Displacement No. 1 - Drainage

Helium was injected at the upper left corner into the pack initially saturated with water. Production occurred at the lower right corner.

Although gas injection pressure was recorded, it was found to correspond closely to the water hydrostatic pressure due to the constant head. This coupled with well effects rendered the measurements insignificant and they are not included.

The integral water production data are listed in Table VI.

TABLE VI

OPERATING SUMMARY

Displacement No. 1
Initial Water in P.V. = 871 cc

Time	Water Produced	Time	Water Produced
2 hrs	9 cc	30 hrs	234 cc
5	32	35	277
10	72	40	319
15	113	45	360
20	152	50	405
25	192	55	458

Breakthrough Water Production = 586 cc
Breakthrough Time = 64.1 hrs.

During the interval from 55 hours to breakthrough, water saturations were not monitored. At breakthrough, production switched sharply from water to gas, the gas injection pressure dropped and the gas rate increased rapidly. This behavior would be expected because of the fingering associated with the gas phase movement.

Water saturation distributions obtained during the displacement appear for six displacement times in Tables VIIa-f. Indicated in each table is the degree of adjustment required to satisfy the material balance. The distributions appear at the odd displacement times because numerical solutions were tabulated at these times. For reasons discussed in Appendix II, time increments for drainage displacements could not always be preset. This is due to the unstable nature of the drainage displacement which is encountered in numerical simulation as well as in the laboratory.

Very little smoothing of raw water saturation data was done in view of the fingering known to be present. As discussed earlier, smoothing was done by plotting water saturation for the points in a row. This procedure has been illustrated in Figures 20 a-c for the top three rows of elements. The top row is numbered 17, with 16 and 15 applying in order of decreasing height. Points denote raw data with the curve denoting smoothed data. Column indices are indicated with the leftmost index corresponds to the leftmost grid element of the row.

It take little imagination to see the formation and dissipation of the fingers. By the five-hour mark in the drainage, regions of low saturation had formed at either end of the top row. These fingers are seen to damp out through the medium at the lower rows. By the 10.59 hour mark, the distribution existing at row 15 was quite similar to that for row 17 at the earlier time. The distribution pattern for the higher rows had changed somewhat. At the top row, the inlet end effect was beginning to appear which remained until the drainage had proceeded

TABLE VII

EXPERIMENTAL WATER SATURATION DISTRIBUTIONS

a. LABORATORY DISPLACEMENT NO. 1 AFTER 5.00 HOURS OF INJECTION

839 CC WATER IN TOTAL MODEL PORE VOLUME OF 871 CC - AVERAGE WATER SATURATION OF 96.33 PER CENT

AVERAGE WATER SATURATION FROM RAW DATA IS 95.88 PER CENT ADJUSTED TO 96.28 PER CENT

ADJUSTED WATER SATURATION AT VIEWABLE POINTS

BY ROWS FROM UPPER LEFT

58.3	65.5	58.3	62.4	66.5	72.5	73.4	71.5	69.5	70.5	74.4	72.5	68.5	62.4	57.3	56.2
78.3	91.3	86.8	89.5	91.3	90.4	90.4	90.4	91.3	92.2	92.2	92.2	91.3	90.4	86.8	82.1
84.9	96.6	91.3	92.2	92.2	93.1	93.1	94.0	94.9	94.9	94.9	93.1	91.3	91.3	92.2	92.2
NOT VIEWABLE - UNDER HOLD-DOWN BAR - NOT VIEWABLE															
97.5	98.3	97.5	98.3	98.3	98.3	98.3	98.3	98.3	98.3	98.3	99.2	99.2	99.2	99.2	96.3
99.2	99.2	99.2	99.2	99.2	99.2	99.2	99.2	99.2	99.2	99.2	99.2	99.2	99.2	99.2	99.2
99.2	99.2	99.2	99.2	99.2	99.2	99.2	99.2	99.2	99.2	99.2	99.2	99.2	99.2	99.2	99.2
NOT VIEWABLE - UNDER HOLD-DOWN BAR - NOT VIEWABLE															
NOT VIEWABLE - UNDER HOLD-DOWN BAR - NOT VIEWABLE															
100.0	100.0	100.0	100.0	100.0	100.0	100.0	100.0	100.0	100.0	100.0	100.0	100.0	100.0	100.0	100.0
100.0	100.0	100.0	100.0	100.0	100.0	100.0	100.0	100.0	100.0	100.0	100.0	100.0	100.0	100.0	100.0
100.0	100.0	100.0	100.0	100.0	100.0	100.0	100.0	100.0	100.0	100.0	100.0	100.0	100.0	100.0	100.0
NOT VIEWABLE - UNDER HOLD-DOWN BAR - NOT VIEWABLE															
100.0	100.0	100.0	100.0	100.0	100.0	100.0	100.0	100.0	100.0	100.0	100.0	100.0	100.0	100.0	100.0
100.0	100.0	100.0	100.0	100.0	100.0	100.0	100.0	100.0	100.0	100.0	100.0	100.0	100.0	100.0	100.0
100.0	100.0	100.0	100.0	100.0	100.0	100.0	100.0	100.0	100.0	100.0	100.0	100.0	100.0	100.0	100.0

b. LABORATORY DISPLACEMENT NO. 1 AFTER 10.59 HOURS OF INJECTION

798 CC WATER IN TOTAL MODEL PORE VOLUME OF 871 CC - AVERAGE WATER SATURATION OF 91.53 PER CENT

AVERAGE WATER SATURATION FROM RAW DATA IS 90.95 PER CENT ADJUSTED TO 91.49 PER CENT

ADJUSTED WATER SATURATION AT VIEWABLE POINTS

BY ROWS FROM UPPER LEFT

45.8	44.7	36.3	35.2	36.3	38.4	41.5	41.5	40.5	41.5	42.6	38.4	38.4	35.2	35.2	37.3
57.3	56.2	55.2	61.4	63.4	63.4	63.4	62.4	65.5	65.5	62.4	60.4	61.4	58.3	53.1	46.8
73.4	73.4	79.3	83.1	84.0	86.8	86.8	86.8	87.7	86.8	85.9	81.2	81.2	82.1	75.4	73.4
NOT VIEWABLE - UNDER HOLD-DOWN BAR - NOT VIEWABLE															
97.5	96.6	94.0	94.9	95.7	96.6	96.6	96.6	96.6	96.6	97.5	97.5	96.6	96.6	96.6	96.6
96.6	97.5	97.5	97.5	98.3	98.3	98.3	98.3	98.3	99.2	99.2	98.3	97.5	97.5	97.5	97.5
96.6	98.3	98.3	98.3	98.3	98.3	98.3	98.3	98.3	99.2	99.2	98.3	98.3	98.3	98.3	97.5
NOT VIEWABLE - UNDER HOLD-DOWN BAR - NOT VIEWABLE															
NOT VIEWABLE - UNDER HOLD-DOWN BAR - NOT VIEWABLE															
100.0	100.0	100.0	100.0	100.0	100.0	100.0	100.0	100.0	100.0	100.0	100.0	100.0	100.0	100.0	100.0
100.0	100.0	100.0	100.0	100.0	100.0	100.0	100.0	100.0	100.0	100.0	100.0	100.0	100.0	100.0	100.0
100.0	100.0	100.0	100.0	100.0	100.0	100.0	100.0	100.0	100.0	100.0	100.0	100.0	100.0	100.0	100.0
NOT VIEWABLE - UNDER HOLD-DOWN BAR - NOT VIEWABLE															
100.0	100.0	100.0	100.0	100.0	100.0	100.0	100.0	100.0	100.0	100.0	100.0	100.0	100.0	100.0	100.0
100.0	100.0	100.0	100.0	100.0	100.0	100.0	100.0	100.0	100.0	100.0	100.0	100.0	100.0	100.0	100.0
100.0	100.0	100.0	100.0	100.0	100.0	100.0	100.0	100.0	100.0	100.0	100.0	100.0	100.0	100.0	100.0

c. LABORATORY DISPLACEMENT NO. 1 AFTER 14.29 HOURS OF INJECTION

765 CC WATER IN TOTAL MODEL PORE VOLUME OF 871 CC - AVERAGE WATER SATURATION OF 87.77 PER CENT

AVERAGE WATER SATURATION FROM RAW DATA IS 86.72 PER CENT ADJUSTED TO 87.73 PER CENT

ADJUSTED WATER SATURATION AT VIEWABLE POINTS

BY ROWS FROM UPPER LEFT

39.2	38.1	27.2	23.9	25.0	27.2	30.5	30.5	29.4	31.6	29.4	28.3	28.3	27.2	28.3	31.6
48.0	46.9	38.1	42.5	43.6	43.6	43.6	43.6	46.9	48.0	45.8	43.6	43.6	42.5	42.5	38.1
58.7	59.7	60.8	68.0	68.0	68.0	67.0	67.0	69.0	69.0	70.0	65.9	65.9	63.9	62.9	59.7
NOT VIEWABLE - UNDER HOLD-DOWN BAR - NOT VIEWABLE															
94.5	93.7	87.8	88.7	92.1	93.7	94.5	94.5	94.5	93.7	95.3	96.1	93.7	92.9	92.9	92.9
96.1	97.7	96.9	96.9	96.9	97.7	97.7	98.5	98.5	97.7	97.7	97.7	96.9	96.9	96.9	96.1
95.3	98.5	98.5	98.5	98.5	98.5	98.5	98.5	99.2	99.2	99.2	99.2	98.5	98.5	97.7	96.1
NOT VIEWABLE - UNDER HOLD-DOWN BAR - NOT VIEWABLE															
NOT VIEWABLE - UNDER HOLD-DOWN BAR - NOT VIEWABLE															
99.2	99.2	99.2	99.2	99.2	99.2	99.2	99.2	99.2	99.2	99.2	99.2	99.2	99.2	99.2	99.2
99.2	99.2	99.2	99.2	99.2	99.2	99.2	99.2	99.2	99.2	99.2	99.2	99.2	99.2	99.2	99.2
99.2	99.2	99.2	99.2	99.2	99.2	99.2	99.2	99.2	99.2	99.2	99.2	99.2	99.2	99.2	99.2
NOT VIEWABLE - UNDER HOLD-DOWN BAR - NOT VIEWABLE															
100.0	100.0	100.0	100.0	100.0	100.0	100.0	100.0	100.0	100.0	100.0	100.0	100.0	100.0	100.0	100.0
100.0	100.0	100.0	100.0	100.0	100.0	100.0	100.0	100.0	100.0	100.0	100.0	100.0	100.0	100.0	100.0
100.0	100.0	100.0	100.0	100.0	100.0	100.0	100.0	100.0	100.0	100.0	100.0	100.0	100.0	100.0	100.0

TABLE VII (CONT'D)

d. LABORATORY DISPLACEMENT NO. 1 AFTER 25.27 HOURS OF INJECTION

674 CC WATER IN TOTAL MODEL PORE VOLUME OF 871 CC - AVERAGE WATER SATURATION OF 77.39 PER CENT

AVERAGE WATER SATURATION FROM RAW DATA IS 75.81 PER CENT ADJUSTED TO 77.35 PER CENT

ADJUSTED WATER SATURATION AT VIEWABLE POINTS

BY ROWS FROM UPPER LEFT

30.8	27.4	17.6	17.6	17.6	18.7	18.7	17.6	18.7	19.8	15.4	14.4	15.4	15.4	18.7	17.6
33.0	31.9	26.3	26.3	27.4	27.4	25.2	25.2	27.4	27.4	24.1	21.9	23.0	23.0	25.2	24.1
33.0	31.9	33.0	33.0	31.9	34.1	35.2	36.3	37.5	33.0	31.9	29.7	28.6	29.7	31.9	35.2
				NOT VIEWABLE - UNDER HOLD-DOWN BAR - NOT VIEWABLE											
56.2	63.6	60.5	57.3	60.5	61.5	62.6	63.6	64.7	64.7	62.6	61.5	59.4	58.4	54.0	56.2
70.8	81.3	73.7	72.8	76.6	78.5	80.4	81.3	81.3	80.4	78.5	78.5	77.6	73.7	71.8	69.8
84.0	94.1	92.5	90.9	92.5	93.3	94.1	92.5	92.5	95.6	95.6	94.1	91.7	90.0	87.5	84.9
				NOT VIEWABLE - UNDER HOLD-DOWN BAR - NOT VIEWABLE											
				NOT VIEWABLE - UNDER HOLD-DOWN BAR - NOT VIEWABLE											
96.4	97.1	97.8	97.8	98.6	98.6	98.6	98.6	98.6	98.6	98.6	98.6	98.6	98.6	98.6	98.6
97.8	98.6	97.1	97.1	99.3	99.3	99.3	99.3	99.3	99.3	99.3	99.3	99.3	99.3	99.3	99.3
99.3	99.3	98.6	99.3	99.3	99.3	99.3	99.3	99.3	99.3	99.3	99.3	99.3	99.3	99.3	99.3
				NOT VIEWABLE - UNDER HOLD-DOWN BAR - NOT VIEWABLE											
99.3	99.3	99.3	99.3	99.3	99.3	99.3	99.3	99.3	99.3	99.3	99.3	99.3	99.3	99.3	99.3
99.3	99.3	99.3	99.3	99.3	99.3	99.3	99.3	99.3	99.3	99.3	99.3	99.3	99.3	99.3	99.3
100.0	100.0	100.0	100.0	100.0	100.0	100.0	100.0	100.0	100.0	100.0	100.0	100.0	100.0	100.0	100.0

e. LABORATORY DISPLACEMENT NO. 1 AFTER 39.80 HOURS OF INJECTION

556 CC WATER IN TOTAL MODEL PORE VOLUME OF 871 CC - AVERAGE WATER SATURATION OF 63.77 PER CENT

AVERAGE WATER SATURATION FROM RAW DATA IS 60.14 PER CENT ADJUSTED TO 63.72 PER CENT

ADJUSTED WATER SATURATION AT VIEWABLE POINTS

BY ROWS FROM UPPER LEFT

14.9	12.6	7.1	7.1	7.1	8.2	9.2	9.2	10.3	10.3	9.2	8.2	7.1	6.0	10.3	12.6
17.2	19.6	12.6	12.6	13.7	13.7	12.6	12.6	14.9	14.9	12.6	11.4	11.4	12.6	13.7	14.9
14.9	18.4	16.0	16.0	14.9	18.4	18.4	17.2	19.6	18.4	17.2	17.2	14.9	14.9	14.9	17.2
				NOT VIEWABLE - UNDER HOLD-DOWN BAR - NOT VIEWABLE											
29.4	31.9	29.4	28.1	29.4	30.7	30.7	31.9	31.9	33.2	31.9	31.9	31.9	31.9	29.4	28.1
34.5	40.8	37.0	37.0	38.3	39.5	39.5	42.1	42.1	42.1	39.5	38.3	38.3	37.0	37.0	34.5
44.6	52.1	52.1	49.6	49.6	50.9	53.4	54.6	55.8	55.8	53.4	50.9	49.6	48.4	47.1	44.6
				NOT VIEWABLE - UNDER HOLD-DOWN BAR - NOT VIEWABLE											
				NOT VIEWABLE - UNDER HOLD-DOWN BAR - NOT VIEWABLE											
78.6	87.1	90.7	92.0	93.9	95.1	95.1	94.5	94.5	95.6	95.6	95.1	93.9	93.3	93.9	92.7
93.9	96.2	93.9	93.9	96.7	97.7	97.7	98.2	97.7	97.2	97.7	97.7	96.7	96.7	97.2	96.2
97.7	97.7	97.2	97.7	97.7	98.7	98.7	98.2	98.7	98.7	98.7	98.7	98.2	97.7	100.0	97.7
				NOT VIEWABLE - UNDER HOLD-DOWN BAR - NOT VIEWABLE											
99.6	99.6	99.6	99.6	99.6	99.6	99.6	99.6	99.6	99.6	99.6	99.6	99.6	99.6	99.6	99.6
99.6	99.6	99.6	99.6	99.6	99.6	99.6	99.6	99.6	99.6	99.6	99.6	99.6	99.6	99.6	99.6
99.6	99.6	99.6	99.6	99.6	99.6	99.6	99.6	99.6	99.6	99.6	99.6	99.6	99.6	99.6	99.6

f. LABORATORY DISPLACEMENT NO. 1 AFTER 50.32 HOURS OF INJECTION

464 CC WATER IN TOTAL MODEL PORE VOLUME OF 871 CC - AVERAGE WATER SATURATION OF 53.22 PER CENT

AVERAGE WATER SATURATION FROM RAW DATA IS 50.39 PER CENT ADJUSTED TO 53.18 PER CENT

ADJUSTED WATER SATURATION AT VIEWABLE POINTS

BY ROWS FROM UPPER LEFT

8.1	11.3	9.2	7.1	6.0	6.0	6.0	6.0	6.0	8.1	8.1	6.0	6.0	6.0	6.0	6.0
10.3	12.4	8.1	8.1	8.1	7.1	6.0	6.0	9.2	9.2	7.1	6.0	6.0	6.0	6.0	6.0
10.3	12.4	9.2	11.3	11.3	11.3	10.3	8.1	13.5	11.3	10.3	12.4	10.3	8.1	6.0	11.3
				NOT VIEWABLE - UNDER HOLD-DOWN BAR - NOT VIEWABLE											
19.2	21.5	19.2	18.0	19.2	20.3	18.0	18.0	20.3	22.6	19.2	26.1	21.5	21.5	18.0	16.9
22.6	21.5	23.8	23.8	23.8	22.6	21.5	21.5	25.0	26.1	23.8	23.8	22.6	22.6	23.8	21.5
27.3	29.7	27.3	28.5	29.7	29.7	27.3	27.3	32.1	32.1	29.7	29.7	28.5	27.3	29.7	30.9
				NOT VIEWABLE - UNDER HOLD-DOWN BAR - NOT VIEWABLE											
				NOT VIEWABLE - UNDER HOLD-DOWN BAR - NOT VIEWABLE											
58.2	65.9	70.1	69.1	69.1	69.1	69.1	68.1	70.1	74.2	70.1	68.1	65.9	63.7	65.9	60.4
74.2	83.5	82.6	83.5	85.2	84.3	84.3	86.0	87.6	88.4	87.6	83.5	81.7	81.7	81.7	76.2
86.8	91.4	91.4	92.1	95.4	94.8	94.1	94.8	94.8	95.4	94.8	94.8	94.1	92.8	94.8	86.8
				NOT VIEWABLE - UNDER HOLD-DOWN BAR - NOT VIEWABLE											
96.7	98.4	97.8	98.4	98.9	98.9	98.9	98.9	98.9	98.9	98.4	96.9	98.4	98.9	98.9	98.9
98.9	98.9	98.4	98.4	98.9	97.8	98.9	98.9	98.9	98.9	98.9	98.9	98.9	98.9	98.9	98.9
98.9	98.9	98.9	98.9	98.9	98.9	98.9	98.9	98.9	98.9	98.9	98.9	98.9	98.9	98.9	98.9

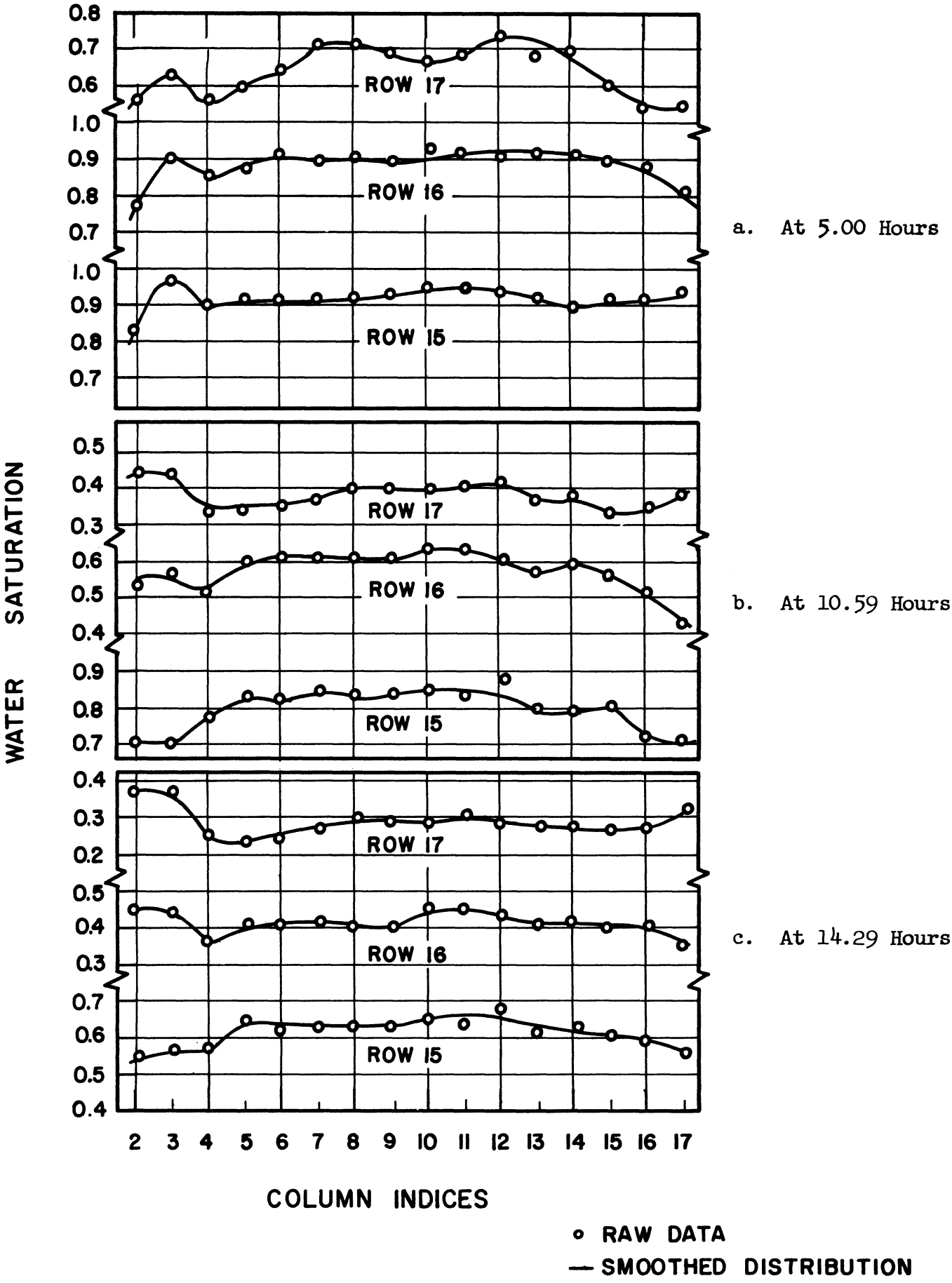

Figure 20. Row-Wise Water Solution Distribution
Displacement No. 1

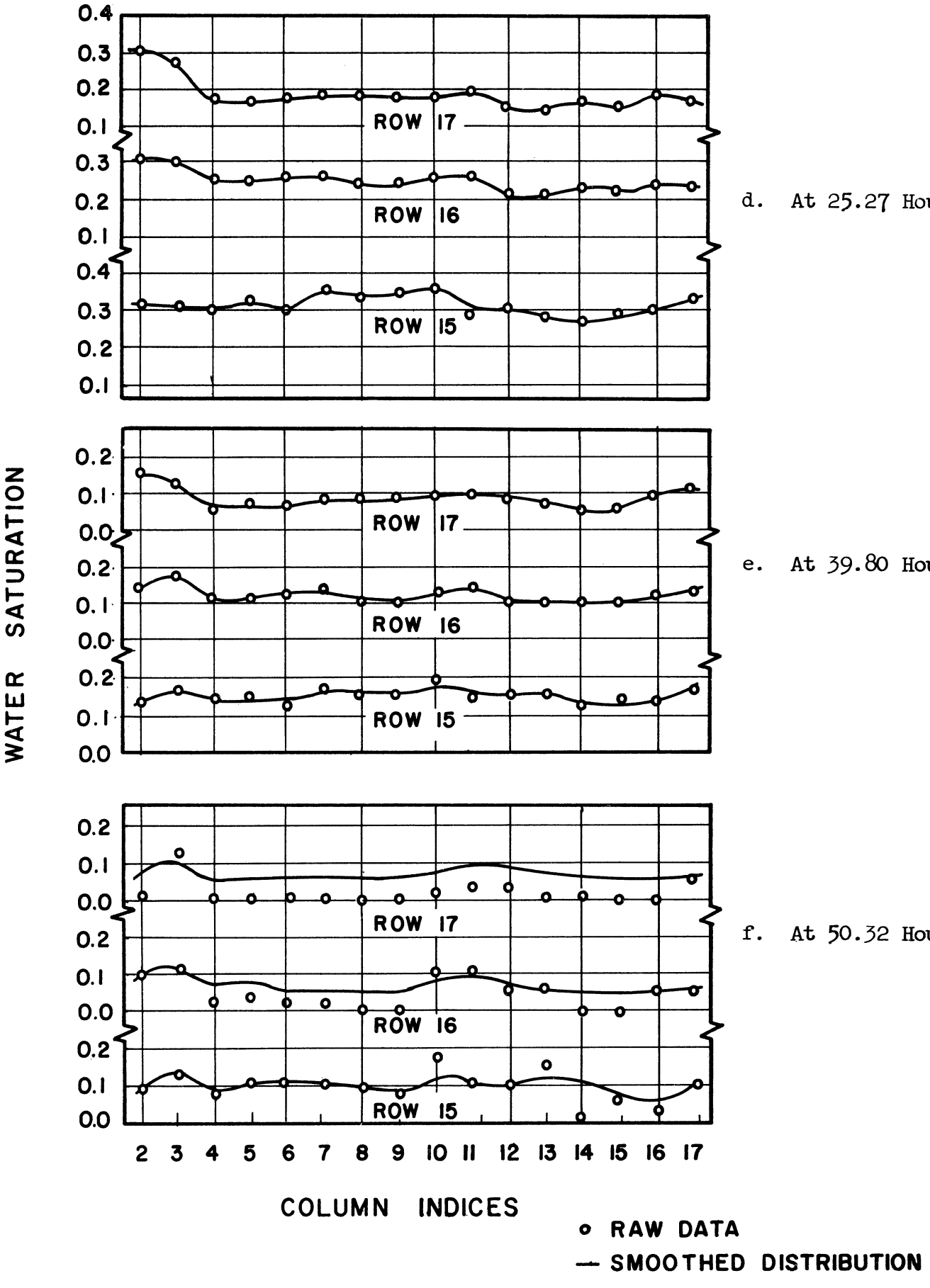

Figure 20 (Cont'd). Row-Wise Water Saturation Distribution
Displacement No. 1

TABLE VIII

COMPARISON OF SMOOTHED WATER SATURATION DATA WITH RAW DATA

LABORATORY DISPLACEMENT NO. 1

AFTER 5.00 HOURS OF INJECTION

AVERAGE AND STANDARD DEVIATION BY WATER SATURATION RANGE EXPRESSED IN SATURATION PER CENT

FROM	TO	NO. PTS	AVG. DEV.	STD. DEV.
.0	20.0	0	.0	.0
20.0	40.0	0	.0	.0
40.0	60.0	6	.2	.4
60.0	80.0	12	1.7	3.5
80.0	96.0	30	.5	.9
96.0	100.0	144	.0	.1
OVERALL		192	.2	.9

AFTER 10.59 HOURS OF INJECTION

AVERAGE AND STANDARD DEVIATION BY WATER SATURATION RANGE EXPRESSED IN SATURATION PER CENT

FROM	TO	NO. PTS	AVG. DEV.	STD. DEV.
.0	20.0	0	.0	.0
20.0	40.0	13	.4	.8
40.0	60.0	14	.8	1.3
60.0	80.0	13	.3	.6
80.0	96.0	23	.3	.8
96.0	100.0	129	.0	.1
OVERALL		192	.1	.5

AFTER 14.29 HOURS OF INJECTION

AVERAGE AND STANDARD DEVIATION BY WATER SATURATION RANGE EXPRESSED IN SATURATION PER CENT

FROM	TO	NO. PTS	AVG. DEV.	STD. DEV.
.0	20.0	0	.0	.0
20.0	40.0	21	.2	.6
40.0	60.0	17	.4	.6
60.0	80.0	10	.8	1.1
80.0	96.0	26	.3	.7
96.0	100.0	118	.0	.2
OVERALL		192	.2	.5

AFTER 25.27 HOURS OF INJECTION

AVERAGE AND STANDARD DEVIATION BY WATER SATURATION RANGE EXPRESSED IN SATURATION PER CENT

FROM	TO	NO. PTS	AVG. DEV.	STD. DEV.
.0	20.0	14	.1	.3
20.0	40.0	34	.4	.9
40.0	60.0	16	.2	.8
60.0	80.0	17	.8	1.8
80.0	96.0	19	.6	1.0
96.0	100.0	92	.0	.0
OVERALL		192	.2	.8

AFTER 50.32 HOURS OF INJECTION

AVERAGE AND STANDARD DEVIATION BY WATER SATURATION RANGE EXPRESSED IN SATURATION PER CENT

FROM	TO	NO. PTS	AVG. DEV.	STD. DEV.
.0	20.0	66	2.6	4.0
20.0	40.0	30	.1	.3
40.0	60.0	8	.0	.0
60.0	80.0	23	.5	1.4
80.0	96.0	20	.3	.7
96.0	100.0	45	.0	.0
OVERALL		192	1.0	2.4

AFTER 39.80 HOURS OF INJECTION

AVERAGE AND STANDARD DEVIATION BY WATER SATURATION RANGE EXPRESSED IN SATURATION PER CENT

FROM	TO	NO. PTS	AVG. DEV.	STD. DEV.
.0	20.0	48	.5	.8
20.0	40.0	35	.1	.4
40.0	60.0	13	.2	.4
60.0	80.0	2	1.5	2.1
80.0	96.0	39	.4	.9
96.0	100.0	55	.0	.0
OVERALL		192	.3	.6

much further. At the 39.80 hour mark the inlet end effect began to disappear. The last time level shows the distributions to be reasonably uniform. Here the measurement quality deteriorates as the photocell operation becomes less reliable. It will be recalled that near connate water the intensity has been attenuated by more than two orders of magnitude. Similar data which were plotted for the remaining nine viewable rows have not been included due to space considerations, but the curves are readily available from Tables VII a-f. For the lower levels, fingering was also apparent but on a reduced scale in most cases.

The smoothing performed on the data is indicated in Table VIII in terms of average and standard deviations by saturation ranges and over-all as before. The deviations indicate that the smoothing done was well within the precision of the measurements. Of course, little if any smoothing was required in regions of high water saturation.

For this displacement as well as the others, graphical presentation and comparison of the data to the numerical solution is deferred until the next section.

2. Displacement No. 2

Water was injected at the lower right corner at the nominal rate of 10 cc/hr. The initial helium-water distribution has been listed in Table IVa. The initial water in the pore volume, the water rate, and breakthrough data are shown in Table IX.

TABLE IX

OPERATING SUMMARY
Displacement No. 2

Initial Water in P.V.	=	344 cc
Water Injection Rate	=	10.23 cc/hr
Breakthrough Time	=	41.68 hours
Water in P.V. at Breakthrough	=	770 cc

At breakthrough, production switched from gas to water with no significant period of two-phase production.

Water saturation distributions are tabulated at six even-hour time levels in Tables X a-f, with material balance adjustments indicated.

Smoothing was done as before by plotting row-wise water saturations. Shown in Figure 21 are the raw and smoothed data for all 12 viewable rows after 5 hours of injection. At the subsequent time levels, plots of raw-smoothed distributions were similar, but at higher water saturation levels.

Fingering as observed during the drainage was conspicuously absent for this displacement. All of the raw data are reasonably smooth except at row 8. The two points showing the greatest deviation in this raw were monitored by photo cell No. 2 which occasionally behaved erratically. Some outlet end effect appeared near the production well (left end of rows 16 and 17). Scrutiny of the data of Tables X a-f shows this effect to be present throughout the displacement.

The average and standard deviations compiled by comparing raw and smoothed water saturations for all 192 viewable points is indicated in Table XI for all six displacement times. The comparison shows the smoothing to be within the precision of the measurements.

3. Displacements No. 3 and 4

Since these displacements were run as duplicates, it is convenient to discuss them together.

TABLE X

EXPERIMENTAL WATER SATURATION DISTRIBUTION

a. LABORATORY DISPLACEMENT NO. 2 — AFTER 5 HOURS OF INJECTION

395 CC WATER IN TOTAL MODEL PORE VOLUME OF 871 CC - AVERAGE WATER SATURATION OF 45.31 PER CENT

AVERAGE WATER SATURATION FROM RAW DATA IS 43.64 PER CENT — ADJUSTED TO 45.30 PER CENT

ADJUSTED WATER SATURATION AT VIEWABLE POINTS

BY ROWS FROM UPPER LEFT

14.3	12.2	11.2	11.2	11.2	11.2	12.2	12.2	12.2	12.2	13.2	13.2	13.2	13.2	14.3	14.3
15.4	14.3	14.3	14.3	14.3	14.3	14.3	14.3	14.3	15.4	15.4	15.4	15.4	15.4	16.4	16.4
16.4	16.4	16.4	16.4	16.4	16.4	16.4	16.4	16.4	17.5	17.5	17.5	17.5	17.5	17.5	17.5
NOT VIEWABLE - UNDER HOLD-DOWN BAR - NOT VIEWABLE															
19.6	19.6	19.6	19.6	19.6	19.6	20.7	20.7	20.7	20.7	20.7	20.7	20.7	21.7	21.7	21.7
20.7	20.7	20.7	20.7	20.7	21.7	21.7	21.7	21.7	21.7	21.7	21.7	21.7	22.8	22.8	22.8
36.9	36.9	36.9	36.9	38.0	38.0	38.0	38.0	38.0	38.0	38.0	38.0	38.0	38.0	39.1	39.1
NOT VIEWABLE - UNDER HOLD-DOWN BAR - NOT VIEWABLE															
NOT VIEWABLE - UNDER HOLD-DOWN BAR - NOT VIEWABLE															
47.7	46.7	45.6	44.5	44.5	44.5	44.5	45.6	45.6	45.6	45.6	45.6	45.6	46.7	46.7	47.7
49.9	49.9	49.9	49.9	49.9	51.0	51.0	51.0	51.0	51.0	52.0	52.0	52.0	52.0	53.1	53.1
59.4	59.4	60.4	60.4	60.4	60.4	61.5	61.5	61.5	61.5	62.5	62.5	62.5	62.5	63.5	63.5
NOT VIEWABLE - UNDER HOLD-DOWN BAR - NOT VIEWABLE															
80.9	80.9	80.9	80.9	80.9	80.9	80.9	81.8	81.8	81.8	81.8	81.8	81.8	82.7	82.7	82.7
90.4	90.4	90.4	90.4	90.4	90.4	90.4	90.4	90.4	90.4	90.4	90.4	90.4	90.4	91.2	91.9
94.3	94.3	94.3	94.3	94.3	94.3	94.3	94.3	94.3	94.3	94.3	94.3	94.3	94.3	94.3	94.3

b. LABORATORY DISPLACEMENT NO. 2 — AFTER 15 HOURS OF INJECTION

497 CC WATER IN TOTAL MODEL PORE VOLUME OF 871 CC - AVERAGE WATER SATURATION OF 57.00 PER CENT

AVERAGE WATER SATURATION FROM RAW DATA IS 53.37 PER CENT — ADJUSTED TO 56.95 PER CENT

ADJUSTED WATER SATURATION AT VIEWABLE POINTS

BY ROWS FROM UPPER LEFT

19.1	16.8	15.7	14.6	14.6	14.6	14.6	14.6	14.6	14.6	14.6	14.6	15.7	15.7	16.8	16.8
19.1	18.0	16.8	16.8	16.8	15.7	15.7	15.7	16.8	16.8	16.8	16.8	18.0	18.0	19.1	20.2
20.2	19.1	18.0	18.0	18.0	18.0	18.0	19.1	19.1	19.1	19.1	20.2	20.2	21.4	21.4	22.5
NOT VIEWABLE - UNDER HOLD-DOWN BAR - NOT VIEWABLE															
30.7	30.7	30.7	30.7	31.9	31.9	31.9	31.9	31.9	33.0	33.0	33.0	33.0	33.0	34.2	34.2
37.8	36.6	35.4	35.4	36.6	36.6	36.6	37.8	37.8	37.8	38.9	38.9	38.9	38.9	40.1	40.1
42.5	43.6	43.6	43.6	43.6	43.6	43.6	44.8	44.8	44.8	44.8	44.8	44.8	46.0	46.0	47.1
NOT VIEWABLE - UNDER HOLD-DOWN BAR - NOT VIEWABLE															
NOT VIEWABLE - UNDER HOLD-DOWN BAR - NOT VIEWABLE															
68.1	69.1	69.1	69.1	69.1	69.1	70.1	70.1	70.1	70.1	70.1	70.1	71.1	71.1	71.1	71.1
77.8	76.9	76.9	76.9	76.9	76.9	77.8	77.8	77.8	77.8	78.7	78.7	78.7	78.7	79.5	79.5
88.3	89.0	89.0	89.0	89.0	89.0	89.6	89.6	89.6	89.6	89.6	89.6	89.6	89.6	90.3	90.3
NOT VIEWABLE - UNDER HOLD-DOWN BAR - NOT VIEWABLE															
86.8	86.8	86.8	86.8	87.5	87.5	87.5	87.5	87.5	88.3	88.3	89.0	89.0	89.6	89.6	90.3
93.9	93.4	92.8	92.8	92.2	92.2	92.2	92.2	92.2	92.2	92.2	92.2	92.2	92.8	92.8	93.4
94.5	94.5	94.5	94.5	94.5	94.5	94.5	94.5	94.5	94.5	94.5	94.5	94.5	94.5	95.0	95.0

c. LABORATORY DISPLACEMENT NO. 2 — AFTER 25 HOURS OF INJECTION

599 CC WATER IN TOTAL MODEL PORE VOLUME OF 871 CC - AVERAGE WATER SATURATION OF 68.69 PER CENT

AVERAGE WATER SATURATION FROM RAW DATA IS 62.66 PER CENT — ADJUSTED TO 68.67 PER CENT

ADJUSTED WATER SATURATION AT VIEWABLE POINTS

BY ROWS FROM UPPER LEFT

29.1	27.9	25.5	24.2	24.2	23.0	21.8	21.8	21.8	21.8	21.8	21.8	23.0	24.2	25.5	26.7
25.5	25.5	24.2	24.2	24.2	24.2	24.2	24.2	24.2	24.2	24.2	24.2	24.2	24.2	25.5	25.5
32.8	31.6	31.6	31.6	31.6	31.6	31.6	31.6	31.6	31.6	31.6	32.8	32.8	34.1	34.1	34.1
NOT VIEWABLE - UNDER HOLD-DOWN BAR - NOT VIEWABLE															
53.7	52.5	52.5	51.3	51.3	51.3	51.3	51.3	51.3	51.3	51.3	51.3	52.5	52.5	52.5	53.7
65.2	64.1	64.1	64.1	64.1	64.1	64.1	65.2	65.2	65.2	65.2	65.2	65.2	66.3	66.3	66.3
76.4	75.5	75.5	75.5	75.5	76.4	76.4	76.4	76.4	77.3	77.3	77.3	77.3	77.3	77.3	78.2
NOT VIEWABLE - UNDER HOLD-DOWN BAR - NOT VIEWABLE															
NOT VIEWABLE - UNDER HOLD-DOWN BAR - NOT VIEWABLE															
84.9	84.1	83.3	83.3	83.3	83.3	83.3	83.3	83.3	83.3	83.3	84.1	84.1	84.1	84.9	
82.5	82.5	82.5	83.3	83.3	83.3	83.3	84.1	84.1	84.1	84.1	84.9	84.9	84.9	85.6	85.6
85.6	85.6	85.6	85.6	85.6	85.6	86.4	86.4	86.4	86.4	86.4	86.4	87.1	87.1	87.1	87.1
NOT VIEWABLE - UNDER HOLD-DOWN BAR - NOT VIEWABLE															
89.7	89.7	89.7	89.7	90.3	90.3	90.3	90.3	90.8	90.8	90.8	90.8	90.8	91.4	91.4	91.4
94.6	94.6	94.2	94.2	93.8	93.4	93.4	93.4	92.9	92.9	92.9	92.9	92.4	92.4	92.4	92.4
95.0	95.0	95.0	94.6	94.6	94.6	94.6	94.2	94.2	94.2	94.2	94.2	94.2	94.2	94.6	95.0

TABLE X (CONT'D)

d. LABORATORY DISPLACEMENT NO. 2 AFTER 30 HOURS OF INJECTION

650 CC WATER IN TOTAL MODEL PORE VOLUME OF 871 CC - AVERAGE WATER SATURATION OF 74.54 PER CENT

AVERAGE WATER SATURATION FROM RAW DATA IS 68.25 PER CENT ADJUSTED TO 74.51 PER CENT

ADJUSTED WATER SATURATION AT VIEWABLE POINTS

BY ROWS FROM UPPER LEFT

34.0	31.6	29.1	27.9	26.7	26.7	25.4	25.4	25.4	25.4	26.7	26.7	27.9	30.3	32.8	35.3
34.0	32.8	32.8	31.6	31.6	31.6	31.6	32.8	32.8	32.8	32.8	32.8	34.0	35.3	36.5	37.7
42.7	41.5	41.5	41.5	41.5	41.5	41.5	42.7	43.9	43.9	45.2	45.2	46.4	47.6	48.8	51.2
NOT VIEWABLE - UNDER HOLD-DOWN BAR - NOT VIEWABLE															
71.4	70.4	70.4	70.4	70.4	70.4	70.4	70.4	70.4	70.4	70.4	71.4	71.4	71.4	72.4	72.4
82.4	82.4	81.6	81.6	81.6	82.4	82.4	82.4	82.4	83.2	83.2	83.2	83.2	83.2	83.2	84.0
84.0	84.0	84.8	84.8	84.8	84.8	84.8	84.8	85.5	85.5	85.5	85.5	85.5	85.5	86.2	86.2
NOT VIEWABLE - UNDER HOLD-DOWN BAR - NOT VIEWABLE															
NOT VIEWABLE - UNDER HOLD-DOWN BAR - NOT VIEWABLE															
84.8	84.0	83.2	83.2	83.2	83.2	83.2	83.2	83.2	83.2	83.2	83.2	84.0	84.0	84.0	84.8
82.4	82.4	83.2	83.2	83.2	83.2	84.0	84.0	84.0	84.0	84.8	84.8	84.8	84.8	85.5	85.5
85.5	85.5	85.5	85.5	85.5	85.5	86.2	86.2	86.2	86.2	86.2	86.2	86.9	86.9	86.9	86.9
NOT VIEWABLE - UNDER HOLD-DOWN BAR - NOT VIEWABLE															
89.6	89.6	89.6	89.6	90.2	90.2	90.2	90.2	90.8	90.8	90.8	90.8	90.8	91.3	91.3	91.3
94.6	94.6	94.2	94.2	93.8	93.3	93.3	93.3	92.9	92.9	92.9	92.9	92.4	92.4	92.4	92.4
95.0	95.0	95.0	94.6	94.6	94.6	94.6	94.2	94.2	94.2	94.2	94.2	94.2	94.2	94.6	95.0

e. LABORATORY DISPLACEMENT NO. 2 AFTER 35 HOURS OF INJECTION

701 CC WATER IN TOTAL MODEL PORE VOLUME OF 871 CC - AVERAGE WATER SATURATION OF 80.41 PER CENT

AVERAGE WATER SATURATION FROM RAW DATA IS 74.38 PER CENT ADJUSTED TO 80.37 PER CENT

ADJUSTED WATER SATURATION AT VIEWABLE POINTS

BY ROWS FROM UPPER LEFT

39.6	37.2	36.0	36.0	36.0	36.0	36.0	36.0	36.0	37.2	37.2	38.4	39.6	40.9	42.1	43.3
59.7	58.6	57.4	57.4	57.4	57.4	57.4	57.4	57.4	57.4	57.4	57.4	57.4	58.6	58.6	59.7
73.4	72.4	72.4	72.4	72.4	72.4	72.4	72.4	72.4	72.4	73.4	73.4	73.4	73.4	74.3	74.3
NOT VIEWABLE - UNDER HOLD-DOWN BAR - NOT VIEWABLE															
83.1	82.3	82.3	82.3	82.3	82.3	82.3	82.3	82.3	82.3	82.3	83.1	83.1	83.1	83.1	83.1
85.5	84.7	83.9	83.9	84.7	84.7	84.7	84.7	84.7	84.7	85.5	85.5	85.5	85.5	85.5	86.2
86.9	86.2	85.5	85.5	85.5	85.5	85.5	85.5	85.5	85.5	85.5	85.5	85.5	85.5	86.2	86.2
NOT VIEWABLE - UNDER HOLD-DOWN BAR - NOT VIEWABLE															
NOT VIEWABLE - UNDER HOLD-DOWN BAR - NOT VIEWABLE															
83.9	83.1	83.1	83.1	83.1	83.1	83.1	83.1	83.1	83.1	83.1	83.1	83.1	83.9	83.9	84.7
82.3	82.3	82.3	82.3	82.3	82.3	83.1	83.1	83.1	83.1	83.1	83.1	83.9	83.9	83.9	84.7
85.5	85.5	85.5	85.5	85.5	85.5	85.5	85.5	85.5	85.5	85.5	85.5	85.5	86.2	86.2	86.9
NOT VIEWABLE - UNDER HOLD-DOWN BAR - NOT VIEWABLE															
89.0	89.0	89.0	89.6	89.6	89.6	89.6	89.6	89.6	89.6	89.6	90.3	90.3	90.3	90.9	90.9
94.6	94.1	93.6	93.6	93.1	93.1	92.6	92.6	92.6	92.6	92.6	92.6	92.0	92.0	92.0	92.0
95.0	95.0	95.0	95.0	95.0	95.0	94.6	94.6	94.6	94.1	94.1	94.1	94.1	94.1	94.6	95.0

f. LABORATORY DISPLACEMENT NO. 2 AFTER 40 HOURS OF INJECTION

752 CC WATER IN TOTAL MODEL PORE VOLUME OF 871 CC - AVERAGE WATER SATURATION OF 86.27 PER CENT

AVERAGE WATER SATURATION FROM RAW DATA IS 80.64 PER CENT ADJUSTED TO 86.24 PER CENT

ADJUSTED WATER SATURATION AT VIEWABLE POINTS

BY ROWS FROM UPPER LEFT

82.2	81.4	80.5	80.5	79.7	79.7	79.7	79.7	78.8	78.8	78.8	77.9	77.9	77.9	78.8	78.8
88.8	88.1	87.5	87.5	87.5	87.5	87.5	87.5	87.5	87.5	87.5	87.5	87.5	87.5	87.5	87.5
88.8	88.8	88.1	88.1	88.1	88.1	87.5	87.5	87.5	87.5	87.5	87.5	88.1	88.1	88.1	88.8
NOT VIEWABLE - UNDER HOLD-DOWN BAR - NOT VIEWABLE															
83.8	83.0	83.0	83.0	83.0	83.0	83.0	83.0	83.0	83.0	83.0	83.0	83.0	83.0	83.0	83.8
86.0	85.3	85.3	85.3	85.3	85.3	85.3	85.3	85.3	86.0	86.0	86.0	86.0	86.0	86.8	86.8
86.8	86.0	85.3	85.3	85.3	85.3	85.3	85.3	85.3	85.3	85.3	85.3	85.3	85.3	86.0	86.0
NOT VIEWABLE - UNDER HOLD-DOWN BAR - NOT VIEWABLE															
NOT VIEWABLE - UNDER HOLD-DOWN BAR - NOT VIEWABLE															
83.8	83.0	83.0	83.0	83.0	83.0	83.0	83.0	83.0	83.0	83.0	83.0	83.8	83.8	84.6	
82.2	82.2	82.2	82.2	82.2	82.2	83.0	83.0	83.0	83.0	83.0	83.0	83.8	83.8	83.8	84.6
85.3	85.3	85.3	85.3	85.3	85.3	85.3	85.3	85.3	85.3	85.3	85.3	85.3	86.0	86.0	86.8
NOT VIEWABLE - UNDER HOLD-DOWN BAR - NOT VIEWABLE															
88.8	88.8	88.8	89.5	89.5	89.5	89.5	89.5	89.5	89.5	89.5	90.1	90.1	90.1	90.7	90.7
94.5	94.0	93.5	93.5	93.0	93.0	92.5	92.5	92.5	92.5	92.5	92.5	91.9	91.9	91.9	91.9
95.0	95.0	95.0	95.0	95.0	95.0	94.5	94.5	94.5	94.0	94.0	94.0	94.0	94.0	94.5	95.0

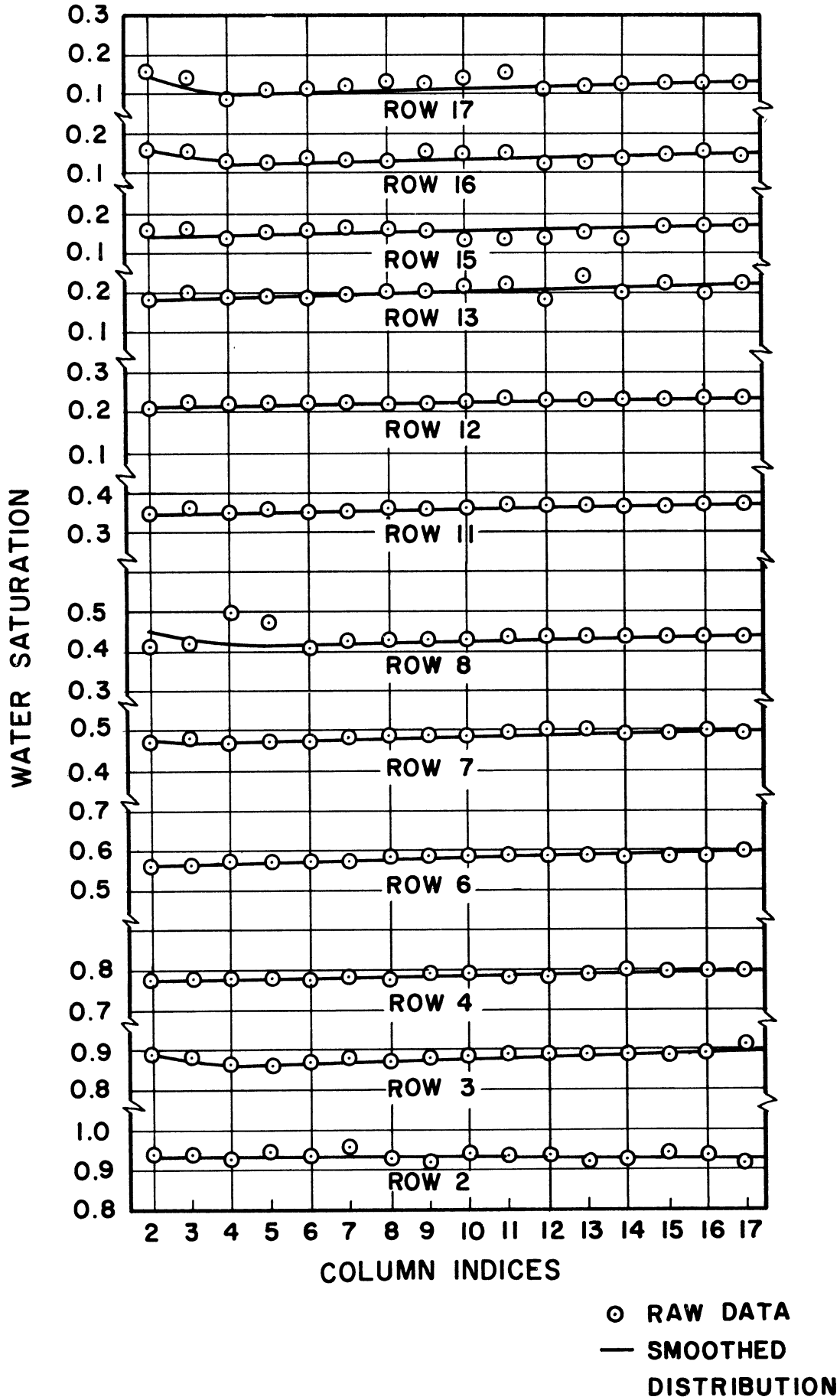

Figure 21. Row-Wise Water Saturation Distribution Displacement No. 2 - At 5.00 Hours.

TABLE XI

COMPARISON OF SMOOTHED WATER SATURATION DATA

WITH RAW DATA

LABORATORY DISPLACEMENT NO. 2

AFTER 5 HOURS OF INJECTION

AVERAGE AND STANDARD DEVIATION BY WATER SATURATION RANGE

EXPRESSED IN SATURATION PER CENT

FROM	TO	NO. PTS	AVG. DEV.	STD. DEV.
.0	20.0	66	1.1	1.5
20.0	40.0	30	.9	1.2
40.0	60.0	48	.9	1.6
60.0	80.0	16	.3	.5
80.0	100.0	32	.8	1.2
OVERALL		192	.9	1.4

AFTER 15 HOURS OF INJECTION

AVERAGE AND STANDARD DEVIATION BY WATER SATURATION RANGE

EXPRESSED IN SATURATION PER CENT

FROM	TO	NO. PTS	AVG. DEV.	STD. DEV.
.0	20.0	47	1.0	1.4
20.0	40.0	46	.4	.7
40.0	60.0	3	.7	.8
60.0	80.0	32	1.3	1.5
80.0	100.0	64	1.3	1.7
OVERALL		192	1.0	1.4

AFTER 25 HOURS OF INJECTION

AVERAGE AND STANDARD DEVIATION BY WATER SATURATION RANGE

EXPRESSED IN SATURATION PER CENT

FROM	TO	NO. PTS	AVG. DEV.	STD. DEV.
.0	20.0	6	.8	1.1
20.0	40.0	42	1.7	2.3
40.0	60.0	32	1.5	1.8
60.0	80.0	64	1.3	1.7
80.0	100.0	48	1.3	1.9
OVERALL		192	1.4	1.9

AFTER 30 HOURS OF INJECTION

AVERAGE AND STANDARD DEVIATION BY WATER SATURATION RANGE

EXPRESSED IN SATURATION PER CENT

FROM	TO	NO. PTS	AVG. DEV.	STD. DEV.
.0	20.0	0	.0	.0
20.0	40.0	45	2.1	2.5
40.0	60.0	3	2.3	3.1
60.0	80.0	96	1.2	1.7
80.0	100.0	48	1.3	1.9
OVERALL		192	1.5	2.0

AFTER 35 HOURS OF INJECTION

AVERAGE AND STANDARD DEVIATION BY WATER SATURATION RANGE

EXPRESSED IN SATURATION PER CENT

FROM	TO	NO. PTS	AVG. DEV.	STD. DEV.
.0	20.0	0	.0	.0
20.0	40.0	16	1.8	2.3
40.0	60.0	16	2.3	3.0
60.0	80.0	110	1.2	1.7
80.0	100.0	50	1.3	1.8
OVERALL		192	1.3	1.9

AFTER 40 HOURS OF INJECTION

AVERAGE AND STANDARD DEVIATION BY WATER SATURATION RANGE

EXPRESSED IN SATURATION PER CENT

FROM	TO	NO. PTS	AVG. DEV.	STD. DEV.
.0	20.0	0	.0	.0
20.0	40.0	0	.0	.0
40.0	60.0	0	.0	.0
60.0	80.0	108	1.3	2.1
80.0	100.0	84	1.3	1.9
OVERALL		192	1.3	2.0

Water was injected at a nominal rate of 5 cc/hr through each of two wells located at the upper and lower right corners. Initial phase distributions appear in Tables IVb and c for the two displacements. The operating summary is listed in Table XII.

TABLE XII

OPERATING SUMMARY

Displacements No. 3 and 4

		No. 3	No. 4
Initial Water in P.V.	=	531 cc	534 cc
Water Injection Rate (Upper well)		5.11 cc/hr	5.13 cc/hr
(Lower well)		5.11 cc/hr	5.13 cc/hr
Breakthrough Time		24.25 hrs	23.75 hrs
Water in P.V. at Breakthrough		778 cc	777 cc

Again, production was observed to switch abruptly from gas to water at breakthrough.

Water saturation distributions at five corresponding time levels are presented in Tables XIII a-e and XIV a-e for the two displacements. The difference of 0.3 hour between corresponding times is approximate as the initial water volumes are known at best to 1 cc. The tabulated distributions are based on the same average water saturation at corresponding times. The row-wise plots of water saturation used in smoothing the raw data were very similar to that shown in Figure 21 for Displacement No. 2, but at higher water saturation levels.

Fingering was again absent with the outlet end effects similar to those observed in Displacement No. 2. Reference to the tabulated distributions shows inlet end effects (upper right corner) as well as outlet effects to be present throughout both displacements. Average and standard deviations between raw and smoothed distributions presented in Tables XV and XVI show the smoothing to be within the precision of the measurements.

D. Overall Displacement Reproducibility

Reproducibility of the technique was assessed by making duplicate measurements on several stationary water saturation distributions. Displacement No. 4 was run to determine how closely the transient behavior observed in Displacement No. 3 could be reproduced.

The integral agreement shown by the respective water contents of the pore volume at breakthrough is excellent. A more meaningful comparison has been made between corresponding water saturation distributions. Table XVII presents the average and standard deviations resulting from point by point comparison between the distributions of Tables XIII(a - e) and XIV(a - e). It must be emphasized that any smoothing of the raw distributions was done separately for the two displacements with no attempt being made to minimize differences between the corresponding distributions. The deviations shown in Table XVII indicate the over-all reproducibility to be at least as good as the reproducibility of the technique of measurement.

TABLE XIII

EXPERIMENTAL WATER SATURATION DISTRIBUTIONS

a. LABORATORY DISPLACEMENT NO. 3 AFTER 4.3 HOURS OF INJECTION

575 CC WATER IN TOTAL MODEL PORE VOLUME OF 871 CC - AVERAGE WATER SATURATION OF 65.98 PER CENT

AVERAGE WATER SATURATION FROM RAW DATA IS 61.36 PER CENT ADJUSTED TO 65.96 PER CENT

ADJUSTED WATER SATURATION AT VIEWABLE POINTS

BY ROWS FROM UPPER LEFT

18.2	15.9	14.8	13.6	13.6	14.8	14.8	15.9	17.1	18.2	19.4	20.6	21.8	23.0	25.4	26.6
24.2	23.0	21.8	21.8	21.8	21.8	21.8	23.0	23.0	24.2	24.2	25.4	25.4	26.6	27.8	29.0
27.8	26.6	26.6	26.6	27.8	27.8	27.8	29.0	29.0	30.2	30.2	30.2	31.5	31.5	31.5	32.7
NOT VIEWABLE - UNDER HOLD-DOWN BAR - NOT VIEWABLE															
43.8	42.5	41.3	41.3	41.3	42.5	42.5	42.5	43.8	43.8	43.8	43.8	43.8	45.0	45.0	45.0
53.4	52.2	52.2	52.2	52.2	52.2	52.2	53.4	53.4	53.4	53.4	53.4	53.4	54.6	54.6	54.6
62.5	61.4	62.5	62.5	62.5	62.5	63.6	63.6	63.6	63.6	63.6	63.6	64.7	64.7	64.7	64.7
NOT VIEWABLE - UNDER HOLD-DOWN BAR - NOT VIEWABLE															
NOT VIEWABLE - UNDER HOLD-DOWN BAR - NOT VIEWABLE															
86.5	85.0	83.5	83.5	83.5	83.5	83.5	83.5	83.5	84.3	84.3	85.0	85.7	85.7	87.2	87.8
88.5	87.8	87.8	87.8	87.8	88.5	88.5	88.5	88.5	88.5	89.1	89.1	89.1	89.1	89.8	89.8
90.4	90.4	90.4	91.0	91.0	91.0	91.0	91.5	91.5	91.5	91.5	92.1	92.1	92.1	92.1	92.6
NOT VIEWABLE - UNDER HOLD-DOWN BAR - NOT VIEWABLE															
92.6	92.6	92.6	93.1	93.1	93.1	93.1	93.1	93.6	93.6	93.6	93.6	93.6	94.1	94.1	94.1
93.1	93.1	93.1	93.1	93.6	93.6	93.6	93.6	93.6	94.1	94.1	94.1	94.1	94.1	94.1	94.6
93.1	93.1	93.1	93.1	93.1	93.6	93.6	93.6	93.6	93.6	94.1	94.1	94.1	94.1	94.1	94.6

b. LABORATORY DISPLACEMENT NO. 3 AFTER 10.3 HOURS OF INJECTION

636 CC WATER IN TOTAL MODEL PORE VOLUME OF 871 CC - AVERAGE WATER SATURATION OF 73.03 PER CENT

AVERAGE WATER SATURATION FROM RAW DATA IS 68.08 PER CENT ADJUSTED TO 73.00 PER CENT

ADJUSTED WATER SATURATION AT VIEWABLE POINTS

BY ROWS FROM UPPER LEFT

24.3	23.1	21.9	20.7	20.7	20.7	20.7	20.7	21.9	21.9	23.1	24.3	25.5	26.7	27.9	29.2
29.2	27.9	27.9	27.9	27.9	27.9	29.2	29.2	30.4	30.4	30.4	31.6	32.9	32.9	34.1	35.4
37.9	36.6	36.6	35.4	35.4	36.6	36.6	37.9	37.9	39.1	39.1	40.4	40.4	40.4	40.4	40.4
NOT VIEWABLE - UNDER HOLD-DOWN BAR - NOT VIEWABLE															
59.6	58.5	57.3	57.3	57.3	57.3	57.3	58.5	58.5	58.5	59.6	59.6	59.6	59.6	59.6	60.7
71.4	70.4	70.4	70.4	70.4	70.4	70.4	70.4	71.4	71.4	71.4	72.4	72.4	72.4	72.4	73.3
82.2	81.4	81.4	81.4	81.4	82.2	82.2	82.2	82.2	82.2	82.2	82.2	83.0	83.0	83.0	83.0
NOT VIEWABLE - UNDER HOLD-DOWN BAR - NOT VIEWABLE															
NOT VIEWABLE - UNDER HOLD-DOWN BAR - NOT VIEWABLE															
89.9	88.6	88.0	87.3	87.3	87.3	87.3	87.3	88.0	88.0	88.6	88.6	89.3	89.9	90.5	91.6
89.9	88.6	88.6	88.6	88.6	88.6	89.3	89.3	89.3	89.9	89.9	90.5	90.5	91.0	91.0	91.6
92.1	91.6	91.0	91.0	91.0	91.0	91.0	91.6	91.6	91.6	92.1	92.1	92.1	92.7	93.2	93.7
NOT VIEWABLE - UNDER HOLD-DOWN BAR - NOT VIEWABLE															
92.7	92.7	93.2	93.2	93.2	93.2	93.7	93.7	93.7	93.7	94.1	94.1	94.1	94.1	94.6	94.6
93.2	93.2	93.2	93.2	93.7	93.7	93.7	93.7	93.7	94.1	94.1	94.1	94.1	94.6	94.6	94.6
93.2	93.2	93.2	93.2	93.2	93.7	93.7	93.7	93.7	93.7	94.1	94.1	94.1	94.1	94.1	94.6

c. LABORATORY DISPLACEMENT NO. 3 AFTER 15.3 HOURS OF INJECTION

687 CC WATER IN TOTAL MODEL PORE VOLUME OF 871 CC - AVERAGE WATER SATURATION OF 78.89 PER CENT

AVERAGE WATER SATURATION FROM RAW DATA IS 74.33 PER CENT ADJUSTED TO 78.86 PER CENT

ADJUSTED WATER SATURATION AT VIEWABLE POINTS

BY ROWS FROM UPPER LEFT

32.5	30.0	30.0	30.0	30.0	30.0	31.2	31.2	31.2	31.2	32.5	32.5	33.7	33.7	34.9	36.1
39.8	41.0	41.0	41.0	42.2	42.2	42.2	42.2	42.2	42.2	43.4	43.4	43.4	42.2	42.2	42.2
57.5	57.5	57.5	57.5	58.7	58.7	58.7	58.7	58.7	58.7	58.7	57.5	57.5	57.5	56.4	56.4
NOT VIEWABLE - UNDER HOLD-DOWN BAR - NOT VIEWABLE															
74.3	73.3	73.3	73.3	73.3	73.3	74.3	74.3	74.3	74.3	75.2	75.2	75.2	75.2	76.1	
84.5	83.7	82.9	82.1	82.1	82.9	82.9	82.9	82.9	82.9	82.9	82.9	82.9	83.7	83.7	
85.2	84.5	83.7	83.7	83.7	83.7	83.7	83.7	83.7	83.7	83.7	83.7	83.7	84.5	84.5	
NOT VIEWABLE - UNDER HOLD-DOWN BAR - NOT VIEWABLE															
NOT VIEWABLE - UNDER HOLD-DOWN BAR - NOT VIEWABLE															
89.4	88.7	88.1	87.4	87.4	87.4	87.4	87.4	88.1	88.1	88.7	88.7	89.4	90.0	91.2	
89.4	88.7	88.1	88.1	88.1	88.1	88.7	88.7	89.4	89.4	90.0	90.0	90.0	90.6	90.6	91.2
91.8	91.2	90.6	90.6	90.6	90.6	90.6	91.2	91.2	91.2	91.8	91.8	91.8	92.4	92.9	93.5
NOT VIEWABLE - UNDER HOLD-DOWN BAR - NOT VIEWABLE															
93.5	93.5	93.5	93.5	93.5	93.5	94.0	94.0	94.0	94.0	94.0	94.0	94.0	94.5	94.5	94.5
93.5	93.5	93.5	93.5	94.0	94.0	94.0	94.0	94.0	94.0	94.0	94.0	94.0	94.5	94.5	94.5
92.9	92.9	92.9	92.9	92.9	93.5	93.5	93.5	93.5	93.5	94.0	94.0	94.0	94.0	94.0	94.5

TABLE XIII (CONT'D)

d. LABORATORY DISPLACEMENT NO. 3 AFTER 20.3 HOURS OF INJECTION

739 CC WATER IN TOTAL MODEL PORE VOLUME OF 871 CC - AVERAGE WATER SATURATION OF 84.77 PER CENT

AVERAGE WATER SATURATION FROM RAW DATA IS 79.46 PER CENT ADJUSTED TO 84.74 PER CENT

ADJUSTED WATER SATURATION AT VIEWABLE POINTS

BY ROWS FROM UPPER LEFT

48.8	47.6	46.4	46.4	47.6	47.6	48.8	48.8	50.0	50.0	50.0	50.0	51.2	51.2	52.4	52.4
68.1	69.1	71.1	72.1	72.1	73.1	73.1	73.1	73.1	73.1	72.1	72.1	71.1	70.1	69.1	68.1
81.1	81.9	81.9	82.7	82.7	82.7	82.7	82.7	82.7	82.7	82.7	82.7	82.7	81.9	81.1	80.3
NOT VIEWABLE - UNDER HOLD-DOWN BAR - NOT VIEWABLE															
81.9	81.1	81.1	81.1	81.1	81.1	81.1	81.1	81.1	81.1	81.1	81.1	81.9	81.9	81.9	81.9
85.7	85.0	84.3	84.3	84.3	83.5	83.5	84.3	84.3	84.3	84.3	84.3	84.3	84.3	85.0	85.0
86.4	85.7	85.0	85.0	84.3	84.3	84.3	84.3	84.3	84.3	84.3	85.0	85.0	85.0	85.7	85.7
NOT VIEWABLE - UNDER HOLD-DOWN BAR - NOT VIEWABLE															
NOT VIEWABLE - UNDER HOLD-DOWN BAR - NOT VIEWABLE															
90.3	89.7	89.1	88.5	87.8	87.8	87.8	87.8	87.8	87.8	88.5	88.5	89.1	89.7	90.9	92.0
90.9	89.7	89.7	89.1	89.1	89.1	89.1	89.7	89.7	89.7	90.3	90.3	90.3	90.9	90.9	91.5
92.6	91.5	90.9	90.9	90.9	90.9	90.9	90.9	91.5	91.5	91.5	92.0	92.0	92.6	93.1	93.6
NOT VIEWABLE - UNDER HOLD-DOWN BAR - NOT VIEWABLE															
93.6	93.6	93.6	93.6	94.1	94.1	94.1	94.1	94.1	94.1	94.5	94.5	94.5	94.5	94.5	94.5
94.1	94.1	94.1	94.1	94.5	94.5	94.5	94.5	94.5	94.5	94.5	94.5	94.5	95.0	95.0	95.0
93.1	93.1	93.1	93.1	93.1	93.6	93.6	93.6	93.6	93.6	94.1	94.1	94.1	94.1	94.1	94.5

e. LABORATORY DISPLACEMENT NO. 3 AFTER 22.3 HOURS OF INJECTION

759 CC WATER IN TOTAL MODEL PORE VOLUME OF 871 CC - AVERAGE WATER SATURATION OF 87.12 PER CENT

AVERAGE WATER SATURATION FROM RAW DATA IS 81.69 PER CENT ADJUSTED TO 87.08 PER CENT

ADJUSTED WATER SATURATION AT VIEWABLE POINTS

BY ROWS FROM UPPER LEFT

70.4	69.4	69.4	69.4	69.4	69.4	69.4	68.4	68.4	68.4	68.4	68.4	68.4	68.4	69.4	70.4
83.7	84.4	84.4	84.4	84.4	84.4	84.4	84.4	84.4	84.4	84.4	84.4	84.4	84.4	84.4	84.4
86.6	85.9	85.2	85.2	85.2	85.2	85.2	85.2	85.2	85.2	85.2	85.2	85.2	85.9	85.9	85.9
NOT VIEWABLE - UNDER HOLD-DOWN BAR - NOT VIEWABLE															
82.1	81.3	81.3	81.3	81.3	81.3	81.3	81.3	81.3	81.3	81.3	81.3	81.3	81.3	82.1	82.1
85.9	85.2	84.4	83.7	83.7	83.7	83.7	83.7	83.7	84.4	84.4	84.4	84.4	84.4	85.2	85.2
86.6	85.2	84.4	84.4	83.7	83.7	84.4	84.4	84.4	84.4	84.4	85.2	85.2	85.2	85.9	85.9
NOT VIEWABLE - UNDER HOLD-DOWN BAR - NOT VIEWABLE															
NOT VIEWABLE - UNDER HOLD-DOWN BAR - NOT VIEWABLE															
90.4	89.8	89.2	88.6	87.9	87.9	87.9	87.9	87.9	87.9	87.9	88.6	89.2	89.8	91.0	92.1
91.6	90.4	89.8	89.2	89.8	89.8	89.8	89.8	89.8	90.4	90.4	90.4	90.4	91.0	91.0	91.6
92.6	91.6	91.0	91.0	91.0	91.0	91.0	91.6	91.6	91.6	91.6	92.1	92.1	92.6	93.1	93.6
NOT VIEWABLE - UNDER HOLD-DOWN BAR - NOT VIEWABLE															
93.6	93.6	93.6	94.1	94.1	94.1	94.1	94.1	94.1	94.1	94.6	94.6	94.6	94.6	94.6	94.6
94.1	94.1	94.1	94.1	94.6	94.6	94.6	94.6	94.6	94.6	94.6	94.6	94.6	95.0	95.0	95.0
93.1	93.1	93.1	93.1	93.1	93.6	93.6	93.6	93.6	93.6	94.1	94.1	94.1	94.1	94.1	94.6

TABLE XIV

EXPERIMENTAL WATER SATURATION DISTRIBUTIONS

a. LABORATORY DISPLACEMENT NO. 4 AFTER 4.0 HOURS OF INJECTION

575 CC WATER IN TOTAL MODEL PORE VOLUME OF 871 CC - AVERAGE WATER SATURATION OF 65.98 PER CENT

AVERAGE WATER SATURATION FROM RAW DATA IS 63.88 PER CENT ADJUSTED TO 65.96 PER CENT

ADJUSTED WATER SATURATION AT VIEWABLE POINTS

BY ROWS FROM UPPER LEFT

22.9	21.9	20.8	20.8	20.8	20.8	20.8	20.8	21.9	21.9	21.9	21.9	21.9	22.9	22.9	22.9
25.1	26.2	26.2	26.2	26.2	26.2	26.2	26.2	26.2	26.2	26.2	26.2	26.2	26.2	27.3	27.3
29.5	29.5	29.5	29.5	30.6	30.6	30.6	30.6	30.6	30.6	30.6	30.6	31.7	31.7	31.7	31.7
				NOT VIEWABLE - UNDER HOLD-DOWN BAR - NOT VIEWABLE											
43.8	43.8	43.8	43.8	43.8	43.8	43.8	43.8	43.8	43.8	43.8	43.8	43.8	43.8	43.8	43.8
52.5	52.5	52.5	52.5	52.5	53.6	53.6	53.6	53.6	53.6	53.6	53.6	53.6	53.6	53.6	54.6
60.9	60.9	60.9	60.9	60.9	60.9	62.0	62.0	62.0	62.0	62.0	62.0	62.0	62.0	62.0	62.0
				NOT VIEWABLE - UNDER HOLD-DOWN BAR - NOT VIEWABLE											
				NOT VIEWABLE - UNDER HOLD-DOWN BAR - NOT VIEWABLE											
82.2	82.2	82.2	82.2	82.2	82.2	82.2	82.2	83.0	83.0	83.0	83.0	83.0	83.0	83.0	83.9
87.3	87.3	87.3	88.1	88.1	88.1	88.1	88.1	88.1	88.1	88.9	88.9	88.9	88.9	88.9	88.9
91.3	91.3	91.3	91.3	91.3	92.0	92.0	92.0	92.0	92.0	92.0	92.0	92.0	92.8	92.8	92.8
				NOT VIEWABLE - UNDER HOLD-DOWN BAR - NOT VIEWABLE											
92.0	92.0	92.0	92.0	92.0	92.0	92.0	92.0	92.8	92.8	92.8	92.8	92.8	92.8	92.8	92.8
92.8	92.8	92.8	92.8	92.8	92.8	93.5	93.5	93.5	93.5	93.5	93.5	93.5	94.3	94.3	94.3
92.8	92.8	92.8	92.8	92.8	92.8	93.5	93.5	93.5	93.5	93.5	93.5	93.5	94.3	94.3	94.3

b. LABORATORY DISPLACEMENT NO. 4 AFTER 10.0 HOURS OF INJECTION

636 CC WATER IN TOTAL MODEL PORE VOLUME OF 871 CC - AVERAGE WATER SATURATION OF 73.03 PER CENT

AVERAGE WATER SATURATION FROM RAW DATA IS 69.08 PER CENT ADJUSTED TO 72.99 PER CENT

ADJUSTED WATER SATURATION AT VIEWABLE POINTS

BY ROWS FROM UPPER LEFT

26.1	24.9	23.8	23.8	23.8	23.8	23.8	23.8	24.9	24.9	24.9	26.1	26.1	27.3	28.4	29.6
29.6	29.6	29.6	30.8	30.8	30.8	32.0	32.0	32.0	32.0	33.2	33.2	33.2	34.4	34.4	34.4
36.8	36.8	36.8	36.8	37.9	37.9	37.9	37.9	37.9	39.1	39.1	39.1	39.1	39.1	40.3	40.3
				NOT VIEWABLE - UNDER HOLD-DOWN BAR - NOT VIEWABLE											
59.9	59.9	59.9	59.9	59.9	61.0	61.0	61.0	61.0	61.0	61.0	61.0	61.0	61.0	62.1	62.1
71.3	71.3	71.3	71.3	71.3	72.3	72.3	72.3	72.3	72.3	72.3	72.3	72.3	73.3	73.3	73.3
79.6	79.6	79.6	79.6	79.6	79.6	79.6	79.6	79.6	80.5	80.5	80.5	80.5	80.5	80.5	80.5
				NOT VIEWABLE - UNDER HOLD-DOWN BAR - NOT VIEWABLE											
				NOT VIEWABLE - UNDER HOLD-DOWN BAR - NOT VIEWABLE											
84.6	84.6	84.6	84.6	84.6	85.3	85.3	85.3	85.3	85.3	85.3	85.3	85.3	86.1	86.1	86.1
88.9	88.9	88.9	88.9	88.9	89.6	89.6	89.6	89.6	89.6	89.6	89.6	89.6	90.3	90.3	90.3
92.2	92.2	92.8	92.8	92.8	92.8	92.8	92.8	92.8	92.8	93.3	93.3	93.3	93.3	93.3	93.3
				NOT VIEWABLE - UNDER HOLD-DOWN BAR - NOT VIEWABLE											
93.3	93.3	93.3	93.3	93.3	93.3	93.9	93.9	93.9	93.9	93.9	93.9	93.9	94.5	94.5	94.5
93.3	93.3	93.3	93.3	93.3	93.3	93.9	93.9	93.9	93.9	93.9	93.9	93.9	94.5	94.5	94.5
93.3	93.3	93.3	93.3	93.3	93.3	93.9	93.9	93.9	93.9	93.9	93.9	93.9	94.5	94.5	94.5

c. LABORATORY DISPLACEMENT NO. 4 AFTER 15.0 HOURS OF INJECTION

687 CC WATER IN TOTAL MODEL PORE VOLUME OF 871 CC - AVERAGE WATER SATURATION OF 78.89 PER CENT

AVERAGE WATER SATURATION FROM RAW DATA IS 73.50 PER CENT ADJUSTED TO 78.86 PER CENT

ADJUSTED WATER SATURATION AT VIEWABLE POINTS

BY ROWS FROM UPPER LEFT

31.8	29.3	28.0	26.8	26.8	28.0	28.0	29.3	30.5	30.5	31.8	33.0	33.0	34.3	35.5	36.8
40.5	39.3	39.3	39.3	40.5	40.5	41.8	41.8	41.8	43.0	43.0	43.0	43.0	44.3	44.3	44.3
54.0	54.0	55.2	55.2	55.2	55.2	56.4	56.4	56.4	56.4	56.4	57.5	57.5	57.5	57.5	57.5
				NOT VIEWABLE - UNDER HOLD-DOWN BAR - NOT VIEWABLE											
76.2	78.2	78.2	78.2	78.2	78.2	78.2	78.2	78.2	78.2	78.2	78.2	79.1	79.1	79.1	79.1
83.9	83.9	83.9	83.9	83.9	83.9	83.9	84.7	84.7	84.7	84.7	84.7	84.7	84.7	84.7	85.4
83.9	83.1	83.1	83.9	83.9	84.7	84.7	84.7	84.7	84.7	84.7	84.7	84.7	84.7	84.7	84.7
				NOT VIEWABLE - UNDER HOLD-DOWN BAR - NOT VIEWABLE											
				NOT VIEWABLE - UNDER HOLD-DOWN BAR - NOT VIEWABLE											
88.1	86.1	85.4	85.4	85.4	85.4	86.1	86.1	86.1	86.8	86.8	86.8	87.5	87.5	87.5	87.5
88.8	88.1	88.1	88.1	88.8	89.4	90.0	90.0	90.6	90.6	90.6	91.1	91.1	91.1	91.7	91.7
92.7	92.7	93.2	93.2	93.2	93.2	93.2	93.2	93.2	93.2	93.7	93.7	93.7	93.7	93.7	93.7
				NOT VIEWABLE - UNDER HOLD-DOWN BAR - NOT VIEWABLE											
93.7	93.7	93.7	93.7	93.7	93.7	94.1	94.1	94.1	94.1	94.1	94.1	94.1	94.6	94.6	94.6
93.7	93.7	93.7	93.7	93.7	93.7	94.1	94.1	94.1	94.1	94.1	94.1	94.1	94.6	94.6	94.6
93.7	93.7	93.7	93.7	93.7	93.7	94.1	94.1	94.1	94.1	94.1	94.1	94.1	94.6	94.6	94.6

TABLE XIV (CONT'D)

d. LABORATORY DISPLACEMENT NO. 4 AFTER 20.0 HOURS OF INJECTION

739 CC WATER IN TOTAL MODEL PORE VOLUME OF 871 CC - AVERAGE WATER SATURATION OF 84.77 PER CENT

AVERAGE WATER SATURATION FROM RAW DATA IS 79.44 PER CENT ADJUSTED TO 84.72 PER CENT

ADJUSTED WATER SATURATION AT VIEWABLE POINTS

BY ROWS FROM UPPER LEFT

52.2	51.0	51.0	51.0	51.0	51.0	52.2	52.2	52.2	52.2	53.3	53.3	54.5	54.5	55.7	55.7
72.8	71.9	71.9	72.8	73.8	73.8	74.7	74.7	74.7	74.7	74.7	74.7	74.7	74.7	74.7	74.7
82.5	83.3	83.3	83.3	83.3	83.3	83.3	83.3	83.3	83.3	83.3	83.3	83.3	83.3	83.3	84.1
				NOT VIEWABLE - UNDER HOLD-DOWN BAR - NOT VIEWABLE											
81.7	80.1	79.2	79.2	80.1	80.9	80.9	81.7	81.7	81.7	81.7	81.7	81.7	81.7	82.5	82.5
85.6	83.3	82.5	82.5	83.3	83.3	83.3	84.1	84.1	84.1	84.1	84.1	84.8	84.8	84.8	84.8
85.6	83.3	82.5	82.5	82.5	83.3	83.3	84.1	84.1	84.8	84.8	84.8	84.8	85.6	85.6	85.6
				NOT VIEWABLE - UNDER HOLD-DOWN BAR - NOT VIEWABLE											
				NOT VIEWABLE - UNDER HOLD-DOWN BAR - NOT VIEWABLE											
87.7	85.6	84.1	84.1	84.1	84.1	84.8	84.8	84.8	85.6	85.6	86.3	86.3	87.0	87.7	88.3
88.3	87.7	87.7	87.7	88.3	89.0	89.0	89.6	90.2	90.2	90.8	90.8	90.8	91.4	91.4	91.4
93.1	92.5	92.0	92.0	92.0	92.5	92.5	93.1	93.1	93.6	93.6	93.6	94.1	94.1	94.1	94.5
				NOT VIEWABLE - UNDER HOLD-DOWN BAR - NOT VIEWABLE											
93.6	93.6	93.6	93.6	93.6	93.6	94.1	94.1	94.1	94.1	94.1	94.1	94.1	94.5	94.5	94.5
93.6	93.6	93.6	93.6	93.6	93.6	94.1	94.1	94.1	94.1	94.1	94.1	94.1	94.5	94.5	94.5
93.6	93.6	93.6	93.6	93.6	93.6	94.1	94.1	94.1	94.1	94.1	94.1	94.1	94.5	94.5	94.5

e. LABORATORY DISPLACEMENT NO. 4 AFTER 22.0 HOURS OF INJECTION

759 CC WATER IN TOTAL MODEL PORE VOLUME OF 871 CC - AVERAGE WATER SATURATION OF 87.12 PER CENT

AVERAGE WATER SATURATION FROM RAW DATA IS 82.16 PER CENT ADJUSTED TO 87.08 PER CENT

ADJUSTED WATER SATURATION AT VIEWABLE POINTS

BY ROWS FROM UPPER LEFT

73.5	73.5	73.5	73.5	74.5	74.5	74.5	74.5	74.5	75.4	75.4	75.4	75.4	75.4	76.3	76.3
87.5	86.1	85.4	85.4	86.1	86.1	86.1	86.1	86.1	86.1	86.1	86.1	86.1	86.1	86.1	86.1
86.1	85.1	84.6	84.6	84.6	84.6	84.6	85.4	85.4	85.4	85.4	85.4	85.4	85.4	85.4	86.1
				NOT VIEWABLE - UNDER HOLD-DOWN BAR - NOT VIEWABLE											
82.3	81.5	80.7	80.7	80.7	80.7	81.5	81.5	81.5	81.5	81.5	81.5	81.5	81.5	82.3	82.3
86.1	83.1	83.1	83.1	83.1	83.1	83.1	83.9	83.9	83.9	83.9	83.9	83.9	84.6	84.6	84.6
86.1	83.9	83.1	83.1	83.9	83.9	83.9	84.6	84.6	84.6	84.6	84.6	85.4	85.4	85.4	86.1
				NOT VIEWABLE - UNDER HOLD-DOWN BAR - NOT VIEWABLE											
				NOT VIEWABLE - UNDER HOLD-DOWN BAR - NOT VIEWABLE											
87.5	86.1	84.6	83.9	83.9	84.6	84.6	84.6	84.6	85.4	85.4	86.1	86.1	86.8	87.5	88.2
88.8	88.2	87.5	87.5	88.2	88.8	89.5	89.5	90.1	90.1	90.7	90.7	90.7	91.3	91.9	92.4
93.0	92.4	91.9	91.9	91.9	92.4	92.4	93.0	93.0	93.5	93.5	93.5	94.0	94.0	94.0	94.5
				NOT VIEWABLE - UNDER HOLD-DOWN BAR - NOT VIEWABLE											
93.5	93.5	93.5	93.5	93.5	93.5	94.0	94.0	94.0	94.0	94.0	94.0	94.0	94.5	94.5	94.5
93.5	93.5	93.5	93.5	93.5	93.5	94.0	94.0	94.0	94.0	94.0	94.0	94.0	94.5	94.5	94.5
93.5	93.5	93.5	93.5	93.5	93.5	94.0	94.0	94.0	94.0	94.0	94.0	94.0	94.5	94.5	94.5

TABLE XV

COMPARISON OF SMOOTHED WATER SATURATION DATA

WITH RAW DATA

LABORATORY DISPLACEMENT NO. 3

AFTER 4.3 HOURS OF INJECTION

AVERAGE AND STANDARD DEVIATION BY WATER SATURATION RANGE

EXPRESSED IN SATURATION PER CENT

FROM	TO	NO. PTS	AVG. DEV.	STD. DEV.
.0	20.0	18	.9	1.3
20.0	40.0	46	.5	.8
40.0	60.0	32	.8	1.0
60.0	80.0	14	.8	1.0
80.0	100.0	82	2.1	2.9
OVERALL		192	1.3	2.1

AFTER 10.3 HOURS OF INJECTION

AVERAGE AND STANDARD DEVIATION BY WATER SATURATION RANGE

EXPRESSED IN SATURATION PER CENT

FROM	TO	NO. PTS	AVG. DEV.	STD. DEV.
.0	20.0	8	1.0	1.2
20.0	40.0	40	.7	1.0
40.0	60.0	16	.7	.9
60.0	80.0	32	1.0	1.4
80.0	100.0	96	2.0	2.7
OVERALL		192	1.4	2.1

AFTER 15.3 HOURS OF INJECTION

AVERAGE AND STANDARD DEVIATION BY WATER SATURATION RANGE

EXPRESSED IN SATURATION PER CENT

FROM	TO	NO. PTS	AVG. DEV.	STD. DEV.
.0	20.0	0	.0	.0
20.0	40.0	32	.7	.9
40.0	60.0	16	.8	1.2
60.0	80.0	48	.7	1.1
80.0	100.0	96	1.7	2.4
OVERALL		192	1.2	1.9

AFTER 20.3 HOURS OF INJECTION

AVERAGE AND STANDARD DEVIATION BY WATER SATURATION RANGE

EXPRESSED IN SATURATION PER CENT

FROM	TO	NO. PTS	AVG. DEV.	STD. DEV.
.0	20.0	0	.0	.0
20.0	40.0	2	.0	.0
40.0	60.0	18	1.2	1.7
60.0	80.0	76	.9	1.3
80.0	100.0	96	1.5	2.1
OVERALL		192	1.2	1.8

AFTER 22.3 HOURS OF INJECTION

AVERAGE AND STANDARD DEVIATION BY WATER SATURATION RANGE

EXPRESSED IN SATURATION PER CENT

FROM	TO	NO. PTS	AVG. DEV.	STD. DEV.
.0	20.0	0	.0	.0
20.0	40.0	0	.0	.0
40.0	60.0	14	1.6	2.2
60.0	80.0	82	.9	1.5
80.0	100.0	96	1.4	2.1
OVERALL		192	1.2	1.8

TABLE XVI

COMPARISON OF SMOOTHED WATER SATURATION DATA WITH RAW DATA
LABORATORY DISPLACEMENT NO. 4

AFTER 4.0 HOURS OF INJECTION

AVERAGE AND STANDARD DEVIATION BY WATER SATURATION RANGE
EXPRESSED IN SATURATION PER CENT

FROM	TO	NO. PTS	AVG. DEV.	STD. DEV.
.0	20.0	6	.0	.0
20.0	40.0	42	.3	.5
40.0	60.0	48	.6	.9
60.0	80.0	15	.5	.8
80.0	100.0	81	1.5	2.2
OVERALL		192	.9	1.5

AFTER 10.0 HOURS OF INJECTION

AVERAGE AND STANDARD DEVIATION BY WATER SATURATION RANGE
EXPRESSED IN SATURATION PER CENT

FROM	TO	NO. PTS	AVG. DEV.	STD. DEV.
.0	20.0	0	.0	.0
20.0	40.0	48	.8	1.1
40.0	60.0	16	1.3	1.7
60.0	80.0	45	1.1	1.5
80.0	100.0	83	1.7	2.4
OVERALL		192	1.3	1.9

AFTER 15.0 HOURS OF INJECTION

AVERAGE AND STANDARD DEVIATION BY WATER SATURATION RANGE
EXPRESSED IN SATURATION PER CENT

FROM	TO	NO. PTS	AVG. DEV.	STD. DEV.
.0	20.0	0	.0	.0
20.0	40.0	32	.8	1.0
40.0	60.0	16	.8	1.3
60.0	80.0	59	.6	.9
80.0	100.0	85	1.5	2.3
OVERALL		192	1.1	1.7

AFTER 20.0 HOURS OF INJECTION

AVERAGE AND STANDARD DEVIATION BY WATER SATURATION RANGE
EXPRESSED IN SATURATION PER CENT

FROM	TO	NO. PTS	AVG. DEV.	STD. DEV.
.0	20.0	0	.0	.0
20.0	40.0	0	.0	.0
40.0	60.0	16	1.7	2.2
60.0	80.0	92	.9	1.4
80.0	100.0	84	1.6	2.3
OVERALL		192	1.3	1.9

AFTER 22.0 HOURS OF INJECTION

AVERAGE AND STANDARD DEVIATION BY WATER SATURATION RANGE
EXPRESSED IN SATURATION PER CENT

FROM	TO	NO. PTS	AVG. DEV.	STD. DEV.
.0	20.0	0	.0	.0
20.0	40.0	0	.0	.0
40.0	60.0	0	.0	.0
60.0	80.0	107	1.0	1.7
80.0	100.0	85	1.6	2.4
OVERALL		192	1.3	2.0

TABLE XVII

OVER-ALL REPRODUCIBILITY

COMPARISON OF WATER SATURATION DATA

OF DISPLACEMENTS NO. 3 AND NO. 4

AFTER 4.3 HOURS AND 4.0 HOURS

AVERAGE AND STANDARD DEVIATION BY SATURATION RANGE

EXPRESSED IN SATURATION PER CENT

FROM	TO	NO. PTS	AVG. DEV.	STD. DEV.
.0	20.0	11	5.3	5.5
20.0	40.0	37	2.0	2.5
40.0	60.0	32	.8	1.1
60.0	80.0	16	1.8	1.9
80.0	100.0	96	.8	1.1
OVERALL			1.4	2.0

AFTER 10.3 HOURS AND 10.0 HOURS

AVERAGE AND STANDARD DEVIATION BY SATURATION RANGE

EXPRESSED IN SATURATION PER CENT

FROM	TO	NO. PTS	AVG. DEV.	STD. DEV.
.0	20.0	0	.0	.0
20.0	40.0	43	1.6	1.9
40.0	60.0	20	1.8	2.1
60.0	80.0	17	.9	1.1
80.0	100.0	112	1.1	1.7
OVERALL			1.3	1.7

AFTER 15.3 HOURS AND 15.0 HOURS

AVERAGE AND STANDARD DEVIATION BY SATURATION RANGE

EXPRESSED IN SATURATION PER CENT

FROM	TO	NO. PTS	AVG. DEV.	STD. DEV.
.0	20.0	0	.0	.0
20.0	40.0	17	1.3	1.7
40.0	60.0	31	1.6	1.9
60.0	80.0	16	4.0	4.1
80.0	100.0	128	.9	1.2
OVERALL			1.3	1.8

AFTER 20.3 HOURS AND 20.0 HOURS

AVERAGE AND STANDARD DEVIATION BY SATURATION RANGE

EXPRESSED IN SATURATION PER CENT

FROM	TO	NO. PTS	AVG. DEV.	STD. DEV.
.0	20.0	0	.0	.0
20.0	40.0	0	.0	.0
40.0	60.0	16	3.4	3.4
60.0	80.0	16	2.7	3.3
80.0	100.0	160	1.0	1.4
OVERALL			1.3	1.9

AFTER 22.3 HOURS AND 22.0 HOURS

AVERAGE AND STANDARD DEVIATION BY SATURATION RANGE

EXPRESSED IN SATURATION PER CENT

FROM	TO	NO. PTS	AVG. DEV.	STD. DEV.
.0	20.0	0	.0	.0
20.0	40.0	0	.0	.0
40.0	60.0	0	.0	.0
60.0	80.0	16	5.7	5.8
80.0	100.0	176	.9	1.4
OVERALL			1.3	2.1

E. Discussion of Results

The saturation measurement technique developed here has been shown to be reliable and convenient. It should be applicable in any transluscent two-dimensional system employing fluids with markedly different refractive indices. Its advantages over other methods lie in its reliance on external sensing elements, its ease of operation and its relatively low cost.

In its present form, however, the technique is limited to low-rate displacements because of the time required to effectively monitor the two-dimensional system. Based on a 14 minute measurement cycle to obtain light intensities at 8 points, a scan of the full grid system requires about 6 hours. Thus in a 24 hour displacement, only four full scans can be made. By concentrating on zones experiencing most rapid saturation changes, and by staggering the half row measurements, the method was operated at maximum efficiency.

Several improvements could be made to reduce the scan time considerably. In the present circuit, current is the metered variable. Consequently it is necessary to switch each cell into the circuit individually. If voltage across a known resistance were measured, all cells could be activated simultaneously with switching involving the metering element only. This would reduce the cycle time to about four minutes allowing two minutes for cell positioning and the remainder for simultaneous equilibration of all cells and recording. The next logical improvement would be to increase the number of mounting units, with the ultimate solution employing a separate cell fixed at each viewable grid point. With more than eight cells, an automatic recording device would be desirable.

One consideration not discussed so far is the "distribution effect" on the measured distributions. In this application, the effect should not be important because the distributions used in calibration are not far removed from those encountered in the displacements. At much higher rates, however, the saturation gradients should become steeper and this effect might become important. Reference to Figure 18 shows the intensity to fall off roughly by a factor of 4 for each inch the cell is moved laterally from the illuminated area. The representative calibration curve, Figure 19 shows that a saturation gradient of 25 per cent per inch also results in an attenuation of about 4. Qualitatively it would appear that this steep a gradient would result in an appreciable distribution effect. Quantitative elimination of the distribution effect requires the type of approach described earlier [Equations (122a) - (122e)].

Another approach could be used to reduce the distribution effect. This would employ a moving photo cell and a moving narrow beam of light on the other side of the pack. Obviously, this would require a fairly sophisticated traversing mechanism.

More accuracy probably would result in the present system if better photo cells and a constant intensity source were employed. In the absence of a constant intensity source, direct measurement of source intensity would be desirable. It will be recalled that source variation was handled here by monitoring an element experiencing little saturation change during displacement.

Both the measurement technique and the saturation distributions obtained through the use of the technique during displacement were found

to show about the same degree of precision (1.5 per cent average absolute deviation and 2 per cent standard deviation). This indicates that the two-dimensional phase distribution data are probably quite accurate. However, a valid assessment of the accuracy of the data would require knowledge of the true phase distribution. This information can be obtained only through absolute measurements such as physical sampling.

In the absence of absolute data, the imbibition distributions measured just prior to breakthrough allow an estimate of the accuracy to be made. Since breakthrough occurred for all three imbibition displacements at nearly the same average water saturation, the water saturation corresponding to "residual gas" appears to be about 89 per cent. (Breakthrough average saturations were 88.3 per cent for Displacement No. 2 and 89.3 per cent for Displacements No. 3 and 4.) Reference to the tabulated distributions, Tables X(a-f), XIII(a-e), and XIV(a-e) shows the bottom few rows to have water saturations of about 94 per cent. It will be noted, however, that the water saturation of a point initially less than 86 per cent seldom rose about that value. Thus it appears that higher saturations can result only at very low rates of imbibition, and may actually arise because of solubility effects. This premise is borne out in the earlier occurrence of breakthrough for Displacement No. 2 than for No.'s 3 and 4 as the initial average water saturation was lower in the case of the former. Therefore, a better estimate of the effective water saturation corresponding to residual gas would be about 86 per cent.

Near breakthrough (40 and 22 hours for Displacement No. 2, and No.'s 3 and 4, respectively) all points except those in the top row would

be expected to be at or above the residual saturation. Those in the top row would not reach residual until all gas production had ceased. If the water saturation at all points not in the top row but initially below the residual saturation are compared to the residual saturation of 86 per cent, the average deviation is about 2 per cent. Therefore, in the high range of saturation, the accuracy of the measurements should average to about 2 saturation per cent. Since the precision of the measurements is higher in the mid range of water saturation (40-80 per cent), it is reasonable to expect better accuracy there too. The good conformance of the initial distributions to the imbibition capillary pressure curve shown in Figure 26 especially in the mid range of water saturation indicates this. Thus it is concluded that the accuracy of the data is of about the same quality as the precision.

This estimate of accuracy was based on the imbibition displacements. Since the correlation between relative intensity and water saturation was developed using drainage distributions, the accuracy of the data obtained for the drainage displacement may be better.

In view of the precision and apparent accuracy of the data, they should provide an excellent basis for evaluating the degree to which the differential equations describe the displacement process.

VII. NUMERICAL RESULTS FOR LABORATORY DISPLACEMENTS

Numerical solutions of the differential equations have been carried out for the laboratory displacements. The results are presented and compared to experimental data in the following order:

A. Drainage Displacement

B. Imbibition Displacements

C. Discussion of Results

D. Conclusions

The laboratory model was described conveniently in a 16 x 16 grid of elements one inch square by 17/32 inch thick. All elements were assigned the measured over-all permeability (10.2 Darcys) and porosity (39.1 per cent). Injection and production were designated at the appropriate grid elements through circular wells 1/8 inch in diameter with 36 per cent open area.

For both drainage and imbibition displacements, the relative permeability curves shown in Figure 22 were used. Each curve was represented in tabular form with table entries for every 2 per cent interval of water saturation (51 entries in each table). Relative permeabilities corresponding to a given water saturation were interpolated linearly between table entries for the appropriate bracket of water saturation. The curves of Figure 22 are based on the data of Wyckoff and Botset[59] for the flow of air and water in a variety of unconsolidated sands.

Capillary pressure data were determined experimentally for drainage and imbibition. The resulting curves were handled by table look-up much the same as relative permeabilities. However, since phase

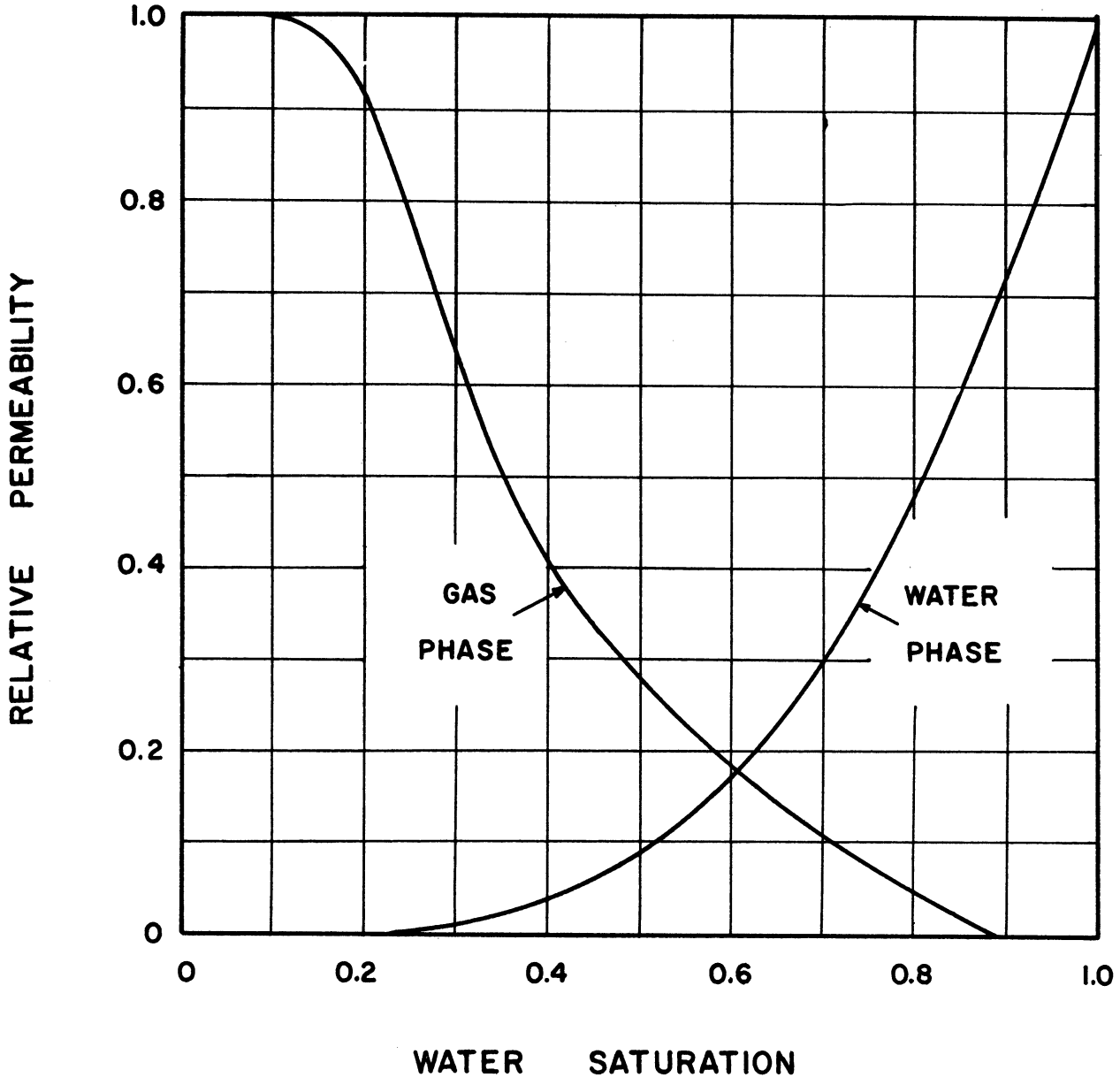

Figure 22. Relative Permeability Curves
Laboratory Medium

[After Wyckoff and Botset(59)]

potentials were the dependent variables it was convenient to tabulate values of water saturation for intervals of capillary pressure. In the mid range of water saturation, equal intervals of capillary pressure were used with coarser spacing near residual saturations.

A. Drainage Displacement

The drainage capillary pressure curve presented in Figure 23 was employed in numerical solution. This is the same curve used in calibration of the light attenuation technique for water saturation measurement. Data points indicated on the curve were obtained by gravity drainage in the cylindrical bead pack as described earlier. Points are the raw data after pack differences had been accounted for by linear transformation of capillary pressure according to Equation (119) with constants A = 1.163 and B = -0.004 atm.

Helium injection rates were varied during the computations closely matching the measured rates presented in Table VI of the previous section.

To cover the 50 hour period over which water saturation distributions were measured a total of 141 time steps of variable length were used. For the 6 displacement times at which computed and experimental water saturation distributions are to be compared, Table XVIII presents a summary of the numerical solution. Time step numbers corresponding to the displacement times have been included to indicate the average time step size over each interval. The water content of the pore volume and the cumulative water phase material balance are listed at the displacement times of interest. The cumulative material balance

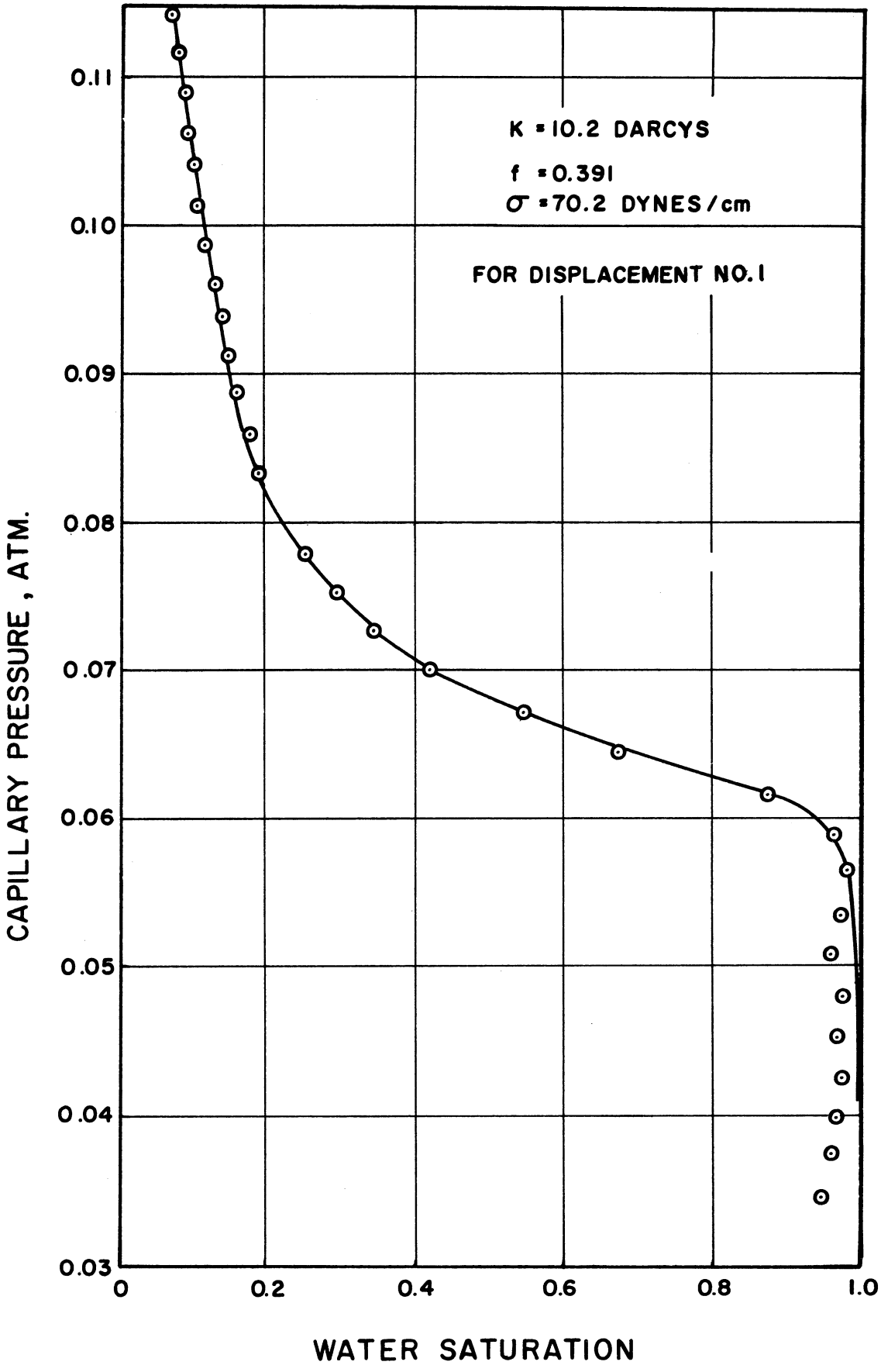

Figure 23. Drainage Capillary Pressure Curve
Laboratory Medium

is an independent check on the numerical solution and is computed according to Equation (II-3b) in Appendix II.

TABLE XVIII

SUMMARY OF NUMERICAL SOLUTION
Displacement No. 1

Time	Time Step No.	Water in P.V.	Cumulative Water Balance
5.00 hrs.	21	839 cc	0.00%
10.59 hrs.	47	798 cc	0.02%
14.29 hrs.	58	765 cc	0.02%
25.27 hrs.	89	674 cc	0.04%
39.80 hrs.	119	556 cc	0.10%
50.32 hrs.	141	464 cc	0.18%

Solution was not carried out to gas breakthrough due to the excessive time requirement and the marginal value of further computations as water saturation had been monitored experimentally only to about 55 hours. Extreme fingering which results in this type of displacement at breakthrough is governed by local inhomogeneities in the porous medium near the production well. Even if these inhomogeneities were known accurately, they could not be described in a one inch grid system. Hence, comparison of computed and experimental breakthrough times would not be expected to be meaningful.

Computed water saturation distributions are listed at the six displacement times in Tables XIX(a-f). Rows and columns of the tables

TABLE XIX

COMPUTED WATER SATURATION DISTRIBUTIONS

a. LABORATORY DISPLACEMENT NO. 1 AFTER 5.00 HOURS OF INJECTION

WATER SATURATION DISTRIBUTION

OBTAINED BY NUMERICAL SOLUTION

BY ROWS FROM UPPER LEFT

78.6	76.1	74.6	68.0	62.8	60.8	60.4	61.9	64.8	70.9	74.7	76.7	77.2	77.3	76.5	76.0
92.2	91.4	89.1	83.7	78.2	75.9	75.7	77.1	80.8	86.3	89.3	91.0	91.5	91.4	91.0	90.6
96.9	96.9	96.3	95.1	92.6	91.3	91.2	92.1	93.9	95.5	96.2	96.6	96.7	96.6	96.5	96.4
97.9	97.9	97.8	97.6	97.1	96.8	96.8	97.0	97.5	97.6	97.8	97.8	97.9	97.8	97.8	97.8
98.5	98.5	98.4	98.2	97.9	97.9	97.9	97.9	98.1	98.2	98.4	98.4	98.4	98.4	98.4	98.4
99.0	99.0	99.0	98.7	98.5	98.4	98.4	98.5	98.6	98.8	98.9	99.0	99.0	99.0	99.0	99.0
99.1	99.1	99.1	99.0	99.0	99.0	99.0	99.0	99.0	99.1	99.1	99.1	99.1	99.1	99.1	99.1
99.2	99.2	99.2	99.1	99.1	99.1	99.1	99.1	99.1	99.1	99.2	99.2	99.2	99.2	99.2	99.2
99.3	99.3	99.3	99.2	99.2	99.2	99.2	99.2	99.2	99.2	99.2	99.3	99.3	99.3	99.3	99.3
99.4	99.4	99.3	99.3	99.3	99.3	99.3	99.3	99.3	99.3	99.3	99.3	99.3	99.3	99.3	99.3
99.4	99.4	99.4	99.4	99.4	99.3	99.3	99.4	99.4	99.4	99.4	99.4	99.4	99.4	99.4	99.4
99.5	99.5	99.5	99.5	99.4	99.4	99.4	99.4	99.5	99.5	99.5	99.5	99.5	99.5	99.5	99.5
99.6	99.6	99.6	99.6	99.5	99.5	99.5	99.5	99.6	99.6	99.6	99.6	99.6	99.6	99.6	99.6
99.7	99.7	99.7	99.7	99.6	99.6	99.6	99.6	99.6	99.7	99.7	99.7	99.7	99.7	99.7	99.7
99.7	99.7	99.7	99.7	99.7	99.7	99.7	99.7	99.7	99.7	99.7	99.7	99.7	99.7	99.7	99.7
99.7	99.7	99.7	99.7	99.7	99.7	99.7	99.7	99.7	99.7	99.7	99.7	99.7	99.7	99.7	99.7

b. LABORATORY DISPLACEMENT NO. 1 AFTER 10.59 HOURS OF INJECTION

WATER SATURATION DISTRIBUTION

OBTAINED BY NUMERICAL SOLUTION

BY ROWS FROM UPPER LEFT

48.9	48.7	49.0	48.9	48.6	48.6	48.3	48.5	48.1	48.7	48.9	48.7	48.6	48.5	48.5	48.5
61.3	61.2	61.0	61.2	61.5	61.4	61.1	61.2	61.3	61.2	61.3	61.4	61.3	61.4	61.2	61.2
76.4	76.3	76.2	76.2	76.6	76.7	76.4	76.6	76.6	76.4	76.7	76.6	76.6	76.6	76.6	76.5
90.6	90.7	90.7	90.7	90.8	90.9	90.9	90.8	90.9	90.9	90.9	90.9	90.9	90.9	90.9	90.9
96.8	96.9	96.9	96.8	96.5	96.4	96.4	96.4	96.5	96.7	96.7	96.6	96.6	96.5	96.5	96.5
97.9	97.9	97.9	97.9	97.8	97.8	97.8	97.8	97.8	97.9	97.9	97.8	97.8	97.8	97.8	97.8
98.5	98.6	98.5	98.5	98.4	98.4	98.4	98.3	98.4	98.4	98.5	98.4	98.4	98.4	98.4	98.4
99.0	99.0	99.0	99.0	99.0	98.9	98.9	98.9	99.0	99.0	99.0	99.0	99.0	99.0	99.0	99.0
99.1	99.1	99.1	99.1	99.1	99.1	99.1	99.1	99.1	99.1	99.1	99.1	99.1	99.1	99.1	99.1
99.2	99.2	99.2	99.2	99.2	99.2	99.2	99.2	99.2	99.2	99.2	99.2	99.2	99.2	99.2	99.2
99.3	99.3	99.3	99.3	99.3	99.2	99.2	99.2	99.3	99.3	99.3	99.3	99.3	99.3	99.3	99.3
99.4	99.4	99.4	99.4	99.3	99.3	99.3	99.3	99.3	99.4	99.4	99.3	99.3	99.3	99.3	99.3
99.5	99.5	99.5	99.5	99.4	99.4	99.4	99.4	99.4	99.4	99.4	99.4	99.4	99.4	99.4	99.4
99.6	99.6	99.6	99.6	99.5	99.5	99.5	99.5	99.5	99.5	99.5	99.5	99.5	99.5	99.5	99.5
99.6	99.6	99.6	99.6	99.6	99.6	99.6	99.6	99.6	99.6	99.6	99.6	99.6	99.6	99.6	99.6
99.7	99.7	99.7	99.7	99.7	99.7	99.7	99.7	99.7	99.7	99.7	99.7	99.7	99.7	99.7	99.7

c. LABORATORY DISPLACEMENT NO. 1 AFTER 14.29 HOURS OF INJECTION

WATER SATURATION DISTRIBUTION

OBTAINED BY NUMERICAL SOLUTION

BY ROWS FROM UPPER LEFT

40.3	40.0	40.1	39.9	39.6	39.4	39.0	39.2	38.8	38.9	38.9	38.9	38.7	38.7	38.6	38.6
49.8	49.5	49.2	49.3	49.4	49.2	48.7	48.9	48.7	48.2	48.2	48.4	48.2	48.3	48.0	48.0
62.7	62.4	62.0	62.0	62.3	62.0	61.4	61.7	61.4	60.7	60.8	60.9	60.7	60.7	60.5	60.4
77.8	77.6	77.3	77.4	77.4	77.2	76.8	76.9	76.6	76.1	76.0	76.2	76.0	75.9	75.7	75.6
91.5	91.7	91.6	91.7	91.0	91.1	91.1	90.8	90.7	90.5	90.3	90.4	90.2	90.0	90.0	90.0
96.9	97.1	97.0	97.0	96.6	96.5	96.5	96.4	96.5	96.5	96.5	96.5	96.4	96.3	96.4	96.3
97.9	97.9	97.9	97.9	97.8	97.8	97.8	97.8	97.8	97.8	97.8	97.8	97.8	97.8	97.8	97.8
98.5	98.6	98.5	98.5	98.4	98.4	98.4	98.4	98.4	98.4	98.4	98.4	98.4	98.4	98.4	98.4
99.0	99.0	99.0	99.0	99.0	99.0	99.0	98.9	99.0	99.0	99.0	99.0	99.0	98.9	98.9	98.9
99.1	99.1	99.1	99.1	99.1	99.1	99.1	99.1	99.1	99.1	99.1	99.1	99.1	99.1	99.1	99.1
99.2	99.2	99.2	99.2	99.2	99.2	99.2	99.2	99.2	99.2	99.2	99.2	99.2	99.2	99.2	99.2
99.3	99.3	99.3	99.3	99.3	99.3	99.2	99.2	99.3	99.3	99.3	99.3	99.3	99.2	99.2	99.2
99.4	99.4	99.4	99.4	99.3	99.3	99.3	99.3	99.3	99.3	99.3	99.3	99.3	99.3	99.3	99.3
99.5	99.5	99.5	99.5	99.4	99.4	99.4	99.4	99.4	99.4	99.4	99.4	99.4	99.4	99.4	99.4
99.5	99.6	99.6	99.5	99.5	99.5	99.5	99.5	99.5	99.5	99.5	99.5	99.5	99.5	99.5	99.5
99.6	99.6	99.6	99.6	99.6	99.6	99.6	99.6	99.6	99.6	99.6	99.6	99.6	99.6	99.6	99.6

TABLE XIX (CONT'D)

d. LABORATORY DISPLACEMENT NO. 1 AFTER 25.27 HOURS OF INJECTION

WATER SATURATION DISTRIBUTION

OBTAINED BY NUMERICAL SOLUTION

BY ROWS FROM UPPER LEFT

27.0	26.7	26.8	26.6	26.6	26.3	25.9	25.6	25.1	25.5	26.2	26.9	27.3	27.7	27.8	27.9
31.0	30.8	30.6	30.6	30.9	30.6	30.3	30.0	29.6	29.7	30.4	31.0	31.4	31.9	31.9	32.0
36.9	36.6	36.5	36.4	36.8	36.5	36.1	35.7	35.2	35.3	36.2	37.1	37.6	38.1	38.2	38.3
44.9	44.5	44.4	44.4	44.9	44.7	44.2	43.6	42.8	43.1	44.4	45.6	46.3	46.9	47.0	47.1
55.0	54.9	55.0	55.2	55.5	55.7	55.7	55.2	54.5	55.0	56.0	57.1	57.7	58.3	58.0	58.1
69.3	69.4	69.5	69.7	69.9	70.1	70.2	70.2	70.5	71.1	71.4	71.8	72.3	72.6	72.7	72.8
84.3	84.4	84.6	84.8	84.9	85.2	85.4	85.6	86.0	86.5	86.8	87.2	87.4	87.6	87.7	87.8
95.1	95.1	95.2	95.2	95.1	95.1	95.2	95.1	95.2	95.3	95.5	95.6	95.7	95.7	95.7	95.8
97.6	97.6	97.6	97.6	97.5	97.6	97.6	97.6	97.6	97.6	97.6	97.6	97.7	97.7	97.7	97.7
98.2	98.2	98.2	98.2	98.1	98.1	98.1	98.1	98.2	98.2	98.2	98.2	98.2	98.2	98.2	98.2
98.7	98.8	98.8	98.8	98.7	98.7	98.7	98.7	98.7	98.8	98.8	98.8	98.8	98.8	98.8	98.8
99.0	99.1	99.1	99.0	99.0	99.0	99.0	99.0	99.0	99.0	99.1	99.1	99.1	99.1	99.1	99.1
99.1	99.1	99.1	99.1	99.1	99.1	99.1	99.1	99.1	99.1	99.1	99.1	99.1	99.1	99.1	99.1
99.2	99.2	99.2	99.2	99.2	99.2	99.2	99.2	99.2	99.2	99.2	99.2	99.2	99.2	99.2	99.2
99.3	99.3	99.3	99.3	99.3	99.3	99.3	99.3	99.3	99.3	99.3	99.3	99.3	99.3	99.3	99.3
99.4	99.4	99.4	99.4	99.4	99.4	99.4	99.4	99.4	99.4	99.4	99.4	99.4	99.4	99.4	99.4

e. LABORATORY DISPLACEMENT NO. 1 AFTER 39.80 HOURS OF INJECTION

WATER SATURATION DISTRIBUTION

OBTAINED BY NUMERICAL SOLUTION

BY ROWS FROM UPPER LEFT

18.9	18.7	18.7	18.6	18.5	18.3	18.0	17.8	17.6	18.1	18.6	19.1	19.4	19.7	19.8	19.8
21.0	20.7	20.6	20.5	20.6	20.3	19.9	19.6	19.5	19.9	20.6	21.3	21.7	22.2	22.3	22.4
23.8	23.5	23.4	23.2	23.3	23.0	22.4	22.0	21.8	22.4	23.4	24.3	25.0	25.5	25.6	25.7
28.2	27.8	27.5	27.2	27.5	26.8	25.9	25.3	25.1	26.0	27.8	28.7	29.1	29.6	29.8	29.9
31.8	31.5	31.3	31.2	31.2	30.9	30.4	29.8	29.7	30.7	32.1	33.4	34.3	34.8	35.0	35.1
37.8	37.5	37.3	37.2	37.2	36.7	36.1	35.6	36.0	37.3	38.6	39.9	41.0	41.7	42.0	42.1
46.2	45.8	45.6	45.5	45.6	45.1	44.5	43.9	44.5	46.3	48.0	49.5	50.5	51.3	51.6	51.7
56.7	56.4	56.2	56.2	56.4	56.6	56.7	56.9	57.7	59.2	60.7	62.2	63.2	63.8	64.2	64.3
70.7	70.6	70.5	70.7	71.0	71.7	72.6	73.6	74.5	75.4	76.3	77.3	77.9	78.3	78.6	78.7
85.1	85.2	85.3	85.5	86.0	86.9	87.7	88.6	89.5	90.3	91.0	91.7	92.3	92.2	92.3	92.3
95.2	95.3	95.3	95.3	95.4	95.5	95.7	95.9	96.2	96.4	96.5	96.7	96.8	96.8	96.9	96.9
97.6	97.6	97.6	97.6	97.6	97.6	97.7	97.7	97.7	97.8	97.8	97.8	97.9	97.9	97.9	97.9
98.2	98.2	98.2	98.2	98.2	98.2	98.2	98.3	98.3	98.4	98.4	98.4	98.4	98.4	98.4	98.5
98.7	98.7	98.7	98.7	98.7	98.8	98.8	98.9	98.9	98.9	99.0	99.0	99.0	99.0	99.0	99.0
99.0	99.0	99.0	99.0	99.0	99.0	99.1	99.1	99.1	99.1	99.1	99.1	99.1	99.1	99.1	99.1
99.1	99.1	99.1	99.1	99.1	99.1	99.1	99.1	99.2	99.2	99.2	99.2	99.2	99.2	99.2	99.2

f. LABORATORY DISPLACEMENT NO. 1 AFTER 50.32 HOURS OF INJECTION

WATER SATURATION DISTRIBUTION

OBTAINED BY NUMERICAL SOLUTION

BY ROWS FROM UPPER LEFT

16.1	15.9	15.8	15.7	15.6	15.3	15.0	14.7	14.5	14.8	15.2	15.6	15.8	16.0	16.1	16.1
17.6	17.4	17.3	17.1	17.1	16.8	16.5	16.1	16.0	16.2	16.6	17.1	17.4	17.6	17.6	17.7
19.3	19.1	18.9	18.8	18.8	18.5	18.1	17.7	17.5	17.8	18.3	18.8	19.1	19.3	19.4	19.4
21.4	21.1	21.0	20.8	20.8	20.4	19.9	19.5	19.3	19.6	20.2	20.8	21.2	21.5	21.6	21.6
24.2	24.0	23.8	23.7	23.6	23.2	22.7	22.0	21.8	22.3	23.1	23.7	24.1	24.4	24.5	24.6
28.5	28.4	28.3	28.1	27.9	27.1	26.1	25.4	25.4	26.1	27.2	28.1	28.4	28.6	28.7	28.7
32.7	32.4	32.2	32.0	31.9	31.2	30.5	29.9	29.9	30.6	31.3	32.0	32.6	33.0	33.1	33.1
38.6	38.4	38.2	38.0	37.9	37.5	37.1	36.6	36.6	37.0	37.7	38.2	38.6	38.9	39.0	39.1
47.3	47.1	46.9	46.7	46.6	46.4	46.2	46.1	46.1	46.2	46.7	47.1	47.4	47.7	47.8	47.9
58.8	58.6	58.4	58.3	58.4	58.4	58.2	58.2	58.3	58.4	58.7	59.0	59.3	59.4	59.5	59.6
73.6	73.4	73.4	73.4	73.4	73.5	73.5	73.5	73.6	73.7	74.0	74.1	74.3	74.4	74.4	74.4
88.3	88.3	88.2	88.2	88.2	88.3	88.4	88.5	88.6	88.7	88.8	88.9	89.0	89.0	89.1	89.1
95.9	95.9	95.9	95.9	95.8	95.8	95.9	95.9	95.9	95.9	96.0	96.0	96.0	96.0	96.0	96.0
97.7	97.7	97.7	97.7	97.7	97.7	97.7	97.7	97.7	97.7	97.7	97.7	97.7	97.7	97.7	97.7
98.3	98.3	98.3	98.3	98.3	98.3	98.3	98.3	98.3	98.3	98.3	98.3	98.3	98.3	98.3	98.3
98.8	98.8	98.8	98.8	98.8	98.8	98.8	98.8	98.8	98.9	98.9	98.9	98.9	98.9	98.9	98.9

correspond to the rows and columns of the grid on the face of the laboratory model. Point by point comparison of the computed distributions of Tables XIX(a-f) to the experimental distributions of Tables VII(a-f) for the 192 viewable grid elements resulted in the average absolute and standard deviations presented in Table XX. Again deviations are listed by saturation ranges and over-all in terms of saturation per cent.

Contours of constant water saturation obtained by cross plotting the computed distributions are shown in Figures 24a and b at 14.29 and 50.32 hours with about one fourth of the experimental data points indicated. The experimental and computed distributions averaged across a horizontal row are plotted for three rows against time in Figure 25.

The two-dimensional saturation contours shown in Figures 24a and 24b do not exhibit the fingering tendency observed experimentally. However, the horizontal variation in water saturation which has developed by the 50 hour mark indicates that inclusion of small pack inhomogeneities at the appropriate grid elements would probably result in fingering similar to that shown by the experimental data. Such effects would have to be explored on a trial and error basis since direct measurement of local porosities and permeabilities would not be possible.

The unstable nature of this displacement was also evidenced in the numerical solution by the severe restriction on time step size required for convergence of the iteration procedure involved in updating the R variable. It will be recalled that the phase saturation distribution follows directly from the R distribution. Such a restriction did not seem to exist in the numerical solution describing the imbibition displacements as time steps of 30 minutes gave satisfactory results. Since the

TABLE XX

COMPARISON OF COMPUTED TO EXPERIMENTAL
WATER SATURATION DISTRIBUTIONS

LABORATORY DISPLACEMENT NO. 1

AFTER 5.00 HOURS OF INJECTION

AVERAGE ABSOLUTE DEVIATION AND STANDARD DEVIATION

FROM NUMERICAL SOLUTION - EXPRESSED IN SATURATION PER CENT

OVERALL AVERAGE DEVIATION = 2.0 STANDARD DEVIATION = 4.5

AVERAGE AND STANDARD DEVIATION BY SATURATION RANGE

FROM	TO	NO. PTS	AVG. DEV.	STD. DEV.
.0	20.0	0	.0	.0
20.0	40.0	0	.0	.0
40.0	60.0	0	.0	.0
60.0	80.0	20	10.9	12.5
80.0	100.0	172	1.0	2.2

LABORATORY DISPLACEMENT NO. 1

AFTER 10.59 HOURS OF INJECTION

AVERAGE ABSOLUTE DEVIATION AND STANDARD DEVIATION

FROM NUMERICAL SOLUTION - EXPRESSED IN SATURATION PER CENT

OVERALL AVERAGE DEVIATION = 2.0 STANDARD DEVIATION = 3.9

AVERAGE AND STANDARD DEVIATION BY SATURATION RANGE

FROM	TO	NO. PTS	AVG. DEV.	STD. DEV.
.0	20.0	0	.0	.0
20.0	40.0	0	.0	.0
40.0	60.0	16	9.3	9.9
60.0	80.0	32	5.1	6.2
80.0	100.0	144	.5	.7

LABORATORY DISPLACEMENT NO. 1

AFTER 14.29 HOURS OF INJECTION

AVERAGE ABSOLUTE DEVIATION AND STANDARD DEVIATION

FROM NUMERICAL SOLUTION - EXPRESSED IN SATURATION PER CENT

OVERALL AVERAGE DEVIATION = 2.2 STANDARD DEVIATION = 3.9

AVERAGE AND STANDARD DEVIATION BY SATURATION RANGE

FROM	TO	NO. PTS	AVG. DEV.	STD. DEV.
.0	20.0	0	.0	.0
20.0	40.0	14	9.9	10.4
40.0	60.0	18	5.2	6.1
60.0	80.0	16	4.9	5.4
80.0	100.0	144	.8	1.3

LABORATORY DISPLACEMENT NO. 1

AFTER 25.27 HOURS OF INJECTION

AVERAGE ABSOLUTE DEVIATION AND STANDARD DEVIATION

FROM NUMERICAL SOLUTION - EXPRESSED IN SATURATION PER CENT

OVERALL AVERAGE DEVIATION = 3.1 STANDARD DEVIATION = 4.7

AVERAGE AND STANDARD DEVIATION BY SATURATION RANGE

FROM	TO	NO. PTS	AVG. DEV.	STD. DEV.
.0	20.0	0	.0	.0
20.0	40.0	48	5.8	6.7
40.0	60.0	16	5.2	6.0
60.0	80.0	16	6.3	7.3
80.0	100.0	112	1.2	2.6

LABORATORY DISPLACEMENT NO. 1

AFTER 39.80 HOURS OF INJECTION

AVERAGE ABSOLUTE DEVIATION AND STANDARD DEVIATION

FROM NUMERICAL SOLUTION - EXPRESSED IN SATURATION PER CENT

OVERALL AVERAGE DEVIATION = 3.6 STANDARD DEVIATION = 5.0

AVERAGE AND STANDARD DEVIATION BY SATURATION RANGE

FROM	TO	NO. PTS	AVG. DEV.	STD. DEV.
.0	20.0	20	8.7	9.1
20.0	40.0	56	4.8	5.8
40.0	60.0	20	5.5	6.3
60.0	80.0	0	.0	.0
80.0	100.0	96	1.3	2.3

LABORATORY DISPLACEMENT NO. 1

AFTER 50.32 HOURS OF INJECTION

AVERAGE ABSOLUTE DEVIATION AND STANDARD DEVIATION

FROM NUMERICAL SOLUTION - EXPRESSED IN SATURATION PER CENT

OVERALL AVERAGE DEVIATION = 5.2 STANDARD DEVIATION = 6.6

AVERAGE AND STANDARD DEVIATION BY SATURATION RANGE

FROM	TO	NO. PTS	AVG. DEV.	STD. DEV.
.0	20.0	48	8.7	8.9
20.0	40.0	48	3.8	4.2
40.0	60.0	16	8.7	9.5
60.0	80.0	16	9.5	10.2
80.0	100.0	64	1.7	2.7

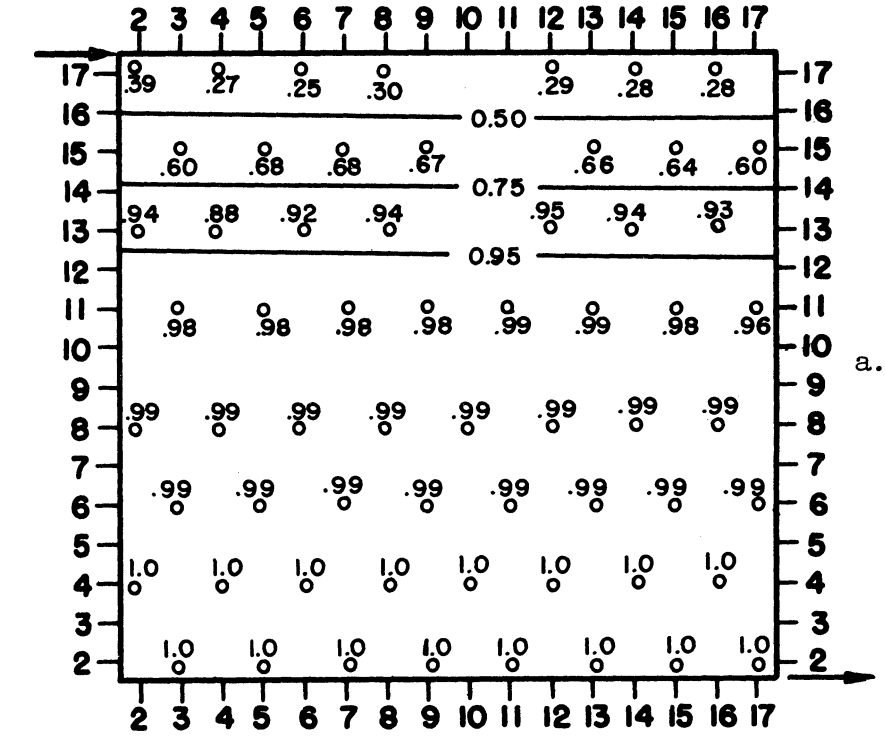

a. At 14.29 Hours

— NUMERICAL SOLUTION

o EXPERIMENTAL DATA

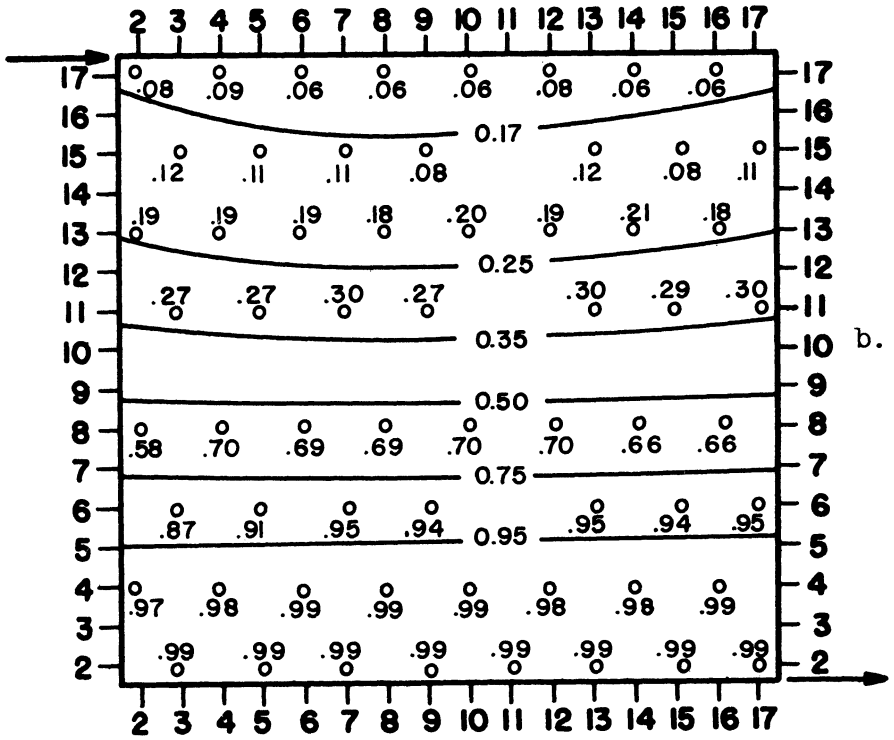

b. At 50.32 Hours

Figure 24. Water Saturation Contours
Displacement No. 1

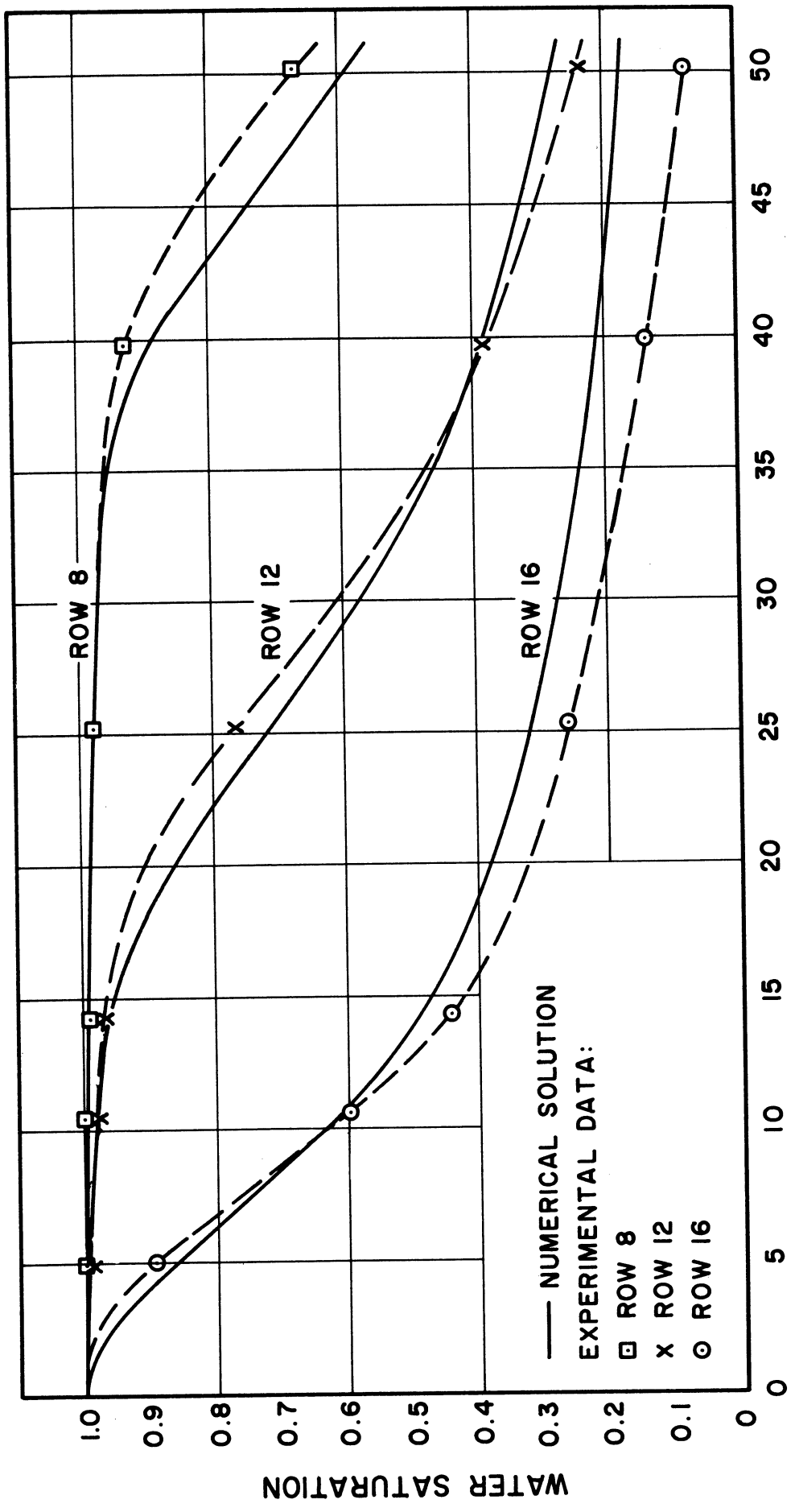

Figure 25. Water Saturation History
Displacement No. 1

same relative permeability functions were used for both types of displacements and the slopes of the capillary pressure curves (Figures 23 and 26) were not greatly different, the time step restriction must have been a reflection of the physical instability of the drainage displacement.

The row-wise saturation history presented by Figure 25 shows the numerical solution to deviate systematically from the experimental data. Agreement could be improved by revision of the capillary pressure curve to have a steeper slope below and a gentler slope above 25 per cent water saturation. The effect would be to cause the elements of the higher levels to approach connate water saturation sooner. From material balance considerations, the saturation at the lower levels would begin to decrease somewhat later in the displacement. This is the behavior shown by the dashed curves passing through the experimental data. Although such revision would be reasonable since the drainage capillary pressure function was obtained in a different medium, its worth is questionable in view of the computational time requirement (about 5 hours of IBM 709 time for 140 time steps).

Over the complete displacement the average and standard deviations between experimental and computed water saturation distributions are shown by Table XX to be about 3.5 and 5 saturation per cent, respectively. The agreement is considered good and it probably could be improved through a revision of the capillary pressure curve and the introduction of small inhomogeneities in the permeability and porosity distributions.

B. Imbibition Displacements

The imbibition capillary pressure curve is shown in Figure 26. Data points were obtained from light intensity scans performed on the imbibition phase distributions existing prior to each of the imbibition displacements. Justification of the 11 per cent residual gas saturation has been discussed earlier.

Water injection rates were set in accordance with the experimental rates listed in Table IX and XII. Half hour time steps were employed after several shorter time steps had been used for the first hour of the displacements.

The numerical solution for Displacement No. 2 will be presented first followed by that for No.'s 3 and 4.

1. Displacement No. 2

The numerical solution is summarized in Table XXI.

TABLE XXI

SUMMARY OF NUMERICAL SOLUTION
Displacement No. 2

Time	Time Step No.	Water in P.V.	Cumulative Water Balance
5 hrs.	13	395.0 cc	0.07%
15 hrs.	33	496.8 cc	0.14%
25 hrs.	53	598.8 cc	0.16%
30 hrs.	63	649.8 cc	0.16%
35 hrs.	73	700.9 cc	0.17%
40 hrs.	83	752.0 cc	0.17%

Breakthrough Time = 42.43 hours

Water Content of P.V. at Breakthrough = 776.6 cc

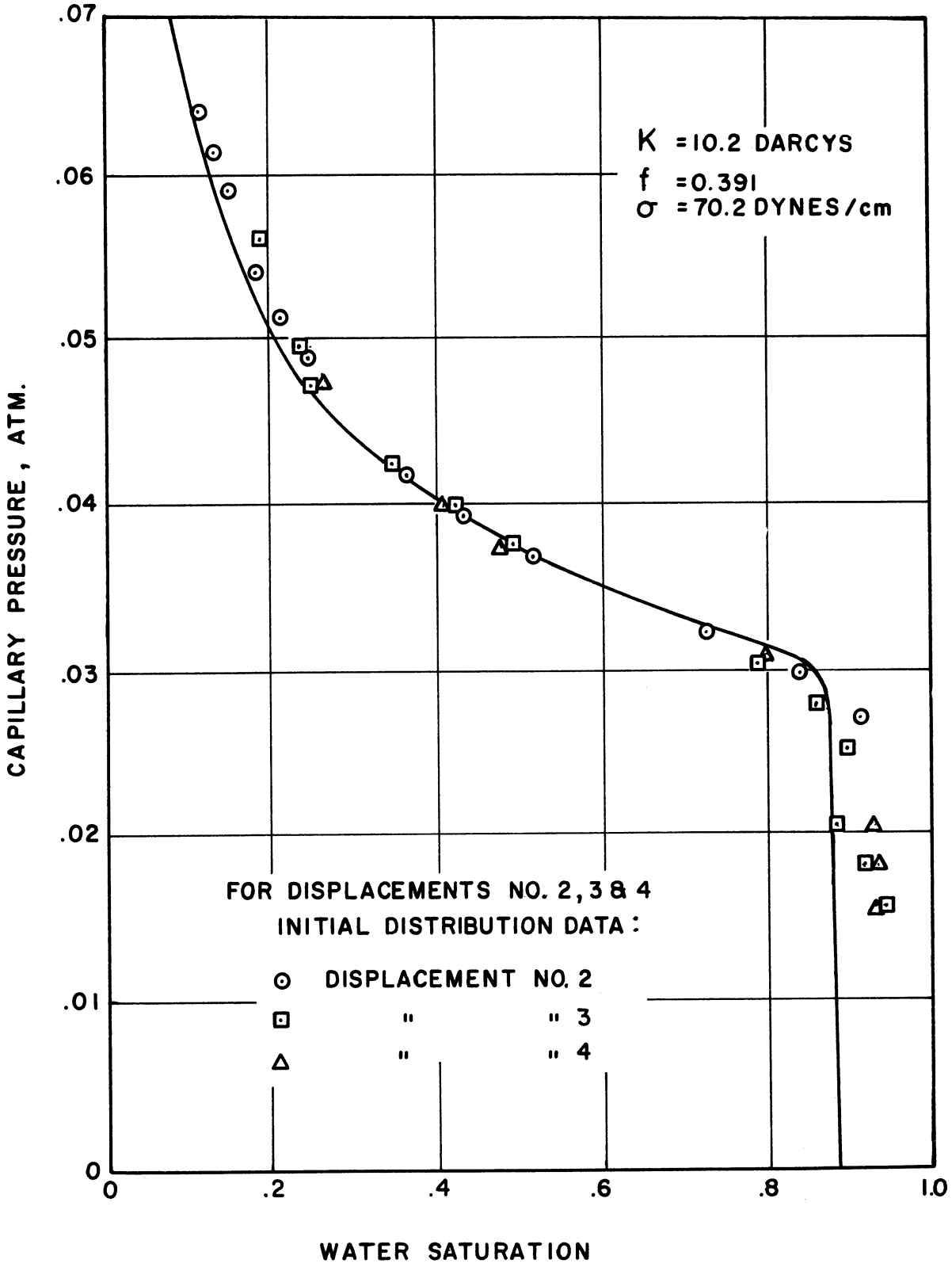

Figure 26. Imbibition Capillary Pressure Curve
Laboratory Medium

The numerical breakthrough behavior was characterized by a short two phase production period with the transition between all gas and all water production occurring over about one hour. This has little significance as it is controlled by the slope of the capillary pressure curve near residual gas saturation. The tighter the curvature displayed in the approach to the vertical slope at residual gas saturation, the more abrupt will be the switch from gas to water production. Subsequent computations not included here demonstrated this, although computational difficulties arose in the assignment of individual phase production rates over the finite time interval in which the sudden transition occurred.

Computed water saturation distributions at the six displacement times are presented in Tables XXII(a-f). Table XXIII shows the results obtained from point by point comparison of these distributions to those found experimentally which were listed in Tables X(a-f).

Two dimensional water saturation contours are drawn with a sampling of the experimental data for two displacement times in Figures 27a and 27b. Saturation history is shown on a row-wise basis for four horizontal rows in Figure 28. A third graphical comparison is shown in Figure 29 where row-wise average water saturations have been plotted for all viewable rows with the numerical solution indicated by the solid curves at the six displacement times.

2. Displacements No. 3 and 4

The final two displacements were run as duplicates so the same numerical solution applies to both. Since the total nominal water

TABLE XXII

COMPUTED WATER SATURATION DISTRIBUTIONS

a. LABORATORY DISPLACEMENT NO. 2 AFTER 5 HOURS OF INJECTION

WATER SATURATION DISTRIBUTION

OBTAINED BY NUMERICAL SOLUTION

BY ROWS FROM UPPER LEFT

13.2	13.2	13.2	13.2	13.2	13.2	13.2	13.2	13.2	13.3	13.3	13.3	13.3	13.3	13.3	13.3
14.4	14.4	14.4	14.4	14.4	14.4	14.5	14.5	14.5	14.5	14.5	14.5	14.6	14.6	14.6	14.6
15.9	15.9	15.9	16.0	16.0	16.0	16.0	16.0	16.0	16.0	16.0	16.1	16.1	16.1	16.1	16.1
17.7	17.7	17.8	17.8	17.8	17.8	17.8	17.8	17.8	17.9	17.9	17.9	17.9	18.0	18.0	18.0
20.1	20.1	20.1	20.1	20.1	20.2	20.2	20.2	20.2	20.3	20.3	20.3	20.4	20.4	20.4	20.4
23.2	23.2	23.2	23.2	23.2	23.2	23.2	23.3	23.3	23.3	23.4	23.4	23.5	23.5	23.5	23.6
27.2	27.2	27.2	27.2	27.2	27.2	27.3	27.3	27.3	27.4	27.4	27.5	27.5	27.6	27.6	27.6
32.0	32.0	32.0	32.0	32.0	32.1	32.1	32.2	32.2	32.3	32.3	32.4	32.5	32.5	32.6	32.6
37.9	37.9	38.0	38.0	38.0	38.1	38.1	38.2	38.3	38.3	38.4	38.5	38.6	38.7	38.8	38.8
46.2	46.2	46.3	46.3	46.3	46.4	46.5	46.5	46.6	46.7	46.8	47.0	47.1	47.2	47.3	47.3
56.5	56.6	56.6	56.6	56.7	56.8	56.9	57.0	57.1	57.2	57.4	57.5	57.7	57.8	57.9	58.0
69.4	69.4	69.4	69.5	69.6	69.6	69.8	69.9	70.0	70.2	70.4	70.6	70.8	71.0	71.1	71.2
83.1	83.1	83.1	83.1	83.2	83.2	83.3	83.3	83.4	83.5	83.6	83.7	83.8	83.9	84.0	84.1
87.7	87.7	87.7	87.7	87.7	87.7	87.7	87.8	87.8	87.8	87.8	87.9	87.9	87.9	87.9	88.0
88.4	88.4	88.4	88.4	88.4	88.4	88.4	88.4	88.4	88.4	88.4	88.4	88.4	88.4	88.4	88.4
88.5	88.5	88.5	88.5	88.5	88.5	88.5	88.5	88.5	88.5	88.5	88.5	88.5	88.5	88.5	88.5

b. LABORATORY DISPLACEMENT NO. 2 AFTER 15 HOURS OF INJECTION

WATER SATURATION DISTRIBUTION

OBTAINED BY NUMERICAL SOLUTION

BY ROWS FROM UPPER LEFT

16.8	16.8	16.8	16.8	16.8	16.9	16.9	16.9	16.9	16.9	16.9	16.9	16.9	16.9	16.9	16.9
18.9	18.9	18.9	18.9	18.9	18.9	18.9	19.0	19.0	19.0	19.0	19.0	19.0	19.0	19.1	19.1
21.6	21.6	21.6	21.6	21.6	21.6	21.6	21.6	21.7	21.7	21.7	21.7	21.7	21.8	21.8	21.8
25.2	25.2	25.2	25.2	25.2	25.2	25.2	25.3	25.3	25.3	25.3	25.4	25.4	25.4	25.4	25.4
29.5	29.5	29.5	29.5	29.5	29.5	29.5	29.6	29.6	29.6	29.6	29.7	29.7	29.7	29.7	29.7
34.9	34.9	34.9	35.0	35.0	35.0	35.0	35.1	35.1	35.1	35.2	35.2	35.2	35.3	35.3	35.3
42.1	42.1	42.1	42.1	42.2	42.2	42.2	42.3	42.3	42.4	42.4	42.5	42.5	42.6	42.6	42.6
51.6	51.6	51.6	51.6	51.6	51.7	51.7	51.8	51.8	51.9	52.0	52.0	52.1	52.2	52.2	52.2
63.1	63.1	63.1	63.2	63.2	63.2	63.3	63.4	63.4	63.5	63.6	63.7	63.8	63.9	63.9	63.9
77.2	77.2	77.2	77.2	77.3	77.3	77.4	77.5	77.6	77.7	77.8	77.9	78.0	78.0	78.1	78.1
86.5	86.5	86.5	86.5	86.5	86.5	86.6	86.6	86.6	86.6	86.6	86.7	86.7	86.7	86.7	86.7
88.2	88.2	88.2	88.3	88.3	88.3	88.3	88.3	88.3	88.3	88.3	88.3	88.3	88.3	88.3	88.3
88.5	88.5	88.5	88.5	88.5	88.5	88.5	88.5	88.5	88.5	88.5	88.5	88.5	88.5	88.5	88.5
88.6	88.6	88.6	88.6	88.6	88.6	88.6	88.6	88.6	88.6	88.6	88.6	88.6	88.6	88.6	88.6
88.7	88.7	88.7	88.7	88.7	88.7	88.7	88.7	88.7	88.7	88.7	88.7	88.7	88.7	88.7	88.7
88.7	88.7	88.7	88.7	88.7	88.7	88.7	88.7	88.8	88.8	88.8	88.8	88.8	88.8	88.8	88.8

c. LABORATORY DISPLACEMENT NO. 2 AFTER 25 HOURS OF INJECTION

WATER SATURATION DISTRIBUTION

OBTAINED BY NUMERICAL SOLUTION

BY ROWS FROM UPPER LEFT

24.0	24.0	24.0	24.0	24.0	24.0	24.0	24.0	24.0	24.0	24.0	24.1	24.1	24.1	24.1	24.1
28.0	28.0	28.1	28.1	28.1	28.1	28.1	28.1	28.1	28.1	28.1	28.2	28.2	28.2	28.2	28.2
33.2	33.2	33.2	33.2	33.2	33.2	33.2	33.2	33.2	33.3	33.3	33.3	33.3	33.3	33.3	33.4
39.6	39.6	39.6	39.6	39.6	39.6	39.7	39.7	39.7	39.7	39.7	39.8	39.8	39.8	39.8	39.8
48.3	48.3	48.3	48.3	48.3	48.4	48.4	48.4	48.5	48.5	48.5	48.6	48.6	48.6	48.7	48.7
59.2	59.2	59.2	59.2	59.2	59.3	59.3	59.3	59.4	59.4	59.5	59.5	59.5	59.6	59.6	59.6
72.6	72.6	72.6	72.6	72.7	72.7	72.7	72.8	72.8	72.9	72.9	73.0	73.0	73.1	73.1	73.1
84.7	84.7	84.8	84.8	84.8	84.8	84.8	84.8	84.9	84.9	84.9	84.9	85.0	85.0	85.0	85.0
88.1	88.1	88.1	88.1	88.1	88.1	88.1	88.1	88.1	88.1	88.1	88.1	88.1	88.1	88.1	88.1
88.4	88.4	88.4	88.4	88.4	88.4	88.4	88.4	88.4	88.4	88.4	88.4	88.4	88.4	88.4	88.4
88.6	88.6	88.6	88.6	88.6	88.6	88.6	88.6	88.6	88.6	88.6	88.6	88.6	88.6	88.6	88.6
88.7	88.7	88.7	88.7	88.7	88.7	88.7	88.7	88.7	88.7	88.7	88.7	88.7	88.7	88.7	88.7
88.7	88.7	88.7	88.7	88.7	88.7	88.7	88.7	88.7	88.7	88.7	88.7	88.7	88.7	88.7	88.7
88.8	88.8	88.8	88.8	88.8	88.8	88.8	88.8	88.8	88.8	88.8	88.8	88.8	88.8	88.8	88.8
88.8	88.8	88.8	88.8	88.8	88.8	88.8	88.8	88.8	88.8	88.8	88.8	88.8	88.8	88.8	88.8
88.8	88.8	88.8	88.8	88.8	88.8	88.8	88.8	88.8	88.8	88.8	88.8	88.8	88.8	88.8	88.8

TABLE XXII (CONT'D)

d. LABORATORY DISPLACEMENT NO. 2 AFTER 30 HOURS OF INJECTION

WATER SATURATION DISTRIBUTION

OBTAINED BY NUMERICAL SOLUTION

BY ROWS FROM UPPER LEFT

30.2	30.2	30.2	30.3	30.3	30.3	30.3	30.3	30.3	30.3	30.3	30.3	30.3	30.3	30.4	30.4
35.9	35.9	36.0	36.0	36.0	36.0	36.0	36.0	36.0	36.0	36.0	36.1	36.1	36.1	36.1	36.1
43.5	43.5	43.5	43.5	43.5	43.5	43.5	43.6	43.6	43.6	43.6	43.6	43.6	43.6	43.7	43.7
53.3	53.3	53.3	53.3	53.3	53.3	53.3	53.3	53.4	53.4	53.4	53.4	53.5	53.5	53.5	53.5
65.1	65.1	65.2	65.2	65.2	65.2	65.2	65.2	65.3	65.3	65.3	65.4	65.4	65.4	65.4	65.4
79.3	79.3	79.3	79.3	79.3	79.3	79.4	79.4	79.4	79.4	79.5	79.5	79.5	79.6	79.6	79.6
87.1	87.1	87.1	87.1	87.1	87.1	87.1	87.1	87.1	87.1	87.1	87.1	87.1	87.1	87.1	87.1
88.3	88.3	88.3	88.3	88.3	88.3	88.3	88.3	88.3	88.3	88.3	88.3	88.3	88.3	88.3	88.3
88.5	88.5	88.5	88.5	88.5	88.5	88.5	88.5	88.5	88.5	88.5	88.5	88.5	88.5	88.5	88.5
88.6	88.6	88.6	88.6	88.6	88.6	88.6	88.6	88.6	88.6	88.6	88.6	88.6	88.6	88.6	88.6
88.7	88.7	88.7	88.7	88.7	88.7	88.7	88.7	88.7	88.7	88.7	88.7	88.7	88.7	88.7	88.7
88.8	88.8	88.8	88.8	88.8	88.8	88.8	88.8	88.8	88.8	88.8	88.8	88.8	88.8	88.8	88.8
88.8	88.8	88.8	88.8	88.8	88.8	88.8	88.8	88.8	88.8	88.8	88.8	88.8	88.8	88.8	88.8
88.8	88.8	88.8	88.8	88.8	88.8	88.8	88.8	88.8	88.8	88.8	88.8	88.8	88.8	88.8	88.8
88.8	88.8	88.8	88.8	88.8	88.8	88.8	88.8	88.8	88.8	88.8	88.8	88.8	88.8	88.8	88.8
88.9	88.9	88.9	88.9	88.9	88.9	88.9	88.9	88.9	88.9	88.9	88.9	88.9	88.9	88.9	88.9

e. LABORATORY DISPLACEMENT NO. 2 AFTER 35 HOURS OF INJECTION

WATER SATURATION DISTRIBUTION

OBTAINED BY NUMERICAL SOLUTION

BY ROWS FROM UPPER LEFT

40.6	40.6	40.6	40.6	40.6	40.6	40.7	40.7	40.7	40.7	40.7	40.7	40.7	40.7	40.7	40.7
49.7	49.7	49.7	49.7	49.7	49.7	49.7	49.7	49.7	49.7	49.7	49.7	49.8	49.8	49.8	49.8
60.7	60.7	60.7	60.7	60.7	60.7	60.7	60.7	60.7	60.8	60.8	60.8	60.8	60.8	60.8	60.8
74.4	74.4	74.4	74.4	74.4	74.4	74.4	74.5	74.5	74.5	74.5	74.5	74.6	74.6	74.6	74.6
85.7	85.7	85.7	85.7	85.7	85.7	85.7	85.7	85.7	85.7	85.7	85.7	85.7	85.7	85.7	85.7
88.1	88.1	88.1	88.1	88.1	88.1	88.1	88.1	88.1	88.1	88.1	88.1	88.1	88.1	88.1	88.1
88.4	88.4	88.4	88.4	88.4	88.4	88.4	88.4	88.4	88.4	88.4	88.4	88.4	88.4	88.4	88.4
88.6	88.6	88.6	88.6	88.6	88.6	88.6	88.6	88.6	88.6	88.6	88.6	88.6	88.6	88.6	88.6
88.7	88.7	88.7	88.7	88.7	88.7	88.7	88.7	88.7	88.7	88.7	88.7	88.7	88.7	88.7	88.7
88.7	88.7	88.7	88.7	88.7	88.7	88.7	88.7	88.7	88.7	88.7	88.7	88.7	88.7	88.7	88.7
88.8	88.8	88.8	88.8	88.8	88.8	88.8	88.8	88.8	88.8	88.8	88.8	88.8	88.8	88.8	88.8
88.8	88.8	88.8	88.8	88.8	88.8	88.8	88.8	88.8	88.8	88.8	88.8	88.8	88.8	88.8	88.8
88.8	88.8	88.8	88.8	88.8	88.8	88.8	88.8	88.8	88.8	88.8	88.8	88.8	88.8	88.8	88.8
88.8	88.8	88.8	88.8	88.8	88.8	88.8	88.8	88.8	88.8	88.8	88.8	88.8	88.8	88.8	88.8
88.9	88.9	88.9	88.9	88.9	88.9	88.9	88.9	88.9	88.9	88.9	88.9	88.9	88.9	88.9	88.9
88.9	88.9	88.9	88.9	88.9	88.9	88.9	88.9	88.9	88.9	88.9	88.9	88.9	88.9	88.9	88.9

f. LABORATORY DISPLACEMENT NO. 2 AFTER 40 HOURS OF INJECTION

WATER SATURATION DISTRIBUTION

OBTAINED BY NUMERICAL SOLUTION

BY ROWS FROM UPPER LEFT

63.5	63.4	63.4	63.3	63.3	63.2	63.2	63.2	63.2	63.1	63.1	63.1	63.1	63.1	63.1	63.1
77.5	77.5	77.4	77.4	77.3	77.3	77.2	77.2	77.2	77.1	77.1	77.1	77.1	77.1	77.1	77.1
86.6	86.6	86.6	86.5	86.5	86.5	86.5	86.5	86.5	86.5	86.5	86.5	86.5	86.5	86.5	86.5
88.3	88.3	88.3	88.3	88.3	88.3	88.3	88.2	88.2	88.2	88.2	88.2	88.2	88.2	88.2	88.2
88.5	88.5	88.5	88.5	88.5	88.5	88.5	88.5	88.5	88.5	88.5	88.5	88.5	88.5	88.5	88.5
88.6	88.6	88.6	88.6	88.6	88.6	88.6	88.6	88.6	88.6	88.6	88.6	88.6	88.6	88.6	88.6
88.7	88.7	88.7	88.7	88.7	88.7	88.7	88.7	88.7	88.7	88.7	88.7	88.7	88.7	88.7	88.7
88.7	88.7	88.7	88.7	88.7	88.7	88.7	88.7	88.7	88.7	88.7	88.7	88.7	88.7	88.7	88.7
88.8	88.8	88.8	88.8	88.8	88.8	88.8	88.8	88.8	88.8	88.8	88.8	88.8	88.8	88.8	88.8
88.8	88.8	88.8	88.8	88.8	88.8	88.8	88.8	88.8	88.8	88.8	88.8	88.8	88.8	88.8	88.8
88.8	88.8	88.8	88.8	88.8	88.8	88.8	88.8	88.8	88.8	88.8	88.8	88.8	88.8	88.8	88.8
88.8	88.8	88.8	88.8	88.8	88.8	88.8	88.8	88.8	88.8	88.8	88.8	88.8	88.8	88.8	88.8
88.9	88.9	88.9	88.9	88.9	88.9	88.9	88.9	88.9	88.9	88.9	88.9	88.9	88.9	88.9	88.9
88.9	88.9	88.9	88.9	88.9	88.9	88.9	88.9	88.9	88.9	88.9	88.9	88.9	88.9	88.9	88.9
89.0	89.0	89.0	89.0	89.0	89.0	89.0	89.0	89.0	89.0	89.0	89.0	89.0	89.0	89.0	89.0
89.0	89.0	89.0	89.0	89.0	89.0	89.0	89.0	89.0	89.0	89.0	89.0	89.0	89.0	89.0	89.0

TABLE XXXII

COMPARISON OF COMPUTED TO EXPERIMENTAL
WATER SATURATION DISTRIBUTIONS

LABORATORY DISPLACEMENT NO. 2

AFTER 5 HOURS OF INJECTION

AVERAGE ABSOLUTE DEVIATION AND STANDARD DEVIATION

FROM NUMERICAL SOLUTION - EXPRESSED IN SATURATION PER CENT

OVERALL AVERAGE DEVIATION = 2.5 STANDARD DEVIATION = 3.3

AVERAGE AND STANDARD DEVIATION BY SATURATION RANGE

FROM	TO	NO. PTS	AVG. DEV.	STD. DEV.
.0	20.0	48	1.0	1.2
20.0	40.0	48	.8	1.0
40.0	60.0	32	2.5	3.0
60.0	80.0	16	6.3	6.4
80.0	100.0	48	4.4	4.6

LABORATORY DISPLACEMENT NO. 2

AFTER 15 HOURS OF INJECTION

AVERAGE ABSOLUTE DEVIATION AND STANDARD DEVIATION

FROM NUMERICAL SOLUTION - EXPRESSED IN SATURATION PER CENT

OVERALL AVERAGE DEVIATION = 3.5 STANDARD DEVIATION = 4.3

AVERAGE AND STANDARD DEVIATION BY SATURATION RANGE

FROM	TO	NO. PTS	AVG. DEV.	STD. DEV.
.0	20.0	32	1.7	2.0
20.0	40.0	48	2.5	2.8
40.0	60.0	16	2.2	2.4
60.0	80.0	16	7.6	7.7
80.0	100.0	80	4.1	5.1

LABORATORY DISPLACEMENT NO. 2

AFTER 25 HOURS OF INJECTION

AVERAGE ABSOLUTE DEVIATION AND STANDARD DEVIATION

FROM NUMERICAL SOLUTION - EXPRESSED IN SATURATION PER CENT

OVERALL AVERAGE DEVIATION = 3.6 STANDARD DEVIATION = 4.0

AVERAGE AND STANDARD DEVIATION BY SATURATION RANGE

FROM	TO	NO. PTS	AVG. DEV.	STD. DEV.
.0	20.0	0	.0	.0
20.0	40.0	48	2.2	2.6
40.0	60.0	32	4.5	4.7
60.0	80.0	16	3.8	3.8
80.0	100.0	96	4.0	4.3

LABORATORY DISPLACEMENT NO. 2

AFTER 30 HOURS OF INJECTION

AVERAGE ABSOLUTE DEVIATION AND STANDARD DEVIATION

FROM NUMERICAL SOLUTION - EXPRESSED IN SATURATION PER CENT

OVERALL AVERAGE DEVIATION = 3.6 STANDARD DEVIATION = 4.0

AVERAGE AND STANDARD DEVIATION BY SATURATION RANGE

FROM	TO	NO. PTS	AVG. DEV.	STD. DEV.
.0	20.0	0	.0	.0
20.0	40.0	32	3.1	3.4
40.0	60.0	16	2.3	2.9
60.0	80.0	32	4.4	4.6
80.0	100.0	112	3.7	4.1

LABORATORY DISPLACEMENT NO. 2

AFTER 35 HOURS OF INJECTION

AVERAGE ABSOLUTE DEVIATION AND STANDARD DEVIATION

FROM NUMERICAL SOLUTION - EXPRESSED IN SATURATION PER CENT

OVERALL AVERAGE DEVIATION = 4.8 STANDARD DEVIATION = 5.6

AVERAGE AND STANDARD DEVIATION BY SATURATION RANGE

FROM	TO	NO. PTS	AVG. DEV.	STD. DEV.
.0	20.0	0	.0	.0
20.0	40.0	0	.0	.0
40.0	60.0	32	5.7	6.3
60.0	80.0	16	12.2	12.2
80.0	100.0	144	3.7	4.1

LABORATORY DISPLACEMENT NO. 2

AFTER 40 HOURS OF INJECTION

AVERAGE ABSOLUTE DEVIATION AND STANDARD DEVIATION

FROM NUMERICAL SOLUTION - EXPRESSED IN SATURATION PER CENT

OVERALL AVERAGE DEVIATION = 5.4 STANDARD DEVIATION = 6.7

AVERAGE AND STANDARD DEVIATION BY SATURATION RANGE

FROM	TO	NO. PTS	AVG. DEV.	STD. DEV.
.0	20.0	0	.0	.0
20.0	40.0	0	.0	.0
40.0	60.0	0	.0	.0
60.0	80.0	32	13.3	13.6
80.0	100.0	160	3.8	4.2

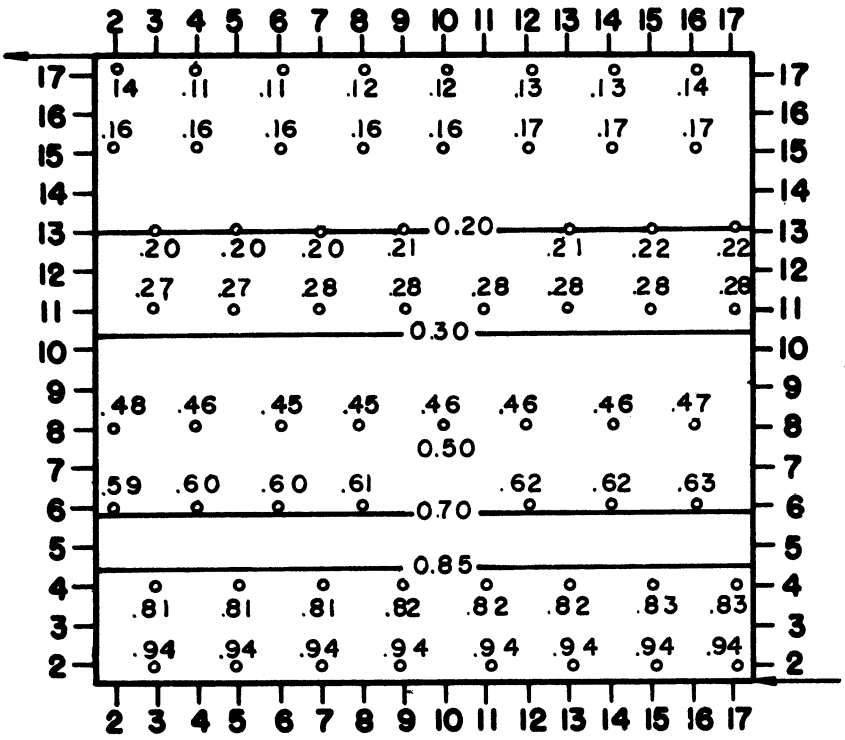

a. At 5 Hours

— NUMERICAL SOLUTION

o EXPERIMENTAL DATA

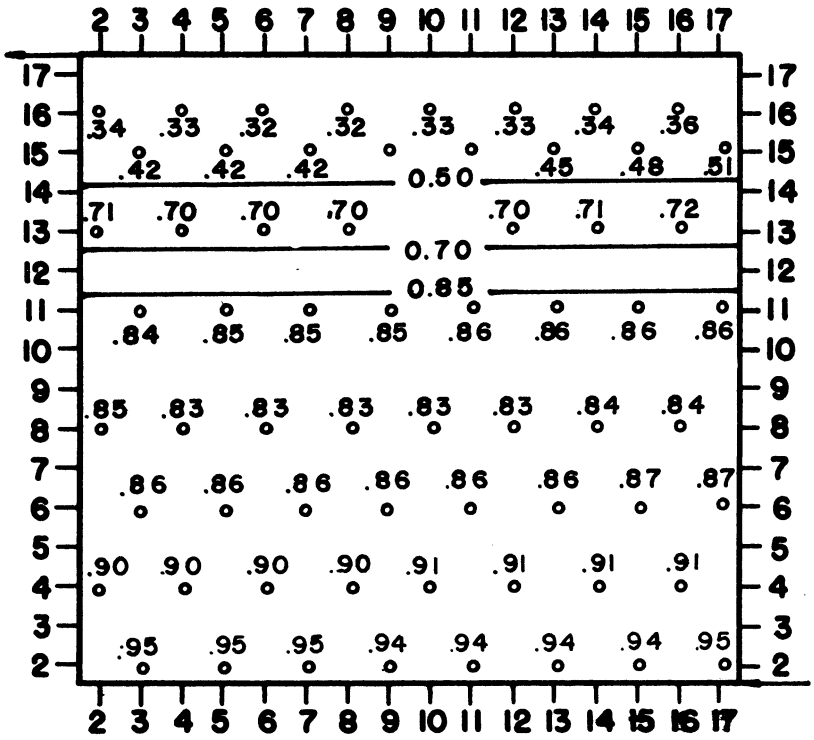

b. At 30 Hours

Figure 27. Water Saturation Contours
Displacement No. 2

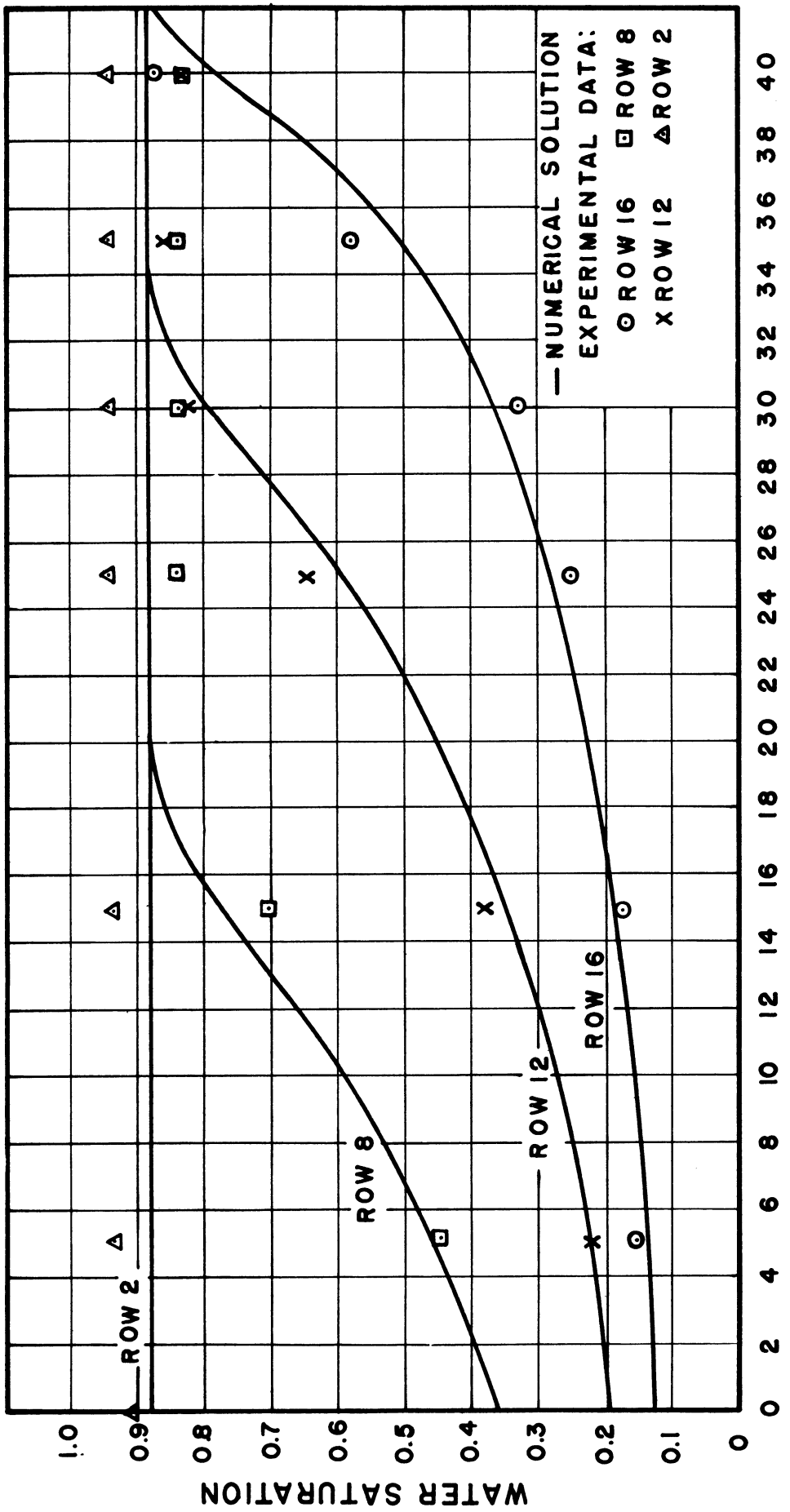

Figure 28. Water Saturation History
Displacement No. 2

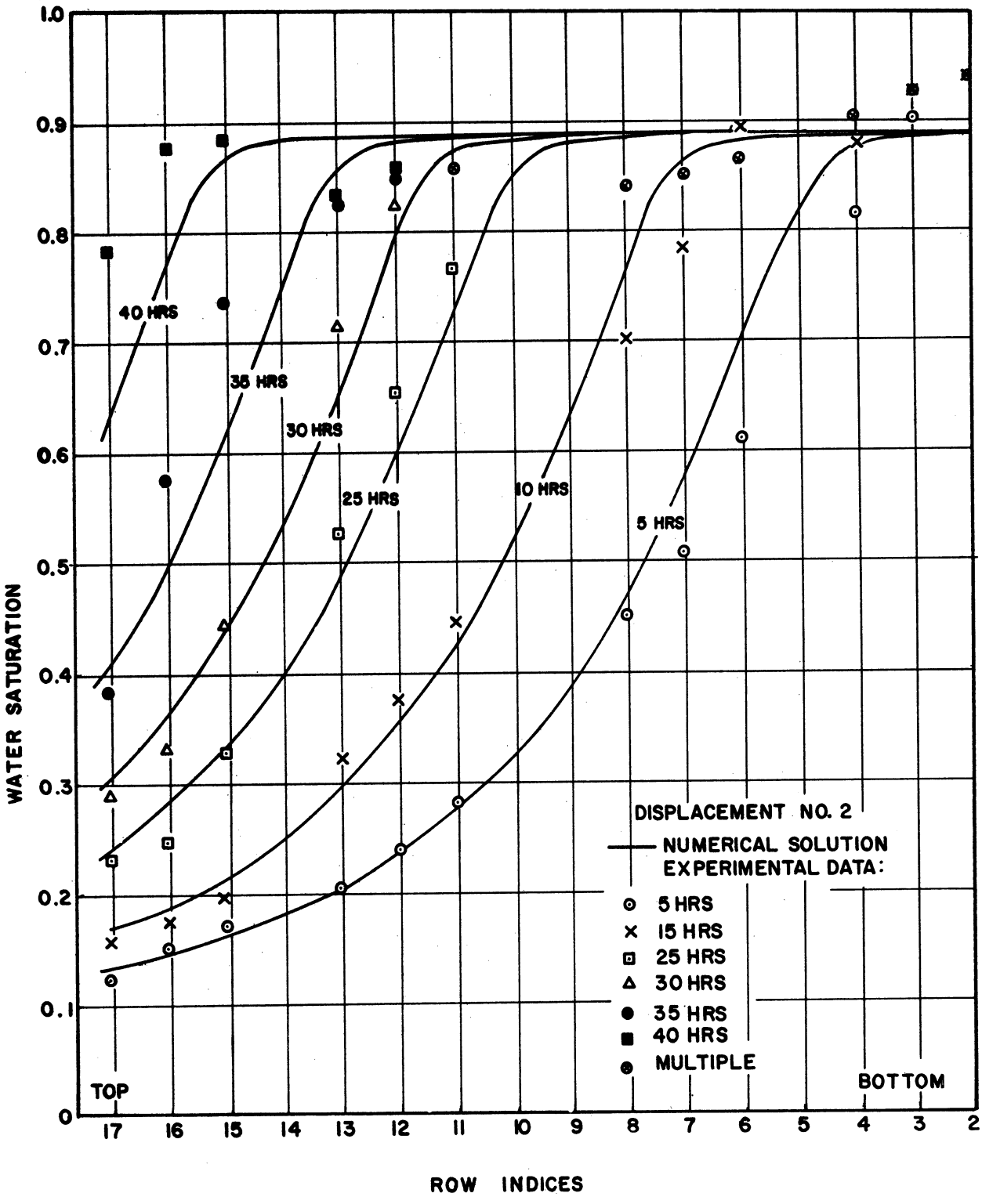

Figure 29. Vertical Water Saturation Distributions

injection rate was 10 cc/hr and the former displacement was begun with 3 cc less water in the pore volume than the latter, the corresponding displacement times were taken to differ by 0.3 hour.

The numerical solution with rates and times based on Displacement No. 4 is summarized in Table XXIV.

TABLE XXIV

SUMMARY OF NUMERICAL SOLUTION
Displacement No. 4 (and No. 3)

Time	Time Step No.	Water in P.V.	Cumulative Water Balance
4 hrs.	11	575.0 cc	0.01%
10 hrs.	23	636.4 cc	0.02%
15 hrs.	33	687.5 cc	0.02%
20 hrs.	43	738.7 cc	0.02%
22 hrs.	47	759.2 cc	0.02%

Breakthrough Time = 23.70 hours

Water Content of P.V. at Breakthrough = 776.6 cc

Computed production history at breakthrough was the same as for Displacement No. 2 as the same capillary pressure function was employed. Again this has little significance for the same reasons discussed previously.

The numerical solution for water saturation distribution is tabulated in Tables XXV(a-e) for the five times of interest. These results are compared to the experimental distributions presented earlier in Tables XIII(a-e) and XIV(a-e) to yield the deviations indicated by Tables XXVI and XXVII for Displacement No. 3 and 4, respectively.

The graphical comparisons of experimental and computed saturation distributions show simiar agreement for both types of imbibition displacements. Numerical solutions shown by solid curves are closest to experimental data at the earlier displacement times. Near breakthrough, experimental water saturations at the upper levels in the model tended to be higher than predicted by numerical solutions. It will be recalled that the saturation measurements were found to be most accurate in the mid range of phase saturation with lower accuracy near connate water and residual gas saturations. Near breakthrough, all elements of the model grid system except those at the upper levels existed at or near the residual gas saturation. Thus the experimental water saturation data for most of the grid elements would be expected to have the lowest accuracy for advanced times in the displacements. Tables X, XIII, and XIV show that positive material balance adjustments were required as the averages of the point-wise water saturations were low. Since these adjustments were made for each element according to Equation (123a) which caused greatest adjustment in the mid range of saturation, the data for the elements in the top rows may have been overadjusted. However, since agreement was quite good even at the higher displacement times, introduction of an improved method of material balance adjustment did not appear warranted.

Contours of constant water saturation along with some of the experimental data for Displacement No. 4 appear in two-dimensional form in Figures 30a and 30b. Figures 31 and 32 show the agreement between the data for Displacement No. 4 and the numerical solution in the form of

TABLE XXV

COMPUTED WATER SATURATION DISTRIBUTIONS

a. LABORATORY DISPLACEMENT NO. 4 (AND NO. 3) AFTER 4.0 HOURS OF INJECTION

WATER SATURATION DISTRIBUTION

OBTAINED BY NUMERICAL SOLUTION

BY ROWS FROM UPPER LEFT

21.9	21.9	21.9	21.9	21.9	21.9	21.9	21.9	21.9	21.9	21.9	21.9	21.9	21.9	21.9	21.9
25.5	25.5	25.5	25.5	25.6	25.6	25.6	25.6	25.6	25.6	25.6	25.6	25.6	25.6	25.6	25.6
29.8	29.8	29.8	29.8	29.8	29.8	29.9	29.9	29.9	29.9	29.9	29.9	29.9	29.9	29.9	29.9
35.4	35.4	35.4	35.4	35.4	35.4	35.4	35.4	35.4	35.4	35.4	35.5	35.5	35.5	35.5	35.5
42.6	42.6	42.6	42.6	42.6	42.6	42.6	42.7	42.7	42.7	42.7	42.7	42.7	42.8	42.8	42.8
52.0	52.0	52.0	52.0	52.1	52.1	52.1	52.1	52.1	52.1	52.2	52.2	52.2	52.2	52.2	52.3
63.5	63.5	63.5	63.5	63.5	63.5	63.5	63.6	63.6	63.6	63.6	63.7	63.7	63.7	63.7	63.7
77.5	77.5	77.5	77.5	77.5	77.5	77.6	77.6	77.6	77.6	77.7	77.7	77.7	77.7	77.8	77.8
86.5	86.6	86.6	86.6	86.6	86.6	86.6	86.6	86.6	86.6	86.6	86.6	86.6	86.6	86.6	86.6
88.3	88.3	88.3	88.3	88.3	88.3	88.3	88.3	88.3	88.3	88.3	88.3	88.3	88.3	88.3	88.3
88.5	88.5	88.5	88.5	88.5	88.5	88.5	88.5	88.5	88.5	88.5	88.5	88.5	88.5	88.5	88.5
88.6	88.6	88.6	88.6	88.6	88.6	88.6	88.6	88.6	88.6	88.6	88.6	88.6	88.6	88.6	88.6
88.7	88.7	88.7	88.7	88.7	88.7	88.7	88.7	88.7	88.7	88.7	88.7	88.7	88.7	88.7	88.7
88.7	88.7	88.7	88.7	88.7	88.7	88.7	88.7	88.7	88.7	88.7	88.7	88.8	88.8	88.8	88.8
88.8	88.8	88.8	88.8	88.8	88.8	88.8	88.8	88.8	88.8	88.8	88.8	88.8	88.8	88.8	88.8
88.8	88.8	88.8	88.8	88.8	88.8	88.8	88.8	88.8	88.8	88.8	88.8	88.8	88.8	88.8	88.8

b. LABORATORY DISPLACEMENT NO. 4 (AND NO. 3) AFTER 10.0 HOURS OF INJECTION

WATER SATURATION DISTRIBUTION

OBTAINED BY NUMERICAL SOLUTION

BY ROWS FROM UPPER LEFT

28.6	28.6	28.6	28.6	28.6	28.6	28.6	28.6	28.6	28.6	28.7	28.7	28.7	28.7	28.7	28.7
33.8	33.8	33.8	33.8	33.8	33.8	33.8	33.8	33.9	33.9	33.9	33.9	33.9	33.9	33.9	33.9
40.3	40.3	40.3	40.3	40.3	40.4	40.4	40.4	40.4	40.4	40.4	40.4	40.4	40.5	40.5	40.5
49.2	49.2	49.2	49.2	49.2	49.2	49.2	49.2	49.2	49.2	49.3	49.3	49.3	49.3	49.3	49.4
59.9	59.9	59.9	59.9	60.0	60.0	60.0	60.0	60.0	60.0	60.1	60.1	60.1	60.1	60.1	60.2
73.3	73.3	73.4	73.4	73.4	73.4	73.4	73.4	73.4	73.5	73.5	73.5	73.5	73.5	73.6	73.6
85.1	85.1	85.1	85.1	85.1	85.1	85.1	85.1	85.1	85.1	85.2	85.2	85.2	85.2	85.2	85.2
88.1	88.1	88.1	88.1	88.1	88.1	88.1	88.1	88.1	88.1	88.1	88.1	88.1	88.1	88.1	88.1
88.4	88.4	88.4	88.4	88.4	88.4	88.4	88.4	88.4	88.4	88.4	88.4	88.4	88.4	88.4	88.4
88.6	88.6	88.6	88.6	88.6	88.6	88.6	88.6	88.6	88.6	88.6	88.6	88.6	88.6	88.6	88.6
88.7	88.7	88.7	88.7	88.7	88.7	88.7	88.7	88.7	88.7	88.7	88.7	88.7	88.7	88.7	88.7
88.7	88.7	88.7	88.7	88.7	88.7	88.7	88.7	88.7	88.7	88.7	88.7	88.7	88.7	88.7	88.7
88.8	88.8	88.8	88.8	88.8	88.8	88.8	88.8	88.8	88.8	88.8	88.8	88.8	88.8	88.8	88.8
88.8	88.8	88.8	88.8	88.8	88.8	88.8	88.8	88.8	88.8	88.8	88.8	88.8	88.8	88.8	88.8
88.8	88.8	88.8	88.8	88.8	88.8	88.8	88.8	88.8	88.8	88.8	88.8	88.8	88.8	88.8	88.8
88.8	88.8	88.8	88.8	88.8	88.8	88.8	88.8	88.8	88.8	88.8	88.8	88.8	88.8	88.8	88.8

c. LABORATORY DISPLACEMENT NO. 4 (AND NO. 3) AFTER 15.0 HOURS OF INJECTION

WATER SATURATION DISTRIBUTION

OBTAINED BY NUMERICAL SOLUTION

BY ROWS FROM UPPER LEFT

37.4	37.4	37.4	37.4	37.4	37.5	37.5	37.5	37.5	37.5	37.5	37.5	37.5	37.6	37.6	37.6
45.5	45.5	45.5	45.5	45.5	45.5	45.5	45.5	45.5	45.5	45.5	45.5	45.6	45.6	45.6	45.6
55.4	55.4	55.4	55.4	55.4	55.4	55.4	55.4	55.4	55.4	55.5	55.5	55.5	55.5	55.6	55.6
67.6	67.6	67.6	67.6	67.6	67.6	67.7	67.7	67.7	67.7	67.7	67.7	67.8	67.8	67.8	67.9
81.5	81.5	81.5	81.5	81.5	81.5	81.5	81.5	81.6	81.6	81.6	81.6	81.6	81.6	81.7	81.7
87.5	87.5	87.5	87.5	87.5	87.5	87.5	87.5	87.5	87.5	87.5	87.5	87.5	87.5	87.5	87.5
88.4	88.4	88.4	88.4	88.4	88.4	88.4	88.4	88.4	88.4	88.4	88.4	88.4	88.4	88.4	88.4
88.5	88.5	88.5	88.5	88.5	88.5	88.5	88.5	88.5	88.5	88.5	88.5	88.5	88.5	88.5	88.5
88.6	88.6	88.6	88.6	88.6	88.6	88.6	88.6	88.6	88.6	88.6	88.6	88.6	88.6	88.6	88.6
88.7	88.7	88.7	88.7	88.7	88.7	88.7	88.7	88.7	88.7	88.7	88.7	88.7	88.7	88.7	88.7
88.8	88.8	88.8	88.8	88.8	88.8	88.8	88.8	88.8	88.8	88.8	88.8	88.8	88.8	88.8	88.8
88.8	88.8	88.8	88.8	88.8	88.8	88.8	88.8	88.8	88.8	88.8	88.8	88.8	88.8	88.8	88.8
88.8	88.8	88.8	88.8	88.8	88.8	88.8	88.8	88.8	88.8	88.8	88.8	88.8	88.8	88.8	88.8
88.8	88.8	88.8	88.8	88.8	88.8	88.8	88.8	88.8	88.8	88.8	88.8	88.8	88.8	88.8	88.8
88.9	88.9	88.9	88.9	88.9	88.9	88.9	88.9	88.9	88.9	88.9	88.9	88.9	88.9	88.9	88.9
88.9	88.9	88.9	88.9	88.9	88.9	88.9	88.9	88.9	88.9	88.9	88.9	88.9	88.9	88.9	88.9

TABLE XXV (CONT'D)

d. LABORATORY DISPLACEMENT NO. 4 (AND NO. 3) AFTER 20.0 HOURS OF INJECTION

WATER SATURATION DISTRIBUTION

OBTAINED BY NUMERICAL SOLUTION

BY ROWS FROM UPPER LEFT

55.3	55.3	55.2	55.2	55.2	55.2	55.2	55.2	55.2	55.2	55.3	55.3	55.3	55.4	55.4	55.5
67.4	67.4	67.3	67.3	67.3	67.3	67.3	67.3	67.3	67.3	67.3	67.4	67.4	67.5	67.5	67.6
81.3	81.2	81.2	81.2	81.2	81.2	81.2	81.2	81.2	81.2	81.2	81.2	81.2	81.3	81.3	81.4
87.5	87.5	87.5	87.5	87.5	87.5	87.5	87.5	87.5	87.5	87.5	87.5	87.5	87.5	87.5	87.5
88.4	88.4	88.4	88.4	88.4	88.4	88.4	88.4	88.4	88.4	88.4	88.4	88.4	88.4	88.4	88.4
88.5	88.5	88.5	88.5	88.5	88.5	88.5	88.5	88.5	88.5	88.5	88.5	88.5	88.5	88.5	88.5
88.6	88.6	88.6	88.6	88.6	88.6	88.6	88.6	88.6	88.6	88.6	88.6	88.6	88.6	88.6	88.6
88.7	88.7	88.7	88.7	88.7	88.7	88.7	88.7	88.7	88.7	88.7	88.7	88.7	88.7	88.7	88.7
88.8	88.8	88.8	88.8	88.8	88.8	88.8	88.8	88.8	88.8	88.8	88.8	88.8	88.8	88.8	88.8
88.8	88.8	88.8	88.8	88.8	88.8	88.8	88.8	88.8	88.8	88.8	88.8	88.8	88.8	88.8	88.8
88.8	88.8	88.8	88.8	88.8	88.8	88.8	88.8	88.8	88.8	88.8	88.8	88.8	88.8	88.8	88.8
88.8	88.8	88.8	88.8	88.8	88.8	88.8	88.8	88.8	88.8	88.8	88.8	88.8	88.8	88.8	88.8
88.9	88.9	88.9	88.9	88.9	88.9	88.9	88.9	88.9	88.9	88.9	88.9	88.9	88.9	88.9	88.9
88.9	88.9	88.9	88.9	88.9	88.9	88.9	88.9	88.9	88.9	88.9	88.9	88.9	88.9	88.9	88.9
88.9	88.9	88.9	88.9	88.9	88.9	88.9	88.9	88.9	88.9	88.9	88.9	88.9	88.9	88.9	88.9
89.0	89.0	89.0	89.0	89.0	89.0	89.0	89.0	89.0	89.0	89.0	89.0	89.0	89.0	89.0	89.0

e. LABORATORY DISPLACEMENT NO. 4 (AND NO. 3) AFTER 22.0 HOURS OF INJECTION

WATER SATURATION DISTRIBUTION

OBTAINED BY NUMERICAL SOLUTION

BY ROWS FROM UPPER LEFT

69.5	69.4	69.3	69.3	69.2	69.1	69.1	69.1	69.1	69.1	69.1	69.2	69.2	69.3	69.5	69.7
83.1	83.0	83.0	82.9	82.9	82.8	82.8	82.7	82.7	82.7	82.7	82.8	82.8	82.9	83.0	83.1
87.7	87.7	87.7	87.7	87.7	87.7	87.7	87.7	87.7	87.7	87.7	87.7	87.7	87.7	87.7	87.7
88.4	88.4	88.4	88.4	88.4	88.4	88.4	88.4	88.4	88.4	88.4	88.4	88.4	88.4	88.4	88.4
88.5	88.5	88.5	88.5	88.5	88.5	88.5	88.5	88.5	88.5	88.5	88.5	88.5	88.5	88.5	88.5
88.6	88.6	88.6	88.6	88.6	88.6	88.6	88.6	88.6	88.6	88.6	88.6	88.6	88.6	88.6	88.6
88.7	88.7	88.7	88.7	88.7	88.7	88.7	88.7	88.7	88.7	88.7	88.7	88.7	88.7	88.7	88.7
88.8	88.8	88.8	88.8	88.8	88.8	88.8	88.8	88.8	88.8	88.8	88.8	88.8	88.8	88.8	88.8
88.8	88.8	88.8	88.8	88.8	88.8	88.8	88.8	88.8	88.8	88.8	88.8	88.8	88.8	88.8	88.8
88.8	88.8	88.8	88.8	88.8	88.8	88.8	88.8	88.8	88.8	88.8	88.8	88.8	88.8	88.8	88.8
88.8	88.8	88.8	88.8	88.8	88.8	88.8	88.8	88.8	88.8	88.8	88.8	88.8	88.8	88.8	88.8
88.9	88.9	88.9	88.9	88.9	88.9	88.9	88.9	88.9	88.9	88.9	88.9	88.9	88.9	88.9	88.9
88.9	88.9	88.9	88.9	88.9	88.9	88.9	88.9	88.9	88.9	88.9	88.9	88.9	88.9	88.9	88.9
88.9	88.9	88.9	88.9	88.9	88.9	88.9	88.9	88.9	88.9	88.9	88.9	88.9	88.9	88.9	88.9
89.0	89.0	89.0	89.0	89.0	89.0	89.0	89.0	89.0	89.0	89.0	89.0	89.0	89.0	89.0	89.0
89.0	89.0	89.0	89.0	89.0	89.0	89.0	89.0	89.0	89.0	89.0	89.0	89.0	89.0	89.0	89.0

TABLE XXVI

COMPARISON OF COMPUTED TO EXPERIMENTAL
WATER SATURATION DISTRIBUTIONS

LABORATORY DISPLACEMENT NO. 3

AFTER 4.3 HOURS OF INJECTION

AVERAGE ABSOLUTE DEVIATION AND STANDARD DEVIATION

FROM NUMERICAL SOLUTION - EXPRESSED IN SATURATION PER CENT

OVERALL AVERAGE DEVIATION = 2.7 STANDARD DEVIATION = 3.4

AVERAGE AND STANDARD DEVIATION BY SATURATION RANGE

FROM	TO	NO. PTS	AVG. DEV.	STD. DEV.
.0	20.0	0	.0	.0
20.0	40.0	48	2.9	3.6
40.0	60.0	32	1.1	1.3
60.0	80.0	16	.7	.9
80.0	100.0	96	3.6	4.0

LABORATORY DISPLACEMENT NO. 3

AFTER 10.3 HOURS OF INJECTION

AVERAGE ABSOLUTE DEVIATION AND STANDARD DEVIATION

FROM NUMERICAL SOLUTION - EXPRESSED IN SATURATION PER CENT

OVERALL AVERAGE DEVIATION = 3.2 STANDARD DEVIATION = 3.7

AVERAGE AND STANDARD DEVIATION BY SATURATION RANGE

FROM	TO	NO. PTS	AVG. DEV.	STD. DEV.
.0	20.0	0	.0	.0
20.0	40.0	32	4.6	5.2
40.0	60.0	24	2.2	2.6
60.0	80.0	24	1.7	2.0
80.0	100.0	112	3.3	3.7

LABORATORY DISPLACEMENT NO. 3

AFTER 15.3 HOURS OF INJECTION

AVERAGE ABSOLUTE DEVIATION AND STANDARD DEVIATION

FROM NUMERICAL SOLUTION - EXPRESSED IN SATURATION PER CENT

OVERALL AVERAGE DEVIATION = 3.9 STANDARD DEVIATION = 4.4

AVERAGE AND STANDARD DEVIATION BY SATURATION RANGE

FROM	TO	NO. PTS	AVG. DEV.	STD. DEV.
.0	20.0	0	.0	.0
20.0	40.0	16	5.6	5.8
40.0	60.0	32	3.0	3.1
60.0	80.0	0	.0	.0
80.0	100.0	144	3.9	4.4

LABORATORY DISPLACEMENT NO. 3

AFTER 20.3 HOURS OF INJECTION

AVERAGE ABSOLUTE DEVIATION AND STANDARD DEVIATION

FROM NUMERICAL SOLUTION - EXPRESSED IN SATURATION PER CENT

OVERALL AVERAGE DEVIATION = 3.9 STANDARD DEVIATION = 4.4

AVERAGE AND STANDARD DEVIATION BY SATURATION RANGE

FROM	TO	NO. PTS	AVG. DEV.	STD. DEV.
.0	20.0	0	.0	.0
20.0	40.0	0	.0	.0
40.0	60.0	16	5.9	6.2
60.0	80.0	16	3.9	4.3
80.0	100.0	160	3.7	4.2

LABORATORY DISPLACEMENT NO. 3

AFTER 22.3 HOURS OF INJECTION

AVERAGE ABSOLUTE DEVIATION AND STANDARD DEVIATION

FROM NUMERICAL SOLUTION - EXPRESSED IN SATURATION PER CENT

OVERALL AVERAGE DEVIATION = 3.4 STANDARD DEVIATION = 3.9

AVERAGE AND STANDARD DEVIATION BY SATURATION RANGE

FROM	TO	NO. PTS	AVG. DEV.	STD. DEV.
.0	20.0	0	.0	.0
20.0	40.0	0	.0	.0
40.0	60.0	0	.0	.0
60.0	80.0	16	.5	.6
80.0	100.0	176	3.6	4.1

TABLE XXVII

COMPARISON OF COMPUTED TO EXPERIMENTAL
WATER SATURATION DISTRIBUTIONS

LABORATORY DISPLACEMENT NO. 4

AFTER 4.0 HOURS OF INJECTION

AVERAGE ABSOLUTE DEVIATION AND STANDARD DEVIATION

FROM NUMERICAL SOLUTION - EXPRESSED IN SATURATION PER CENT

OVERALL AVERAGE DEVIATION = 2.4 STANDARD DEVIATION = 3.0

AVERAGE AND STANDARD DEVIATION BY SATURATION RANGE

FROM	TO	NO. PTS	AVG. DEV.	STD. DEV.
.0	20.0	0	.0	.0
20.0	40.0	48	.8	.9
40.0	60.0	32	1.1	1.2
60.0	80.0	16	2.0	2.1
80.0	100.0	96	3.7	4.1

LABORATORY DISPLACEMENT NO. 4

AFTER 10.0 HOURS OF INJECTION

AVERAGE ABSOLUTE DEVIATION AND STANDARD DEVIATION

FROM NUMERICAL SOLUTION - EXPRESSED IN SATURATION PER CENT

OVERALL AVERAGE DEVIATION = 3.2 STANDARD DEVIATION = 3.6

AVERAGE AND STANDARD DEVIATION BY SATURATION RANGE

FROM	TO	NO. PTS	AVG. DEV.	STD. DEV.
.0	20.0	0	.0	.0
20.0	40.0	32	2.7	3.1
40.0	60.0	24	1.5	2.0
60.0	80.0	24	1.2	1.3
80.0	100.0	112	4.1	4.3

LABORATORY DISPLACEMENT NO. 4

AFTER 15.0 HOURS OF INJECTION

AVERAGE ABSOLUTE DEVIATION AND STANDARD DEVIATION

FROM NUMERICAL SOLUTION - EXPRESSED IN SATURATION PER CENT

OVERALL AVERAGE DEVIATION = 3.8 STANDARD DEVIATION = 4.3

AVERAGE AND STANDARD DEVIATION BY SATURATION RANGE

FROM	TO	NO. PTS	AVG. DEV.	STD. DEV.
.0	20.0	0	.0	.0
20.0	40.0	16	6.7	7.3
40.0	60.0	32	2.4	3.0
60.0	80.0	0	.0	.0
80.0	100.0	144	3.8	4.0

LABORATORY DISPLACEMENT NO. 4

AFTER 20.0 HOURS OF INJECTION

AVERAGE ABSOLUTE DEVIATION AND STANDARD DEVIATION

FROM NUMERICAL SOLUTION - EXPRESSED IN SATURATION PER CENT

OVERALL AVERAGE DEVIATION = 4.3 STANDARD DEVIATION = 4.7

AVERAGE AND STANDARD DEVIATION BY SATURATION RANGE

FROM	TO	NO. PTS	AVG. DEV.	STD. DEV.
.0	20.0	0	.0	.0
20.0	40.0	0	.0	.0
40.0	60.0	16	2.7	3.0
60.0	80.0	16	6.7	6.7
80.0	100.0	160	4.2	4.6

LABORATORY DISPLACEMENT NO. 4

AFTER 22.0 HOURS OF INJECTION

AVERAGE ABSOLUTE DEVIATION AND STANDARD DEVIATION

FROM NUMERICAL SOLUTION - EXPRESSED IN SATURATION PER CENT

OVERALL AVERAGE DEVIATION = 4.2 STANDARD DEVIATION = 4.5

AVERAGE AND STANDARD DEVIATION BY SATURATION RANGE

FROM	TO	NO. PTS	AVG. DEV.	STD. DEV.
.0	20.0	0	.0	.0
20.0	40.0	0	.0	.0
40.0	60.0	0	.0	.0
60.0	80.0	16	5.5	5.6
80.0	100.0	176	4.1	4.4

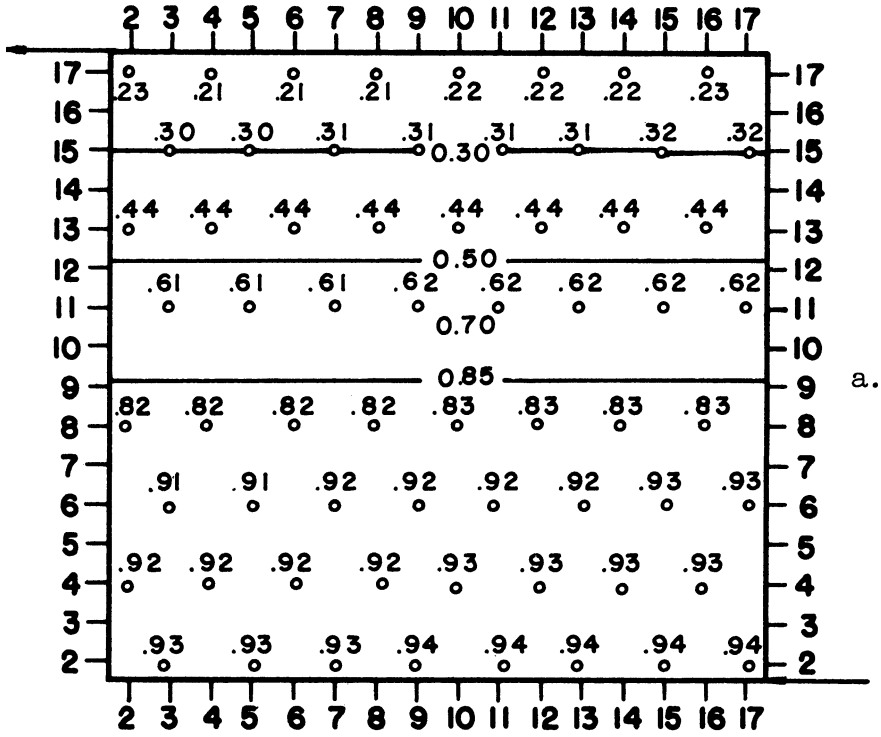

a. At 4 Hours

— NUMERICAL SOLUTION

o EXPERIMENTAL DATA

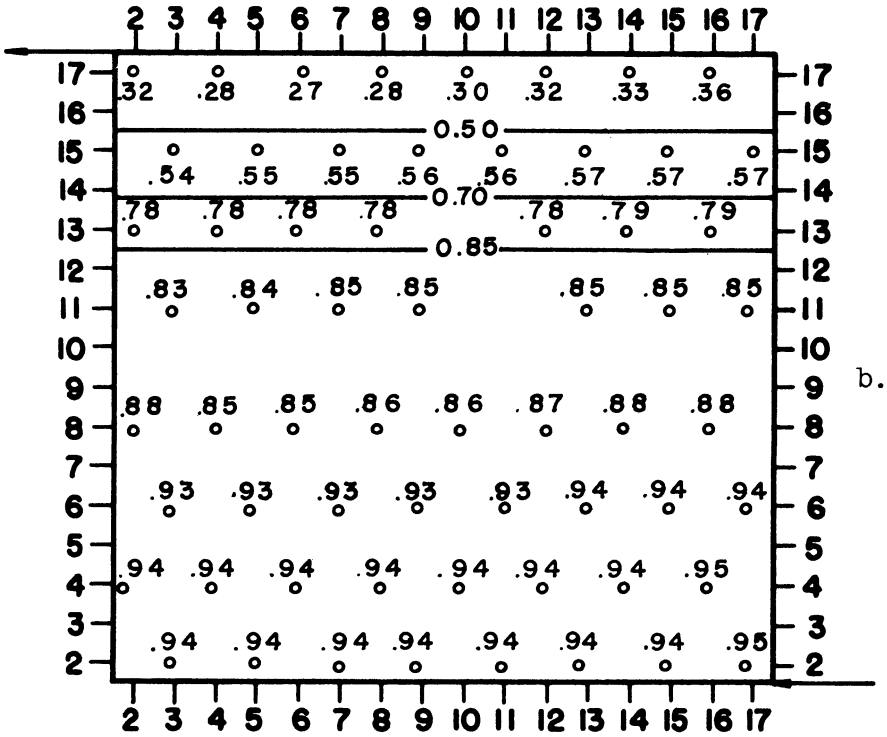

b. At 15 Hours

Figure 30. Water Saturation Contours
Displacement No. 4 (and No. 3)

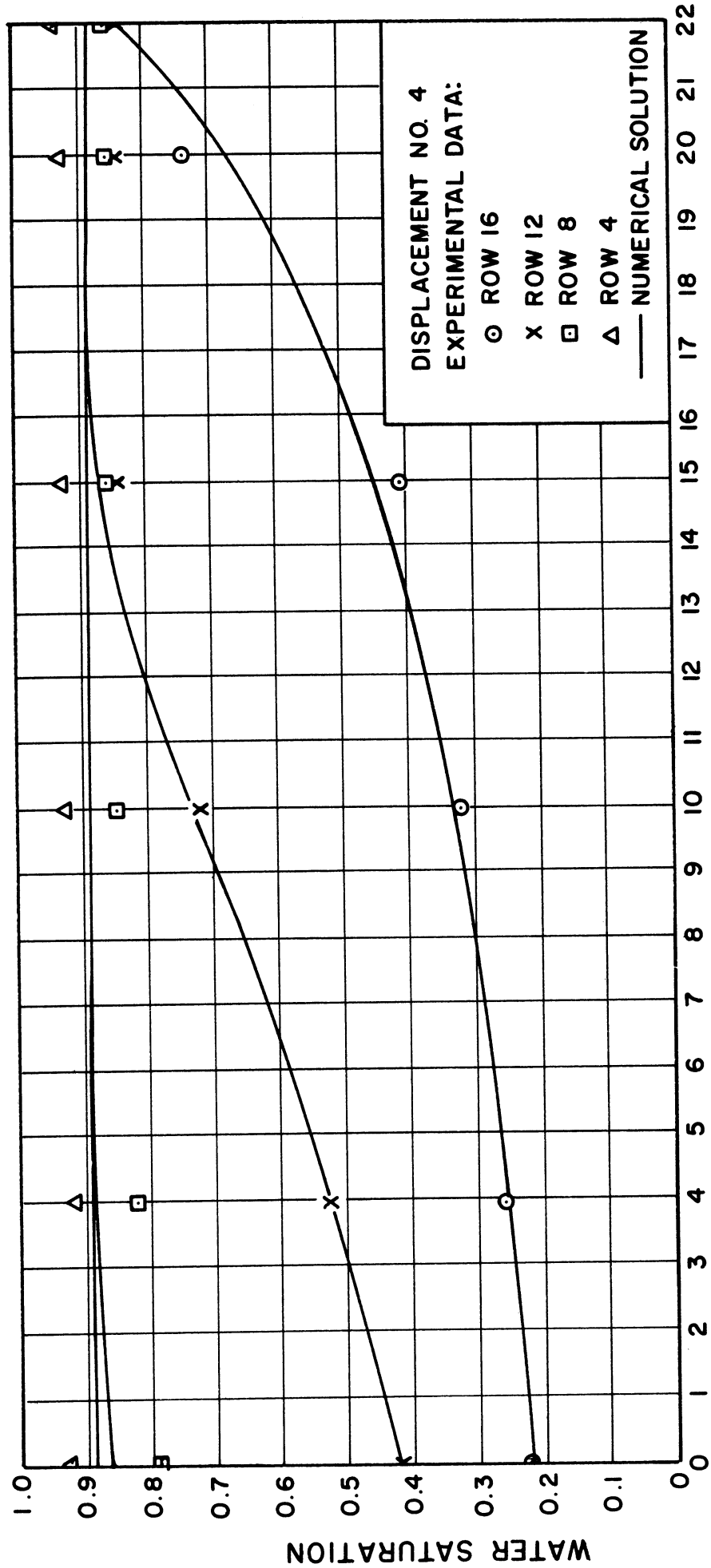

Figure 31. Water Saturation History
Displacement No. 4 (and No. 3)

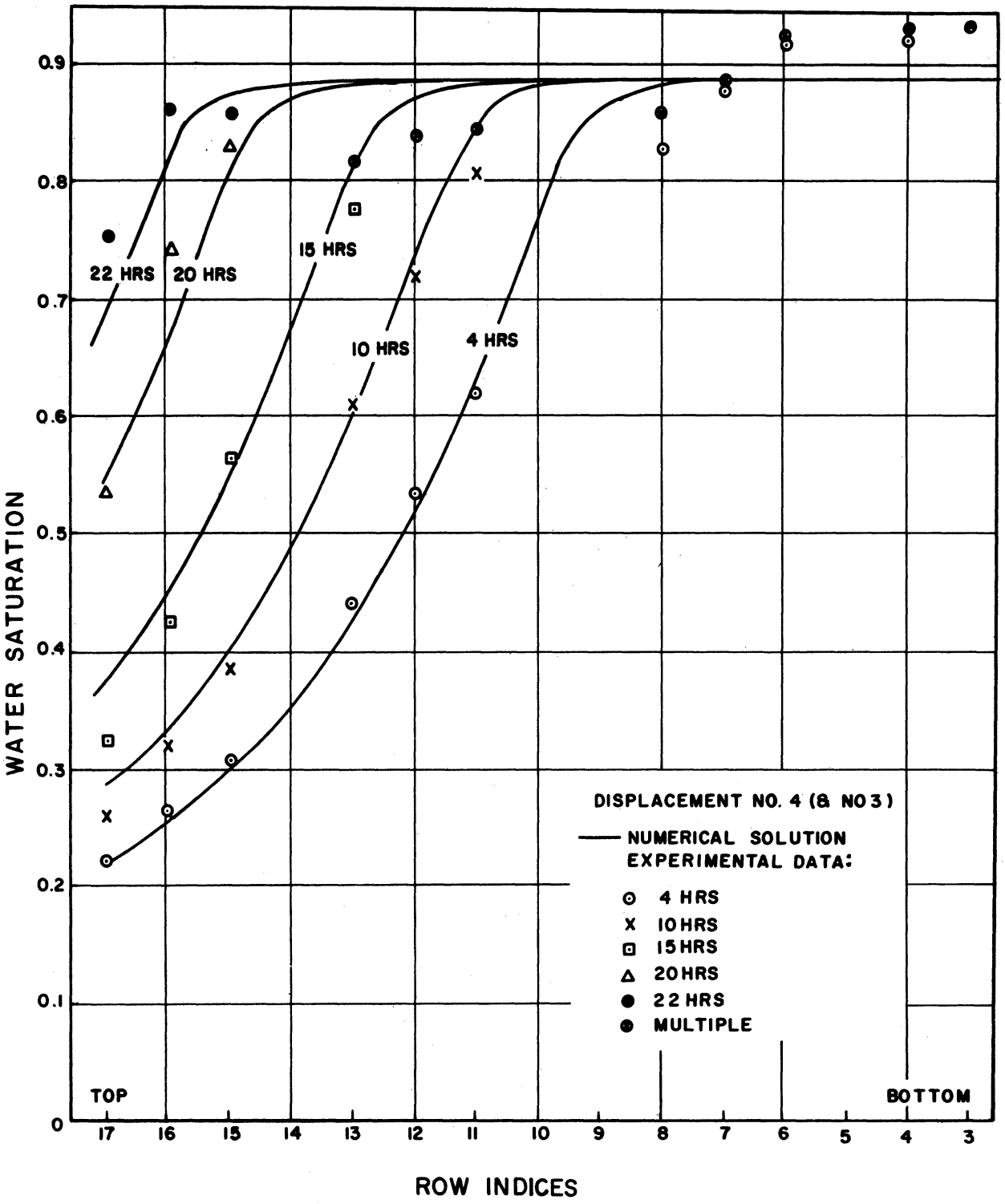

Figure 32. Vertical Water Saturation Distributions

saturation history and vertical distribution, respectively. In these figures, the saturations are again row averages.

The over-all water balances shown in Tables XXI and XXIV are good. For Displacement No. 2, the 0.17 per cent error amounts to about 1.3 cc at the 40 hour mark while the other solution is off by only 0.15 cc at 22 hours. These figures reflect the degree of convergence obtained in the updating of the R variable. Since the former solution began at a lower average water saturation, more grid elements existed in the flat portion of the capillary pressure curve where an increment of capillary pressure covers the greatest range of water saturation. Thus a given error in R or equivalently capillary pressure in this range corresponds to the largest error in water saturation. This behavior was borne out by the lower rate of increase in cumulative water balance error as the water content of the pore volume increased during the former displacement. The material balance would be improved by demanding a stricter tolerance on the R variable during the early phases of Displacement No. 2. This would result of course in a higher computing time requirement.

The good agreement between computed and experimental breakthrough times merely indicates that a proper value had been assigned for residual gas saturation on the imbibition capillary pressure curve.

The average and standard deviations for the complete imbibition displacements are tabulated below.

This agreement is considered to be quite good and is somewhat better than for the drainage displacement as would be expected from the

TABLE XXVIII

OVER-ALL EXPERIMENTAL - NUMERICAL AGREEMENT,
IMBIBITION DISPLACEMENTS

Disp. No.	Avg. Dev.	Std. Dev.
2	3.9%	4.7%
3	3.4%	4.0%
4	3.6%	4.0%
over-all	3.6%	4.2%

stable vs. unstable nature of the two types of displacement. It is felt that the agreement might be improved if it were possible to begin an experimental imbibition from a uniform phase distribution near connate water. It will be recalled that the initial distributions were achieved by following a pressure drainage by a slow counter gravity imbibition. With this technique of operation, it of course would be impossible to fix an imbibition distribution at a significantly lower average water saturation than was employed in Displacement No. 2.

It was rather surprising to find no significant horizontal gradients in water saturation for both experimental and computed imbibition distributions. It would appear that higher rates are required to override the gravitational and capillary effects responsible for the one-dimensional phase saturation distributions. Under the operating techniques employed, appreciably higher injection rates would not have been handled satisfactorily because of the time required to effectively monitor saturation distributions.

Water potential distributions were considerably more interesting. By cross-plotting the computed water potential matrices the contours appearing in Figures 33a - d and 34a - c were constructed. Corresponding water saturation contours have not been included but they were very similar to those shown in Figures 27 and 30 with the appropriate vertical translation. To the author's knowledge, phase potential distributions in two-dimensional, two-phase systems have not appeared in the literature.

Flow lines or streamlines can be imagined crossing perpendicular to each potential contour. Thus for Displacement No. 2 operated with water injection solely at the lower right corner, the water velocity distribution is seen to be directed toward the production well at all times. During the displacement, the contours became skewed and displaced according to the relative permeability distribution. If the contours were plotted subsequent to completion of breakthrough, they would assume the normal single phase flow positions formed by superposition of concentric circles about the injection and production wells.

For the two point injection of water employed in the final two displacements, water is seen to flow from both wells to a pseudo sink along the left edge of the model. In this case the initial position of the sink is about at the mid point of the left boundary. For a lower initial average water saturation, the sink would be expected to be proportionately lower. During displacement, the sink is seen to move vertically and would reach the production well at water breakthrough. Following completion of breakthrough, the single phase potential distribution would result. The influence of gravity is illustrated by the

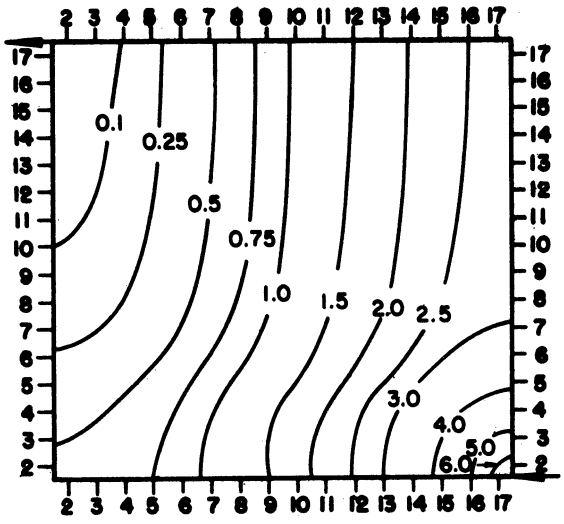

a. At 1 Hour

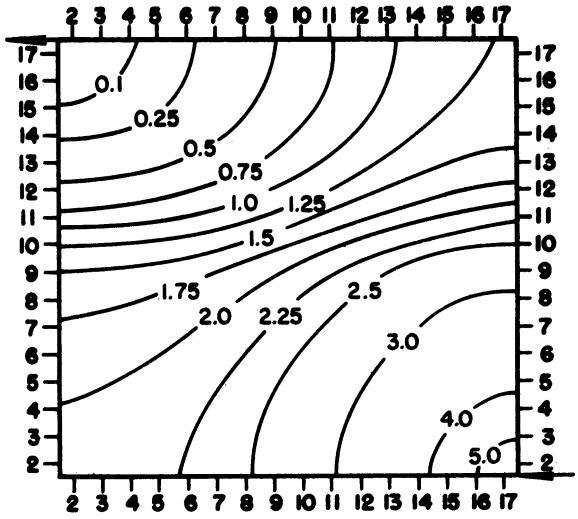

b. At 21 Hours

UNITS OF 0.0001 ATM.

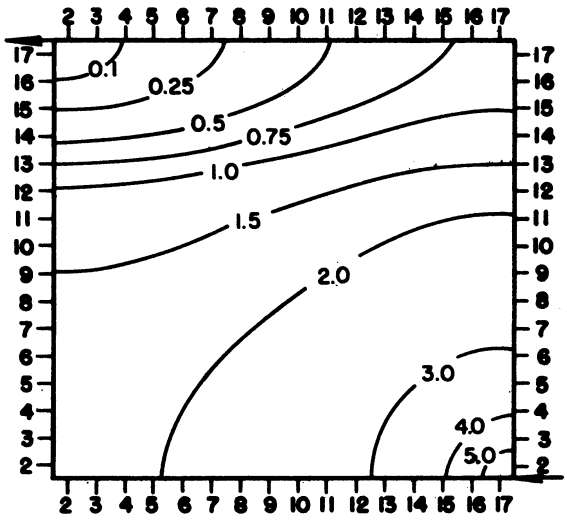

c. At 31 Hours

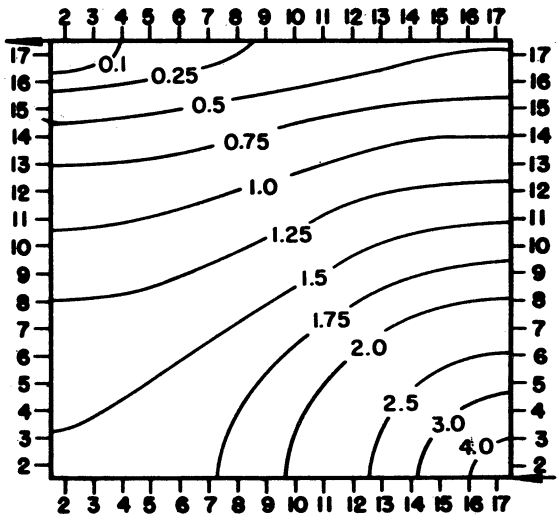

d. At 41 Hours

Figure 33. Water Potential Contours
Displacement No. 2

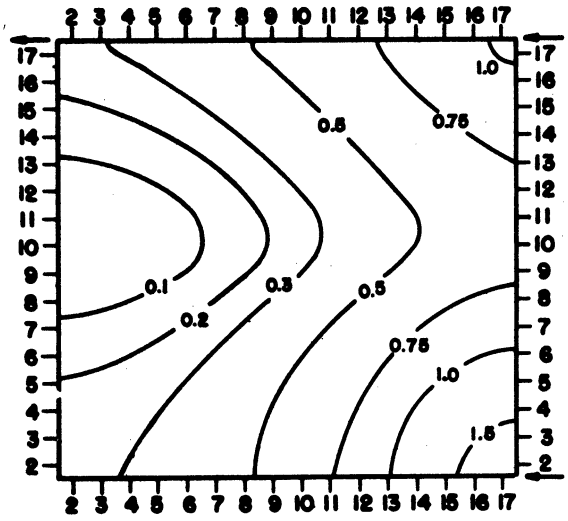

a. At 1 Hour

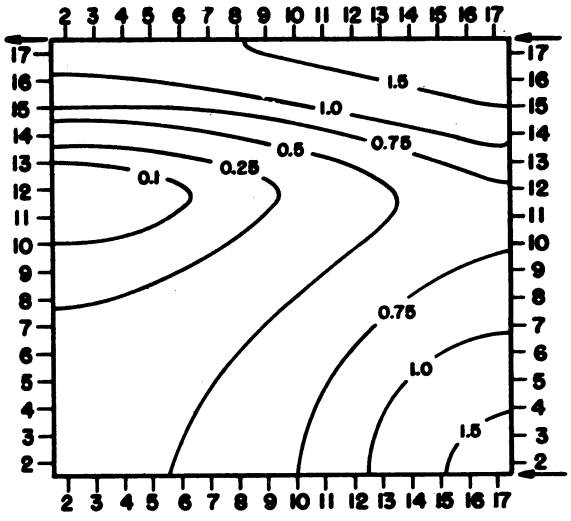

b. At 9 Hours

UNITS OF 0.0001 ATM.

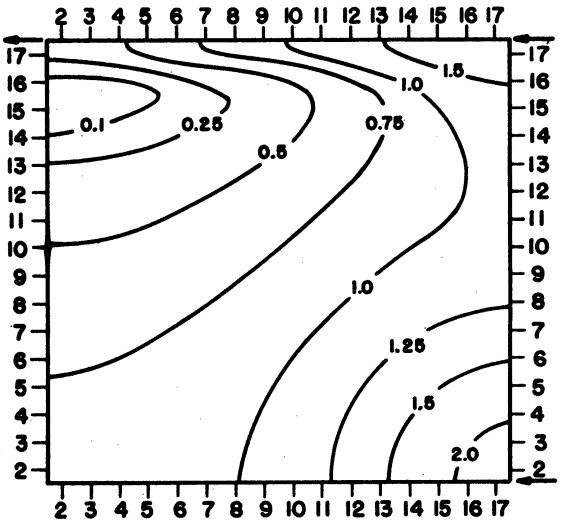

c. At 20 Hours

Figure 34. Water Potential Contours
Displacement No. 4 (and No. 3)

increasing water potential gradient developing near the upper injection well as the displacement proceeds. In the absence of gravity, the potential gradient would be expected to decrease near this well because the water permeability increases as the imbibition proceeds.

As discussed earlier, water potential measurements would require the use of a device permeable to water only. If such measurements were attempted, higher rates would be desirable as the potential unit (0.0001 atm) is equivalent to about 0.04 inch of water. At higher rates, the potential contours would be expected to display roughly the same shapes as obtained for low rates at the corresponding water saturation distributions, but the gradients would be steeper.

C. Discussion of Results

The cumulative water balances constitute good integral checks on the solutions, but they say little about the convergence of the solutions. To investigate convergence, the 11 to 15 hour portion of the solution for Displacement No. 2 was re-evaluated on a series of 15 minute time steps. Included in Appendix III in Tables XXXIV and XXXV are the computed water saturation distributions resulting at the 15 hour mark for solution over this four hour period on 30 and 15 minute time steps, respectively. The phase distributions are seen to agree to two or three digits in the fourth place. From this agreement it was concluded that the solutions were convergent for the imbibition displacements. Since the same tolerances were demanded of the P and R variables calculated in the drainage, it was assumed that this solution was also convergent.

It will be noted that water saturations above 89 per cent appear in Tables XXXIV and XXXV. For these computations a capillary pressure curve somewhat different from that shown in Figure 26 was employed. It had a residual gas saturation of about 6 per cent ($S_w = 0.94$) and was slightly steeper over the saturation mid range. Using these capillary pressure data numerical solutions were carried out for both imbibition displacements. As might be expected, the resulting water saturation distributions were too high over the lower part of the model and too low for the upper part with breakthrough occurring considerably later than observed experimentally. At the 40 hour level in Displacement No. 2, the average deviation from this solution shown by the data was about 12 per cent, which is three times greater than obtained using the proper residual gas saturation.

Subsequent computations for Displacement No. 2 using the high residual saturation capillary pressure data were carried out employing the modified relative permeability data shown in Figure 35a. Comparison to the normal relative permeability curves presented in Figure 22 shows the modified curves to be somewhat lower for the higher water saturations. The gas relative permeability was set to zero for water saturations above 84 per cent. (The approach to zero was roughly exponential between 78 and 84 per cent.) This modification appeared justifiable on the basis of the scatter shown in the Wyckoff and Botset data. It was introduced in an attempt to improve the description of experimental behavior by allowing rows of elements initially above 84 per cent water saturation to remain at the same saturation but to fix 84 per cent as the upper limit for elements initially below that value.

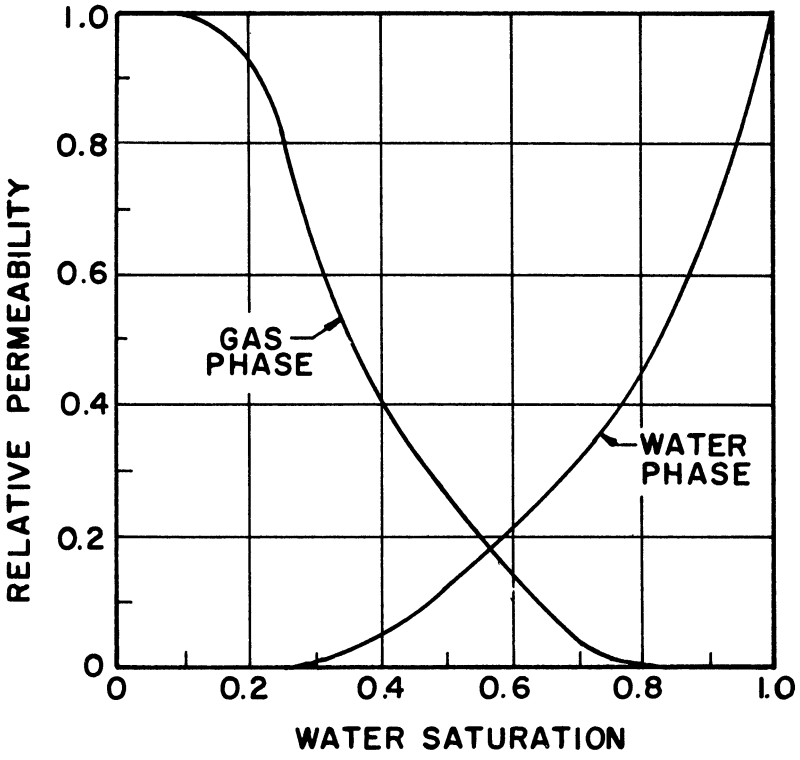

a. Relative Permeability Curves

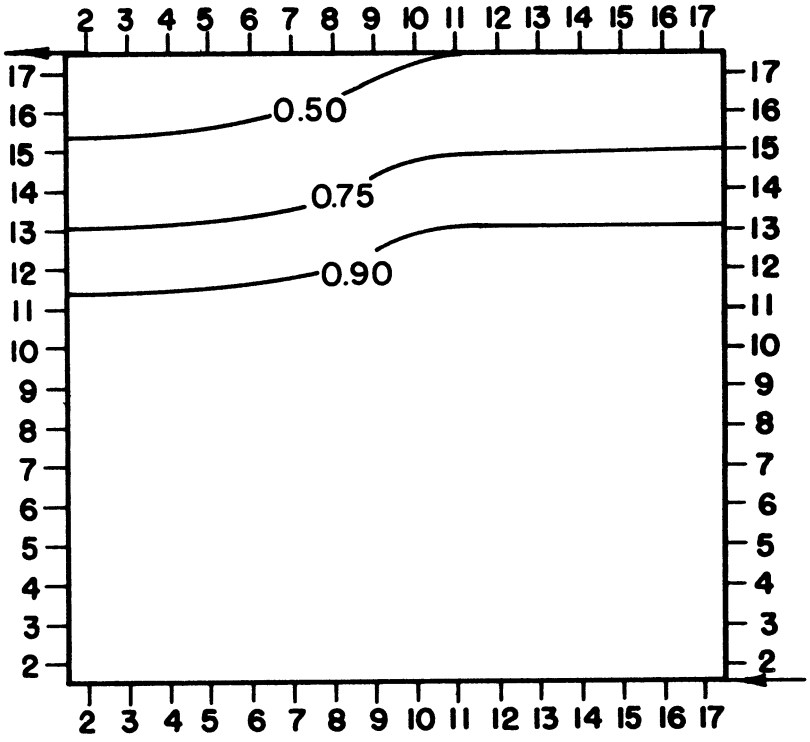

b. Water Saturation Contours at 38 Hours

Figure 35. Modified Simulation of Displacement No. 2

Figure 35b presents the computed phase distribution after 38 hours of water injection. It is not completely understood why water saturations greater than 24 per cent result. This is believed to be a consequence of the use of the P and R forms of the equations where relative permeabilities enter as sums and differences. It is probable that solution for the individual phase potentials would not allow this type of behavior. It might be possible to override the apparent anomaly by freezing the value of R for all elements existing at or above the desired residual saturation. This, however, might introduce convergence problems.

More important, it will be noticed that the horizontal saturation gradients present in the solution are far greater than observed experimentally. For this reason, it was concluded that the modified relative permeability curves must not have been representative of the laboratory medium. Thus it appeared that the best description of the data should result through the use of a capillary pressure curve with a residual gas saturation corresponding to the average saturation existing at breakthrough. Possible reasons for the existence of water saturations greater than the apparent residual have been discussed in the Experimental Results section.

D. Conclusions

The following conclusions have been drawn from comparison of experimental to computed results and the behavior of the numerical solutions.

1. The major conclusion is that phase distributions in the two-dimensional laboratory medium subject to the

simultaneous flow of gas and water can be described very closely by numerical solution of the differential equations taken to apply to the system.

2. Little if any significance should be attached to comparison of integral behavior obtained during the two-phase production period following breakthrough by experimental observation to that resulting from numerical solution of the differential equations. This is because the numerical solution can be shaped to approximate the observed behavior over this period by appropriate choice of the capillary pressure relationship near the residual phase saturation. This portion of the capillary pressure curve is generally ill-defined by experimental data and most any reasonable shape can be justified.

3. For displacements operated at low flow rates, gravitational and capillary effects tend to override viscous effects.

4. A corrollary to the above conclusion is that the phase distributions arising in low rate displacements are much more sensitive to capillary pressure than relative permeability relationships.

5. The numerical solutions appear to converge to the exact solutions of the differential equations. Positive proof cannot be given in the absence of analytic solutions of the equations.

VIII. EVALUATION OF SCALING LAWS

In order to reproduce the behavior of a reservoir system on the laboratory scale, certain relationships must exist among the physical properties of the reservoir and laboratory systems. For cases in which the reservoir fluids may be considered as two immiscible, incompressible phases, the necessary relationships among the physical properties have been formulated by Rapoport(42). These relationships or scaling laws were deduced by performing dimensional analysis on the differential equations taken to describe the immiscible, incompressible two-phase flow system in porous media. The method is illustrated in the Mathematical Analysis section where the scaling laws as set forth by Rapoport for three-dimensional cartesian coordinates have been developed and modified for use in the two dimensional coordinate systems under consideration here.

It will be recalled that the scaling laws presuppose three conditions which normally cannot be satisfied by the laboratory system. These conditions are:

1. The functional dependence of relative permeabilities on phase saturations must be identical for reservoir and laboratory systems.

2. The capillary pressure functions for the two systems must be linearly related.

3. The boundary conditions in the laboratory model must duplicate those in the reservoir system.

On a purely mathematical basis, however, these conditions can be satisfied easily. Thus the importance of these unscalable properties can be assessed by solution of the describing differential equations. In the absence of analytic methods of solution, this sort of evaluation could not have been accomplished prior to the development of large capacity, high speed digital computing facilities which made numerical solutions practical.

This portion of the work has been undertaken to assess the validity of the scaling laws in relation to a practical laboratory system which has been scaled as rigorously as possible to a realistic field system. Numerical solutions in two-dimensional cartesian coordinates have been carried out for a field system, the practical laboratory model of the field system and for several unattainable laboratory models which satisfy the experimentally unscalable requirements to varying degrees.

Presentation appears in the following sequence:

A. Description of the Field System.

B. Description of the Laboratory System.

C. Computations Performed.

D. Results of Computations.

E. Conclusions.

It must be appreciated that an evaluation of the scaling laws on the basis of the performance shown by a series of laboratory displacements scaled to different geometric proportions would be merely a roundabout way of testing the validity of the differential equations

taken to describe the system. Evaluation of the scaling laws in the light of the unscalable properties of the laboratory system can be accomplished only on a mathematical basis.

A. Description of the Field System

The field scale system selected as the basis of this investigation was a natural gas reservoir subject to water-drive. The assumptions of immiscibility and imcompressibility would be approximated closely by both phases at the operating pressure level of 1260 psia. Pressure gradients in the gas phase prevailing at the flow rates encountered would result in little variation of gas phase density throughout the system and the solubility of natural gas in water is not large. The gas phase would be expected to be saturated with water vapor, but again at this pressure level, the concentration of water vapor in the gas phase would be low. Even if mutual solubilities were appreciable, very little mass transfer between phases would occur in view of the small variations in absolute pressure resulting in the respective phases throughout the reservoir. For purposes of the two-phase reservoir problem the water phase would behave incompressibly.

One must clearly recognize the distinction between the treatments of the two-phase reservoir system and the single phase system associated with the large surrounding aquifer. In the latter case, the water phase normally will be treated as slightly compressible to allow analysis of the movement of the water phase. Specifically, the problem posed here centered on finding the phase saturation distributions as a

function of time in the vicinity of the well as gas was produced from the sand face. This section of the formation has been shown in Figure 36. It is seen to consist of five layers of porous rock, each layer having a different permeability but all layers having the same porosity. The outer boundary (right edge) is an artifice which represents no discontinuity in the porous medium and allows flow of both phases across this boundary at all levels in the permeable zone. From a practical standpoint, the field represented by the geometry of Figure 36 would correspond either to a gas reservoir located between parallel faults, or alternatively, to a reservoir of large areal extent produced by a series of aligned wells in line drive fashion. Treatment within the framework of two-dimensional cartesian coordinates assumes that no significant gradients of the system variables occur across the horizontal thickness of the formation. As indicated by Figure 36, the formation was inclined 1° from the horizontal.

The phases initially existed at the capillary-gravitational equilibirum distribution. Gas was produced at a constant rate of 7800 MSCF/Day through the 6 inch diameter, partially penetrating well shown in Figure 36. The properties of the individual phases are listed in Table XXIX. The imbibition capillary pressure relationship shown in Figure 38a was transformed to the indicated basis of porosity, permeability and surface tension through the Leverett J-function from a rather sketchy set of air-water capillary pressure data given by Katz (Reference 25, page 59) for a 175 md permeability, 22.8% porosity sandstone. The relative permeability curves shown in Figure 39a are representative for gas-water systems in consolidated media as determined by Botset[3].

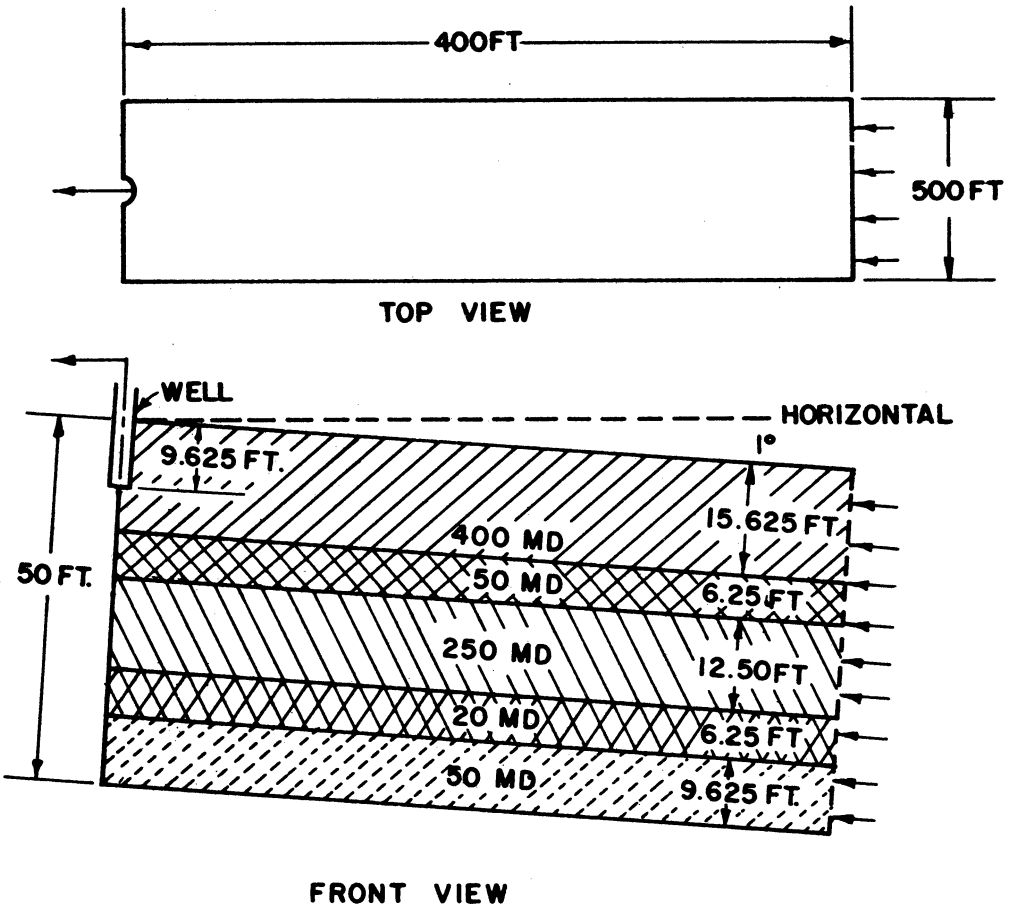

Figure 36. Field System

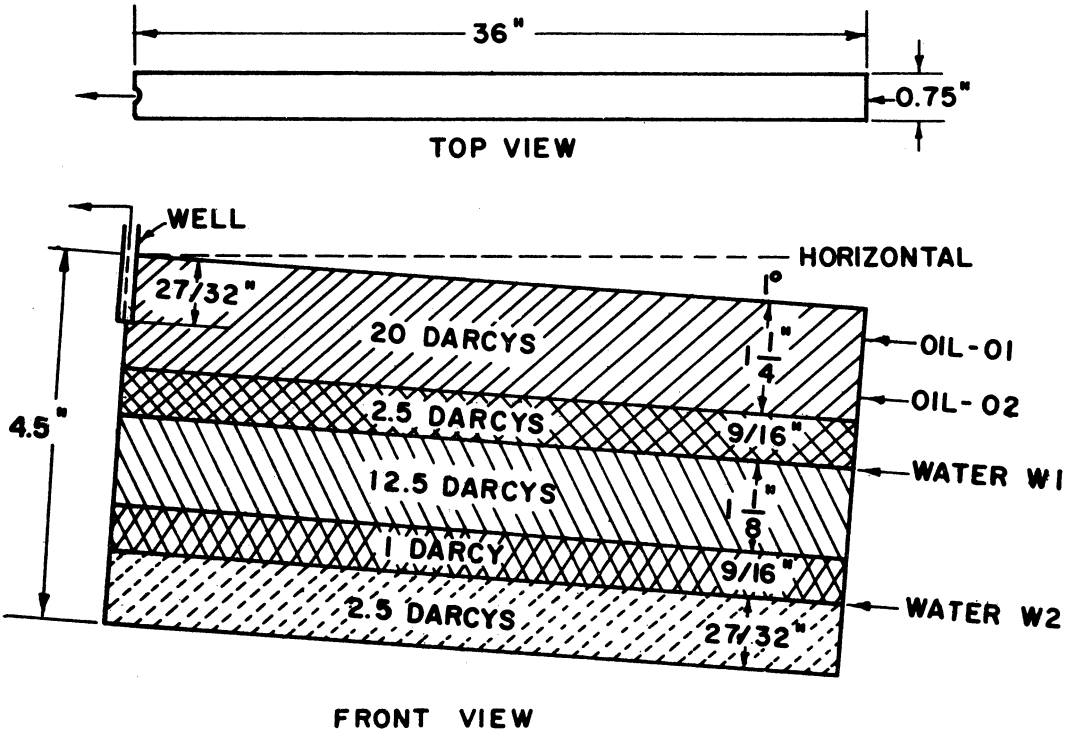

Figure 37. Laboratory Model of Field System

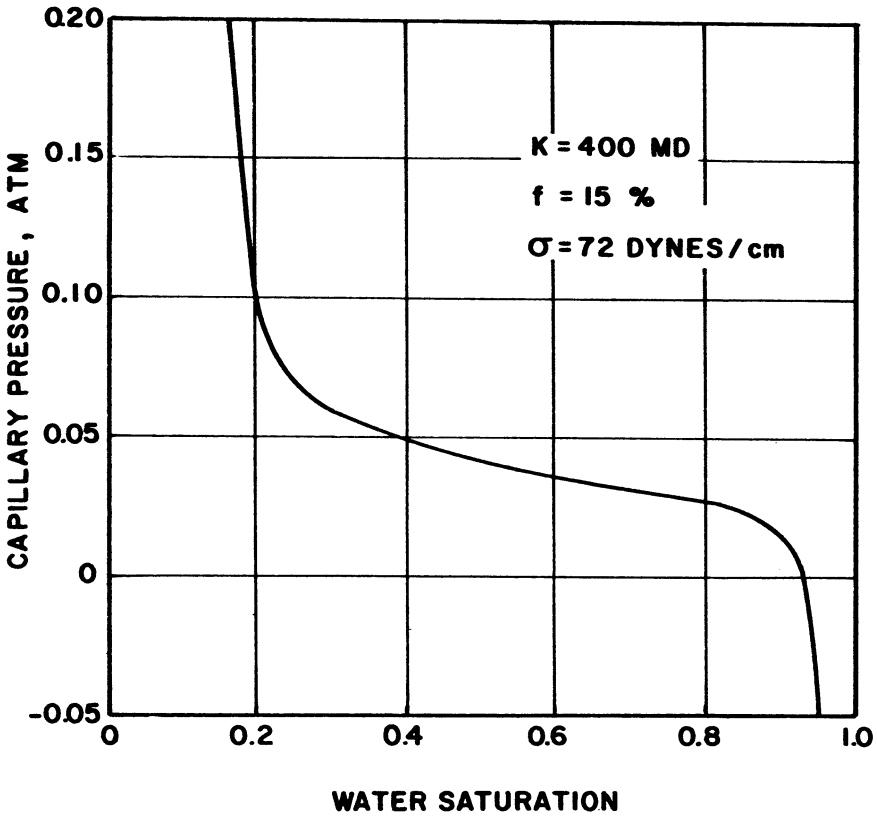

a. Field System

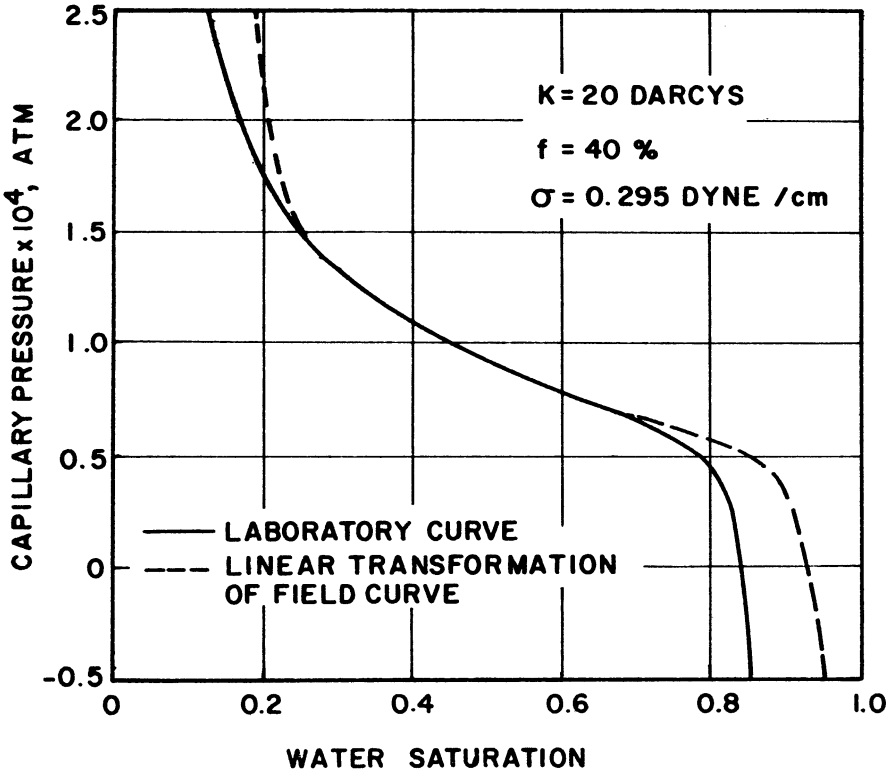

b. Laboratory System [After Katz[25]]

Figure 38. Capillary Pressure Curves

[After Carpenter[8]]

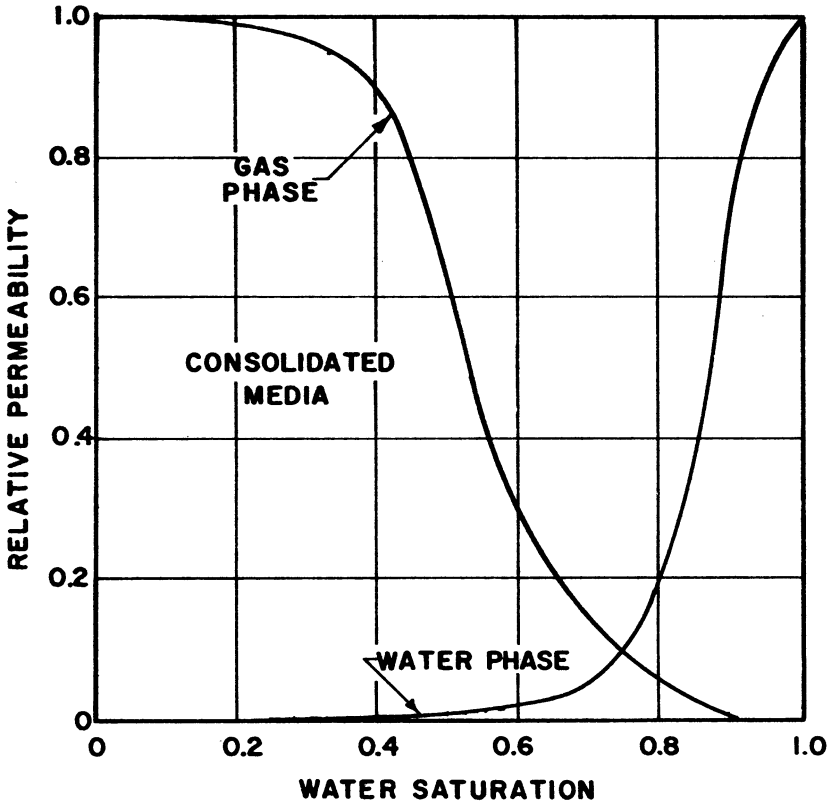

a. Field System

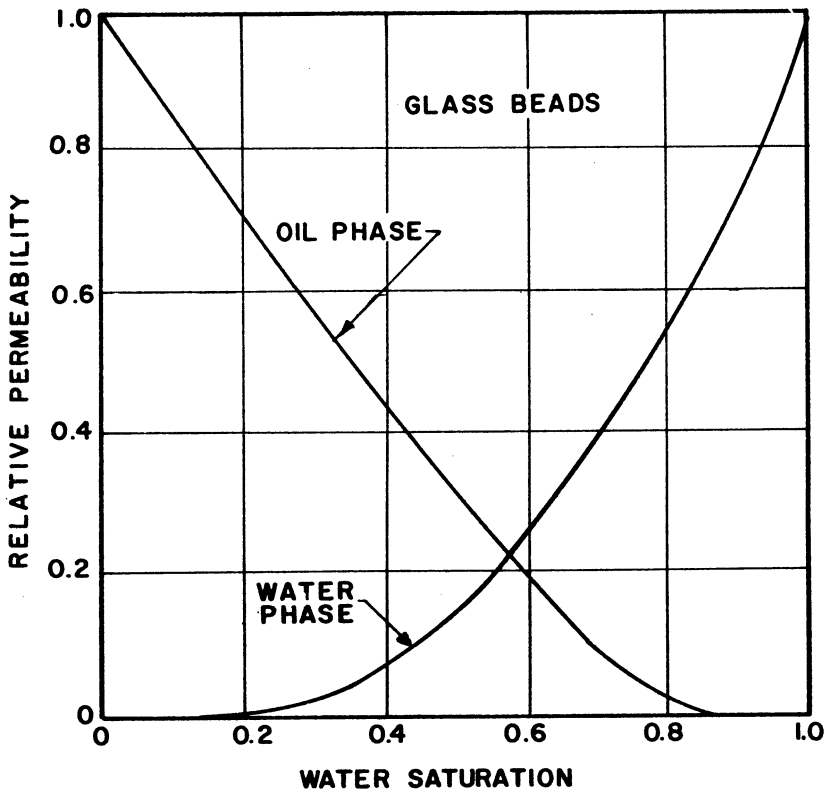

b. Laboratory System

[After Botset(3)]

Figure 39. Relative Permeability Curves

[After Carpenter(8)]

B. Description of the Laboratory System

To simulate the gas-water system of the field, an oil-water system was chosen for the laboratory. This was done as the interfacial tension between oil and water can be adjusted over a wider range than a gas and water. Adjustment of interfacial tension will be seen necessary to scale capillary effects to the laboratory. In addition, the use of an oil-water system can be operated more conveniently in the laboratory. The assumptions of immiscibility and imcompressibility would be satisfied without question by the oil and water phases.

For ease of construction, glass beads were designated for use in the laboratory model. To make the hypothetical model as realistic as possible, the permeabilities of the layers were chosen in ranges which could be realized through the use of glass beads. The porosity of a glass bead pack cannot be fixed arbitrarily as a value of about 40 per cent will result regardless of bead size.

The dimensions of a laboratory model are fixed by practical considerations. Those shown for this particular model in Figure 37 are quite reasonable. At this point, the advantage of the use of the two-dimensional scaling laws becomes obvious because a 3/4 inch thickness would be much more practical than the 45 inch thickness required by the three-dimensional laws for this particular choice of length and height dimensions. At the right boundary of the model, a discontinuity not present in the field exists. In an effort to reproduce the field boundary in a reasonable manner, four injection ports were provided as shown in Figure 37 with the upper two for oil and the lower two for water injection. Rates of injection through each of the ports appear in Table XXX.

If the length and height scale ratio were applied to the diameter of the production well as required by the scaling laws, a microscopic well diameter not obtainable in the laboratory would result. Consequently, the production well was designated to have a 1/8 inch diameter which is a convenient laboratory size.

Properties of the laboratory fluids and bead pack are listed in Table XXIX. All variables except the well diameter have been scaled in accordance with the two-dimensional scaling laws stated by Equations (43) and (44). The scaled well diameter has been placed in parentheses as have the thickness dimension and oil production rate which result from the three-dimensional scaling laws.

The gas gravity indicated for the field system applies at standard conditions in the normal sense. At the pressure and temperature conditions of the reservoir, the compressibility factor should be 0.884 to result in a gas phase density of 0.0813gm/cc. The reservoir water phase was taken to be a brine of the indicated specific gravity and viscosity. The contact angle was assumed to be 0°.

In the laboratory system the desired gravity and viscosity could be obtained by blending a dense halocarbon into a normal hydrocarbon such as octane. Surface active agents would be used to yield the desired interfacial tension. A thickening agent such as glycerine would be added to the water phase to give the proper viscosity. Again the contact angle was assumed to be 0°.

The capillary pressure curve for the oil-water system in unconsolidated glass beads appears in Figure 38b for the indicated porosity,

permeability and interfacial tension. This curve was based on data supplied by Carpenter[8] for an oil-water system in glass beads. The dashed curve superposed on this figure resulted from linear transformation of the consolidated data of the field system. The necessary scale ratio, G, defined by Equation (29a) was 452.6. The constant term Γ of the linear transformation defined by Equation (29b) was set to zero, the value which seemed to yield the best degree of superposition of the two curves.

Figure 39b presents the relative permeability curves expected for the bead pack. These curves were also supplied by Carpenter and were based on data taken for an oil-water system in glass beads.

The conditions imposed by the scaling laws of identical relative permeability and linearly related capillary pressure curves clearly are seen to be in violation. Further, the practical inability to scale well diameters rigorously and to provide laboratory boundaries identical to those of the field has been demonstrated. Because of these unscalable properties, duplication of field behavior in the laboratory would not be expected.

C. Computations Performed

The numerical solutions for the field and laboratory systems were performed in the following sequence:

1. Field system over 30 day production period.
2. Unattainable laboratory systems over the homologous period of time:
   a. Scaled in accordance with three dimensional scaling laws, employing relative permeability curves identical to and

TABLE XXIX

SPECIFICATIONS OF FIELD AND LABORATORY SYSTEMS

Property	Field	Laboratory
length	400 ft.	36 in.
height	50 ft.	4.5 in.
thickness	500 ft.	0.75 in. (45 in.)
angle of inclination	1°	1°
pressure	1260 psia	14.7 psia
temperature	68°F	70°F
well bore diameter	6 in.	1/8 in. (.0450 in.)
gas gravity	0.7	
oil gravity		0.8
water gravity	1.1	1.1
gas viscosity	0.0135 cp.	
oil viscosity		0.6 cp.
water viscosity	1.5 cp.	75.8 cp.
medium	sandstone	glass beads
permeability (layered)	400 md.	20 Darcys
	250 md.	12.5 Darcys
	50 md.	2.5 Darcys
	20 md.	1 Darcy
porosity (uniform)	0.15	0.40
surface tension	72 dynes/cm.	
interfacial tension		0.295 dynes/cm
contact angle	0°	0°
gas production rate	7800 MSCF/day	29.9 cc/hr. (1795 cc/hr.)
operation time	30 days	43.5 hours

TABLE XXX

INJECTION RATE SCHEDULE LABORATORY SYSTEM

Time Interval	Port 01 Oil Rate	Port 02 Oil Rate	Port W1 Water Rate	Port W2 Water Rate
0 - 0.39 days	17.8 cc/hr	11.9 cc/hr	0.119 cc/hr	0.068 cc/hr
0.39 - 0.60	17.8	11.9	0.118	0.068
0.60 - 0.84	17.8	11.9	0.117	0.068
0.84 - 1.09	17.8	11.9	0.116	0.067
1.09 - 1.33	17.8	11.9	0.115	0.066
1.33 - 1.57	17.8	11.9	0.114	0.066
1.57 - 1.81	17.8	11.9	0.113	0.065

capillary pressure curve transformed from field data, and field boundary conditions.

b. Scaled in accordance with two-dimensional scaling laws with relative permeability and capillary pressure relationships and boundary conditions corresponding to the field system.

c. Scaled in accordance with two-dimensional scaling laws using relative permeability and capillary pressure relationships for the unconsolidated bead pack used in the laboratory, but with field boundary conditions.

3. Practical laboratory system over the homologous period of time which was scaled by the two-dimensional laws and employed relative permeability and capillary pressure relationships for the unconsolidated bead pack, with laboratory boundary conditions.

For purposes of numerical solution, the field and model media were partitioned into a 16x16 grid of equally sized elements. Reservoir grid elements of 3.125 ft in height, 25 ft in length and 500 ft in thickness resulted. Corresponding laboratory grid elements were 9/32x2-1/4x3/4 inch except in the simulation of the unattainable laboratory model scaled in three dimensions for which the element thickness was increased to 45 inches. Relative permeability and capillary pressure functions were handled in tabular form as discussed earlier.

All solutions were carried to completion through a sequence of ten time steps. Although higher accuracy would have resulted with a larger number of time steps, the expenditure of additional computational time did not appear justifiable in view of the hypothetical nature of the

problems. Since the lengths of the corresponding time steps in all laboratory solutions were scaled to those used in the field solution, comparisons among the sequence of solutions should give an accurate picture of the trends introduced by the unscalable properties.

D. Results of Computations

Water saturation distributions at the times of interest are tabulated in Appendix III. Plots of water saturation contours have been included for the reservoir and practical laboratory systems in Figures 40a-c and 41a-c. These figures are focused on the levels in which the sharpest water saturation gradients occur. Element indexing has been indicated. (Lower left element indexed 2, 2). In all five solutions, overall water balance errors were never greater than 0.01%.

The results are summarized in the above sequence.

1. Field System

The initial phase distribution is shown in Figure 40a. Lines of constant water saturation are horizontal and discontinuous at the layer boundaries. Gas was produced at the specified rate through the partially penetrating well shown extending into the upper left corner of the illustrated section. The well was taken to be circular with a 6 inch diameter and 100 per cent open area (open hole). At the right edge, the aquifer boundary condition was employed. The resulting phase distributions after 14 days and 30 days of production are presented in Figures 40b and 40c, respectively. Water saturation distributions at 6.5, 14, and 30 days (time steps 4, 6, and 10) are reproduced in Tables XXXVI(a) through XXXVI(c).

Figures 40a-c give a clear picture of the water coning which was found to occur near the production well.

2. Unattainable Laboratory Systems

a. Rigorous three-dimensional scaling

The initial phase distribution existing in the reservoir was reproduced on the laboratory scale since the capillary pressure curve corresponded linearly to that of the reservoir prototype. The relative permeability relationships were identical to those of the field system. Field boundary conditions were reproduced by using the aquifer boundary condition at the right edge and by scaling the producing well to the required 0.045 inch diameter. Computations proceeded on a sequence of homologous time steps with the phase distribution presented in Table XXXVII(a) resulting after 9.41 hours of operation (time step 4).

Comparison of the distribution in Table XXXVII for this experimentally unattainable version of the laboratory model to that in Table XXXVI for the reservoir prototype at the corresponding homologous time shows the water saturations to be the same at all grid elements to at least one digit in the fourth place.

b. Rigorous two-dimensional scaling

Specifications for this experimentally unattainable version of the laboratory displacement were the same as above except with the thickness dimension compressed to 3/4 inch and the production rate reduced accordingly. Presented in Table XXXVII is the computed water saturation distribution after 9.41 hours of operation (time step 4).

Again excellent agreement is seen to exist between water saturation distributions in the field and laboratory systems.

c. Semi-rigorous two-dimensional scaling

Problem specifications are the same as previously, including treatment of boundary conditions, but relative permeability and capillary pressure relationships for the unconsolidated bead pack were introduced. Since this capillary pressure curve departs from the required linear relationship to the field curve, the initial phase distribution cannot be identical to that of the prototype. Consequently, the distribution was fixed so that the 50 per cent contours would match up. The distribution is shown in Figure 41a.

Table XXXVII(c) reproduced the computed water saturation distribution obtained after 9.41 hours of production (time step 4). This distribution is to be compared with that for the practical laboratory system (Table XXXVIII(a)).

3. Practical Laboratory System

The only changes from the third version of the experimentally unattainable laboratory model were in the treatment of the boundary conditions. The practical diameter of 1/8 inch and 40 per cent open area were assigned to the production well, and the aquifer boundary formerly applied at the right edge was replaced by the four injection wells. Injection rates were assigned in accordance with Table XXX. Since rates at each injection well were specified, a description of each well was not required. (Well-bore diameter and open area enter only in computation of the distribution of the total injection or production rates over the grid elements open to the well.) The initial phase distribution is shown in Figure 41a.

Reproduced in Tables XXXVIII(a) through XXXVIII(c) are the computed water saturation distributions existing after 9.41, 20.3, and 43.5 hours of

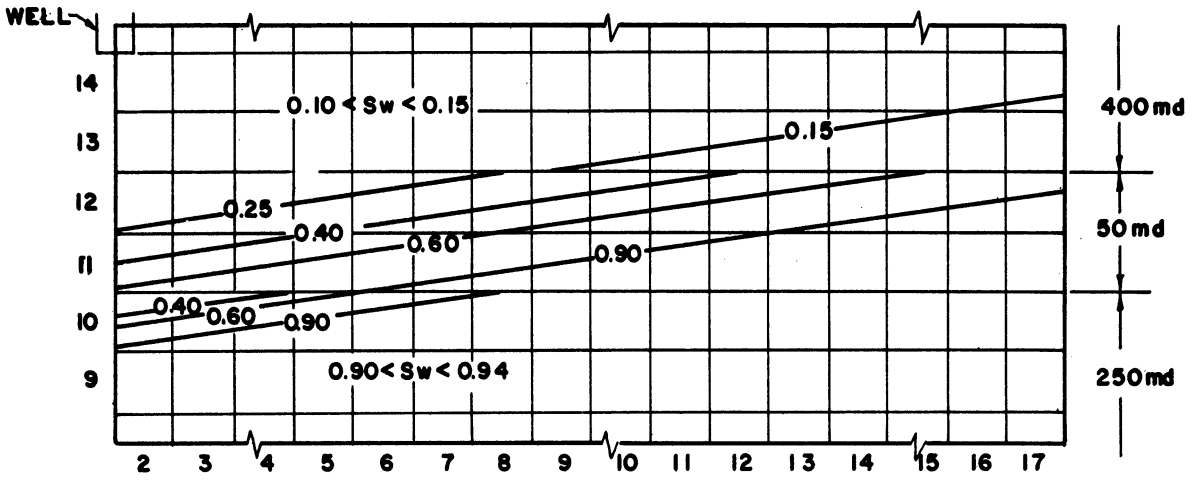

a. Initial

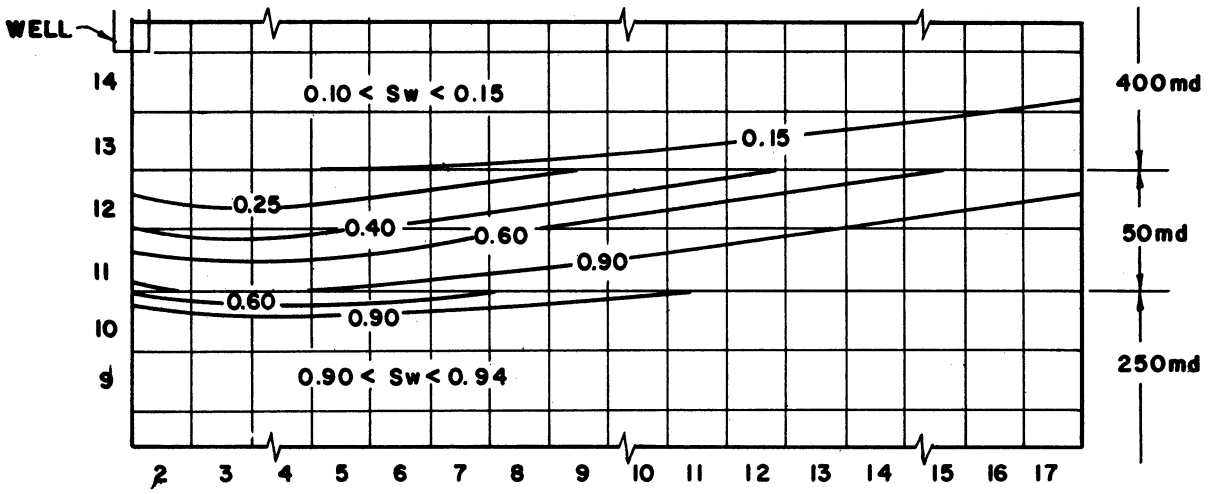

b. At 14 Days

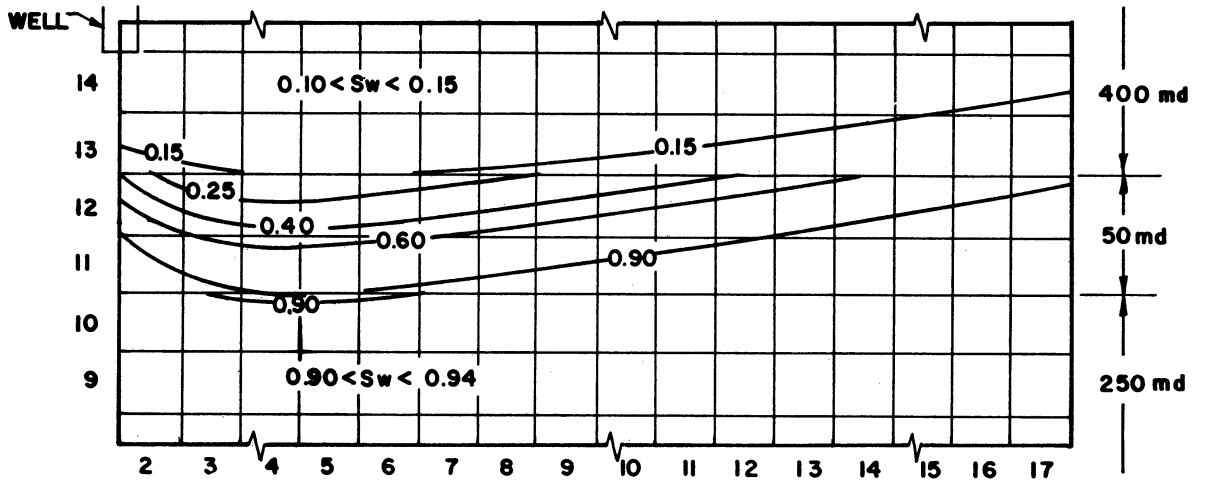

c. At 30 Days

Figure 40. Water Saturation Contours Field System

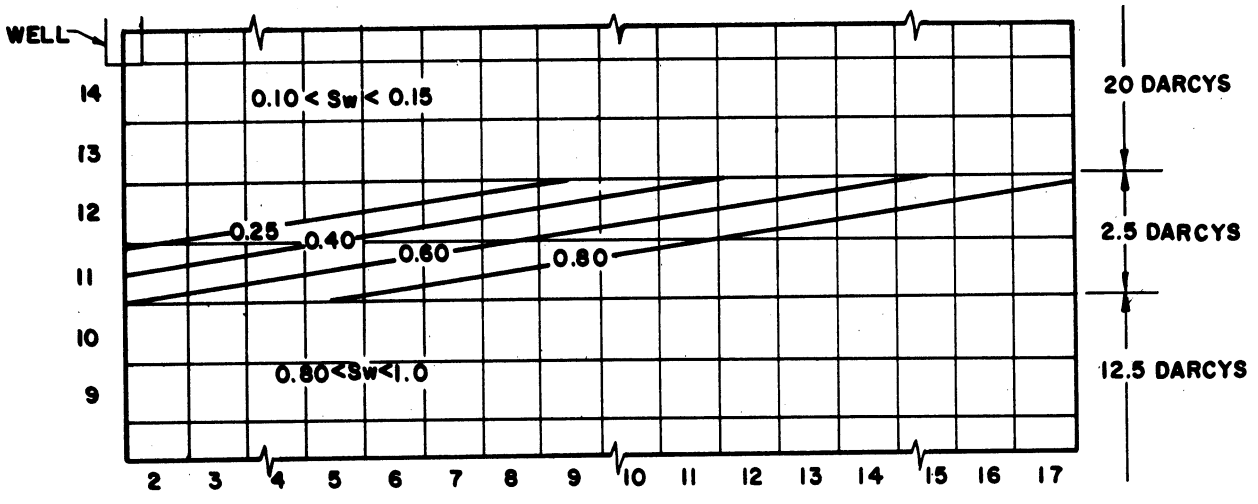

a. Initial

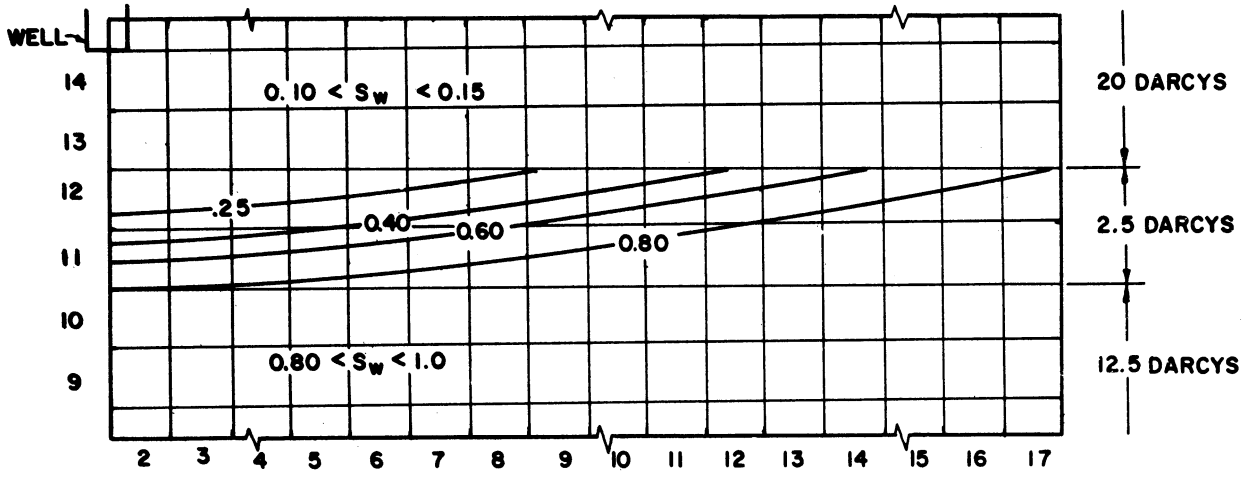

b. At 20.3 Hours

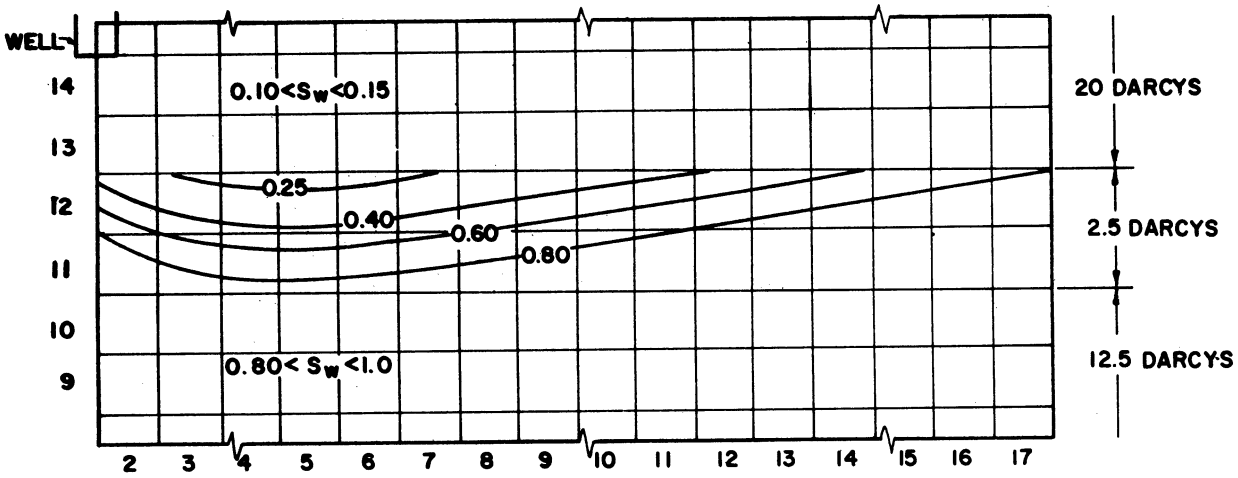

c. At 43.5 Hours

Figure 41. Water Saturation Contours
Laboratory System

production (time steps 4, 6, and 10). Water saturation contours were constructed for the latter two time levels and they appear in Figures 41b and 41c.

Comparison of Tables XXXVII(c) and XXXVIII(a) shows that the two different sets of boundary conditions apparently caused little change in the water saturation distributions. As would be expected, the largest difference between the two distributions accrue near the right boundary.

It must be admitted, however, that the flow rates which resulted over the aquifer boundary in the previous problems were used as a guide in assigning the injection rates listed in Table XXX. This was considered legitimate since the purpose of this investigation was to see how closely laboratory performance could be matched to field performance in view of the unscalable properties. The good experimentalist might be able to deduce rates similar to these from knowledge of the oil production rate and the approximate water saturation distribution existing near the right edge.

Comparison of Figures 41b and 41c for the laboratory system to Figures 40b and 40c for the reservoir prototype shows that the behavior of the two systems was qualitatively similar. However, the water coning exhibited in the reservoir was somewhat more pronounced than in the laboratory. Thus if the purpose of such a model study were to investigate the severity of water coning for a given production rate in the reservoir, erroneous conclusions probably would be drawn. No doubt the differences shown between the two systems would become magnified for longer periods of operation.

The effects introduced by unscalable relative permeability and capillary pressure relationships cannot be separated in a strict sense. However in very rough terms, it appears that the different spacings between the saturation contours were controlled by capillary pressure curves while the different shapes of the contours were controlled by the relative permeability curves.

It should be recognized that the laboratory model was scaled as rigorously as possible within practical limits to the reservoir system. No attempt was made to investigate how closely the scalable properties such as permeability, viscosity, and interfacial tension must satisfy the scaling laws without introducing serious error. In view of the non-linear character of the mathematical description of the flow system, it is felt that no general conclusions may be drawn from the analysis of one system which would assess the importance of scaling deviations in a different system.

Up to this point, intimate knowledge of the reservoir prototype properties has been assumed. This of course seldom, if ever will be the case. Thus a laboratory model scaled as rigorously as practically possible may lead to erroneous conclusions because of faulty reservoir description.

E. Conclusions

The results of this study allow the following conclusions to be drawn. It is assumed that the model and prototype systems are described accurately by the differential equations resulting for the flow of two immiscible, incompressible phases in porous media.

1. Homologous behavior will result in the laboratory model and the reservoir if the model is scaled in accordance with the three dimensional scaling laws.

2. For systems which may be described in two-dimensional cartesian coordinates, the laboratory model may be scaled to the prototype with equal validity through use of the two-dimensional scaling laws.

3. In the particular case studied, distortion of the producing well and in-flow face appears to have little effect on water saturation distributions resulting during operation of the laboratory model.

4. The experimental unattainability of relative permeability and capillary pressure relationships required by the scaling laws must be expected to introduce deviations between prototype and model performance.

5. In the mathematical development of the scaling laws, it was shown that all variant dimensions of the reservoir prototype must be scaled in the same ratio, and that the angle at which the reservoir prototype is inclined from the horizontal cannot be changed by scaling.

IX. GAS CONTAINMENT BY WATER INJECTION

Natural gas is often stored underground in dome-shaped permeable formations capped by a layer of impermeable rock. Such formations are usually water-bearing (aquifers) and may or may not have contained natural gas prior to the initiation of storage operations. If a saddle is present on the surface defined by the dome, the effective capacity of the formation for storage purposes is limited. After a critical volume of gas has been injected into the storage sand, further gas injection will lead to spillage at the saddle point. A plausible means for increasing the storage capacity in a formation of this sort is to provide water injection at the spillpoint. This would be expected to maintain total water saturation in the sand under the saddle retaining a very low (or zero) gas permeability at the spillpoint and causing downward growth of the region of gas saturation on continued gas injection.

From single phase flow theory, an estimation of the minimum required water injection rate can be made for an assumed water velocity distribution below the saddle due to gas injection alone. At this water rate, the resultant horizontal component of the water velocity vector at the spillpoint should be zero. Analysis of this sort yields no information about the most critical aspect of such a system -- the effect of water injection on phase distributions existing in the reservoir. Such information can result only from mathematical treatment of the multiphase flow system. For a gas storage reservoir, mathematical description in terms of two immiscible incompressible phases will usually be possible because of the following considerations.

An oil phase generally is not present. Where an oil phase is present, its volumetric concentration often will be low enough to render the phase immobile. In either case, reservoir analysis may be undertaken on the basis of two immiscible phases because of the low mutual solubilities of natural gas and water.

The normal operation of gas storage reservoirs is cyclic due to seasonal injection and production schedules. Consequently the insitu pressure of both phases is subject to cyclic variation accompanied by compression and expansion of the gas phase primarily and of the water phase to a much smaller extent. For purposes of the spillpoint problem, however, the half cycle over which gas injection occurs is most important as this is the period during which leakage would begin. Since pressure differences within each phase should be small in comparison to the reservoir pressure level over the half cycle, assumption of phase incompressibility would be reasonable.

Numerical solutions of the differential equations describing the flow of two immiscible, incompressible phases have been carried out for a hypothetical reservoir of this type. The analysis has been done within an inclined system of two-dimensional cartesian coordinates. The study is presented in the following sequence:

A. Description of Reservoir System.

B. Computations Performed.

C. Results of Computations.

D. Conclusions.

A. Description of Reservoir System

The hypothetical storage reservoir which served as the basis for this study is illustrated in Figure 42. The rectangular block superposed on the homogeneous sand outlines the portion of the reservoir subjected to analysis. In addition to the x- and y- dimensions indicated, the horizontal thickness was taken to be 100 ft. This region was subdivided into a 16x16 grid network, each grid element measuring 2 ft by 20 ft (and 100 ft thick). The coordinate system was inclined by 2° from the horizontal.

The size of the hypothetical reservoir is recognized as being smaller than that of actual reservoirs normally encountered. However, the qualitative aspects of its behavior would be expected to be representative of an actual reservoir with similar geometry. These dimensions were chosen to allow description within a reasonably small grid network since computational time requirements increase rapidly with increased grid size. Additionally, the dimensions of the individual grid elements is fixed by the magnitude of the phase saturation (or equivalently, the phase potential) gradients which occur. Considering gravitational and capillary effects it follows that sufficient resolution of water saturations would not be expected for a "vertical" grid spacing much greater than 2 ft. Stability considerations fix the length to height ratio of a grid element at about 20 in most instances with more rapid convergence resulting for smaller ratios. (A ratio of 10 was used here.) The 2° tilt is considered to be representative of an actual reservoir.

From a practical standpoint, the geometry of Figure 42 may correspond to several different reservoir formations.

1. The reservoir actually may be dome shaped with a saddle point existing as shown in Figure 42. In this case, the area treated represents a vertical cross section in the direction of the saddle with any desired thickness. For a field of the specified size, rates should be scaled in proportion to the thickness considered.

2. The reservoir may be bounded by fault planes parallel to the indicated vertical cross section. This case would of course correspond directly to the system studied.

3. Alternatively, the reservoir may be of large areal extent produced at equal rates through a series of evenly spaced aligned wells.

In any of the above interpretations, it is felt that the solutions obtained would be approximately correct if the portion of the reservoir treated were localized in the vicinity of the spillpoint with gas injection occurring some distance to the left of the indicated position.

The porous medium considered was a consolidated sand with a permeability of 50 md and a porosity of 15 per cent. The drainage capillary pressure curve expected for this sand is plotted in Figure 43. This curve was based on data for the 175 md, 22.8 per cent (porosity) sand given by Katz (Reference 25, page 59). Relative permeability curves for gas and water in consolidated media used earlier in the scaling study and appearing in Figure 39a were employed.

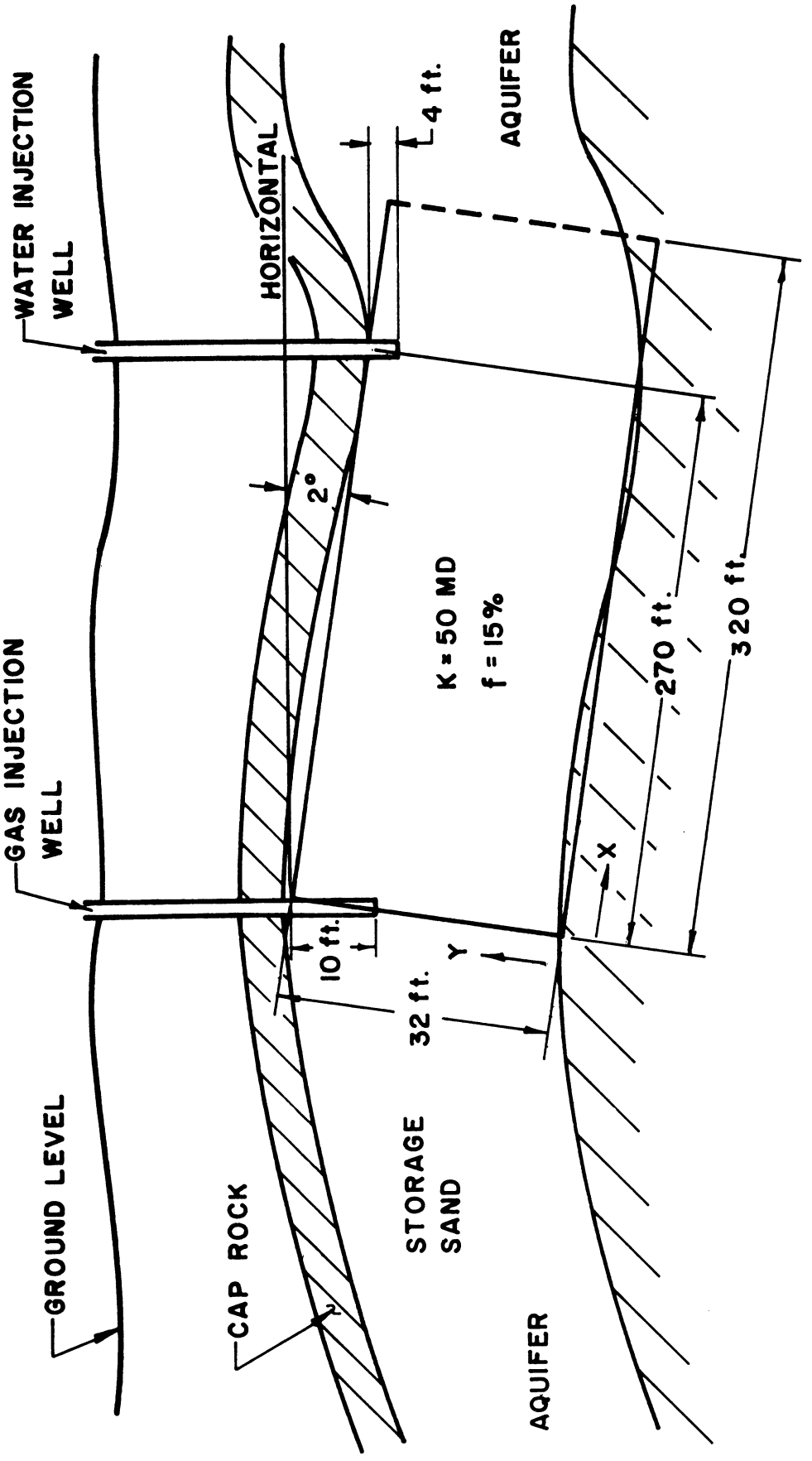

Figure 42. Gas Storage Reservoir

Gas and water injection occurred through wells having a 6 inch diameter and 50 per cent open area. Both wells were partially penetrating as indicated in Figure 42 with the gas well open to the top five layers of grid elements at the left edge and the water well open to the top two layers at the middle of the 13th column of elements. The reservoir pressure level was fixed at 2000 psia and the temperature at 80°F. The gravity of the natural gas was 0.78 and its compressibility factor was taken to be 0.625. Gas was injected at a constant rate of 50 MSCF/day into the sand initially at capillary-gravitational equilibrium with 1.126 MMSCF of gas in place. Operation was simulated for two water injection rates of 25 Bbl/day and 100 Bbl/day with water injection accompanying gas injection over the entire duration of the problems.

B. Computations Performed

Solutions were carried out for the five different modes of operation which follow. Starting from the equilibrium distribution resulting with 1.126 MMSCF of gas in place, gas was injected at a constant rate of 50 MSCF/day accompanied by:

1. No water injection.
2. 25 Bbl/day water injection.
3. 100 Bbl/day water injection.

Solutions for these cases all were carried out past 20 days. Using the phase potential (and therefore saturation) distributions resulting after 14.38 days (34th time step) for the case with 25 Bbl/day water injection, gas injection was ceased and solutions proceeded with:

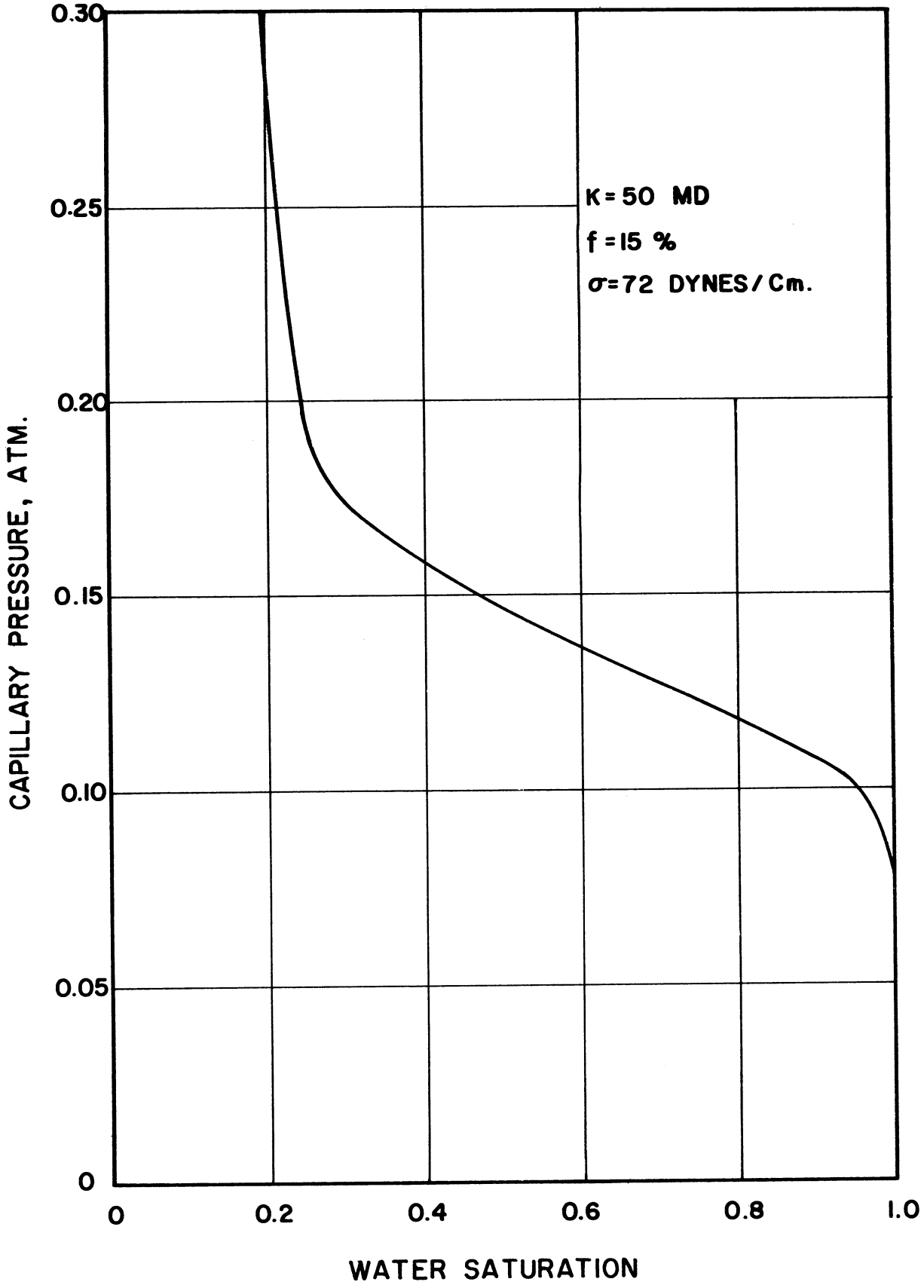

Figure 43. Capillary Pressure Curve
Gas Storage Reservoir

[After Katz(25)]

4. 25 Bbl/day water injection.

5. No further water injection.

Solutions for the latter two cases were advanced over the additional periods of 15 and 20 days.

C. Results of Computations

Phase saturation distributions were considered to be the most interesting and significant aspect of the reservoir behavoir as simulated for the various modes of operation. These results are presented as two-dimensional contour plots of water saturation for several time levels in each mode of operation by Figures 44 - 50. Row and column indices have been included to fix the position of the reservoir section shown. As before, the element indexed 2,2, is situated in the lower left corner of the grid. Column and row indices of 17 are associated with the rightmost column and topmost row of the 16x16 grid. The position of the gas injection well has been shown with its actual penetration into the sand indicated. The spillpoint is taken to be the element in the upper row of column index 14. Any gas existing to the right of column 14 is considered lost past the spillpoint. The water injection well at the spillpoint has been denoted by an arrow. In keeping with the dimensions appearing in Figure 42, the well penetration was through the top two rows of elements.

Water potential distributions are significant also, but to a smaller extent in the interpretation of reservoir behavior. Computed water potential distributions appear in tabular form in Appendix III for several time levels in the various modes of operation. Although potential

contours were constructed from these arrays, they have not been included since the tabulated forms show the distributions just as clearly. In interpreting the tables, the indicated x-index corresponds to column and y-index to row in the grid system. It will be observed that the water potential along the aquifer boundary was set to 5 atm.

The numerical solutions for the first three cases, all of which involved gas injection, showed excellent cumulative water balances with a maximum discrepancy of 0.01 per cent. For the last two cases, cumulative water balance errors of about 2.5 per cent resulted. These errors, though far greater than any encountered in the other phase of this work, were not considered sufficient to invalidate the results. Apparently they were due to the sudden cessation of gas injection, and better material balances probably would have resulted if the rate had been reduced to zero gradually over several time steps.

For each mode of operation, a sequence of unequal time steps was used. In view of the physical instability associated with drainage displacements of this type, it was always not possible to predetermine a sequence of time steps which would lead to convergent solution. It will be recalled that the numerical simulation of the drainage displacement performed in the laboratory presented the same type of behavior. Consequently it was convenient to introduce an internal control in the computer program which would reduce the length of a time step if the desired rate of convergence was not resulting in the updating of the R distribution. This control is discussed in Appendix II. As a result, the computed water saturation and potential distributions were printed

out at rather odd times in the displacements. To give an indication of the lengths of time steps used, time step numbers corresponding to the distributions presented in Figures 45-50 have been listed in Table XXXI.

TABLE XXXI

TIME STEP SUMMARY

Mode of Operation	Time	Figure No.	Time Step
1	10.00 days	45	23
1	17.22	46a	42
1	21.72	46b	51
2	10.00	45	20
2	14.38	47a	34
2	16.09	47b	43
2	20.59	47c	52
3	10.00	45	24
3	14.23	48a	45
3	16.06	48b	62
3	19.19	48c	87
3	20.30	48d	121
4	4.00	49a	9
4	15.36	49b	17
5	3.85	50a	9
5	19.85	50b	17

For the first three modes of operation, the initial water saturation distribution is plotted in Figure 44. Since the distribution is at a condition of capillary-gravitational equilibrium, contours of constant water saturation are horizontal lines. The operating distributions are presented in Figures 45 through 48. At the 10 day mark a slightly different distribution developed for each water injection rate, but the differences were too small to be seen on the contour plot. Thus,

the distributions at 10 days for all three modes are described by Figure 45. Distributions for the final two modes of operation appear in Figures 49 and 50 with the "initial" distribution shown by Figure 47a.

It will be noticed that all saturation contours show a consistently wavy appearance. This behavior appears to demonstrate the unstable nature of these drainage displacements. It should be contrasted with the behavior resulting from the field scale imbibition displacement simulated in the scaling law evaluation. There water saturation contours were always smooth, and further, much larger time steps gave satisfactory convergence properties.

The progress of the water saturation distributions resulting from gas injection only is seen starting with Figure 44, and moving according to Figures 45, 46a, and 46b. After the first 10 days of injection, most of the thickening of the gas saturation zone near the gas well had occurred. During the next 10 days little movement of the 25 per cent water saturation contour (75 per cent gas) was in evidence. The contours of higher water saturation (lower gas) moved in an orderly fashion extending further and further down the inclined bedding plane. After the first 10 day period, gas leakage past the spillpoint began, and by the most advanced time (21.72 days), the leakage rate was appreciable. The leakage rate can be seen from Figures 51 and 52 where the net gas in place to the left of the spillpoint (columns 2 through 14) and the total gas lost past the spillpoint have been plotted. Net gas in place is defined as the total gas volume to the left of the spillpoint minus the initial gas volume in that region. The volume of gas lost is the differ-

ence between the total volume injected and the net volume in place at a given time. The indicated points were obtained by summing all of the four place water saturations computed for the appropriate elements, and multiplying by the pore volume of each element.

For the case of gas injection accompanied by 25 Bbl/day water injection the movement of the water saturation contours follows the sequence of Figures 44, 45, 47a, 47b, and 47c. The first departure from the behavior exhibited under conditions of no water injection arose at about the 11 day mark, and by 14.38 days, this rate of water injection showed a tendency to pinch off gas leakage at the spillpoint. Although some gas leakage did occur by this time, Figures 51 and 52 show the rate of leakage to have been reduced. As injection of both phases continued, saturation distributions in the region between the gas well and column 11 (60 ft left of the spillpoint) changed very little although some thickening of the gas saturation zone did occur. Just to the left of the spillpoint however, the gas phase accumulated causing a pronounced downward growth of the gas containing zone. By the 16.09 day mark, the 95 per cent water saturation (5 per cent gas) contour nearly had reached its maximum depth of penetration and the effectiveness of the water barrier diminished. At the most advanced time of solution (20.59 days), Figures 51 and 52 show the leakage rate to be only slighter less than for no water injection. (These curves represent volumes, so their slopes correspond to rates.)

At the highest water rate (100 Bbl/day), the phase distribution behavior follows the sequence of Figures 44, 45, 48a through 48d. Comparison

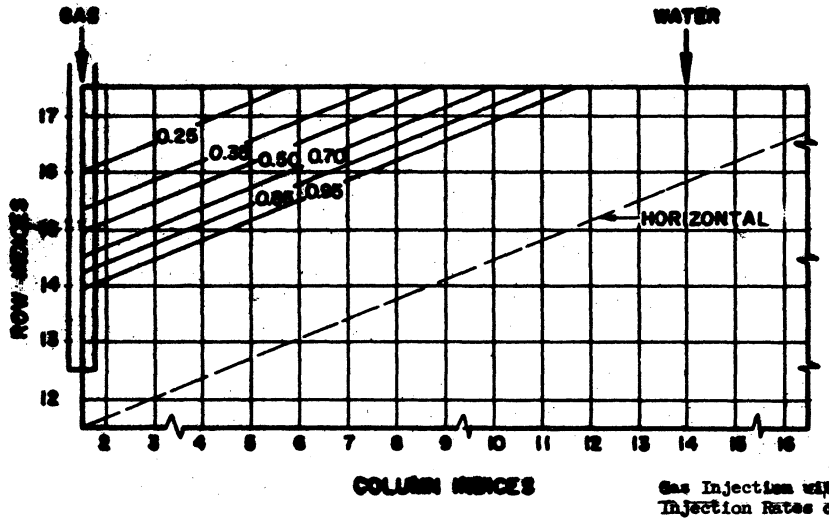

Figure 44. Water Saturation Contours
Prior to Gas Injection

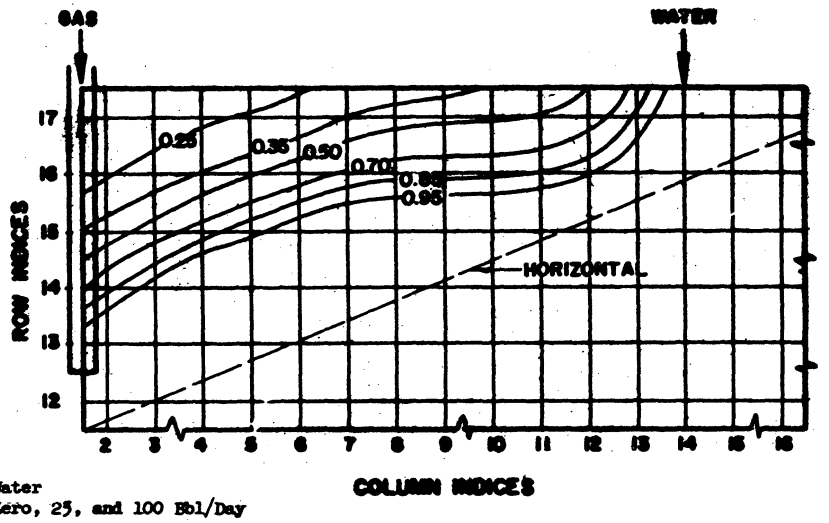

Figure 45. Water Saturation Contours
After 10.00 Days Gas Injection

Gas Injection with Water
Injection Rates of Zero, 25, and 100 Bbl/Day

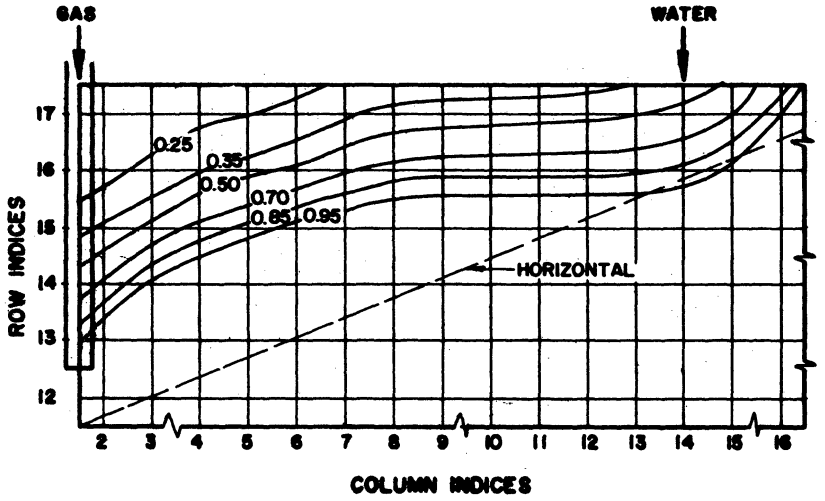

a. At 17.22 Days

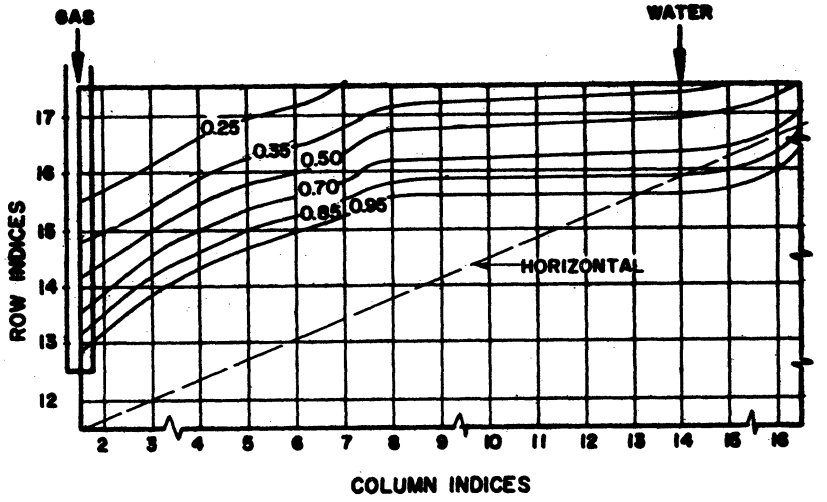

b. At 21.72 Days

Figure 46. Water Saturation Contours
Gas Injection with No Water Injection

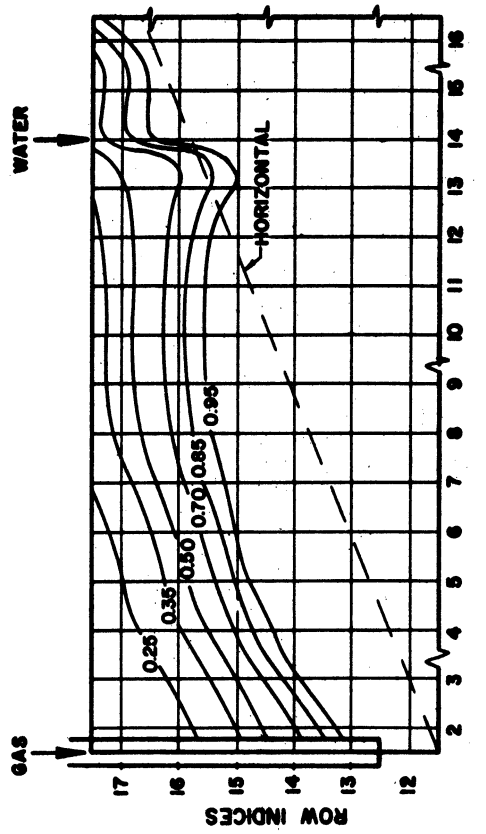

b. At 16.09 Days

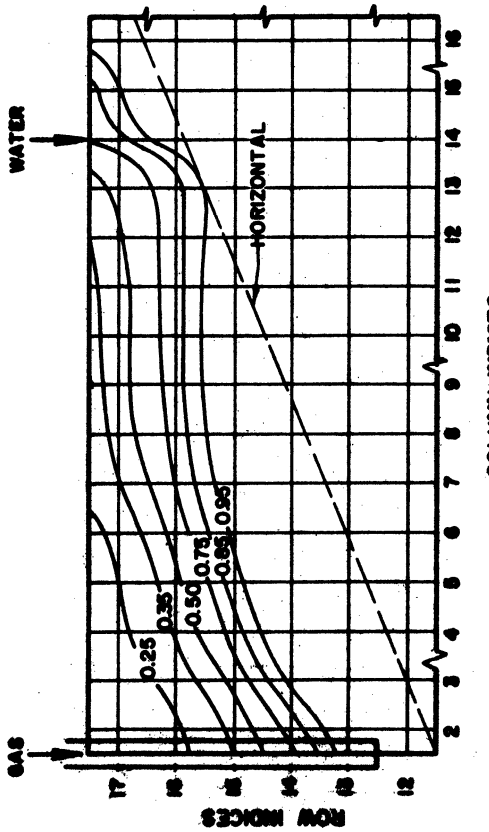

a. At 14.38 Days

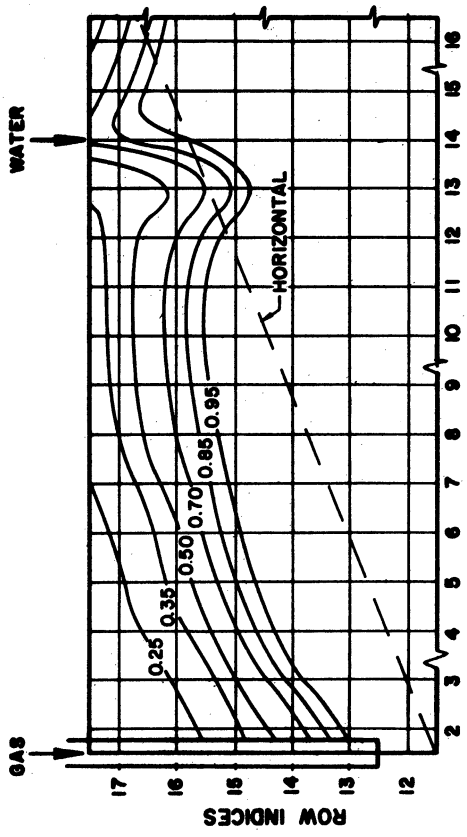

c. At 20.59 Days

Figure 47. Water Saturation Contours
Gas Injection with 25 Bbl/Day Water Injection

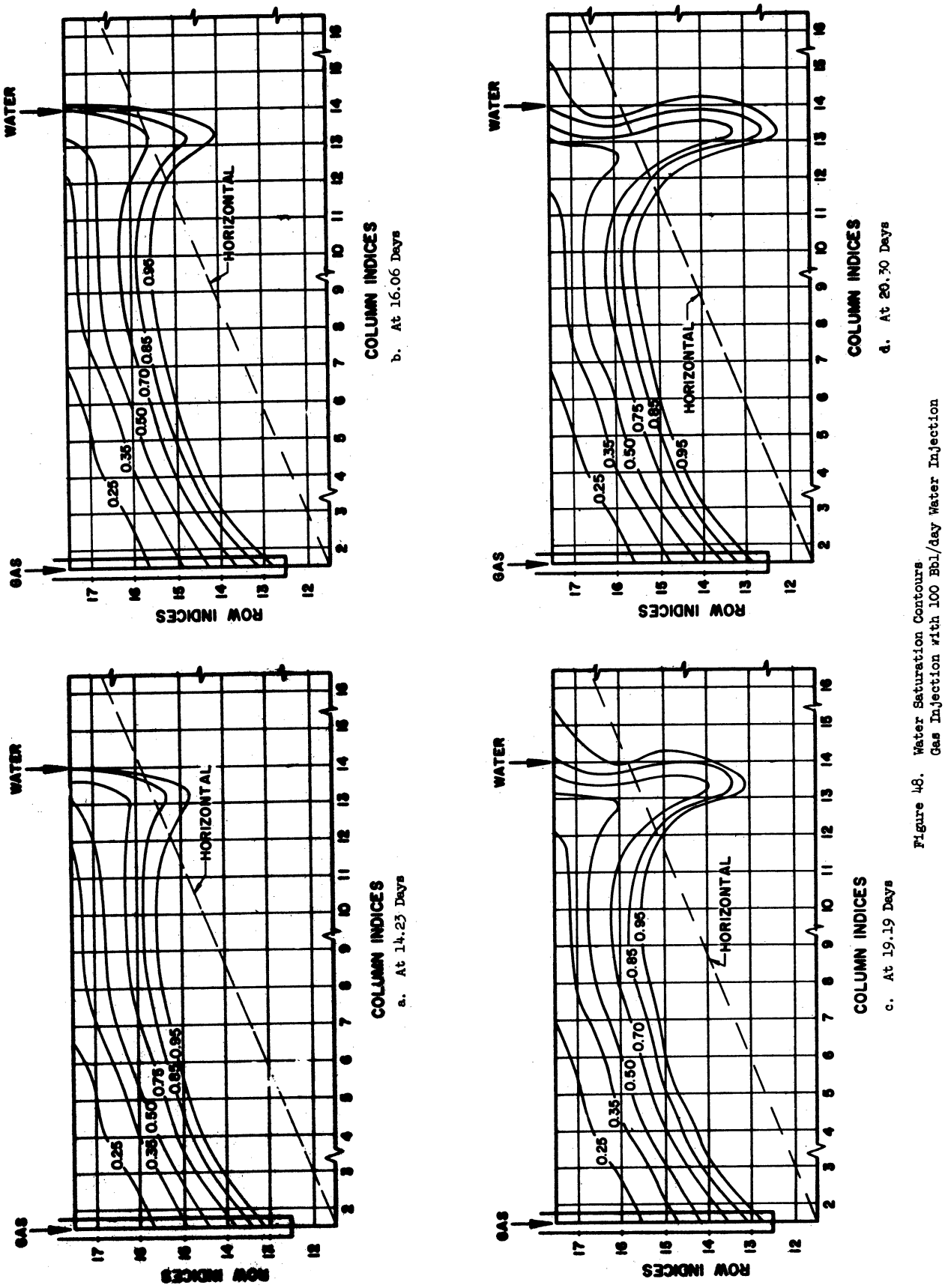

a. At 14.23 Days

b. At 16.06 Days

c. At 19.19 Days

d. At 20.30 Days

Figure 48. Water Saturation Contours
Gas Injection with 100 Bbl/day Water Injection

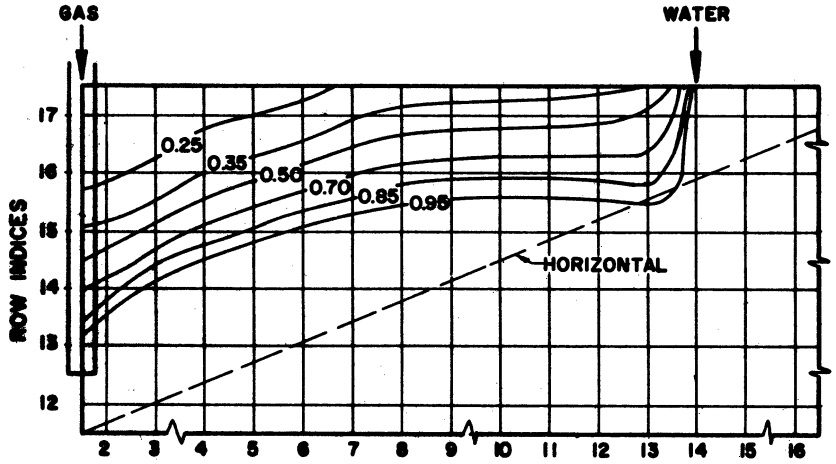

a. At 4.00 Days

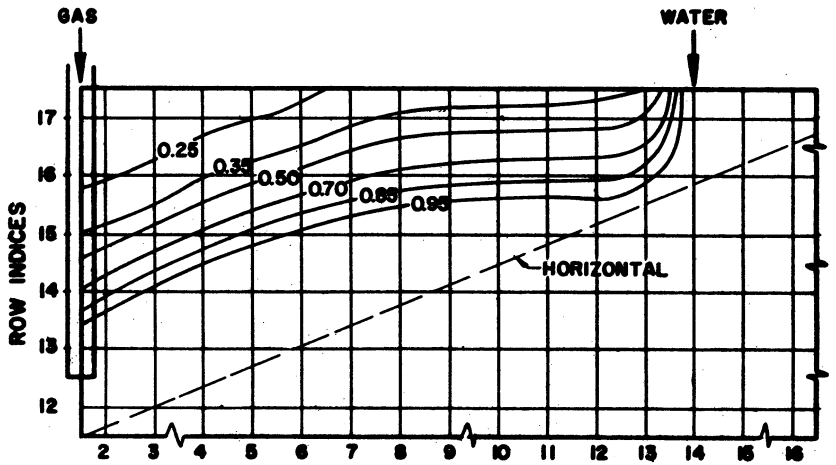

b. At 15.36 Days

Figure 49. Water Saturation Contours
No Gas Injection, 25 Bbl/Day Water Injection

Initial Distribution - 14.38 Days with Gas Injection and 25 Bbl/Day Water Injection (See Figure 47a)

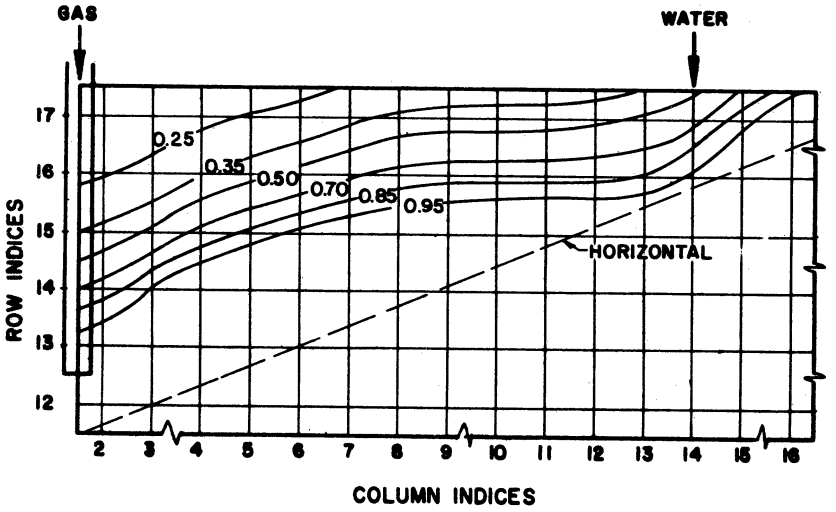

a. At 3.85 Days

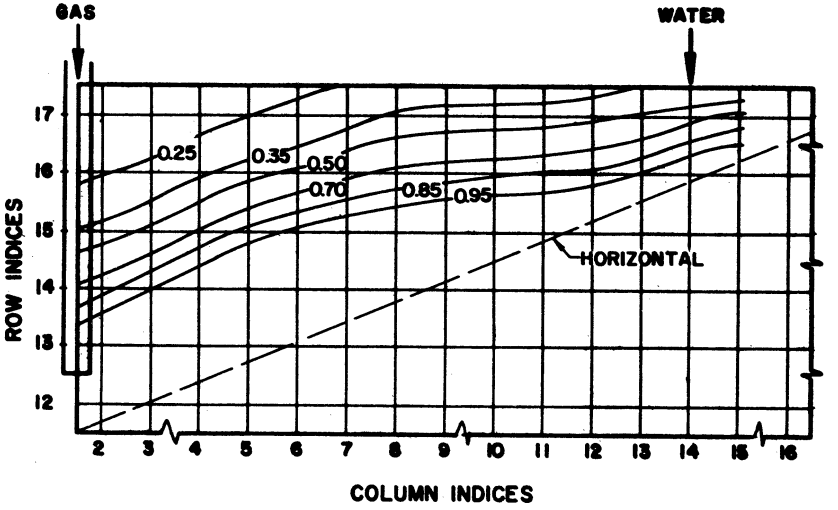

b. At 19.85 Days

Figure 50. Water Saturation Contours
No Gas Injection, No Water Injection

of Figures 48a and 47a which apply at nearly the same times shows this rate of injection to provide a much more effective water seal. Once again, very little effect was noticeable between the gas well and column 11 by the 14.23 day mark although as injection continued the zone of gas saturation did appear to thicken. The most striking change however was exhibited in the vicinity of the spillpoint. Here the gas accumulation was much greater and the gas zone fingered deeply into the storage sand. By the most advanced time of solution (20.30 days, Figure 48d) the 70, 85, and 95 per cent water saturation contours reached about 6-1/2 feet deeper into the sand near the spillpoint than at column 10 (80 feet left of the spillpoint). Although some gas leakage was apparent from about 18 days on, the seal provided by this rate of water injection remained quite effective.

In the fourth mode of operation, gas injection was discontinued at the 14.38 day mark in the second mode and water injection remained at 25 Bbl/day. The resulting phase distributions follow the sequence Figures 47a, 49a, and 49b. Four days after gas injection was stopped, the water injection apparently had swept the gas existing to the right of the spillpoint out into the aquifer. The remaining gas in the reservoir was confined to the region between the gas well and the spillpoint. The distribution resulting 15.36 days after cessation of gas injection (Figure 49b) shows that the distribution had changed very little during the intervening 11.36 day period except in the immediate vicinity of the gas well where the longitudinal saturation gradients became somewhat more gentle.

For the fifth mode of operation in which water injection was also discontinued, the distributions were found to follow the sequence of Figures 47a, 50a, and 50b. Immediately, the pinching tendency caused earlier by the water injection began to wash out. In this case, redistribution of the phases proceeded toward the equilibrium distribution composed of horizontal contour lines as would be expected.

The gross effect of continued water injection is shown in Figure 53. Here the gas content of the pore volume to the left of the spillpoint for no water injection has been subtracted from that for continued injection. For these particular reservoir conditions, continued water injection is seen to result in a saving of about 22 MSCF of gas.

Several computed water potential distributions are reproduced in Tables XXXIX through XLII. Scrutiny of these distributions reveals the following.

1. In all cases, the water potential gradients existing to the left of the spillpoint decreased as the gas saturation increased in this zone.

2. When water injection was present, the water potential gradients existing left of the spillpoint were essentially unaffected. The longitudinal gradients right of the spillpoint increased in proportion to the water injection rate. Also the "vertical" gradients increased immediately below the spillpoint in proportion to injection rate. The greatest effects were present for the top two rows of grid elements as this was the extent of penetration of the water injection well.

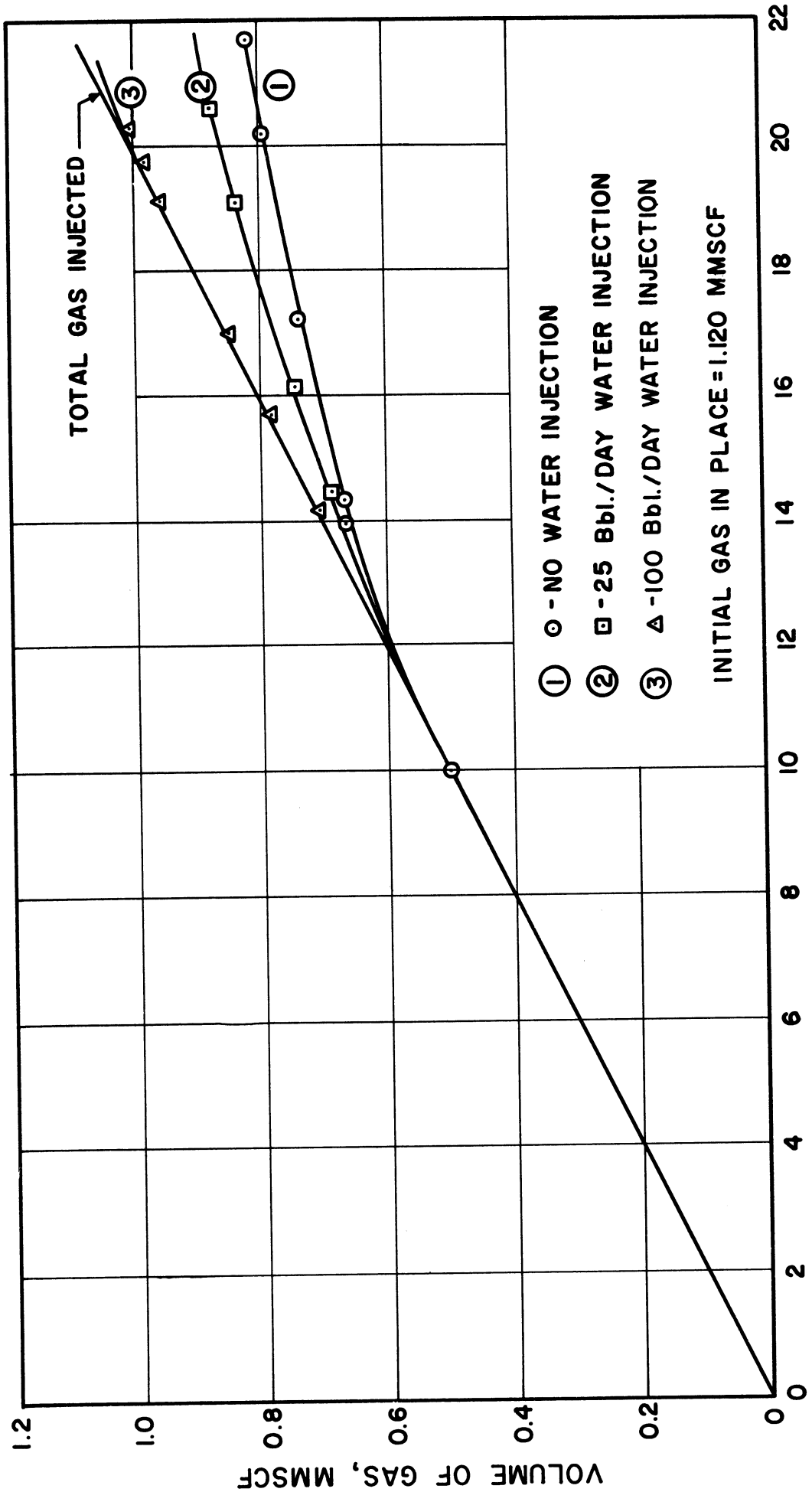

Figure 51. Net Gas In Place

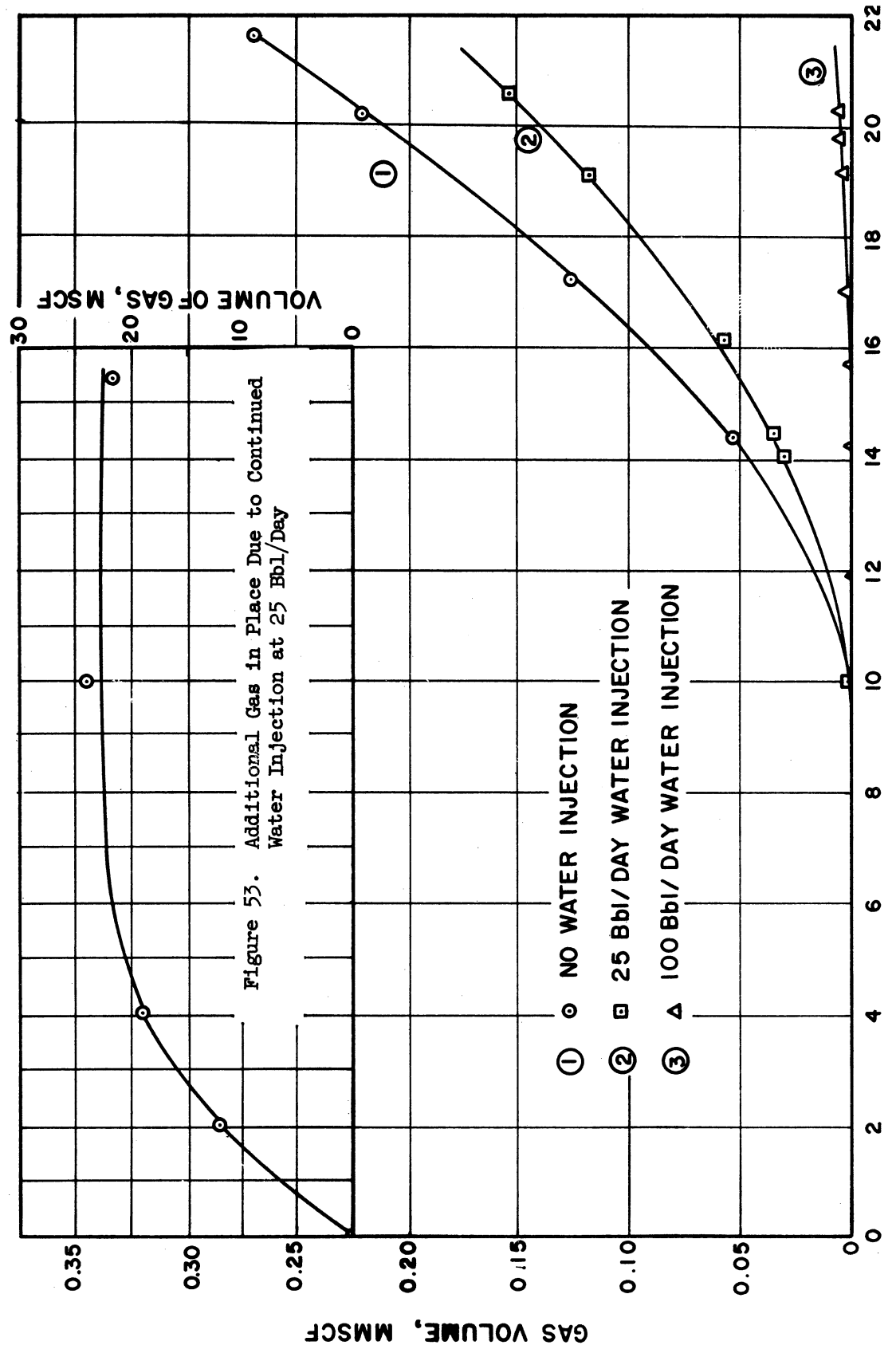

Figure 52. Gas Lost Past Spillpoint

Figure 53. Additional Gas in Place Due to Continued Water Injection at 25 Bbl/Day

3. Only for the higher rate of water injection (100 Bbl/day) did the sign of the gradient reverse to the left of the spillpoint (between elements 13, 17, and 14, 17). The reversed gradient was present throughout the solution and appeared not to change in magnitude.

4. After gas injection was halted, the water potential distribution to the left of the spillpoint approached a constant potential level. The presence of a constant water potential in all elements would correspond to no water movement. For the case in which water injection was continued, the potential gradient again was reversed to the left of the spillpoint.

5. Whenever the gradient was reversed to the left of the spillpoint, reversal occurred only at the upper levels of the sand. Thus, all of the injected water eventually flowed into the aquifer across the right boundary, but a fraction did flow away from the aquifer at the upper levels. After a short distance, the stream lines for this fraction curved downward and to the right intersecting the aquifer boundary at the lower levels of the sand.

Another interesting result of the computations is shown in Figure 54. This is a plot of the gas well-bore potential referred to the 5 atm potential level at the aquifer boundary. Thus it is a measure of the pressure drop which was found to exist in the gas phase during the first three modes of operation. For all three modes, the gas phase pressure drop is seen to decrease as the relative permeability to the gas phase increased with growth of the zone of appreciable gas saturation. The hump in the curve for the second mode of operation (25 Bbl/day water

injection) occurred at the time when the seal provided by water injection was broken. Since the water seal was never broken effectively for the high rate of water injection over the period studied, such a hump did not appear.

The predicted tendency for the pressure drop in the gas phase to rise and then fall off again as the water seal is broken might be of value in field tests investigating gas containment by water injection. Interpretation of field data in this light must recognize that the injection pressure is the sum of the pressure drop in the gas phase and the gas pressure at the aquifer boundary. The latter term should be essentially equivalent to the water pressure at the boundary which would follow from calculations based on water movement within the aquifer. (Ideally, at the aquifer boundary, water and gas phase pressures differ by the "displacement pressure", or the capillary pressure at 100 per cent water saturation.)

D. Conclusions

The following conclusions have been drawn from the behavior of the reservoir as simulated under the various modes of operation studied.

1. The use of water injection near a reservoir spillpoint appears to increase the gas storage capacity of the reservoir.

2. To provide an effective water seal at a spillpoint, the water injection rate must be high enough to cause some water to flow toward the gas injection well at the upper levels of the storage sand below the spillpoint.

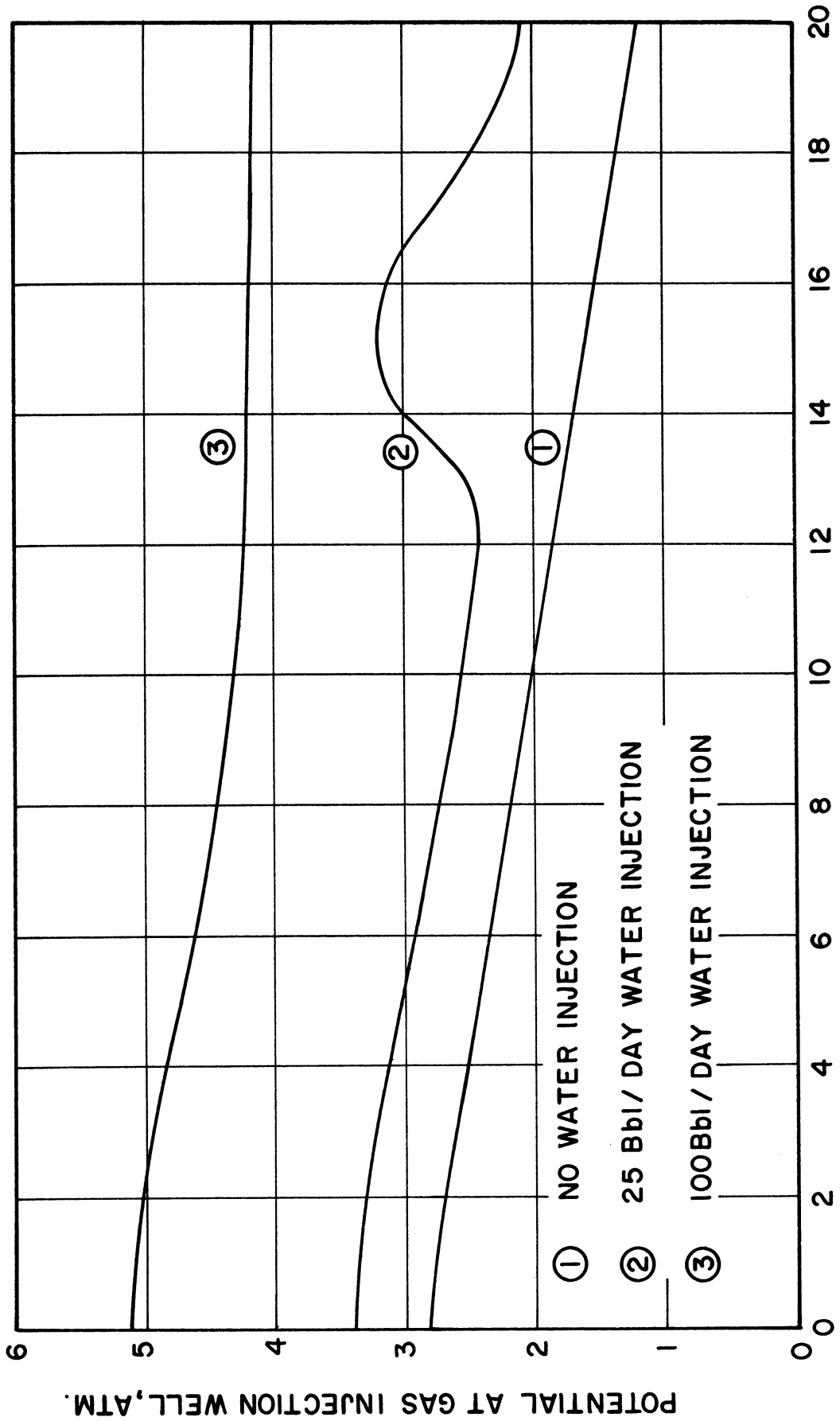

Figure 54. Potential at Gas Injection Well

3. The increase in capacity realized through water injection would be expected to be greater for higher water injection rates.

4. When gas is injected into a reservoir formation, a sheet of appreciable gas saturation advances into the sand directly below the cap rock. If the cap rock is inclined downward from the horizontal, the sheet will advance in spite of gravitational forces which oppose its advance. Where the permeability and porosity are in the range of those studied here (50 md, 15 per cent), the gas saturation in this sheet should vary from about 70 to 5 per cent over the top four feet of the sand. For other permeabilities and porosities the thickness of the sheet would be expected to vary as the square root of the ratio of porosity to permeability.

5. When a sufficient rate of water injection is employed, the thickness of the gas saturation zone between the gas injection well and the spillpoint should increase. The gas phase would be expected to accumulate in the reservoir sand near the water injection well, with contours of gas saturation fingering deeply into the sand.

6. When a water injection rate is insufficient to cause a flow reversal beneath the spillpoint, the volume of gas lost should be less than would be lost if no water injection were provided.

7. If a zone of high gas saturation has been developed in the presence of a water seal, the seal should be maintained after gas injection has ceased. If the seal is not maintained, gas leakage at the spillpoint would be expected. Although not investigated here, the water rate necessary to provide the seal after gas injection has halted might be lower than required in the presence of gas injection.

8. The pressure drop between the gas injection well and the "aquifer boundary" appears to decrease as the zone of gas saturation grows. If an insufficient water seal is broken, the pressure drop in the gas phase would be expected to increase as the seal is being broken and then to drop back to its former level as the rate of gas leakage approaches the injection rate.

The results of this study also should provide some insight into the allied problem of gas storage in a horizontal aquifer. In such a reservoir the region of gas saturation would be localized about the gas injection well (or wells) by providing water injection through a series of wells surrounding the gas well. Numerical solutions for this type of system were attempted employing the techniques outlined in the Mathematical Analysis section for two-dimensional domal coordinates. In order to treat the problem in this axisymmetric coordinate system, it was necessary to replace the finite number of water injection wells by a circular line source about a centrally located gas injection well.

Unfortunately no significant results were obtained because of convergence problems which arose during the solutions. Possible causes for the difficulties are discussed in Appendix II. Since a considerable amount of computing time had been required for the other phases of this research (about 70 hours of IBM 709 time), further work on the horizontal aquifer problem did not seem justifiable. Specifications of the system considered and computed water saturation and water potential distributions have been included in Tables XLIII for the sake of completeness.

X. RECOMMENDATIONS FOR FUTURE WORK

The experimental work done in this research was limited to a gas-water system in a particular two-dimensional geometry. Likewise, the numerical work was confined to two-dimensional treatment of the flow of two immiscible, incompressible phases in porous media. These areas will be recognized as only small segments of the general topic of multi-phase flow in porous media. Except for the area of completely miscible fluid flow, other segments of the general topic remain essentially untouched. The other segments encompass experimental and numerical work on compressible and partially miscible two- and three-phase systems in two-dimensions and extension of all areas to three-dimensional geometries. The recommendations, however, have been confined to the areas investigated here.

1. The technique developed for measurement of local water saturations was highly satisfactory. Its advantages over other techniques lie mainly in its use of external sensing elements, its ease of operation, and its relatively low cost. It is felt that the applicability of the method can be extended through several modifications which were discussed in the Experimental Method section. The object of these modifications would be to reduce the time required to effectively determine a two-dimensional distribution of phase saturation. Further development of the technique seems to be warranted, and it is anticipated that this might be done in connection with an experimental investigation such as this one which would study higher rate two-phase displacements. Investigation of its applicability to oil-water systems is also suggested.

2. The basic purpose of this research was to determine how closely controlled two-phase displacements could be simulated by numerical solutions of the differential equations taken to describe the systems. It has been seen that good agreement resulted in the cases studied However, in all of these displacements, capillary and gravitational effects tended to override the viscous effects. Therefore additional investigations of this type are called for in which viscous effects play a greater role. Particularly in gas-water systems, imbibition displacements would be recommended because of their relative insensitivity to the slight inhomogeneities bound to be present in even the most carefully constructed laboratory model. Suggested displacements to be performed in the same or similar laboratory porous medium are:

a. Higher rate gas-water displacements retaining pack orientation in a vertical plane.

b. A series of gas-water or oil-water displacements with pack orientation varied from vertical to horizontal in in several steps. Because of the thinness of the pack, the two-dimensional nature of the displacement would be preserved, but gravitational effects would diminish as horizontal orientation was approached.

3. Fingering associated with unstable displacements was not studied on a quantitative basis although it occurred in the drainage displacement. The tendency toward instability in gas-water drainage displacements also appeared to be shown in the numerical solutions. It is felt that some very interesting numerical and experimental work could be done to see how well a deliberately triggered finger can be described by

these numerical techniques. The study envisioned would employ a similar two-dimensional glass bead pack with injection of the less viscous phase (oil or gas) occurring at the mid point of one edge. The location of water production would not be considered critical, but provision of a number of wells along the opposite edge might prove most satisfactory. Fingering would be initiated by a rectangular zone of high permeability situated adjacent to and centered on the injection well. Both vertical and horizontal pack orientation might be investigated. Displacements at several injection rates should be performed with measurements of phase saturation distribution being made.

4. Many field problems can be described more accurately in an axisymmetric system of two-dimensional radial coordinates than in two-dimensional cartesian coordinates. For this reason, the numerical technique for solution of the differential equations under consideration here was developed within a general system of domal coordinates. A discussion of the convergence problems encountered in most applications of this coordinate system has been included in Appendix II. Basically, the difficulties appeared to derive from the method of selection employed in setting the values of the iteration parameters required in the solution of the P equation. It is felt that some further work on this phase of the problem will result in an extremely useful numerical method of reservoir simulation.

5. The field applications of the numerical techniques represent only a sample of the type of problems that can be treated in two-dimensional cartesian coordinates. In these applications, only vertical

orientation of the grid system has been demonstrated. Many multiple-well reservoir problems can be analyzed more conveniently within a horizontal or inclined orientation of the grid. The inclined orientation considered here refers to an inclination of the coordinate plane rather than an inclination of the axes, as was employed in several cases treated in this research. Although horizontal or inclined orientation assumes that no gradients exist in the third or invariant dimension, in oil-water systems with a small density difference where the pay thickness is not great, this condition is approximated. Further, no investigations have been made of the effects on recovery controlled by such reservoir variables as production rate and well penetration. Also the effects of gross reservoir inhomogeneities were not studied. Thus it is seen that many additional problems of practical and academic interest could be considered. No specific problems are recommended, however, as the reader's background and interests should provide many interesting ones.

BIBLIOGRAPHY

1. Archie, G., Trans. AIME, 146, (1942), 54.

2. Blair, P.M., Douglas, Jim Jr., and Wagner, R.J., Trans. AIME, 213, (1958), 96.

3. Botset, H.G., Trans. AIME, 136, (1940), 91.

4. Boyer, R.L., Morgan, F., and Muskat, M., Trans.AIME, 170, (1947), 15.

5. Briggs, J.E., PH.D. Dissertation (yet to be completed), The University of Michigan, Ann Arbor, Michigan.

6. Buckley, S.E., and Leverett, M.C., Trans. AIME, 142, (1942), 107.

7. Calhoun, J.C., Oil and Gas J., 50, No. 21, (1951), 117.

8. Carpenter, C.W., Jr., Jersey Production Research Co., Tulsa, Okla. (Private Communication).

9. Cloud, W.F., Trans. AIME, 86, (1930), 337.

10. Coats, K.H., Selected Topics in Numerical Analysis, (unpublished notes), University of Michigan, Ann Arbor, Michigan.

11. Coomber, S.E., and Tiratsoo, E.N., Inst. of Petr., 36, (1950), 543.

12. Darcy, Henry, Les Fontaines Publiques de la Ville de Dijon, Victor Dalmont, Paris (1856).

13. Denekas, M.O., Mattax, C.C., and Davis, G.T., Trans. AIME, 216, (1959), 330.

14. Deutsch, E.R., Nature, 185, (March 5, 1960), 675.

15. Douglas, Jim Jr., J. Soc. Ind. Appl. Math., 4, (1958), 20.

16. Douglas, Jim Jr., Peaceman, D.W., and Rachford, H.H., Trans.AIME, 216, (1959), 297.

17. Fayers, F.J., and Sheldon, J.W., Trans. AIME, 216, (1959), 147.

18. Gorring, R.L., Ph.D. Dissertation, The University of Michigan, Ann Arbor, Michigan, 1962.

19. Heller, J.P., Rev. Sci. Instr., 30, (1959), 1056.

20. Hildebrand, F.B., Introduction to Numerical Analysis, McGraw-Hill Co., New York, 1956.

21. Hovanessian, S.A., and Fayers, F.J., Soc. Pet. Engrs. J., 1, (1961),32.

22. Hubbert, M.K., Trans. AIME, 207, (1956), 222.

23. Josendal, V.A., Sandiford, B.V., and Wilson, J.W., Trans. AIME, 195, (1952), 65.

24. Kaplan, W., Advanced Calculus, Addison-Wesley Co., Cambridge, Mass.

25. Katz, D.L., et al., Handbook of Natural Gas Engineering, McGraw-Hill Co., New York, 1959.

26. Katz, D.L., and Tek, M.R., (Private Communication).

27. Laird, A.D.K., and Putnam, J.A., Trans. AIME, 192, (1951), 275.

28. Leverett, M.C., Trans. AIME, 142, (1941), 152.

29. Leverett, M.C., and Lewis, W.B., Trans. AIME, 142, (1941), 107.

30. Leverett, M.C., Lewis, W.B., and True, M.E., Petroleum Technology, 5, (Jan. 1942), 1.

31. Levine, J., Trans. AIME, 201, (1954), 21.

32. McEwen, C.R., Trans. AIME, 216, (1957), 412.

33. Melrose, J.C., Am. Inst. Chem. Engrs., Preprint No. 63, Kansas City, May 17-20, 1959.

34. Muskat, M., Physical Principles of Oil Production, McGraw-Hill Co., New York, 1949.

35. Muskat, M., and Meres, M.W., Physics, 7, (1936), 346.

36. Naar, J., and Wygal, R.J., Soc. Pet. Engrs. J., 1, No.4, (Dec. 1961), 254.

37. Naar, J., Wygal, R.J., and Henderson, J.H., Soc. Pet. Engrs. J., 2, No. 1, (March, 1962), 13.

38. Osaba, J.S., Richardson, J.G., Kerver, J.K., Hafford, J.A., and Blair, P.M., Trans. AIME, 192, (1951), 47.

39. Peaceman, D.W., and Rachford, H.H., Jr., J. Soc. Ind. Appl. Math., 3,No.1, (March, 1955), 28.

40. Peaceman, D.W., and Rachford, H.H., Paper presented SPE of AIME Meeting, Denver, Colo., Oct. 2-5, 1960.

41. Pirson, S.J., Oil Reservoir Engineering, McGraw-Hill Co., New York, 1958.

42. Rapoport, L.A., Trans. AIME, 204, (1955), 143.

43. Rapoport, L.A., Carpenter, C.W., Jr., and Leas, W.J., Trans. AIME, 213, (1958), 113.

44. Rapoport, L.A., and Leas, W.J., Trans. AIME, 198, (1953), 139.

45. Richardson, J.G., and Perkins, F.M., Jr., Trans. AIME, 210, (1957), 114.

46. Richtmeyer, R.D., Difference Methods for Initial Value Problems, Interscience Publishers Inc., New York, 1957.

47. Scheidegger, A.E., Physics of Flow Through Porous Media, McMillan Co., 1957.

48. Sheffield, M., Jersey Production Research Co., Tulsa, Okla., (Private Communication).

49. Sheldon, J.W., Zondek, B., and Cardwell, W.T., Jr., Trans. AIME, 216, (1959), 290.

50. Terwilliger, P.L., Wilsey, L.E., Hall, H.N., Bridges, P.M., and Morse, R.A., Trans. AIME, 192, (1951), 285.

51. Terwilliger, P.L., and Yuster, S.T., Oil Weekly, 126, No.1, (1947), 54.

52. Uren, L.C., and Bradshaw, E.J., Trans. AIME, 98, (1932), 438.

53. Van Everdingen, A.F., and Hurst, W., Trans. AIME, 186, (1949), 305.

54. Wagner, O.R., and Leach, R.O., Trans. AIME, 216, (1959), 65.

55. Welge, H.J., Trans. AIME, 192, (1952), 91.

56. Welge, H.J., Johnson, E.F., Ewing, S.P., Jr., and Brinkman, F.H., J. Pet. Tech., 13, No. 8, (Aug. 1961), 787.

57. West, W.J., Garvin, W.W., and Sheldon, J.W., Trans. AIME, 201, (1954), 217.

58. Whalen, J., Trans. AIME, 198, (1954), 111.

59. Wyckoff, R.D., and Botset, H.G., Physics, 7, (1936), 325.

APPENDICES

APPENDIX I

ITERATION PARAMETERS - ELLIPTIC EQUATION BY STABILITY ANALYSIS

The stability of the alternating direction methods has been analyzed by Peaceman and Rachford[39] for the two-dimensional diffusion equation and Laplace's equation. For the former equation their analysis showed the alternating direction method of solution to be unconditionally stable (no limitations on Δx , Δy , Δt). For the elliptic case of the latter equation, solution is reached by treating the equation as parabolic and iterating to the steady state. This concept has been discussed in Mathematical Analysis. Thus it is apparent that the same stability must exist for solution of Laplace's equation as for the diffusion equation. However, stability analysis also indicates the optimum choice of the artificial time step sequence to effect the most rapid convergence of the elliptic equation.

The partial differential equations treated by Peaceman and Rachford were linear with coefficients of unity. In the numerical solution of the P equations, the difference equations are linearized by the use of coefficients evaluated at the end of the previous time step (n). These coefficients vary from element to element within the grid system. Consequently some further complications arise in the stability analysis, but the final result is similar in form to the simpler case of Laplace's equation.

The method of analysis follows that presented by Coats[10]. The P equation in each coordinate system has been reduced to Equation

(75) which restated is:

$$a_{i+1,j}\,P_{i+1,j} + b_{i,j}\,P_{i,j} + c_{i-1,j}\,P_{i-1,j} + d_{i,j+1}\,P_{i,j+1} + e_{i,j}P_{i,j} + g_{i,j-1}\,P_{i,j+1} - G_{i,j} = 0 \qquad \text{(I-1)}$$

Time subscripts of $n + 1$ are associated with all P terms, while subscripts of n are associated with the coefficients and G. The coefficients and constant term G are defined by Equations (73a) - (73f), (74a) - (74f), (72a) and (72b).

The following terms are defined:

P^* = exact solution of difference equation (I-2a)

P = numerical solution of difference equation (I-2b)

E = $P^* - P$, error present in numerical solution (I-2c)

Difference Equation (I-1) is subtracted from the identical equation in P^* to give the difference equation in E.

$$a_{i+1,j}\,E_{i+1,j} + b_{i,j}\,E_{i,j} + c_{i-1,j}\,E_{i-1,j} + d_{i,j+1}\,E_{i,j+1} + e_{i,j}\,E_{i,j} + g_{i,j-1}\,E_{i,j-1} = 0 \qquad \text{(I-3)}$$

To save writing space, indices on the coefficients will be dropped, but they will be understood to occur as indicated in Equation (I-3).

The x-direction equation corresponding to Equation (I-3) after introduction of the iteration parameter $\not{\alpha}$ becomes:

$$a\,E_{i+1,j}^{K+1/2} + b\,E_{i,j}^{K+1/2} + c\,E_{i-1,j}^{K+1/2} + d\,E_{i,j+1}^{K} + e\,E_{i,j}^{K} + g\,E_{i,j-1}^{K} = \not{\alpha}^{(K+1)}\left(E_{i,j}^{K+1/2} - E_{i,j}^{K}\right) \qquad \text{(I-4a)}$$

and the y-direction form is:

$$a E_{i+1,j}^{K+1/2} + b E_{i,j}^{K+1/2} + c E_{i,j}^{K+1/2} + d E_{i,j+1}^{K+1} + e E_{i,j}^{K+1} + g E_{i,j-1}^{K+1} = \beta^{(K+1)} \left(E_{i,j}^{K+1} - E_{i,j}^{K+1/2} \right) \quad \text{(I-4b)}$$

The bracketed superscript on the iteration parameter is taken to indicate that the same value is used in both x- and y-directions in performing the complete iteration advancing pseudo time from k to k + 1 .

The criterion of stability is that the error shall not be amplified from iteration to iteration.

$$\left| \frac{E_{i,j}^{K+1}}{E_{i,j}^{K}} \right| \leq 1 \quad \text{(I-5)}$$

Solution of Equations (I-4a) and (I-4b) is by separation of variables. The error is factored into its components:

$$E_{i,j}^{K} = I_i \cdot J_j \cdot K^k \quad \text{(I-6)}$$

It is seen that Equation (I-5) is equivalent to:

$$\left| \frac{K^{K+1}}{K^{K}} \right| \leq 1 \quad \text{(I-7)}$$

The purpose of the analysis is to obtain an expression for this ratio.

Substituting Equation (I-6) into (I-4a) and dividing by $E_{i,j}^{k}$:

$$a\frac{I_{i+1}J_j K^{k+1/2}}{I_i J_j K^k} + b\frac{I_i J_j K^{k+1/2}}{I_i J_j K^k} + c\frac{I_{i-1}J_j K^{k+1/2}}{I_i J_j K^k} + d\frac{I_i J_{j+1} K^k}{I_i J_j K^k}$$

$$+ e\frac{I_i J_j K^k}{I_i J_j K^k} + g\frac{I_i J_{j-1} K^k}{I_i J_j K^k} = \not{\alpha}^{(k+1)}\left(\frac{I_i J_j K^{k+1/2}}{I_i J_j K^k} - \frac{I_i J_j K^k}{I_i J_j K^k}\right) \qquad \text{(I-8)}$$

rearranging

$$\frac{K^{k+1/2}}{K^k}\left[a\frac{I_{i+1}}{I_i} + b + c\frac{I_{i-1}}{I_i} - \not{\alpha}^{(k+1)}\right]$$

$$= -\left[d\frac{J_{j+1}}{J_j} + e + g\frac{J_{j-1}}{J_j} + \not{\alpha}^{(k+1)}\right] = \gamma_1 \qquad \text{(I-9)}$$

Since the j-component is equal to a combination of the i- and k-components, both the j-component and the combination of i- and k-components must equal some constant, γ_1 .

By similar reasoning it follows that:

$$\gamma_1 \frac{K^k}{K^{k+1/2}} = \lambda_1 \qquad \text{(I-10)}$$

Rearrangement gives:

$$d\,J_{j+1} - \left(-e - \not{\alpha}^{(k+1)} - \gamma_1\right) J_j + g\,J_{j-1} = 0 \qquad \text{(I-11a)}$$

$$a\,I_{i+1} - \left(-b + \not{\alpha}^{(k+1)} + \lambda_1\right) I_i + c\,I_{i-1} = 0 \qquad \text{(I-11b)}$$

Up to this point the coefficients of the difference equation vary from element to element of the grid system. Further operations will

deal with the most "adverse" values of the coefficients and a bar over the coefficients will be used to denote this.

Since the coefficients on the I_i and the J_j terms in Equations (I-11a) and (I-11b) are now treated as constants, the following substitutions will be convenient as solutions in the form of sines and cosines is anticipated.

$$(-\bar{e} - \mathcal{H}^{(k+1)} - \gamma_1) = 2\sqrt{\bar{a}\bar{g}}\,\cos\alpha_j \qquad \text{(I-12a)}$$

$$(-\bar{b} + \mathcal{H}^{(k+1)} + \lambda_1) = 2\sqrt{\bar{a}\bar{c}}\,\cos\alpha_i \qquad \text{(I-12b)}$$

The α_i and α_j are constants with subscripts indicating the components with which they will be used. (At this point the α's may be real or complex.)

The solution for (I-11a) will be of the form

$$J_j = A\beta^j \qquad \text{(I-13)}$$

where A is a constant, and β is raised to the j-th power.

Substitution of Equations (I-13) and (I-12a) into Equation (I-11a) gives:

$$\bar{a}\beta^2 - (2\sqrt{\bar{a}\bar{g}}\,\cos\alpha_j)\beta + \bar{g} = 0 \qquad \text{(I-14a)}$$

from which

$$\beta_{1,2} = \sqrt{\bar{g}/\bar{a}}\,(\cos\alpha_j \pm \sqrt{-1}\,\sin\alpha_j) \qquad \text{(I-14b)}$$

The general solution is therefore:

$$J_j = A_1 \beta_1^j + A_2 \beta_2^j = \bar{A}_1 \cos(j \cdot \alpha_j) + \bar{A}_2 \sin(j \cdot \alpha_j) \qquad \text{(I-15)}$$

The expansion follows from the trignometric identity:

$$(\cos\theta + \sqrt{-1}\,\sin\theta)^n = \cos n\theta + \sqrt{-1}\,\sin n\theta \qquad \text{(I-16)}$$

Similar manipulations show the i component to be:

$$I_i = \bar{B}_1 \cos(i \cdot \alpha_i) + \bar{B}_2 \sin(i \cdot \alpha_i) \qquad \text{(I-17)}$$

In this problem, all boundaries are treated as reflecting. Thus the sine terms of Equations (I-15) and (I-17) must have coefficients of zero to obtain zero derivatives at $i = 0$ and $j = 0$. The zero derivatives at the boundaries $i = i_m$ and $j = j_m$ give only real eigenvalues for each component.

at i_m :

$$\sin i_m \cdot \alpha_i = 0 \qquad \text{(I-18a)}$$

$$\alpha_i = i\pi / i_m \qquad \text{for } i = 1, 2, \cdots, i_m - 1 \qquad \text{(I-18b)}$$

at j_m :

$$\alpha_j = j\pi / j_m \qquad \text{for } j = 1, 2, \cdots, j_m - 1 \qquad \text{(I-18c)}$$

Returning to Equations (I-12a) and (I-12b) there results:

$$-\gamma_1 = 2\sqrt{d\bar{g}}\cos j\pi/j_m + \bar{e} + \not{H}^{(K+1)} \tag{I-19a}$$

$$\lambda_1 = 2\sqrt{\bar{a}\bar{c}}\cos i\pi/i_m + \bar{b} - \not{H}^{(K+1)} \tag{I-19b}$$

Substitution of Equations (I-19a) and (I-19b) into Equation (I-10) and taking the absolute value yields:

$$\left|\frac{K^{K+1/2}}{K^K}\right| = \left|\frac{\gamma_1}{\lambda_1}\right| = \left|\frac{\not{H}^{(K+1)} - [-\bar{e} - 2\sqrt{d\bar{g}}\cos j\pi/j_m]}{\not{H}^{(K+1)} + [-\bar{b} - 2\sqrt{\bar{a}\bar{c}}\cos i\pi/i_m]}\right| \tag{I-20}$$

Similar operation on the y-direction Equations (I-4b) yields a relationship analogous to Equation (I-9)

$$\frac{K^{K+1}}{K^{K+1/2}}\left[d\frac{J_{j+1}}{J_j} + e + g\frac{J_{j-1}}{J_j} - \not{H}^{(K+1)}\right] = -\left[a\frac{I_{i+1}}{I_i} + b + c\frac{I_{i-1}}{I_i} + \not{H}^{(K+1)}\right] = \gamma_2 \tag{I-21}$$

Proceeding as before, there results:

$$\lambda_2\frac{K^{K+1}}{K^{K+1/2}} = \gamma_2 \tag{I-22a}$$

$$a\,I_{i+1} - (-b - \not{H}^{(K+1)} - \gamma_2)I_i + c\,I_{i-1} = 0 \tag{I-22b}$$

$$d\,J_{j+1} - (-e + \not{H}^{(K+1)} + \lambda_2)J_j + g\,J_{j-1} = 0 \tag{I-22c}$$

Again the most adverse values of the coefficients are used and trignometric substituion is made:

$$(-\bar{e} + \mathcal{H}^{(k+1)} + \lambda_2) = 2\sqrt{\bar{d}\bar{g}}\,\cos\alpha_j \qquad \text{(I-23a)}$$

$$(-\bar{b} - \mathcal{H}^{(k+1)} - \gamma_2) = 2\sqrt{\bar{a}\bar{c}}\,\cos\alpha_i \qquad \text{(I-23b)}$$

The general solution for each component is obtained as before and the same eigenvalues result. Rearrangement of Equations (I-23a) and (I-23b) with the proper α's yields:

$$\lambda_2 = 2\sqrt{\bar{d}\bar{g}}\,\cos j\pi/j_m + \bar{e} - \mathcal{H}^{(k+1)} \qquad \text{(I-24a)}$$

$$-\gamma_2 = 2\sqrt{\bar{a}\bar{c}}\,\cos i\pi/i_m + \bar{b} + \mathcal{H}^{(k+1)} \qquad \text{(I-24b)}$$

Substitution of Equations (I-24a) and (I-24b) into Equation (I-22a) and taking the absolute value gives:

$$\left|\frac{K^{K+1}}{K^{K+1/2}}\right| = \left|\frac{\mathcal{H}^{(k+1)} - [-\bar{b} - 2\sqrt{\bar{a}\bar{c}}\,\cos i\pi/i_m]}{\mathcal{H}^{(k+1)} + [-\bar{e} - 2\sqrt{\bar{d}\bar{g}}\,\cos j\pi/j_m]}\right| \qquad \text{(I-25)}$$

The over-all amplification factor results from multiplication of Equations (I-20) and (I-25):

$$\left|\frac{K^{K+1}}{K^{K}}\right| = \left|\frac{K^{K+1}}{K^{K+1/2}}\right| \cdot \left|\frac{K^{K+1/2}}{K^{K}}\right|$$

$$= \left|\frac{\mathcal{H}^{(k+1)} - [-\bar{e} - 2\sqrt{\bar{d}\bar{g}}\,\cos j\pi/j_m]}{\mathcal{H}^{(k+1)} + [-\bar{b} - 2\sqrt{\bar{a}\bar{c}}\,\cos i\pi/i_m]}\right| \cdot \left|\frac{\mathcal{H}^{(k+1)} - [-\bar{b} - 2\sqrt{\bar{a}\bar{c}}\,\cos i\pi/i_m]}{\mathcal{H}^{(k+1)} + [-e - 2\sqrt{\bar{d}\bar{g}}\,\cos j\pi/j_m]}\right| \qquad \text{(I-26)}$$

Definition of the coefficients has been made in Equations (73a) - (73f) and (74a) - (74f). They are all interblock values of M multiplied by the appropriate geometric factors.

$$M = K\left(k_n/\mu_n + k_w/\mu_w\right) \tag{I-27}$$

Relative permeabilities are always positive, so the same is true for the M's . The geometric factors also are always positive.

The coefficients a , c , d and g are <u>positive</u> products of a geometric factor and a value of M while the coefficients b and e are <u>negative</u> products of a geometric factor and two adjacent M values. For any five adjacent grid elements about which the difference equations are written, four interblock positions enter. The coefficients associated with these elements can be written:

$$a = \gamma_x M_{x2} \tag{I-28a}$$

$$b = -\gamma_x\left(M_{x2} + M_{x1}\right) \tag{I-28b}$$

$$c = \gamma_x M_{x1} \tag{I-28c}$$

$$d = \gamma_y M_{y2} \tag{I-28d}$$

$$e = -\gamma_y\left(M_{y2} + M_{y1}\right) \tag{I-28e}$$

$$g = \gamma_y M_{y1} \tag{I-28f}$$

The γ's are the geometric factors and M's the interblock properties in the x- (or r-) and y-directions.

If the iteration technique is stable, the amplification factor must be less than or equal to unity. For positive values of the iteration

parameter γ_x , this requirement will be met if the bracketed terms in Equation (I-27) are positive. Using the above values of the coefficients, the bracketed terms become:

$$\left[-b-2\sqrt{ac}\cos i\pi/i_m\right] = \gamma_x\left[(M_{x_2}+M_{x_1})-2\sqrt{M_{x_2}M_{x_1}}\cos i\pi/i_m\right] \qquad \text{(I-29a)}$$

The requirement reduces to:

$$(M_{x_2}+M_{x_1})-2\sqrt{M_{x_2}M_{x_1}}\cos i\pi/i_m \geq 0 \qquad \text{(I-29b)}$$

$$M_{x_2}+M_{x_1} \geq 2\sqrt{M_{x_2}M_{x_1}}\cos i\pi/i_m \qquad \text{(I-29c)}$$

Since $0 < \cos i\pi/i_m < 1$, inequality (I-29c) will always be satisfied if

$$M_{x_2}+M_{x_1} \geq 2\sqrt{M_{x_2}M_{x_1}} \qquad \text{(I-29d)}$$

Squaring and rearranging, this condition is:

$$(M_{x_2}-M_{x_1})^2 \geq 0 \qquad \text{(I-29e)}$$

The above inequality is always satisfied.

The other bracketed term is treated in the same way and the condition corresponding to (I-29e) is:

$$(M_{y_2}-M_{y_1})^2 \geq 0 \qquad \text{(I-29f)}$$

This inequality is always satisfied too.

Thus for adjacent elements, the amplification factor is seen to be less than unity for any positive $\mathcal{H}$.

$$\left|\frac{K^{k+1}}{K^{k}}\right| = \left|\frac{\mathcal{H}^{(k+1)} - \epsilon}{\mathcal{H}^{(k+1)} + \epsilon}\right|^2 < 1 \qquad \text{(I-30)}$$

where

$$\epsilon = \min\left\{\begin{matrix}[-b - 2\sqrt{ac}\cos i\pi/i_m] \\ [-e - 2\sqrt{dg}\cos j\pi/j_m]\end{matrix}\right\} \qquad \text{(I-31)}$$

It is assumed that favorable stability will result from the most adverse values of the coefficients also.

For purposes of estimating the optimum iteration parameters, each part of the numerator is set to zero.

$$\mathcal{H}^{(k+1)} = \left[-\bar{e} - 2\sqrt{d\bar{g}}\cos j\pi/j_m\right] \qquad \text{(I-32a)}$$

$$\mathcal{H}^{(k+1)} = \left[-\bar{b} - 2\sqrt{ac}\cos i\pi/i_m\right] \qquad \text{(I-32b)}$$

An average coefficient $\bar{M}$ is assumed to factor out leaving:

$$\mathcal{H}^{(k+1)} = 2\gamma_y \bar{M}\left[1 - \cos j\pi/j_m\right] \qquad \text{(I-33a)}$$

$$\mathcal{H}^{(k+1)} = 2\gamma_x \bar{M}\left[1 - \cos i\pi/i_m\right] \qquad \text{(I-33b)}$$

Again the γ's are the geometric factors.

It will be noted that Equations (I-33a) and (I-33b) are the relationships resulting from stability analysis on Laplace's equation in which the geometric factors are $(\Delta x)^{-2}$ and $(\Delta y)^{-2}$ and $\bar{M}$ is unity.

The average coefficient $\bar{M}$ is factored from the definition of the "pure" iteration parameter.

$$\frac{\beta}{4\bar{M}} = HK_1 = \frac{\gamma_y}{2}\left[1-\cos j\pi/j_m\right] \qquad (I-34a)$$

$$\frac{\beta}{4\bar{M}} = HK_2 = \frac{\gamma_x}{2}\left[1-\cos i\pi/i_m\right] \qquad (I-34b)$$

Minimum and maximum values of HK are selected as:

$$HK_{\substack{min\\max}} = \min_{\max}\left\{\begin{matrix}\gamma_x[1-\cos i\pi/i_m]\\ \gamma_y[1-\cos j\pi/j_m]\end{matrix}\right\} \qquad (I-35)$$

The geometric factors for the two coordinate systems are:

Cartesian: Domal:

$$\gamma_x = 1/\Delta x^2 \qquad \gamma_x = \alpha_i = \frac{2\Delta x}{\left\{r_1^2 e^{2(i-1)\Delta x}[1-e^{-2\Delta x}][e^{\Delta x}-1]^2\right\}} \qquad (I-36a,b)$$

$$\gamma_y = 1/\Delta y^2 \qquad \gamma_y = 1/\Delta y^2 \qquad (I-36c,d)$$

Substitution of the geometric factors and expansion of the cosine term results in:

Cartesian:

$$HK_{min} = \min\left\{\begin{array}{l} \frac{1}{2\Delta x^2}\left[\pi^2/(2i_m^2)\right] \\ \frac{1}{2\Delta y^2}\left[\pi^2/(2j_m^2)\right] \end{array}\right\} \tag{I-37a}$$

$$HK_{max} = \max\left\{\begin{array}{l} \frac{1}{2\Delta x^2}\left[2 - \pi^2/(2i_m^2)\right] \\ \frac{1}{2\Delta y^2}\left[2 - \pi^2/(2j_m^2)\right] \end{array}\right\} \tag{I-37b}$$

Domal:

$$HK_{min} = \min\left\{\begin{array}{l} \frac{\alpha_{im}}{2}\left[\pi^2/(2i_m^2)\right] \\ \frac{1}{2\Delta y^2}\left[\pi^2/(2j_m^2)\right] \end{array}\right\} \tag{I-37c}$$

$$HK_{max} = \max\left\{\begin{array}{l} \frac{\alpha_1}{2}\left[2 - \pi^2/(2i_m^2)\right] \\ \frac{1}{2\Delta y^2}\left[2 - \pi^2/(2j_m^2)\right] \end{array}\right\} \tag{I-37d}$$

The average coefficient $\bar{M}$ is taken to be:

$$4\bar{M} = \sum M = M_{i+1/2,j} + M_{i-1/2,j} + M_{i,j+1/2} + M_{i,j-1/2} \tag{I-38}$$

The iteration parameter $\mathscr{H}$ to be used is:

$$\mathscr{H} = \left(\sum M\right) HK \tag{I-39}$$

The minimum values of HK is employed on the first iteration of a cycle with the maximum value on the last. Here, iteration parameters between the minimum and maximum are obtained by logarithmic interpolation.

In view of the approximations involved in treating the stability analysis in this manner, it must be realized that the "theoretically" best minimum and maximum values of the iteration parameter should serve only as a guide in the selection. It would appear advisable to test a number of sets of iteration parameters for a particular distribution of coefficients before proceeding with the solution of the problem. It is the author's personal knowledge that one production research organization handles the iteration parameter problem by means of on-line adjustment based on experience[48].

APPENDIX II

PROGRAM CAPABILITIES AND PERFORMANCE

During the course of this work a considerable amount of effort and computing time has been expended in the writing, checking-out and operation of the computer programs through which the numerical solutions have been accomplished. This section has been included primarily for the benefit of those who might continue the work begun here or seek solutions for other types of problems through similar numerical techniques.

A listing of the computer programs has not been included because of the space requirement and the marginal value that their inclusion is felt to afford in view of the transient nature of the computing art. However the programs should be available at this institution for some time. It is hoped that the description of the numerical methods employed here is complete enough to allow development of similar programs with a minimum amount of effort.

A. Program Characteristics and Capabilities

Programs were written for both cartesian and domal coordinate systems. The programs are quite similar as would be expected from the similarity of the difference equations. They were written separately due to storage capacity considerations, but they could be combined into a single program if desired.

Each program was written for the Fortran compiler in conjunction with the University of Michigan Executive System. Fortran was selected in preference to the MAD compiler basically because of the increased

efficiency of the resulting program. Even though significantly less compiling time would have resulted with the MAD language, the saving in execution time has far outweighed this consideration in view of the extensive use made of the programs.

In the Fortran language each complete program is rather lengthy and occupies approximately two thousand cards. To reduce compilation time each was segmented into a number of subroutines. Main programs control data input and the calling sequence with the majority of the computations and output split up among the subroutines.

In this work an IBM 709 computer with 32,000 word core-storage was used. By utilizing this space as economically as possible a maximum grid size of 50 row by 20 column elements could be handled in both coordinate systems.

All internal computations are done in the cgs unit system, but input and output can be specified in any one of the three unit systems in Table XXXII.

TABLE XXXII

SYSTEMS OF UNITS

System	Length	Time	Water Rate	Gas Rate
1	cm	sec	cc/sec	std cc/sec
2	inches	sec	cc/sec	std cc/sec
3	feet	days	BBl/day	MSCF/day

As evidenced by the above table, the programs were written specifically for gas-water systems, but due to the incompressibility of the phases, computations for oil-water systems are identical and may be performed by specification of the appropriate phase properties. In the calculations performed here, the maximum grid size was never used. For most problems, as coarse a grid system as possible should be used in the interest of computational time requirements.

For the solution of long problems requiring more than one hour of execution time, provisions were made for stopping and restarting with punch-out and read-in of the dependent variables P and R. This was found to be wise because of the frequency of machine error. Punch out can be triggered after a specified time step or after a specified number of minutes of execution.

In addition to efforts to minimize unnecessarily repetitious calculations, another feature has been included to increase the efficiency of operation. Reference to the difference equations shows the size of the time step to enter only the R equations. Too large a time step causes the iterative scheme to be non-convergent with the resulting loss of the updated P matrix and several days waiting time. Consequently a routine was included to sense the rate of convergence of the R equation and to automatically reduce the size of the time step accordingly.

Relative permeability and capillary pressure functions were handled by linear interpolation of tables. Relative permeability tables had 51 entries on evenly spaced increments of wetting phase saturation (2%). The main capillary pressure table was used to obtain wetting phase

saturation and the derivative dS_w/dp_c from values of capillary pressure. This table utilized 51 entries of saturation on semi-evenly spaced increments of capillary pressure. (Near residual saturations, coarser spacing was used.)

The derivative $dS_w\ dp_c$ was obtained from the table in the following manner:

$$\frac{dS_w}{dp_c} \cong \frac{S_w(p_c+\delta) - S_w(p_c-\delta)}{2\delta} \qquad \text{(II-1)}$$

where δ was taken as one half the spacing used in the table. To facilitate the treatment of an arbitrarily specified initial saturation distribution, a second capillary pressure table was employed with 51 entries on evenly spaced increments of wetting phase saturation.

To give an indication of the performance of the solution, material balance calculations were made at the end of each time step on a differential and over-all basis for the wetting phase.

$$QT_{n+1} = \sum_{i=1}^{im} \sum_{j=1}^{jm} Qw_{i,j,n+1/2} \cdot \Delta t_{n+1} \qquad \text{(II-2a)}$$

$$W_n = \sum_{i=1}^{im} \sum_{j=1}^{jm} S_{w_{i,j,n}} \cdot \Delta V_{i,j} \qquad \text{(II-2b)}$$

$$error_d = \left(QT_{n+1} - W_{n+1} + W_n \right) / W_{n+1} \qquad \text{(II-3a)}$$

$$error_c = \left(\sum_{m=1}^{n+1} QT_m - W_{n+1} + W_0 \right) / W_{n+1} \qquad \text{(II-3b)}$$

The problems treated had homogeneous or layered porous media, but specification of unique porosity and permeability for each grid element is allowed. Likewise, any initial wetting phase saturation and potential distribution can be specified, but the normal procedure is to begin with an equilibrium distribution which is obtained automatically from specification of the desired capillary pressure at the base elevation $(h = 0)$.

The difference equations indicate that injection may exist for any element of the grid system. However in all physical problems, the elements actually experiencing injection or production will be few in comparison with the total number of elements. Consequently, to conserve storage space, injection terms were treated as singly-subscripted variables. In both programs a maximum of 60 elements can have two-phase injection-production. This number includes elements in communication with wells and the producing face (if used) for which total rates are specified on an individual basis.

In the cartesian system injection of a single phase or production of both phases may be accomplished through circular wells at either edge $(i = 1$ and $i = i_m)$ of the porous medium. In addition wetting phase injection can occur through a circular well in any column $(1 < i < i_m)$ of the grid system. In the domal system, single phase injection or two-phase production may be specified through an axial well and a producing face at the outer radius $(r = r_m + \frac{1}{2})$. Wetting phase injection is permitted through a line source for any interior radius $(1 \leq i < i_m)$. These injection-production provisions may communicate with the porous medium at all or any prescribed levels of the grid system. To treat the case of slotted or

perforated well liners, any fraction of the well bore area may be open to flow. Both systems can also employ the aquifer boundary at the outer edge in which communication occurs at all levels.

B. Performance

In the early phases of this work, numerical solution to difference equations corresponding to the following rearrangement of the differential equations was attempted. Here the differential equations are written in cartesian coordinates with y in the vertical direction.

$$\nabla\cdot(M\nabla P) + \tfrac{1}{2}\nabla\cdot(N p_c' \nabla S_w) - \tfrac{1}{2}\frac{\partial}{\partial y}(N\Delta\rho g) = 0 \qquad \text{(II-4a)}$$

$$\nabla\cdot(N\nabla P) + \tfrac{1}{2}\nabla\cdot(M p_c' \nabla S_w) - \tfrac{1}{2}\frac{\partial}{\partial y}(M\Delta\rho g) = -2f\frac{\partial S_w}{\partial t} \qquad \text{(II-4b)}$$

Comparison of these equations to the P and R forms Equations (55a) and (55b) shows the primary difference to be the presence of the capillary pressure derivative in the coefficients of the spatial derivatives rather than the time derivative. It would appear that the above equations might be easier to handle because of the choice of wetting phase saturation as one of the dependent variables. The numerical techniques were very similar to those presented for the P and R equations as the above forms can easily be reduced to difference equations of the standard from Equation (93). The convergence properties of the P equation resulting from Equation (II-4a) were very similar to those obtained in the P and R form. However convergence of the S equation corresponding to Equation (II-4b) was obtained for only a few simple cases. The conclusion is that although

several forms of the differential equations describing a system may be equivalent, successful numerical solution may depend critically on the arrangement of the terms of the difference equations.

In general, numerical solution of the P and R equations in cartesian coordinates behaved satisfactorily. In domal coordinates considerable difficulty arose. For both coordinate systems when convergence problems were encountered, invariably they were associated with solution of the P equation. Convergence of the P equation seems to be very sensitive to both the number of iterations employed per cycle and the values of the iteration parameters used within a cycle. A discussion of the behavior of the P equation for each coordinate system follows.

1. Cartesian Coordinates

The best results were obtained when square elements ($\Delta x = \Delta y$) were used in a square grid ($i_m = j_m$) . This was the case in the solutions associated with the laboratory displacements. The other problems treated also employed a 16x16 grid with non-square grid elements. Calculations for the spillpoint problem were begun on a 15x30 grid of non-square elements, but due to the excessive execution time requirement grid size was subsequently reduced. The non-square elements had length to height ratios of 8.3 and 10 in the scaling and spillpoint problems, respectively, with faster convergence resulting for the former. Earlier efforts on the latter problem found slow convergence at a ratio of 20 and non-convergence at 100. This behavior should be expected from the results of the stability analysis as summarized in Equations (84a) and (84b). It is seen that as the elements and grid become more and more assymetric, the minima and maxima

of the iteration parameters theoretically most effective in the two directions depart further and further. Because of the influence grid and element sizes have on the rate of convergence, it is wise to test the convergence of the P equation in several grid systems before choosing the one to be used.

Serious convergence problems were never encountered in solution of the R equation. It was found that larger time steps could be used successfully for imbibition type displacements than for drainage displacements in gas-water systems. This might be expected due to the physical instability associated with displacements carried out under conditions of unfavorable mobility ratios as are present when gas displaces water.

The over-all convergence of the "simultaneous" difference equations was investigated by rerunning a portion of the solution for the second laboratory displacement on a series of shorter time steps. The water saturation distribution obtained at 15 hours of operation is presented in Table XXXIV. This resulted when a basic time step of 30 minutes was used. The saturation distribution obtained at 15 hours by rerunning the solution from 11 hours on a 15 minute time step appears in Table XXXV. Thus the four hour period was covered first in 8 time steps and later in 16 time steps. Comparison of the respective saturation distributions shows agreement to two or three digits in the fourth place. On this basis, the overall convergence must be considered very good. Although this was the only cartesian solution tested in this manner, it was assumed that the other solutions presented would exhibit similarly good over-all convergence.

For purposes of check out, computations were made for horizontal single phase (water) flow. The resulting pressure distribution was in excellent agreement with Darcy's law. Because of the unavailability of analytic solutions for two phase problems, conclusive two-phase checkout was not possible. However, qualitatively good behavior was obtained for a two-phase system in which the initial phase distribution was removed from capillary equilibrium. Both two-dimensional checkout problems showed the one-dimensional character that would be expected. It should be noted that solution of the single phase problem is just as difficult as a two-phase problem as far as computational methods are concerned. The only difference is that functions of phase saturation are the same for all grid elements.

2. Domal Coordinates

In an effort to assess the conditions required for convergence of the P equation, a number of single phase radial flow problems were solved. The results are summarized in Table XXXIII. All convergent solutions showed excellent agreement with Darcy's law integrated over the radial system. The description of convergence refers to the rate of convergence with good indicating that the tolerance was satisfied on the first iteration (largest pseudo time step) of the indicated cycle. In all cases seven iterations were used per cycle.

The number in parenthesis following the cycle number is the first iteration in that cycle on which the tolerance was met. Because several differently sized systems were studied, tolerance limits had to be adjusted in order to be approximately equivalent.

TABLE XXXIII

CONVERGENCE PROPERTIES - DOMAL COORDINATES SINGLE PHASE RADIAL FLOW

r_1	r_m	i_m	Δ_y	j_m	Convergence	Cycle
2 cm	20 cm	10	1 cm	5	good	5
2 ft	20 ft	10	1 ft	5	good	5
2 ft	20 ft	12	1 ft	5	slow	5(7)
2 ft	20 ft	14	1 ft	5	slow	5(6)
2 ft	20 ft	20	1 ft	5	slow	5(7)
2 ft	40 ft	13	1 ft	5	slow	5(7)
6 ft	60 ft	10	1 ft	5	good	5
6 ft	100 ft	10	1 ft	5	slow	5(7)
6 ft	100 ft	13	1 ft	5	slow	5(7)
6 ft	150 ft	15	1 ft	5	slow	5(7)
6 ft	200 ft	10	1 ft	5	slow	5(7)
6 ft	200 ft	15	1 ft	5	slow	5(7)
6 ft	200 ft	20	1 ft	5	non-convergent	

From these studies it appears that a ratio of no more than 10 can exist between outer and inner radii in order to achieve good convergence. Also it appears that better convergence generally results when fewer radial increments are used. This may seem surprising, but it might be expected from the results of the stability analysis Equations (84c) and (84d) for the same reasons discussed above.

The convergence difficulties seem basically to be due to the larger logarithmic range between minimum and maximum iteration parameters which result in this coordinate system compared to those of the former. It would seem logical that it might be beneficial to use a greater number of iteration parameters per cycle to allow more complete coverage of the desired range. Some calculations performed with ten iterations per cycle instead of the normal seven showed the rate of convergence to be somewhat improved. However, the use of a greater number of iterations per cycle also means more computation per cycle. Perhaps for this coordinate system a better means could be found both for choosing minimum and maximum iteration parameters and for assigning values between the minima and maxima.

One reservoir system was studied which was divided into a 14x20 grid with inner and outer radii of 2 ft and 7000 ft and a vertical spacing of 2 ft. The problem consisted of producing gas through an axial well from a dome-shaped formation initially at capillary equilibrium. As would be expected from the cases cited above, the P equation was non-convergent when the normal choice of iteration parameters was made. Solution was obtained by increasing the minimum parameter computed from Equation (84c) by a factor of 10,000. The parameters were assigned by logarithmic interpolation between the modified minimum of 6×10^{-9} and the normal maximum of 6×10^{-4}. The P equation was usually within tolerance by the fifth or sixth iteration of cycle five. No difficulties were encountered in solution of the R equation and the material balances were excellent. However when the same problem was run on shorter time steps the computed water saturation

distributions were considerably different. For purposes of comparison, the saturation distributions after 30 days of gas production are presented in Tables XLIV(a) and XLIV(b) for five and ten time steps, respectively. Since the minimum iteration parameter corresponds to the maximum step in pseudo time, the total time covered per cycle was far less than specified by the stability analysis. Thus the specified tolerance was met only because a very small pseudo time step had been experienced, and the P matrix must not have reached the stabilized state. The conclusion is that true convergence of the P equation will not result from an arbitrary choice of iteration parameters.

After the study summarized in Table XXXIII was concluded, an attempt at solution of the horizontal aquifer problem was made. In keeping with the conclusions reached with respect to radius limitations, a grid system was set up to cover radii of 14 to 140 ft in 10 increments with 14 vertical increments of 0.1 ft each. Seven iterations were employed per cycle with parameters logarithmically interpolated between the minimum and maximum values prescribed by the stability analysis. Gas was injected into the formation through an axial well, first, with no water injection and, second, with water injection through a line source at a radius of 97 ft. The initial water saturation distribution was essentially uniform ranging from .99 at the top layer to unity for the bottom eight layers.

For the first few time steps a satisfactory convergence rate was obtained for the P equation. However, as soon as the upper element at the interior radius decreased in water saturation to 0.7 for both

problems, the P equation failed to converge. Since the likelihood of a machine error occurring at the same stage of solution in two parallel problems is extremely small, the non-convergence must have been due to the variation among the coefficients in the region of most rapidly changing water saturation (i.e., the vicinity of element $(1, j_m)$).

Although a series of small time steps were used (6 to cover the first hour), it might have been possible to smooth the saturation gradients and preserve convergence of the P equation by operating with a series of much smaller time steps. Also, satisfactory solutions might have resulted if the tolerance on the P equation had been relaxed somewhat during the initial phases of the solutions. This approach is viewed rather dimly though because it would seem that any reasonable tolerance should be met after 15 cycles (the limit set in these problems) if the solutions were even slowly converging. However, at this point a considerable amount of computing time had been used and embarkation on another lengthy project did not seem justifiable.

The solutions were not carried out far enough to establish a basis for assessment of the feasibility of gas containment through peripheral water injection in a horizontal aquifer. However, the computed saturation distributions just prior to non-convergence of the P equation have been included in Tables XLIII(a) through XLIII(c) for the indicated times of operation.

In view of the success obtained in the cartesian system, it was disappointing that the domal system did not turn out more profitable. It is hoped that additional work can be done on the latter as the coordinate system is adaptable to a great many reservoir problems.

APPENDIX III

SELECTED NUMERICAL RESULTS

TABLE XXXIV

COMPUTED WATER SATURATION DISTRIBUTION, DISPLACEMENT NO. 2
(11 TO 15 HOURS COVERED ON 30 MINUTES TIME STEPS)

WATER SATURATION DISTRIBUTION

FOR TIME STEP [illegible], ADVANCING TIME FROM 14.50 HRS TO 15.00 HRS

WITH 16 X-INCREMENTS OF 1.00 IN, 16 Y-INCREMENTS OF 1.00 IN, AND HORIZONTAL THICKNESS OF .53 IN

BLOCK (2,2) - LOWER LEFT CORNER BLOCK (17,2) - LOWER RIGHT CORNER

ANGLE OF INCLINATION = .0 DEGREES (FROM LEFT EDGE)

Y-INDEX / X-INDEX	4	6	7	8	11	12	13	15	16	17
2	.9403	.8954	.7960	.6802	.4009	.3410	.2958	.2314	.2045	.1809
3	.9403	.8954	.7961	.6803	.4010	.3410	.2959	.2314	.2045	.1809
4	.9403	.8956	.7963	.6805	.4011	.3411	.2959	.2314	.2045	.1810
5	.9403	.8957	.7966	.6808	.4013	.3412	.2960	.2315	.2046	.1810
6	.9403	.8959	.7969	.6811	.4015	.3414	.2961	.2316	.2047	.1811
7	.9403	.8962	.7974	.6816	.4018	.3416	.2963	.2317	.2048	.1812
8	.9403	.8966	.7980	.6822	.4021	.3418	.2965	.2318	.2049	.1813
9	.9403	.8970	.7987	.6828	.4025	.3421	.2967	.2319	.2050	.1814
10	.9403	.8974	.7994	.6835	.4029	.3424	.2969	.2321	.2052	.1815
11	.9403	.8979	.8002	.6843	.4034	.3427	.2971	.2323	.2053	.1816
12	.9403	.8985	.8010	.6852	.4039	.3430	.2974	.2324	.2055	.1818
13	.9403	.8991	.8019	.6860	.4044	.3434	.2977	.2326	.2057	.1819
14	.9403	.8996	.8027	.6868	.4049	.3437	.2979	.2328	.2059	.1821
15	.9403	.9002	.8035	.6876	.4053	.3440	.2981	.2329	.2060	.1822
16	.9403	.9006	.8041	.6881	.4056	.3442	.2983	.2330	.2061	.1823
17	.9403	.9009	.8044	.6884	.4057	.3443	.2984	.2331	.2062	.1823

TABLE XXXV

COMPUTED WATER SATURATION DISTRIBUTION, DISPLACEMENT NO. 2
(11 TO 15 HOURS COVERED ON 15 MINUTES TIME STEPS)

WATER SATURATION DISTRIBUTION

FOR TIME STEP 16, ADVANCING TIME FROM 14.75 HRS TO 15.00 HRS

WITH 16 X-INCREMENTS OF 1.00 IN, 16 Y-INCREMENTS OF 1.00 IN, AND HORIZONTAL THICKNESS OF .53 IN

BLOCK (2,2) - LOWER LEFT CORNER BLOCK (17,2) - LOWER RIGHT CORNER

ANGLE OF INCLINATION = .0 DEGREES (FROM LEFT EDGE)

Y-INDEX / X-INDEX	4	6	7	8	11	12	13	15	16	17
2	.9403	.8955	.7963	.6805	.4008	.3407	.2956	.2312	.2042	.1807
3	.9403	.8956	.7964	.6806	.4009	.3408	.2956	.2312	.2043	.1808
4	.9403	.8957	.7966	.6808	.4010	.3409	.2957	.2312	.2043	.1808
5	.9403	.8959	.7969	.6811	.4011	.3410	.2958	.2313	.2044	.1808
6	.9403	.8961	.7972	.6815	.4014	.3412	.2959	.2314	.2045	.1809
7	.9403	.8964	.7977	.6820	.4017	.3414	.2961	.2315	.2046	.1810
8	.9403	.8968	.7983	.6826	.4020	.3416	.2963	.2316	.2047	.1811
9	.9403	.8972	.7990	.6832	.4024	.3419	.2965	.2317	.2048	.1812
10	.9403	.8976	.7997	.6840	.4028	.3422	.2967	.2319	.2050	.1813
11	.9403	.8982	.8005	.6847	.4033	.3425	.2969	.2321	.2051	.1815
12	.9403	.8987	.8014	.6856	.4038	.3429	.2972	.2322	.2053	.1816
13	.9403	.8993	.8022	.6864	.4043	.3432	.2975	.2324	.2055	.1818
14	.9403	.8999	.8031	.6873	.4048	.3435	.2977	.2326	.2057	.1819
15	.9403	.9004	.8038	.6880	.4052	.3438	.2979	.2327	.2058	.1820
16	.9403	.9008	.8044	.6885	.4055	.3440	.2981	.2328	.2059	.1821
17	.9403	.9011	.8047	.6888	.4056	.3441	.2981	.2329	.2060	.1821

TABLE XXXVI

COMPUTED WATER SATURATION DISTRIBUTIONS, FIELD SYSTEM

a. WATER SATURATION DISTRIBUTION

FOR TIME STEP 4, ADVANCING TIME FROM 3.50 DAYS TO 6.50 DAYS

WITH 16 X-INCREMENTS OF 25.00 FT, 16 Y-INCREMENTS OF 3.12 FT, AND HORIZONTAL THICKNESS OF 500.00 FT

BLOCK (2,2) - LOWER LEFT CORNER BLOCK (17,2) - LOWER RIGHT CORNER

ANGLE OF INCLINATION = -1.0 DEGREES (FROM LEFT EDGE)

Y-INDEX / X-INDEX	6	9	10	11	12	13	14	15	16	17
2	.9367	.9341	.8362	.4744	.2208	.1263	.1185	.1107	.1100	.1100
3	.9369	.9348	.9059	.5318	.2295	.1271	.1194	.1116	.1100	.1100
4	.9370	.9352	.9154	.5751	.2377	.1278	.1200	.1123	.1100	.1100
5	.9373	.9361	.9217	.6443	.2497	.1287	.1210	.1132	.1100	.1100
6	.9375	.9372	.9274	.7470	.2773	.1298	.1220	.1143	.1100	.1100
7	.9378	.9382	.9296	.8304	.3100	.1326	.1231	.1153	.1100	.1100
8	.9381	.9391	.9309	.8820	.3580	.1359	.1242	.1164	.1100	.1100
9	.9384	.9397	.9322	.9047	.4140	.1391	.1253	.1175	.1100	.1100
10	.9386	.9404	.9335	.9144	.4791	.1435	.1263	.1186	.1108	.1100
11	.9389	.9410	.9347	.9182	.5501	.1483	.1274	.1197	.1119	.1100
12	.9391	.9413	.9359	.9216	.6231	.1532	.1285	.1207	.1130	.1100
13	.9393	.9418	.9370	.9248	.7286	.1581	.1296	.1218	.1141	.1100
14	.9395	.9424	.9380	.9272	.8224	.1631	.1321	.1229	.1152	.1100
15	.9397	.9431	.9390	.9287	.8751	.1681	.1354	.1241	.1163	.1100
16	.9398	.9437	.9396	.9294	.9033	.1729	.1387	.1251	.1174	.1100
17	.9400	.9443	.9402	.9299	.9122	.1788	.1424	.1261	.1184	.1106

b. WATER SATURATION DISTRIBUTION

FOR TIME STEP 6, ADVANCING TIME FROM 10.00 DAYS TO 14.00 DAYS

WITH 16 X-INCREMENTS OF 25.00 FT, 16 Y-INCREMENTS OF 3.12 FT, AND HORIZONTAL THICKNESS OF 500.00 FT

BLOCK (2,2) - LOWER LEFT CORNER BLOCK (17,2) - LOWER RIGHT CORNER

ANGLE OF INCLINATION = -1.0 DEGREES (FROM LEFT EDGE)

Y-INDEX / X-INDEX	6	9	10	11	12	13	14	15	16	17
2	.9374	.9370	.9261	.6663	.2540	.1289	.1211	.1134	.1100	.1100
3	.9371	.9355	.9180	.5902	.2403	.1280	.1202	.1125	.1100	.1100
4	.9371	.9355	.9177	.5971	.2418	.1281	.1203	.1126	.1100	.1100
5	.9373	.9363	.9227	.6586	.2531	.1289	.1211	.1133	.1100	.1100
6	.9376	.9373	.9277	.7556	.2795	.1299	.1221	.1143	.1100	.1100
7	.9378	.9383	.9297	.8341	.3132	.1328	.1232	.1154	.1100	.1100
8	.9381	.9391	.9310	.8855	.3610	.1361	.1243	.1165	.1100	.1100
9	.9384	.9398	.9323	.9053	.4178	.1393	.1253	.1176	.1100	.1100
10	.9387	.9404	.9336	.9150	.4826	.1438	.1264	.1186	.1109	.1100
11	.9389	.9410	.9348	.9184	.5535	.1486	.1275	.1197	.1120	.1100
12	.9391	.9413	.9359	.9218	.6269	.1534	.1285	.1208	.1130	.1100
13	.9393	.9418	.9371	.9250	.7339	.1583	.1296	.1219	.1141	.1100
14	.9395	.9425	.9381	.9273	.8261	.1634	.1323	.1230	.1153	.1100
15	.9397	.9431	.9390	.9288	.8791	.1685	.1357	.1241	.1164	.1100
16	.9399	.9438	.9397	.9295	.9038	.1732	.1388	.1252	.1174	.1100
17	.9400	.9444	.9403	.9300	.9130	.1793	.1428	.1262	.1184	.1107

c. WATER SATURATION DISTRIBUTION

FOR TIME STEP 10, ADVANCING TIME FROM 26.00 DAYS TO 30.00 DAYS

WITH 16 X-INCREMENTS OF 25.00 FT, 16 Y-INCREMENTS OF 3.12 FT, AND HORIZONTAL THICKNESS OF 500.00 FT

BLOCK (2,2) - LOWER LEFT CORNER BLOCK (17,2) - LOWER RIGHT CORNER

ANGLE OF INCLINATION = -1.0 DEGREES (FROM LEFT EDGE)

Y-INDEX / X-INDEX	6	9	10	11	12	13	14	15	16	17
2	.9386	.9403	.9335	.9143	.4578	.1419	.1260	.1182	.1105	.1100
3	.9377	.9379	.9292	.7912	.2870	.1304	.1224	.1146	.1100	.1100
4	.9375	.9368	.9260	.6954	.2622	.1292	.1214	.1137	.1100	.1100
5	.9375	.9369	.9266	.7144	.2678	.1294	.1217	.1139	.1100	.1100
6	.9377	.9376	.9287	.7871	.2877	.1305	.1224	.1146	.1100	.1100
7	.9379	.9385	.9300	.8448	.3227	.1334	.1234	.1156	.1100	.1100
8	.9382	.9392	.9312	.8938	.3683	.1366	.1244	.1167	.1100	.1100
9	.9384	.9398	.9325	.9066	.4261	.1397	.1255	.1177	.1100	.1100
10	.9387	.9405	.9337	.9154	.4904	.1443	.1265	.1188	.1110	.1100
11	.9389	.9411	.9349	.9188	.5615	.1491	.1276	.1198	.1121	.1100
12	.9391	.9414	.9361	.9222	.6381	.1539	.1287	.1209	.1131	.1100
13	.9393	.9419	.9372	.9254	.7467	.1589	.1298	.1220	.1143	.1100
14	.9395	.9426	.9383	.9275	.8339	.1642	.1328	.1232	.1154	.1100
15	.9397	.9432	.9391	.9289	.8861	.1691	.1361	.1243	.1165	.1100
16	.9399	.9438	.9397	.9295	.9048	.1739	.1392	.1253	.1175	.1100
17	.9400	.9444	.9403	.9300	.9134	.1796	.1430	.1262	.1185	.1107

TABLE XXXVII

COMPUTED WATER SATURATION DISTRIBUTIONS,
UNATTAINABLE LABORATORY SYSTEMS

a. Rigorous Three-Dimensional Scaling Laws

WATER SATURATION DISTRIBUTION

FOR TIME STEP 4, ADVANCING TIME FROM 5.07 HRS TO 9.41 HRS

WITH 16 X-INCREMENTS OF 2.25 IN, 16 Y-INCREMENTS OF .28 IN, AND HORIZONTAL THICKNESS OF 45.00 IN

BLOCK (2,2) - LOWER LEFT CORNER BLOCK (17,2) - LOWER RIGHT CORNER

ANGLE OF INCLINATION = -1.0 DEGREES (FROM LEFT EDGE)

Y-INDEX / X-INDEX	6	9	10	11	12	13	14	15	16	17
2	.9367	.9341	.8362	.4744	.2208	.1263	.1185	.1107	.1100	.1100
3	.9369	.9348	.9059	.5318	.2295	.1271	.1194	.1116	.1100	.1100
4	.9370	.9352	.9154	.5751	.2378	.1278	.1200	.1123	.1100	.1100
5	.9373	.9361	.9217	.6443	.2497	.1287	.1210	.1132	.1100	.1100
6	.9375	.9372	.9274	.7470	.2772	.1298	.1220	.1143	.1100	.1100
7	.9378	.9382	.9296	.8304	.3100	.1326	.1231	.1153	.1100	.1100
8	.9381	.9391	.9309	.8819	.3580	.1359	.1242	.1164	.1100	.1100
9	.9384	.9397	.9322	.9047	.4140	.1391	.1253	.1175	.1100	.1100
10	.9386	.9404	.9335	.9144	.4791	.1435	.1263	.1186	.1108	.1100
11	.9389	.9410	.9347	.9182	.5501	.1483	.1274	.1197	.1119	.1100
12	.9391	.9413	.9359	.9216	.6232	.1532	.1285	.1207	.1130	.1100
13	.9393	.9418	.9370	.9248	.7286	.1581	.1296	.1218	.1141	.1100
14	.9395	.9424	.9380	.9272	.8225	.1631	.1321	.1229	.1152	.1100
15	.9397	.9431	.9390	.9287	.8752	.1681	.1355	.1241	.1163	.1100
16	.9398	.9437	.9396	.9294	.9033	.1729	.1387	.1251	.1174	.1100
17	.9400	.9443	.9402	.9300	.9123	.1789	.1425	.1261	.1184	.1106

b. Rigorous Two-Dimensional Scaling Laws

WATER SATURATION DISTRIBUTION

FOR TIME STEP 4, ADVANCING TIME FROM 5.07 HRS TO 9.41 HRS

WITH 16 X-INCREMENTS OF 2.25 IN, 16 Y-INCREMENTS OF .28 IN, AND HORIZONTAL THICKNESS OF .75 IN

BLOCK (2,2) - LOWER LEFT CORNER BLOCK (17,2) - LOWER RIGHT CORNER

ANGLE OF INCLINATION = -1.0 DEGREES (FROM LEFT EDGE)

Y-INDEX / X-INDEX	6	9	10	11	12	13	14	15	16	17
2	.9367	.9341	.8362	.4744	.2208	.1263	.1185	.1107	.1100	.1100
3	.9369	.9348	.9058	.5318	.2295	.1271	.1194	.1116	.1100	.1100
4	.9370	.9352	.9154	.5751	.2378	.1278	.1200	.1123	.1100	.1100
5	.9373	.9361	.9217	.6443	.2497	.1287	.1210	.1132	.1100	.1100
6	.9375	.9372	.9274	.7470	.2772	.1298	.1220	.1143	.1100	.1100
7	.9378	.9382	.9296	.8304	.3100	.1326	.1231	.1153	.1100	.1100
8	.9381	.9391	.9309	.8819	.3580	.1359	.1242	.1164	.1100	.1100
9	.9384	.9397	.9322	.9047	.4140	.1391	.1253	.1175	.1100	.1100
10	.9386	.9404	.9335	.9144	.4791	.1435	.1263	.1186	.1108	.1100
11	.9389	.9410	.9347	.9182	.5501	.1483	.1274	.1197	.1119	.1100
12	.9391	.9413	.9359	.9216	.6232	.1532	.1285	.1207	.1130	.1100
13	.9393	.9418	.9370	.9248	.7287	.1581	.1296	.1218	.1141	.1100
14	.9395	.9424	.9380	.9272	.8225	.1631	.1321	.1229	.1152	.1100
15	.9397	.9431	.9390	.9287	.8752	.1681	.1355	.1241	.1163	.1100
16	.9398	.9437	.9396	.9294	.9034	.1730	.1387	.1251	.1174	.1100
17	.9400	.9443	.9402	.9300	.9125	.1790	.1426	.1261	.1184	.1106

c. Two-Dimensional Scaling Laws with Laboratory Relative Permeability and Capillary Pressure Relationships

WATER SATURATION DISTRIBUTION

FOR TIME STEP 4, ADVANCING TIME FROM 5.07 HRS TO 9.41 HRS

WITH 16 X-INCREMENTS OF 2.25 IN, 16 Y-INCREMENTS OF .28 IN, AND HORIZONTAL THICKNESS OF .75 IN

BLOCK (2,2) - LOWER LEFT CORNER BLOCK (17,2) - LOWER RIGHT CORNER

ANGLE OF INCLINATION = -1.0 DEGREES (FROM LEFT EDGE)

Y-INDEX / X-INDEX	6	9	10	11	12	13	14	15	16	17
2	.8556	.8361	.7194	.4574	.2000	.1070	.1070	.1070	.1070	.1070
3	.8617	.8361	.8205	.5305	.2172	.1070	.1070	.1070	.1070	.1070
4	.8684	.8555	.8341	.6165	.2439	.1070	.1070	.1070	.1070	.1070
5	.8704	.8552	.8350	.6506	.2592	.1070	.1070	.1070	.1070	.1070
6	.8749	.8692	.8357	.7043	.2820	.1070	.1070	.1070	.1070	.1070
7	.8797	.8854	.8359	.7584	.3098	.1070	.1070	.1070	.1070	.1070
8	.8848	.9033	.8360	.8039	.3516	.1070	.1070	.1070	.1070	.1070
9	.8899	.9213	.8360	.8223	.4118	.1070	.1070	.1070	.1070	.1070
10	.8950	.9394	.8361	.8299	.4823	.1070	.1070	.1070	.1070	.1070
11	.9001	.9573	.8361	.8323	.5561	.1070	.1070	.1070	.1070	.1070
12	.9057	.9787	.8496	.8345	.6336	.1070	.1070	.1070	.1070	.1070
13	.9105	.9946	.8661	.8354	.6898	.1070	.1070	.1070	.1070	.1070
14	.9155	1.0000	.8829	.8357	.7481	.1070	.1070	.1070	.1070	.1070
15	.9205	1.0000	.9003	.8359	.7979	.1070	.1070	.1070	.1070	.1070
16	.9257	1.0000	.9194	.8359	.8208	.1071	.1070	.1070	.1070	.1070
17	.9301	1.0000	.9352	.8360	8290	.1232	.1070	.1070	.1070	.1070

TABLE XXXVIII

COMPUTED WATER SATURATION DISTRIBUTIONS;
PRACTICAL LABORATORY SYSTEM

a. WATER SATURATION DISTRIBUTION

FOR TIME STEP 4, ADVANCING TIME FROM 5.07 HRS TO 9.41 HRS

WITH 16 X-INCREMENTS OF 2.25 IN, 16 Y-INCREMENTS OF .28 IN, AND HORIZONTAL THICKNESS OF .75 IN

BLOCK (2,2) - LOWER LEFT CORNER BLOCK (17,2) - LOWER RIGHT CORNER

ANGLE OF INCLINATION = -1.0 DEGREES (FROM LEFT EDGE)

Y-INDEX / X-INDEX	6	9	10	11	12	13	14	15	16	17
2	.8556	.8361	.7194	.4574	.2000	.1070	.1070	.1070	.1070	.1070
3	.8617	.8361	.8205	.5305	.2172	.1070	.1070	.1070	.1070	.1070
4	.8684	.8555	.8341	.6165	.2439	.1070	.1070	.1070	.1070	.1070
5	.8704	.8552	.8350	.6506	.2592	.1070	.1070	.1070	.1070	.1070
6	.8749	.8692	.8357	.7043	.2820	.1070	.1070	.1070	.1070	.1070
7	.8797	.8854	.8359	.7584	.3098	.1070	.1070	.1070	.1070	.1070
8	.8848	.9033	.8360	.8039	.3516	.1070	.1070	.1070	.1070	.1070
9	.8899	.9213	.8360	.8223	.4118	.1070	.1070	.1070	.1070	.1070
10	.8950	.9394	.8361	.8299	.4823	.1070	.1070	.1070	.1070	.1070
11	.9001	.9573	.8361	.8323	.5562	.1070	.1070	.1070	.1070	.1070
12	.9057	.9788	.8497	.8345	.6337	.1070	.1070	.1070	.1070	.1070
13	.9106	.9956	.8667	.8354	.6903	.1070	.1070	.1070	.1070	.1070
14	.9155	1.0000	.8830	.8357	.7485	.1070	.1070	.1070	.1070	.1070
15	.9206	1.0000	.9008	.8359	.7987	.1070	.1070	.1070	.1070	.1070
16	.9257	1.0000	.9189	.8359	.8207	.1070	.1070	.1070	.1070	.1070
17	.9303	1.0000	.9345	.8360	.8288	.1224	.1070	.1070	.1070	.1070

b. WATER SATURATION DISTRIBUTION

FOR TIME STEP 8, ADVANCING TIME FROM .60 DAYS TO .84 DAYS

WITH 16 X-INCREMENTS OF 2.25 IN, 16 Y-INCREMENTS OF .28 IN, AND HORIZONTAL THICKNESS OF .75 IN

BLOCK (2,2) - LOWER LEFT CORNER BLOCK (17,2) - LOWER RIGHT CORNER

ANGLE OF INCLINATION = -1.0 DEGREES (FROM LEFT EDGE)

Y-INDEX / X-INDEX	6	9	10	11	12	13	14	15	16	17
2	.8607	.8361	.8248	.5475	.2216	.1070	.1070	.1070	.1070	.1070
3	.8686	.8626	.8351	.6338	.2497	.1070	.1070	.1070	.1070	.1070
4	.8682	.8517	.8346	.6342	.2534	.1070	.1070	.1070	.1070	.1070
5	.8715	.8599	.8354	.6680	.2647	.1070	.1070	.1070	.1070	.1070
6	.8758	.8725	.8358	.7143	.2872	.1070	.1070	.1070	.1070	.1070
7	.8801	.8874	.8359	.7649	.3135	.1070	.1070	.1070	.1070	.1070
8	.8852	.9052	.8360	.8066	.3554	.1070	.1070	.1070	.1070	.1070
9	.8903	.9231	.8360	.8235	.4185	.1070	.1070	.1070	.1070	.1070
10	.8954	.9413	.8361	.8302	.4887	.1070	.1070	.1070	.1070	.1070
11	.9005	.9595	.8361	.8326	.5619	.1070	.1070	.1070	.1070	.1070
12	.9065	.9827	.8537	.8348	.6407	.1070	.1070	.1070	.1070	.1070
13	.9112	.9984	.8691	.8355	.6986	.1070	.1070	.1070	.1070	.1070
14	.9159	1.0000	.8848	.8357	.7545	.1070	.1070	.1070	.1070	.1070
15	.9209	1.0000	.9024	.8359	.8019	.1070	.1070	.1070	.1070	.1070
16	.9259	1.0000	.9198	.8359	.8210	.1075	.1070	.1070	.1070	.1070
17	.9294	1.0000	.9327	.8360	.8284	.1212	.1070	.1070	.1070	.1070

c. WATER SATURATION DISTRIBUTION

FOR TIME STEP 10, ADVANCING TIME FROM 1.57 DAYS TO 1.81 DAYS

WITH 16 X-INCREMENTS OF 2.25 IN, 16 Y-INCREMENTS OF .28 IN, AND HORIZONTAL THICKNESS OF .75 IN

BLOCK (2,2) - LOWER LEFT CORNER BLOCK (17,2) - LOWER RIGHT CORNER

ANGLE OF INCLINATION = -1.0 DEGREES (FROM LEFT EDGE)

Y-INDEX / X-INDEX	6	9	10	11	12	13	14	15	16	17
2	.8842	.9436	.8361	.8294	.4424	.1070	.1070	.1070	.1070	.1070
3	.8761	.8927	.8360	.7706	.3117	.1070	.1070	.1070	.1070	.1070
4	.8725	.8679	.8357	.6965	.2761	.1070	.1070	.1070	.1070	.1070
5	.8739	.8667	.8357	.7020	.2794	.1070	.1070	.1070	.1070	.1070
6	.8772	.8788	.8359	.7359	.2971	.1070	.1070	.1070	.1070	.1070
7	.8812	.8923	.8360	.7794	.3249	.1070	.1070	.1070	.1070	.1070
8	.8861	.9096	.8360	.8125	.3648	.1070	.1070	.1070	.1070	.1070
9	.8913	.9276	.8360	.8260	.4328	.1070	.1070	.1070	.1070	.1070
10	.8964	.9457	.8361	.8308	.5046	.1070	.1070	.1070	.1070	.1070
11	.9016	.9642	.8361	.8332	.5765	.1070	.1070	.1070	.1070	.1070
12	.9082	.9905	.8611	.8351	.6567	.1070	.1070	.1070	.1070	.1070
13	.9122	1.0000	.8729	.8355	.7140	.1070	.1070	.1070	.1070	.1070
14	.9166	1.0000	.8880	.8358	.7663	.1070	.1070	.1070	.1070	.1070
15	.9213	1.0000	.9041	.8359	.8051	.1070	.1070	.1070	.1070	.1070
16	.9258	1.0000	.9191	.8359	.8206	.1070	.1070	.1070	.1070	.1070
17	.9267	1.0000	.9279	.8359	.8271	.1178	.1070	.1070	.1070	.1070

TABLE XXXIX

COMPUTED WATER POTENTIAL DISTRIBUTIONS;
GAS INJECTION, NO WATER INJECTION

a. WATER POTENTIAL (ATM) DISTRIBUTION

FOR TIME STEP 3, ADVANCING TIME FROM 6.04 DAYS TO 9.96 HRS

WITH 16 X-INCREMENTS OF 20.00 FT, 16 Y-INCREMENTS OF 2.00 FT, AND HORIZONTAL THICKNESS OF 100.00 FT

BLOCK (2,2) - LOWER LEFT CORNER BLOCK (17,2) - LOWER RIGHT CORNER

ANGLE OF INCLINATION = -2.0 DEGREES (FROM LEFT EDGE)

Y-INDEX / X-INDEX	4	7	10	11	12	13	14	15	16	17
2	8.19E 00	8.20E 00	8.21E 00	8.21E 00	8.21E 00	8.22E 00	8.22E 00	8.22E 00	8.22E 00	8.22E 00
3	8.16E 00	8.16E 00	8.17E 00	8.17E 00	8.17E 00	8.17E 00	8.17E 00	8.18E 00	8.18E 00	8.18E 00
4	8.11E 00	8.11E 00	8.12E 00	8.12E 00	8.12E 00	8.12E 00	8.12E 00	8.13E 00	8.13E 00	8.13E 00
5	8.05E 00	8.05E 00	8.05E 00	8.06E 00	8.06E 00	8.06E 00	8.06E 00	8.06E 00	8.07E 00	8.07E 00
6	7.97E 00	7.97E 00	7.98E 00	7.98E 00	7.98E 00	7.98E 00	7.98E 00	7.99E 00	7.99E 00	7.99E 00
7	7.86E 00	7.87E 00	7.88E 00	7.88E 00	7.88E 00	7.89E 00	7.89E 00	7.90E 00	7.90E 00	7.91E 00
8	7.71E 00	7.72E 00	7.74E 00	7.74E 00	7.75E 00	7.76E 00	7.76E 00	7.77E 00	7.78E 00	7.79E 00
9	7.50E 00	7.51E 00	7.52E 00	7.53E 00	7.54E 00	7.54E 00	7.55E 00	7.56E 00	7.57E 00	7.59E 00
10	7.23E 00	7.23E 00	7.24E 00	7.24E 00	7.25E 00	7.25E 00	7.26E 00	7.26E 00	7.26E 00	7.27E 00
11	6.92E 00	6.92E 00	6.92E 00	6.92E 00	6.92E 00	6.92E 00	6.92E 00	6.92E 00	6.92E 00	6.92E 00
12	6.60E 00	6.60E 00	6.60E 00	6.60E 00	6.60E 00	6.60E 00	6.60E 00	6.60E 00	6.60E 00	6.60E 00
13	6.28E 00	6.28E 00	6.28E 00	6.28E 00	6.28E 00	6.28E 00	6.28E 00	6.28E 00	6.28E 00	6.28E 00
14	5.96E 00	5.96E 00	5.96E 00	5.96E 00	5.96E 00	5.96E 00	5.96E 00	5.96E 00	5.96E 00	5.96E 00
15	5.64E 00	5.64E 00	5.64E 00	5.64E 00	5.64E 00	5.64E 00	5.64E 00	5.64E 00	5.64E 00	5.64E 00
16	5.32E 00	5.32E 00	5.32E 00	5.32E 00	5.32E 00	5.32E 00	5.32E 00	5.32E 00	5.32E 00	5.32E 00
17	5.00E 00	5.00E 00	5.00E 00	5.00E 00	5.00E 00	5.00E 00	5.00E 00	5.00E 00	5.00E 00	5.00E 00

b. FOR TIME STEP 51, ADVANCING TIME FROM 21.22 DAYS TO 21.72 DAYS

Y-INDEX / X-INDEX	4	7	10	11	12	13	14	15	16	17
2	6.45E 00	6.45E 00	6.45E 00	6.46E 00	6.46E 00	6.46E 00	6.46E 00	6.48E 00	6.48E 00	6.48E 00
3	6.43E 00	6.43E 00	6.43E 00	6.43E 00	6.44E 00	6.44E 00	6.44E 00	6.44E 00	6.45E 00	6.45E 00
4	6.39E 00	6.39E 00	6.39E 00	6.39E 00	6.40E 00	6.40E 00	6.40E 00	6.40E 00	6.41E 00	6.41E 00
5	6.34E 00	6.34E 00	6.34E 00	6.34E 00	6.35E 00	6.35E 00	6.35E 00	6.35E 00	6.35E 00	6.35E 00
6	6.28E 00	6.28E 00	6.28E 00	6.28E 00	6.28E 00	6.29E 00	6.29E 00	6.29E 00	6.29E 00	6.30E 00
7	6.21E 00	6.21E 00	6.21E 00	6.21E 00	6.21E 00	6.22E 00	6.22E 00	6.22E 00	6.22E 00	6.23E 00
8	6.13E 00	6.13E 00	6.13E 00	6.13E 00	6.13E 00	6.13E 00	6.13E 00	6.13E 00	6.14E 00	6.14E 00
9	6.03E 00	6.03E 00	6.04E 00	6.04E 00	6.04E 00	6.04E 00	6.04E 00	6.04E 00	6.04E 00	6.05E 00
10	5.93E 00	5.94E 00	5.94E 00	5.94E 00	5.94E 00	5.94E 00	5.94E 00	5.94E 00	5.94E 00	5.95E 00
11	5.83E 00	5.83E 00	5.83E 00	5.83E 00	5.83E 00	5.83E 00	5.83E 00	5.83E 00	5.84E 00	5.84E 00
12	5.73E 00	5.73E 00	5.73E 00	5.73E 00	5.73E 00	5.73E 00	5.73E 00	5.73E 00	5.73E 00	5.74E 00
13	5.61E 00	5.62E 00	5.62E 00	5.62E 00	5.62E 00	5.62E 00	5.62E 00	5.62E 00	5.62E 00	5.63E 00
14	5.50E 00	5.50E 00	5.50E 00	5.50E 00	5.50E 00	5.51E 00	5.51E 00	5.51E 00	5.51E 00	5.53E 00
15	5.36E 00	5.37E 00	5.37E 00	5.37E 00	5.38E 00	5.38E 00	5.38E 00	5.39E 00	5.39E 00	5.41E 00
16	5.20E 00	5.21E 00	5.21E 00	5.22E 00	5.22E 00	5.22E 00	5.23E 00	5.23E 00	5.24E 00	5.25E 00
17	5.01E 00	5.01E 00	5.01E 00	5.01E 00	5.01E 00	5.01E 00	5.01E 00	5.02E 00	5.02E 00	5.02E 00

TABLE XL

COMPUTED WATER POTENTIAL DISTRIBUTIONS;
GAS INJECTION, 25 BBL/DAY WATER INJECTION

WATER POTENTIAL (ATM) DISTRIBUTION

a. FOR TIME STEP 3, ADVANCING TIME FROM 4.56 HRS TO 9.96 HRS

WITH 16 X-INCREMENTS OF 20.00 FT, 16 Y-INCREMENTS OF 2.00 FT, AND HORIZONTAL THICKNESS OF 100.00 FT

BLOCK (2,2) - LOWER LEFT CORNER BLOCK (17,2) - LOWER RIGHT CORNER

ANGLE OF INCLINATION = -2.0 DEGREES (FROM LEFT EDGE)

Y-INDEX / X-INDEX	4	7	10	11	12	13	14	15	16	17
2	8.76E 00	8.77E 00	8.77E 00	8.78E 00	8.78E 00	8.78E 00	8.79E 00	8.79E 00	8.79E 00	8.79E 00
3	8.73E 00	8.73E 00	8.74E 00	8.74E 00	8.74E 00	8.74E 00	8.74E 00	8.75E 00	8.75E 00	8.75E 00
4	8.68E 00	8.68E 00	8.69E 00	8.69E 00	8.69E 00	8.69E 00	8.69E 00	8.69E 00	8.69E 00	8.69E 00
5	8.62E 00	8.62E 00	8.62E 00	8.63E 00	8.63E 00	8.63E 00	8.63E 00	8.63E 00	8.63E 00	8.63E 00
6	8.54E 00	8.54E 00	8.54E 00	8.55E 00	8.55E 00	8.55E 00	8.55E 00	8.56E 00	8.56E 00	8.56E 00
7	8.43E 00	8.44E 00	8.44E 00	8.45E 00	8.45E 00	8.46E 00	8.46E 00	8.47E 00	8.47E 00	8.47E 00
8	8.28E 00	8.29E 00	8.30E 00	8.31E 00	8.32E 00	8.32E 00	8.33E 00	8.34E 00	8.35E 00	8.36E 00
9	8.07E 00	8.08E 00	8.09E 00	8.10E 00	8.11E 00	8.11E 00	8.12E 00	8.13E 00	8.14E 00	8.16E 00
10	7.80E 00	7.80E 00	7.81E 00	7.81E 00	7.82E 00	7.82E 00	7.82E 00	7.83E 00	7.83E 00	7.84E 00
11	7.49E 00	7.49E 00	7.49E 00	7.49E 00	7.49E 00	7.49E 00	7.49E 00	7.49E 00	7.49E 00	7.49E 00
12	7.17E 00	7.17E 00	7.17E 00	7.17E 00	7.17E 00	7.17E 00	7.17E 00	7.17E 00	7.17E 00	7.17E 00
13	6.84E 00	6.84E 00	6.85E 00	6.85E 00	6.85E 00	6.86E 00	6.86E 00	6.86E 00	6.86E 00	6.86E 00
14	6.48E 00	6.49E 00	6.52E 00	6.53E 00	6.54E 00	6.54E 00	6.58E 00	6.60E 00	6.62E 00	6.63E 00
15	6.01E 00	6.01E 00	6.02E 00	6.02E 00	6.02E 00	6.03E 00	6.03E 00	6.03E 00	6.03E 00	6.03E 00
16	5.51E 00	5.51E 00	5.51E 00	5.51E 00	5.51E 00	5.51E 00	5.51E 00	5.51E 00	5.51E 00	5.51E 00
17	5.00E 00	5.00E 00	5.00E 00	5.00E 00	5.00E 00	5.00E 00	5.00E 00	5.00E 00	5.00E 00	5.00E 00

b. FOR TIME STEP 52, ADVANCING TIME FROM 20.09 DAYS TO 20.59 DAYS

Y-INDEX / X-INDEX	4	7	10	11	12	13	14	15	16	17
2	7.54E 00	7.55E 00	7.55E 00	7.55E 00	7.56E 00	7.56E 00	7.56E 00	7.57E 00	7.58E 00	7.58E 00
3	7.52E 00	7.53E 00	7.53E 00	7.53E 00	7.53E 00	7.53E 00	7.54E 00	7.54E 00	7.54E 00	7.54E 00
4	7.49E 00	7.49E 00	7.49E 00	7.49E 00	7.49E 00	7.49E 00	7.50E 00	7.50E 00	7.50E 00	7.50E 00
5	7.44E 00	7.44E 00	7.44E 00	7.44E 00	7.44E 00	7.44E 00	7.44E 00	7.45E 00	7.45E 00	7.45E 00
6	7.38E 00	7.38E 00	7.38E 00	7.38E 00	7.38E 00	7.38E 00	7.38E 00	7.39E 00	7.39E 00	7.39E 00
7	7.30E 00	7.30E 00	7.31E 00	7.31E 00	7.31E 00	7.31E 00	7.31E 00	7.31E 00	7.32E 00	7.32E 00
8	7.22E 00	7.22E 00	7.22E 00	7.22E 00	7.22E 00	7.23E 00	7.23E 00	7.23E 00	7.23E 00	7.24E 00
9	7.13E 00	7.13E 00	7.13E 00	7.13E 00	7.13E 00	7.13E 00	7.13E 00	7.13E 00	7.13E 00	7.14E 00
10	7.03E 00	7.03E 00	7.03E 00	7.03E 00	7.03E 00	7.03E 00	7.03E 00	7.03E 00	7.03E 00	7.04E 00
11	6.92E 00	6.92E 00	6.92E 00	6.92E 00	6.92E 00	6.92E 00	6.93E 00	6.93E 00	6.93E 00	6.94E 00
12	6.80E 00	6.80E 00	6.81E 00	6.81E 00	6.81E 00	6.82E 00	6.82E 00	6.82E 00	6.83E 00	6.84E 00
13	6.65E 00	6.66E 00	6.67E 00	6.68E 00	6.69E 00	6.70E 00	6.71E 00	6.72E 00	6.73E 00	6.76E 00
14	6.41E 00	6.43E 00	6.48E 00	6.50E 00	6.53E 00	6.56E 00	6.59E 00	6.63E 00	6.68E 00	6.71E 00
15	5.96E 00	5.97E 00	5.97E 00	5.97E 00	5.97E 00	5.97E 00	5.97E 00	5.96E 00	5.96E 00	5.95E 00
16	5.49E 00	5.49E 00	5.49E 00	5.49E 00	5.49E 00	5.49E 00	5.49E 00	5.49E 00	5.49E 00	5.49E 00
17	5.02E 00	5.02E 00	5.02E 00	5.02E 00	5.02E 00	5.02E 00	5.02E 00	5.02E 00	5.02E 00	5.01E 00

TABLE XLI

COMPUTED WATER POTENTIAL DISTRIBUTIONS;
GAS INJECTION, 100 BBL/DAY WATER INJECTION

a. WATER POTENTIAL (ATM) DISTRIBUTION

FOR TIME STEP 3, ADVANCING TIME FROM 4.56 HRS TO 9.96 HRS

WITH 16 X-INCREMENTS OF 20.00 FT, 16 Y-INCREMENTS OF 2.00 FT, AND HORIZONTAL THICKNESS OF 100.00 FT

BLOCK (2,2) - LOWER LEFT CORNER BLOCK (17,2) - LOWER RIGHT CORNER

ANGLE OF INCLINATION = -2.0 DEGREES (FROM LEFT EDGE)

Y-INDEX / X-INDEX	4	7	10	11	12	13	14	15	16	17
2	1.05E 01	1.05E 01	1.05E 01	1.05E 01	1.05E 01	1.05E 01	1.05E 01	1.05E 01	1.05E 01	1.05E 01
3	1.04E 01	1.04E 01	1.04E 01	1.04E 01	1.04E 01	1.04E 01	1.04E 01	1.05E 01	1.05E 01	1.05E 01
4	1.04E 01	1.04E 01	1.04E 01	1.04E 01	1.04E 01	1.04E 01	1.04E 01	1.04E 01	1.04E 01	1.04E 01
5	1.03E 01	1.03E 01	1.03E 01	1.03E 01	1.03E 01	1.03E 01	1.03E 01	1.03E 01	1.03E 01	1.03E 01
6	1.02E 01	1.02E 01	1.03E 01	1.03E 01	1.03E 01	1.03E 01	1.03E 01	1.03E 01	1.03E 01	1.03E 01
7	1.01E 01	1.01E 01	1.02E 01	1.02E 01	1.02E 01	1.02E 01	1.02E 01	1.02E 01	1.02E 01	1.02E 01
8	9.99E 00	10.00E 00	1.00E 01	1.00E 01	1.00E 01	1.00E 01	1.00E 01	1.00E 01	1.01E 01	1.01E 01
9	9.78E 00	9.79E 00	9.80E 00	9.80E 00	9.81E 00	9.82E 00	9.83E 00	9.84E 00	9.85E 00	9.86E 00
10	9.50E 00	9.51E 00	9.52E 00	9.52E 00	9.52E 00	9.53E 00	9.53E 00	9.53E 00	9.54E 00	9.55E 00
11	9.19E 00	9.19E 00	9.20E 00	9.20E 00	9.20E 00	9.20E 00	9.20E 00	9.20E 00	9.20E 00	9.20E 00
12	8.87E 00	8.87E 00	8.88E 00	8.88E 00	8.88E 00	8.88E 00	8.88E 00	8.88E 00	8.88E 00	8.89E 00
13	8.52E 00	8.53E 00	8.56E 00	8.57E 00	8.57E 00	8.58E 00	8.59E 00	8.60E 00	8.61E 00	8.61E 00
14	8.04E 00	8.09E 00	8.19E 00	8.23E 00	8.29E 00	8.35E 00	8.42E 00	8.50E 00	8.59E 00	8.64E 00
15	7.12E 00	7.13E 00	7.16E 00	7.17E 00	7.18E 00	7.18E 00	7.19E 00	7.20E 00	7.21E 00	7.21E 00
16	6.07E 00	6.07E 00	6.08E 00	6.08E 00	6.08E 00	6.08E 00	6.08E 00	6.09E 00	6.09E 00	6.09E 00
17	5.00E 00	5.00E 00	5.00E 00	5.00E 00	5.00E 00	5.00E 00	5.00E 00	5.00E 00	5.00E 00	5.00E 00

b. FOR TIME STEP121, ADVANCING TIME FROM 20.26 DAYS TO 20.30 DAYS

Y-INDEX / X-INDEX	4	7	10	11	12	13	14	15	16	17
2	9.60E 00	9.60E 00	9.60E 00	9.61E 00	9.61E 00	9.61E 00	9.61E 00	9.63E 00	9.63E 00	9.63E 00
3	9.58E 00	9.58E 00	9.58E 00	9.58E 00	9.59E 00	9.59E 00	9.59E 00	9.59E 00	9.60E 00	9.60E 00
4	9.54E 00	9.54E 00	9.54E 00	9.54E 00	9.55E 00	9.55E 00	9.55E 00	9.55E 00	9.56E 00	9.56E 00
5	9.49E 00	9.49E 00	9.49E 00	9.49E 00	9.49E 00	9.50E 00	9.50E 00	9.50E 00	9.50E 00	9.50E 00
6	9.43E 00	9.43E 00	9.43E 00	9.43E 00	9.43E 00	9.44E 00	9.44E 00	9.44E 00	9.44E 00	9.45E 00
7	9.36E 00	9.36E 00	9.36E 00	9.36E 00	9.36E 00	9.36E 00	9.37E 00	9.37E 00	9.37E 00	9.38E 00
8	9.27E 00	9.27E 00	9.28E 00	9.28E 00	9.28E 00	9.28E 00	9.28E 00	9.28E 00	9.28E 00	9.29E 00
9	9.18E 00	9.18E 00	9.18E 00	9.18E 00	9.18E 00	9.18E 00	9.19E 00	9.19E 00	9.19E 00	9.20E 00
10	9.08E 00	9.08E 00	9.08E 00	9.08E 00	9.08E 00	9.08E 00	9.08E 00	9.09E 00	9.09E 00	9.10E 00
11	8.96E 00	8.96E 00	8.97E 00	8.97E 00	8.97E 00	8.98E 00	8.98E 00	8.98E 00	8.99E 00	9.00E 00
12	8.82E 00	8.83E 00	8.84E 00	8.85E 00	8.86E 00	8.86E 00	8.87E 00	8.88E 00	8.89E 00	8.92E 00
13	8.59E 00	8.62E 00	8.66E 00	8.68E 00	8.69E 00	8.71E 00	8.74E 00	8.78E 00	8.83E 00	8.87E 00
14	8.17E 00	8.23E 00	8.35E 00	8.40E 00	8.46E 00	8.54E 00	8.63E 00	8.74E 00	8.85E 00	8.90E 00
15	7.22E 00	7.24E 00	7.27E 00	7.28E 00	7.29E 00	7.30E 00	7.31E 00	7.32E 00	7.33E 00	7.33E 00
16	6.13E 00	6.14E 00	6.14E 00	6.14E 00	6.15E 00	6.15E 00	6.15E 00	6.15E 00	6.15E 00	6.15E 00
17	5.01E 00	5.01E 00	5.01E 00	5.01E 00	5.01E 00	5.01E 00	5.01E 00	5.02E 00	5.02E 00	5.02E 00

TABLE XLII

COMPUTED WATER POTENTIAL DISTRIBUTIONS
AFTER CESSATION OF GAS INJECTION

a. Water Injection: 25 Bbl/Day

WATER POTENTIAL (ATM) DISTRIBUTION

FOR TIME STEP 17, ADVANCING TIME FROM 14.64 DAYS TO 15.36 DAYS

WITH 16 X-INCREMENTS OF 20.00 FT, 16 Y-INCREMENTS OF 2.00 FT, AND HORIZONTAL THICKNESS OF 100.00 FT

BLOCK (2,2) - LOWER LEFT CORNER BLOCK (17,2) - LOWER RIGHT CORNER

ANGLE OF INCLINATION = -2.0 DEGREES (FROM LEFT EDGE)

Y-INDEX / X-INDEX	4	7	10	11	12	13	14	15	16	17
2	5.50E 00	5.50E 00	5.50E 00	5.50E 00	5.50E 00	5.50E 00	5.50E 00	5.51E 00	5.51E 00	5.51E 00
3	5.51E 00	5.51E 00	5.51E 00	5.51E 00	5.51E 00	5.51E 00	5.51E 00	5.51E 00	5.51E 00	5.51E 00
4	5.51E 00	5.51E 00	5.51E 00	5.51E 00	5.51E 00	5.51E 00	5.51E 00	5.51E 00	5.51E 00	5.51E 00
5	5.51E 00	5.51E 00	5.51E 00	5.51E 00	5.51E 00	5.51E 00	5.51E 00	5.51E 00	5.51E 00	5.51E 00
6	5.50E 00	5.50E 00	5.50E 00	5.50E 00	5.50E 00	5.50E 00	5.50E 00	5.50E 00	5.51E 00	5.51E 00
7	5.50E 00	5.50E 00	5.50E 00	5.50E 00	5.50E 00	5.50E 00	5.50E 00	5.50E 00	5.50E 00	5.51E 00
8	5.49E 00	5.49E 00	5.49E 00	5.49E 00	5.49E 00	5.49E 00	5.49E 00	5.49E 00	5.49E 00	5.50E 00
9	5.48E 00	5.48E 00	5.48E 00	5.48E 00	5.48E 00	5.48E 00	5.48E 00	5.48E 00	5.49E 00	5.49E 00
10	5.47E 00	5.47E 00	5.47E 00	5.47E 00	5.47E 00	5.47E 00	5.47E 00	5.47E 00	5.47E 00	5.48E 00
11	5.46E 00	5.46E 00	5.46E 00	5.46E 00	5.46E 00	5.46E 00	5.46E 00	5.46E 00	5.46E 00	5.47E 00
12	5.45E 00	5.45E 00	5.45E 00	5.45E 00	5.45E 00	5.45E 00	5.45E 00	5.45E 00	5.45E 00	5.46E 00
13	5.44E 00	5.44E 00	5.44E 00	5.45E 00	5.45E 00	5.45E 00	5.45E 00	5.45E 00	5.45E 00	5.46E 00
14	5.39E 00	5.41E 00	5.43E 00	5.45E 00	5.46E 00	5.48E 00	5.49E 00	5.51E 00	5.54E 00	5.55E 00
15	5.24E 00	5.25E 00	5.26E 00	5.26E 00	5.27E 00	5.27E 00	5.27E 00	5.28E 00	5.28E 00	5.29E 00
16	5.04E 00	5.04E 00	5.05E 00	5.05E 00	5.05E 00	5.06E 00	5.06E 00	5.06E 00	5.07E 00	5.07E 00
17	4.80E 00	4.80E 00	4.79E 00	4.79E 00	4.79E 00	4.79E 00	4.79E 00	4.79E 00	4.79E 00	4.79E 00

b. Water Injection: None

FOR TIME STEP 17, ADVANCING TIME FROM 17.85 DAYS TO 19.85 DAYS

Y-INDEX / X-INDEX	4	7	10	11	12	13	14	15	16	17
2	5.10E 00	5.10E 00	5.10E 00	5.10E 00	5.10E 00	5.10E 00	5.10E 00	5.10E 00	5.11E 00	5.11E 00
3	5.10E 00	5.10E 00	5.10E 00	5.10E 00	5.10E 00	5.10E 00	5.10E 00	5.10E 00	5.11E 00	5.11E 00
4	5.10E 00	5.10E 00	5.10E 00	5.10E 00	5.10E 00	5.10E 00	5.10E 00	5.10E 00	5.11E 00	5.11E 00
5	5.10E 00	5.10E 00	5.10E 00	5.10E 00	5.10E 00	5.10E 00	5.10E 00	5.10E 00	5.10E 00	5.11E 00
6	5.10E 00	5.10E 00	5.10E 00	5.10E 00	5.10E 00	5.10E 00	5.10E 00	5.10E 00	5.10E 00	5.11E 00
7	5.09E 00	5.09E 00	5.09E 00	5.09E 00	5.09E 00	5.09E 00	5.10E 00	5.10E 00	5.10E 00	5.10E 00
8	5.09E 00	5.09E 00	5.09E 00	5.09E 00	5.09E 00	5.09E 00	5.09E 00	5.09E 00	5.09E 00	5.10E 00
9	5.08E 00	5.08E 00	5.08E 00	5.08E 00	5.08E 00	5.08E 00	5.08E 00	5.08E 00	5.08E 00	5.09E 00
10	5.07E 00	5.07E 00	5.07E 00	5.07E 00	5.07E 00	5.07E 00	5.07E 00	5.07E 00	5.07E 00	5.08E 00
11	5.06E 00	5.06E 00	5.06E 00	5.06E 00	5.06E 00	5.06E 00	5.06E 00	5.06E 00	5.06E 00	5.06E 00
12	5.05E 00	5.05E 00	5.05E 00	5.05E 00	5.05E 00	5.05E 00	5.05E 00	5.05E 00	5.05E 00	5.06E 00
13	5.05E 00	5.05E 00	5.05E 00	5.05E 00	5.05E 00	5.05E 00	5.05E 00	5.05E 00	5.05E 00	5.05E 00
14	5.04E 00	5.04E 00	5.04E 00	5.04E 00	5.04E 00	5.04E 00	5.05E 00	5.05E 00	5.05E 00	5.05E 00
15	5.02E 00	5.02E 00	5.03E 00	5.03E 00	5.03E 00	5.03E 00	5.04E 00	5.04E 00	5.04E 00	5.05E 00
16	4.96E 00	4.97E 00	4.98E 00	4.99E 00	4.99E 00	5.00E 00	5.00E 00	5.01E 00	5.02E 00	5.03E 00
17	4.88E 00	4.87E 00	4.85E 00	4.84E 00	4.82E 00	4.81E 00	4.81E 00	4.81E 00	4.81E 00	4.81E 00

[redacted] XXIII

[redacted] AQUIFER

a. SYSTEM SPECIFICATION

INDEPENDENT VARIABLES

10 RADIAL INCREMENTS — 14 VERTICAL INCREMENTS OF — 20 TIME INCREMENTS OF

FROM RMIN OF 14.17 TO RMAX OF 141.70 FEET — .10 FEET — VARIABLE LENGTH

RADII OF ELEMENTS AND ELEVATION OF BOTTOM LAYER, FEET

R-INDEX	R-INNER	R-CENTER	R-OUTER	YB-CENTER	R-INDEX	R-INNER	R-CENTER	R-OUTER	YB-CENTER
1	12.50	14.17	16.15	.00	2	16.15	18.30	20.86	.00
3	20.86	23.64	26.94	.00	4	26.94	30.53	34.79	.00
5	34.79	39.43	44.93	.00	6	44.93	50.92	58.03	.00
7	58.03	65.77	74.95	.00	8	74.95	84.95	96.80	.00
9	96.80	109.71	125.03	.00	10	125.03	141.70	161.48	.00

WELL BORE DIAMETER = .42 (ON AXIS) FRACTION OF AREA OPEN TO EACH LAYER = .50

RING OF WATER INJECTION WELLS - RADIAL INCREMENT NO. 8, RADIUS = 84.95

COMMUNICATION WITH SURROUNDING AQUIFER AT OUTER BOUNDARY

WATER GRAVITY = 1.000 VISCOSITY = 1.000 CP GAS GRAVITY = 1.000 VISCOSITY = .01750 CP

SURFACE TENSION = 72.00 DYNES/CM

STANDARD GAS VOLUME MEASURED AT 14.68 PSIA AND 60.0 DEG F

INSITU CONDITIONS OF 304.00 PSIA AND 157.0 DEG F COMPRESSIBILITY FACTOR = .990

MODAL PERMEABILITY = 1.0700 DARCIES POROSITY = 19.30 PER CENT

b. GAS RATE = 2.0000E 00 MSCF/DAY WATER INJECTION RATE = 1.0000E 02 BBL/DAY

WATER SATURATION DISTRIBUTION

FOR TIME STEP 8, ADVANCING TIME FROM 1.16 HRS TO 1.28 HRS

WITH 10 LOGARITHMIC RADIAL INCREMENTS AND 14 VERTICAL INCREMENTS

ANNULAR RINGS (2,2) AT INNER RADIUS, LOWER LAYER AND (10,2) AT OUTER RADIUS, LOWER LAYER

Y-INDEX / R-INDEX	6	7	8	9	10	11	12	13	14	15
1	.9990	.9971	.9952	.9933	.9912	.9870	.9725	.8986	.7828	.6684
2	1.0000	1.0000	.9991	.9972	.9953	.9933	.9913	.9883	.9832	.9413
3	1.0000	1.0000	1.0000	1.0000	.9985	.9967	.9949	.9931	.9912	.9886
4	1.0000	1.0000	1.0000	1.0000	.9992	.9974	.9955	.9937	.9918	.9900
5	1.0000	1.0000	1.0000	1.0000	.9993	.9975	.9957	.9938	.9920	.9901
6	1.0000	1.0000	1.0000	1.0000	.9992	.9973	.9955	.9936	.9918	.9899
7	1.0000	1.0000	1.0000	1.0000	.9992	.9974	.9955	.9937	.9919	.9900
8	1.0000	1.0000	1.0000	1.0000	.9992	.9974	.9955	.9937	.9919	.9900
9	1.0000	1.0000	1.0000	1.0000	.9992	.9973	.9955	.9937	.9918	.9900
10	1.0000	1.0000	1.0000	1.0000	.9992	.9973	.9955	.9937	.9918	.9900

WATER POTENTIAL (ATM) DISTRIBUTION

FOR TIME STEP 8, ADVANCING TIME FROM 1.16 HRS TO 1.28 HRS

Y-INDEX / R-INDEX	6	7	8	9	10	11	12	13	14	15
1	1.00E 00	1.00E 00	1.00E 00	1.00E 00	1.00E 00	1.00E 00	10.00E-01	10.00E-01	10.00E-01	1.00E 00
2	1.04E 00	1.04E 00	1.04E 00	1.04E 00	1.04E 00	1.04E 00	1.04E 00	1.04E 00	1.04E 00	1.04E 00
3	1.07E 00	1.07E 00	1.07E 00	1.07E 00	1.07E 00	1.07E 00	1.07E 00	1.07E 00	1.07E 00	1.07E 00
4	9.90E-01	9.90E-01	9.90E-01	9.90E-01	9.90E-01	9.90E-01	9.90E-01	9.90E-01	9.90E-01	9.90E-01
5	9.32E-01	9.32E-01	9.32E-01	9.32E-01	9.32E-01	9.32E-01	9.32E-01	9.32E-01	9.32E-01	9.32E-01
6	9.14E-01	9.14E-01	9.14E-01	9.14E-01	9.14E-01	9.14E-01	9.14E-01	9.14E-01	9.14E-01	9.14E-01
7	8.97E-01	8.97E-01	8.97E-01	8.97E-01	8.97E-01	8.97E-01	8.97E-01	8.97E-01	8.97E-01	8.97E-01
8	8.76E-01	8.76E-01	8.76E-01	8.76E-01	8.76E-01	8.76E-01	8.76E-01	8.76E-01	8.76E-01	8.76E-01
9	6.88E-01	6.88E-01	6.88E-01	6.88E-01	6.88E-01	6.88E-01	6.88E-01	6.88E-01	6.88E-01	6.88E-01
10	5.00E-01	5.00E-01	5.00E-01	5.00E-01	5.00E-01	5.00E-01	5.00E-01	5.00E-01	5.00E-01	5.00E-01

c. GAS RATE = 2.0000E 00 MSCF/DAY NO WATER INJECTION

WATER SATURATION DISTRIBUTION

FOR TIME STEP 6, ADVANCING TIME FROM .95 HRS TO 1.19 HRS

WITH 10 LOGARITHMIC RADIAL INCREMENTS AND 14 VERTICAL INCREMENTS

ANNULAR RINGS (2,2) AT INNER RADIUS, LOWER LAYER AND (10,2) AT OUTER RADIUS, LOWER LAYER

Y-INDEX / R-INDEX	6	7	8	9	10	11	12	13	14	15
1	.9990	.9972	.9953	.9933	.9912	.9873	.9761	.9099	.7934	.6770
2	1.0000	1.0000	.9995	.9977	.9958	.9938	.9919	.9897	.9847	.9610
3	1.0000	1.0000	1.0000	.9992	.9974	.9956	.9938	.9919	.9901	.9858
4	1.0000	1.0000	1.0000	1.0000	.9994	.9976	.9958	.9939	.9921	.9903
5	1.0000	1.0000	1.0000	1.0000	.9994	.9975	.9957	.9939	.9920	.9902
6	1.0000	1.0000	1.0000	1.0000	.9992	.9973	.9955	.9937	.9918	.9900
7	1.0000	1.0000	1.0000	1.0000	.9992	.9974	.9955	.9937	.9918	.9900
8	1.0000	1.0000	1.0000	1.0000	.9992	.9973	.9955	.9937	.9918	.9900
9	1.0000	1.0000	1.0000	1.0000	.9992	.9973	.9955	.9937	.9918	.9900
10	1.0000	1.0000	1.0000	1.0000	.9992	.9973	.9955	.9937	.9918	.9900

WATER POTENTIAL (ATM) DISTRIBUTION

FOR TIME STEP 6, ADVANCING TIME FROM .95 HRS TO 1.19 HRS

Y-INDEX / R-INDEX	6	7	8	9	10	11	12	13	14	15
1	6.94E-01	6.94E-01	6.94E-01	6.94E-01	6.94E-01	6.94E-01	6.94E-01	6.94E-01	6.94E-01	6.94E-01
2	7.16E-01	7.16E-01	7.16E-01	7.16E-01	7.16E-01	7.16E-01	7.16E-01	7.16E-01	7.16E-01	7.16E-01
3	7.26E-01	7.26E-01	7.26E-01	7.26E-01	7.26E-01	7.26E-01	7.26E-01	7.26E-01	7.26E-01	7.26E-01
4	6.66E-01	6.66E-01	6.66E-01	6.66E-01	6.66E-01	6.66E-01	6.66E-01	6.66E-01	6.66E-01	6.66E-01
5	6.20E-01	6.20E-01	6.20E-01	6.20E-01	6.20E-01	6.20E-01	6.20E-01	6.20E-01	6.20E-01	6.20E-01
6	5.97E-01	5.97E-01	5.97E-01	5.97E-01	5.97E-01	5.97E-01	5.97E-01	5.97E-01	5.97E-01	5.97E-01
7	5.75E-01	5.75E-01	5.75E-01	5.75E-01	5.75E-01	5.75E-01	5.75E-01	5.75E-01	5.75E-01	5.75E-01
8	5.51E-01	5.51E-01	5.51E-01	5.51E-01	5.51E-01	5.51E-01	5.51E-01	5.51E-01	5.51E-01	5.51E-01
9	5.26E-01	5.26E-01	5.26E-01	5.26E-01	5.26E-01	5.26E-01	5.26E-01	5.26E-01	5.26E-01	5.26E-01
10	5.00E-01	5.00E-01	5.00E-01	5.00E-01	5.00E-01	5.00E-01	5.00E-01	5.00E-01	5.00E-01	5.00E-01

TABLE XLIV

GAS PRODUCTION FROM DOMAL RESERVOIR

a. SYSTEM SPECIFICATION

INDEPENDENT VARIABLES

14 RADIAL INCREMENTS FROM RMIN OF 2.00 TO RMAX OF7022.38 FEET

20 VERTICAL INCREMENTS OF 2.00 FEET

5 TIME INCREMENTS OF VARIABLE LENGTH

RADII OF ELEMENTS AND ELEVATION OF BOTTOM LAYER, FEET

R-INDEX	R-INNER	R-CENTER	R-OUTER	YB-CENTER	R-INDEX	R-INNER	R-CENTER	R-OUTER	YB-CENTER
1	1.49	2.00	2.78	.00	2	2.78	3.75	5.21	-.00
3	5.21	7.02	9.77	-.00	4	9.77	13.16	18.31	-.01
5	18.31	24.66	34.31	-.01	6	34.31	46.20	64.29	-.05
7	64.29	86.58	120.47	-.11	8	120.47	162.23	225.73	-.27
9	225.73	303.98	422.98	-.83	10	422.98	569.61	792.60	-2.23
11	792.60	1067.34	1485.18	-6.80	12	1485.18	2000.00	2782.95	-20.00
13	2782.95	3747.63	5214.75	-35.00	14	5214.75	7022.38	9771.48	-40.00

WELL BORE DIAMETER = .50 (ON AXIS) FRACTION OF AREA OPEN TO EACH LAYER = 1.00

COMMUNICATION WITH SURROUNDING AQUIFER AT OUTER BOUNDARY

WATER GRAVITY = 1.100 VISCOSITY = 1.500 CP GAS GRAVITY = .700 VISCOSITY = .01350 CP

SURFACE TENSION = 72.00 DYNES/CM

STANDARD GAS VOLUME MEASURED AT 14.68 PSIA AND 60.0 DEG F

INSITU CONDITIONS OF 1260.00 PSIA AND 68.0 DEG F COMPRESSIBILITY FACTOR = .884

MODAL PERMEABILITY = .2000 DARCIES POROSITY = 15.00 PER CENT

GAS PRODUCTION RATE THROUGH WELL ON AXIS = 2.0000E 03 MSCF/DAY

b. WATER SATURATION DISTRIBUTION

FOR TIME STEP 5, ADVANCING TIME FROM 19.20 DAYS TO 30.00 DAYS

WITH 14 LOGARITHMIC RADIAL INCREMENTS AND 20 VERTICAL INCREMENTS

ANNULAR RINGS (2,2) AT INNER RADIUS, LOWER LAYER AND (14,2) AT OUTER RADIUS, LOWER LAYER

Y-INDEX / R-INDEX	11	13	14	15	16	17	18	19	20	21
1	.9405	.9308	.9057	.3146	.1954	.1719	.1561	.1403	.1299	.1264
2	.9405	.9308	.9052	.3119	.1952	.1718	.1560	.1402	.1299	.1263
3	.9400	.9300	.8721	.2716	.1910	.1697	.1539	.1387	.1294	.1259
4	.9383	.9236	.5217	.2094	.1796	.1621	.1463	.1337	.1277	.1242
5	.9356	.8914	.2826	.1923	.1703	.1545	.1392	.1295	.1260	.1225
6	.9318	.4122	.2029	.1759	.1594	.1436	.1318	.1271	.1236	.1201
7	.9279	.2260	.1839	.1654	.1496	.1359	.1285	.1249	.1214	.1179
8	.9271	.2213	.1828	.1645	.1487	.1353	.1283	.1247	.1212	.1177
9	.9295	.2501	.1887	.1684	.1526	.1379	.1291	.1256	.1221	.1186
10	.9333	.5925	.2177	.1819	.1639	.1481	.1348	.1281	.1246	.1211
11	.9413	.9345	.9293	.8061	.2433	.1873	.1676	.1518	.1373	.1289
12	.9589	.9496	.9483	.9470	.9457	.9437	.9413	.9390	.9347	.9295
13	.9961	.9855	.9803	.9750	.9697	.9644	.9592	.9539	.9497	.9483

c. WATER SATURATION DISTRIBUTION

FOR TIME STEP 10, ADVANCING TIME FROM 24.30 DAYS TO 30.00 DAYS

WITH 14 LOGARITHMIC RADIAL INCREMENTS AND 20 VERTICAL INCREMENTS

ANNULAR RINGS (2,2) AT INNER RADIUS, LOWER LAYER AND (14,2) AT OUTER RADIUS, LOWER LAYER

Y-INDEX / R-INDEX	11	13	14	15	16	17	18	19	20	21
1	.9430	.9357	.9297	.8433	.2552	.1891	.1687	.1529	.1380	.1292
2	.9428	.9352	.9293	.8077	.2431	.1872	.1675	.1517	.1373	.1289
3	.9415	.9334	.9243	.5359	.2104	.1800	.1625	.1467	.1339	.1278
4	.9399	.9303	.8980	.2859	.1927	.1705	.1547	.1393	.1296	.1261
5	.9365	.9158	.3709	.2001	.1743	.1582	.1424	.1310	.1268	.1233
6	.9318	.4100	.2028	.1759	.1594	.1436	.1319	.1271	.1236	.1201
7	.9280	.2269	.1841	.1656	.1498	.1360	.1285	.1250	.1215	.1180
8	.9273	.2229	.1832	.1649	.1491	.1355	.1283	.1248	.1213	.1178
9	.9297	.2587	.1896	.1690	.1532	.1383	.1293	.1257	.1222	.1187
10	.9334	.6039	.2193	.1823	.1642	.1484	.1351	.1282	.1247	.1212
11	.9413	.9345	.9293	.8121	.2447	.1876	.1678	.1520	.1374	.1290
12	.9586	.9495	.9482	.9469	.9456	.9435	.9412	.9387	.9343	.9290
13	.9961	.9856	.9803	.9750	.9697	.9644	.9592	.9539	.9497	.9483